THE PETROLOGY AND GEOCHEMISTRY OF THE MERENSKY REEF IN THE RUSTENBURG AREA

by

RAYLAN TALBOT BROWN

Submitted in partial fulfilment
of the requirements for the degree of
Master of Science
in the Department of Geology,
University of Natal,
Pietermaritzburg,
South Africa.

1994

DECLARATION

I, RAYLAN TALBOT BROWN, hereby declare that the
work and results embodied in this dissertation
are my own, except where otherwise stated or
acknowledged.   I further declare that no part
of this dissertation has been, or is being
concurrently, submitted for a degree or other
qualification at any other university or
educational institution.

i

RESTRICTION

No part of this unpublished thesis, nor any data used in it, including tables, figures and appendices, may be used, referenced, reproduced or published in any form without the explicit written permission of the author, and the Head of Department of Geology, University of Natal.

ACKNOWLEDGEMENTS

DEDICATION

I dedicate this thesis to my father, Clive Melville Brown.

ABSTRACT

Four Merensky reef underground exposures of different reef thickness, representative of the lithological variations exposed in mining, have been drilled and mapped. The relationship of the Merensky reef to the underlying rocks is paraconformable, and a broad-based definition of the highly variable Merensky reef, on the basis of detailed mine-wide mapping, is presented. Fifty two whole-rock samples from one drill intersection were analysed for major and trace elements by X-Ray Fluorescence spectrometry, and for platinum-group elements (PGE) by Neutron Activation analysis. The remaining three drill intersections were analysed for trace elements, and for PGE in one instance. Orthopyroxene and plagioclase mineral separates from one intersection were analysed for major elements by XRF, and the mineral compositions determined. The results of the whole-rock and silicate mineral chemistry are presented and discussed.

Whole-rock geochemistry is controlled by modal composition, as are most trace elements. Incompatible elements such as Nb, Zr, Ba, Y and Rb occur in elevated abundances in the feldspathic pyroxenites and show systematic low-correlation relationships with Cu, Ni, S and the PGE. These patterns are ascribed to the pore space competition between incompatible element enriched silicate melt and sulphide melt. The PGE are systematically associated with the base metal sulphide elements, with some localised decoupling, with Pd and Au showing the greatest chalcophile nature. The other PGE are highly correlated. Deviations in the geochemistry relative to the mode are analysed and discussed.

Orthopyroxene and plagioclase mineral compositions consistently define three-way lithological associations, demonstrating limited geochemical relationship between the lithologies. These lithologies represent the footwall and hangingwall norites/anorthosites and the Merensky reef/Merensky pyroxenite sequence. The Merensky reef pegmatoid and the overlying Merensky pyroxenite have more evolved Mg# and Ca# than the norite or anorthosite. Ni in orthopyroxene correlates with whole-rock Ni, providing evidence of re-equilibration. A systematic relationship exists between plagioclase and orthopyroxene mineral compositions, with Ti in both phases defining primary and re-equilibrated trends.

Apart from the elevated PGE abundances in the Merensky reef, the Merensky reef and overlying Merensky pyroxenite are geochemically indistinguishable. Certain evolved element

distribution patterns coincide with the zone of elevated PGE, Cu and Ni abundances. Abundant geochemical evidence is consistent with late-stage *in situ* hydromagmatic alteration and modification to the Merensky reef, and in part, the Merensky pyroxenite. In contrast, the texturally similar footwall and hangingwall norites show very little evidence of hydromagmatic effects, where magmatic and submagmatic processes are well preserved.

The whole-rock and mineral geochemistry defines and characterises the Merensky succession and provides certain constraints for petrogenetic modelling. A multi-stage process is envisaged for the petrogenesis and evolution of the Merensky succession, involving, 1) a magmatic stage, 2) a submagmatic stage, and 3) a hydromagmatic stage.

CONTENTS

APPENDICES

LIST OF TABLES

LIST OF FIGURES

Figure 4.26 Upper portion of thick Merensky reef showing typical partial pegmatoidal development and large interstitial plagioclase crystals.

Figure 4.27 Middle portion of thick Merensky reef showing a partially pegmatoidal texture. Note the large plagioclase crystals and the rimming of orthopyroxene crystals.

Figure 4.28 Thick Merensky reef showing typical scattered partially pegmatoidal texture.

Figure 4.29 Close-up view of thick Merensky reef showing the partially pegmatoidal texture and large variation in crystal size.

Figure 4.30 Top contact of thick Merensky reef (upper chromitite layer at 10cm down from top of scale) showing patchy pegmatoidal development associated with the upper chromitite layer.

Figure 4.31 Top contact of thick Merensky reef (at 5cm up from base of scale) showing patchy pegmatoid, where in this case is largely confined to immediately beneath the uppermost chromitite layer.

Figure 4.32 Upper portion of thick Merensky reef showing long vertically orientated channel-like plagioclase occurrences.

Figure 4.33 Close-up view of thick Merensky reef showing channel-like plagioclase occurrences.

Figure 4.34 Basal contact of thick Merensky reef (top of cm scale on contact). Note there is no basal chromitite or footwall anorthosite layers developed. Note too in this case the undulatory nature of the contact.

Figure 4.35 Basal contact of thick Merensky reef. In this case there is some disseminated chromite concentrated in places along the contact, hence the thin localised footwall anorthosite layer.

Figure 4.36 Basal contact of thick Merensky reef with some disseminated chromite along contact, and the resultant, in this case very thin, footwall anorthosite layer.

Figure 5.1 Photomicrograph of footwall leuconorite showing the cumulus plagioclase and intercumulus orthopyroxene. Note the Carlsbad and albite twinning in the plagioclase.

Figure 5.2 Footwall leuconorite showing typical textural relationships between cumulus plagioclase and intercumulus orthopyroxene and clinopyroxene.

Figure 5.3 Footwall leuconorite with intercumulus orthopyroxene showing bleby clinopyroxene exsolution lamellae parallel to the (100) crystallographic axis.

Figure 5.4 Footwall leuconorite showing a local abundance of interstitial phlogopite.

Figure 5.5 Examples of intergrown pyrrhotite and chalcopyrite, where chalcopyrite has partially replaced pyrrhotite in footwall leuconorite.

Figure 5.6 Merensky reef showing cumulus subhedral to euhedral orthopyroxene crystals with intercumulus plagioclase displaying both albite and pericline twinning. Note the interstitial

euhedral BMS grain in the plagioclase.

Figure 5.24 An example of almost total replacement of pyrrhotite by chalcopyrite, resulting in relict islands of pyrrhotite.

Figure 5.25 Another example of near complete replacement of pyrrhotite by chalcopyrite. Remnant islands of pyrrhotite remain scattered throughout the chalcopyrite.

Figure 5.26 Rectangular-shaped chalcopyrite grain enclosed in a chromite grain (light grey-brown) of a Merensky reef basal chromitite layer. The adjacent plagioclase crystal encloses pyrrhotite and chalcopyrite intergrowths.

Figure 5.27 Interstitial chalcopyrite-pyrrhotite intergrowth in a Merensky reef basal chromitite layer.

Figure 5.28 Intergrowth of pyrrhotite (pink-yellow) and chalcopyrite (yellow) interstitial to chromite grains of a Merensky reef basal chromitite layer.

Figure 5.29 Base metal sulphide grains, plus minor plagioclase and phlogopite, enclosed within a cumulus pegmatoidal orthopyroxene crystal of the Merensky reef.

Figure 5.30 A base metal sulphide grain and some associated phlogopite enclosed within a cumulus pegmatoidal orthopyroxene crystal of the Merensky reef.

Figure 5.31 A base metal sulphide grain with a small amount of plagioclase enclosed in a pegmatoidal orthopyroxene crystal of the Merensky reef. Note the alteration in the orthopyroxene and particularly the adjacent plagioclase crystal.

Figure 5.32 Interstitial pyrrhotite grains showing advanced caries replacement by chalcopyrite. Note the small, elongate remobilised? chalcopyrite grains developed along cleavage planes in the adjacent orthopyroxene crystals.

Figure 5.33 Large interstitial pyrrhotite grain showing some caries replacement by chalcopyrite. The adjacent orthopyroxene crystal contains secondary? elongate blebs of chalcopyrite developed along cleavage planes.

Figure 5.34 Subhedral to euhedral cumulus orthopyroxene and intercumulus plagioclase crystals of the Merensky pyroxenite. Note the albite and pericline twinning in the plagioclase.

Figure 5.35 Subhedral cumulus orthopyroxene and intercumulus plagioclase and phlogopite of the Merensky pyroxenite.

Figure 5.36 Merensky pyroxenite cumulus orthopyroxene with interstitial base metal sulphide developed to the total exclusion of plagioclase.

Figure 5.37 Intergrown pyrrhotite and chalcopyrite grain in intercumulus plagioclase, and in contact with cumulus orthopyroxene crystal to the left. Note the remnant islands of pyrrhotite within the chalcopyrite.

Figure 5.38 Chalcopyrite replacing large pyrrhotite grain. The replacement front shows the typical caries texture.

Figure 5.39 Numerous small chalcopyrite grains enclosed in intercumulus plagioclase, with a

few elongate grains occupying cleavage planes of the adjacent cumulus orthopyroxene crystal.

Figure 6.32 R27A whole-rock log S v log tenor PGE, Au and Cu. Note that there are no convincing trends.

ERRATA

Figure 4.25: 'variety' should read 'variation'.

Figure 4.28: Caption should read 'Thick Merensky reef showing typical limited pegmatoidal development'.

Figure 4.31: 'where' should read 'which'.

Figure 5.3: 'bleby' should read 'blebby'. '100' should read '(100)'.

Figures 5.16 and 5.17: 'BMS isotropic' should read 'BMS opaque'.

CHAPTER 1

INTRODUCTION

1.1 GENERAL

The Bushveld Complex is the world's largest layered mafic to ultramafic intrusion and is a major resource of many economic minerals. It is the main constituent of the multi-complex Bushveld Magmatic Province (Irvine, 1982; Kruger, 1990, 1991) and is located in the central part of the Transvaal Province of the Republic of South Africa (Figure 1.1). It is essentially an inward dipping sheet-like body with east-west and north-south outcrop extremities of approximately 400km and 270km respectively. This does not necessarily imply a continuous body. The exposed parts of the complex occur in an area of 12200km^2 and attain apparent thicknesses of nearly 9000m in the eastern Bushveld, 7750m in the western Bushveld and 7000m in the northern Bushveld (SACS, 1980). The complex is almost entirely surrounded by older sedimentary and volcanic successions of the Transvaal Sequence, dated at 2224 ± 21 Ma (Burger and Coertze, 1975; Rb-Sr), into which it was intruded. Part of the northern Bushveld Complex abuts directly against Archaean granites.

The central portion of the Bushveld Complex has been extensively intruded by the Rashoop Granophyre Complex (the Rashoop Granophyre Suite of SACS, 1980), dated at 2000 ± 30 Ma (Faurie and Von Gruenewaldt, 1979; U-Pb), and the Lebowa Granite Complex (the Lebowa Granite Suite of SACS,1980), dated between 2010 ± 20 Ma (Von Gruenewaldt et al, 1985; U-Pb) and 1670 ± 30 Ma (Coertze et al, 1978; U-Pb). These acid intrusions were emplaced in batholithic proportions of thickness in excess of 3000m (Tankard et al, 1982). This central portion is partially covered by younger sedimentary rocks of the Waterberg Group (± 1800 Ma, Button 1977, in Tankard et al, 1982) and Karoo Sequence (c.200 Ma, Tankard et al, 1982). The western Bushveld, in addition, has been intruded by the alkaline Pilanesberg Complex, dated at 1330 ± 80 Ma (Van Niekerk, 1962, in Lurie, 1986). Irvine (1982) and Kruger (1990, 1991) have recommended that the complete array of ultrabasic to acid plutonic, hypabyssal and volcanic rocks that formally comprise the Bushveld (including the Rashoop Granophyre and Lebowa Granite Suites of SACS, 1980), the Bushveld-related mafic Losberg (Coetzee & Kruger, 1989) and Molopo Farms (Von Gruenewaldt et al, 1989) complexes, be collectively

termed the Bushveld Magmatic Province.

The Bushveld Complex (the Rustenburg Layered Suite of SACS, 1980) is informally divided, on the basis of dominant rock types and geochemistry, into four zones; the Lower Zone (LZ), Critical Zone (CZ), Main Zone (MZ) and Upper Zone (UZ), with the Marginal Zone (BZ) locally developed beneath the Lower Zone at the contact with the Transvaal Sequence. The Bushveld Complex has been dated, using Sm-Nd and Rb-Sr systematics, at 2049 ± 152 Mα and 2057 ± 24 Mα respectively (Von Gruenewaldt et al, 1985). A Rb-Sr isochron (recalculated to λ = 1,39 x 10^{-11} years for the decay constant of Rb^{87} (Hamilton, 1977) yields an age of 2050 ± 22 Mα, which along with the age of 2050 ± 25 Mα calculated by Harmer and Sharpe (1985), is the generally accepted age of the Bushveld Complex. More recent work in the eastern Bushveld by Lee and Butcher (1990) yields an age of 2025 ± 40 Mα.

1.2 GEOLOGY OF THE BUSHVELD COMPLEX

1.2.1 DISTRIBUTION AND STRUCTURE

The Bushveld Complex exists as a roughly subcircular-shaped body which consists of five lobes (Figure 1.1). For the purposes of this study, the five lobes are referred to as the western Bushveld, eastern Bushveld, northern Bushveld (includes both the Potgietersrus and Villa Nora compartments), south eastern Bushveld and far-western Bushveld respectively. The latter occurs as a limb-like extension to the west of the western Bushveld and largely comprises rocks of the Marginal and Lower Zones, with some Critical and Main Zone development. The south eastern Bushveld is completely covered by sedimentary successions of the Karoo Sequence, while the remaining four lobes are variably exposed, with some areas under extensive soil cover.

The Bushveld Complex layered succession generally dips inward towards the centre of the complex, with the exception of the northern Bushveld, which dips in a westerly direction. It is generally accepted by Bushveld scholars that the layered rocks are not continuous beneath the granites, granophyres and sedimentary cover surrounded by the complex. Geophysical studies indicate that the complex consists of several feeder compartments (Tankard et al, 1982), as was originally suggested by Cousins (1959). It is suggested that there are at least four,
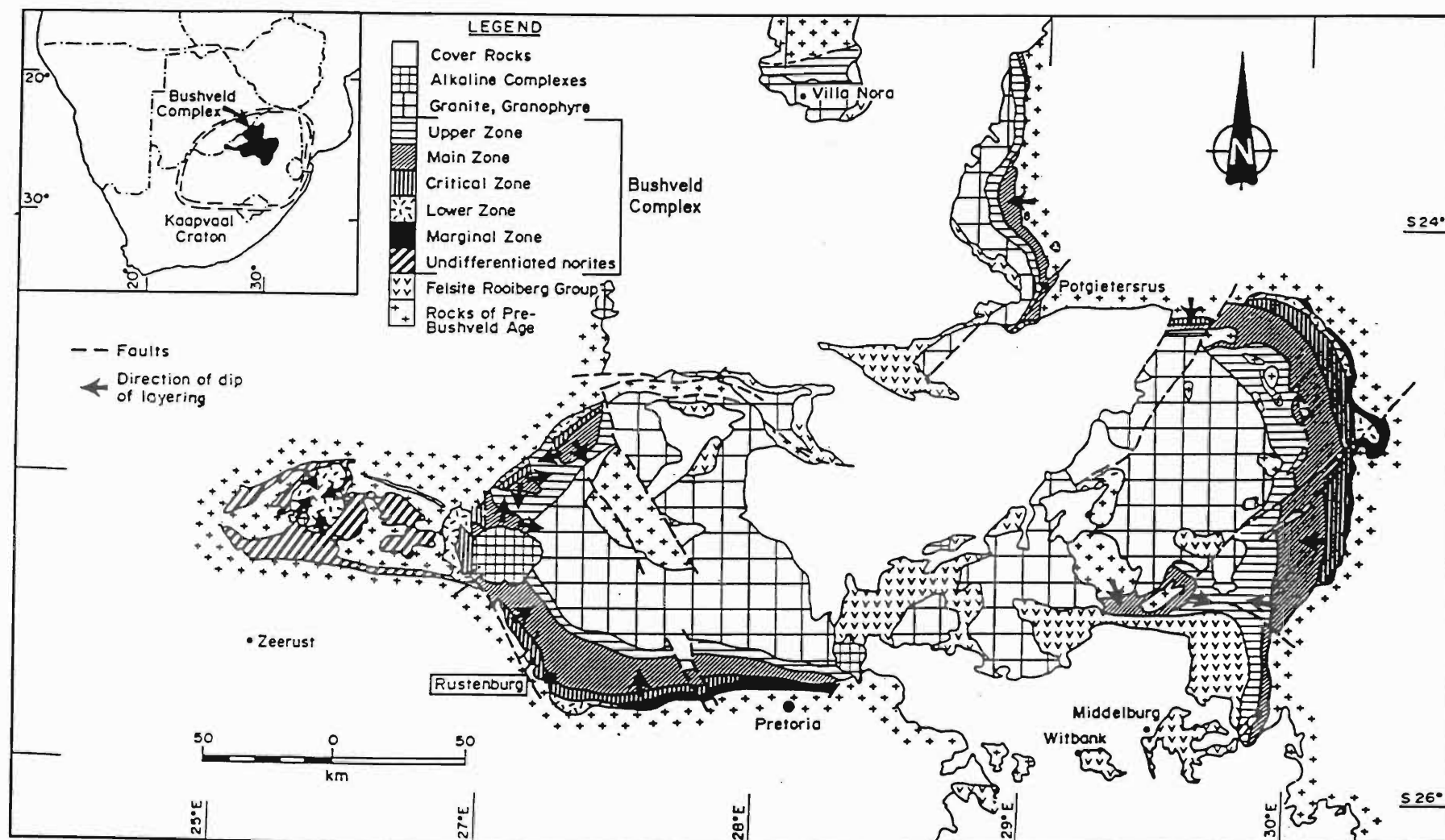
Figure 1.1   The Bushveld Complex

possibly five, intrusive centres coincident with the lobes (Tankard *et al*, 1982). Sharpe *et al* (1981) have suggested that the compartments were interconnected to a large master magma chamber at depth during the early stages of crystallisation of the Bushveld Complex. To this they attribute the similarities in crystallisation sequences between the eastern and western lobes.

1.2.2 <u>STRATIGRAPHY</u>

Numerous attempts have been made over the years, from Wagner (1929) to Kruger (1990, 1991), to stratigraphically subdivide the Bushveld Complex. To date there is still no firm consensus of opinion.

The stratigraphy of the Bushveld Complex has been formalised by the South African Committee for Stratigraphy (SACS, 1980), in which it is fundamentally divided into three suites; the Rustenburg Layered Suite, the Rashoop Granophyre Suite, and the Lebowa Granite Suite.

In 1980, SACS and later Walraven (1986), relegated the well established zonal nomenclature to informal status, having formally subdivided the complex into suites, subsuites and formations. This was an attempt to bring the Bushveld stratigraphy in line with the more traditional sedimentary-type stratigraphic nomenclature based on local place names (Tables 1.1 & 1.2). SACS (1980) attempted to correlate their stratigraphic division system with the `informal' zonal system by the introduction of subsuites. However, this system as a whole has not found much favour amongst geologists and has been all but totally ignored. To date (some 13 years later) it is very seldom referred to in the literature and has been strongly criticised by Irvine (1982) and Kruger (1990).

For the purpose of this work, the zonal nomenclature is retained, and more specifically, the hierarchy of zones, subzones, macrounits, units and layers as proposed by Kruger (1990) is considered appropriate. So too is his proposal to relocate the lower boundary of the Main Zone from the top of the Bastard Unit giant mottled anorthosite to the base of the Merensky Unit (*ie* the Merensky reef basal contact). Quite contrary to what is suggested by Mitchell & Scoon (1991), the base of the Merensky reef is one of the most frequently and most extensively exposed and mapped contacts within the entire Bushveld Complex (Kruger, 1991), and

The more important lithological units in the eastern part		The more important lithological units in the western part		Approx. thickness (m)	
Subdivision by SACS	Lithology	Subdivision by SACS	Lithology	E Bushveld	W Bushveld
Luipershoek Olivine Diorite	Diorite and olivine diorite / Uppermost magnetite layer / Olivine diorite	Bierkraal Magnetite Gabbro	Magnetite gabbro with layers of magnetitite and anorthosite	1 000	1 700
Ironstone Magnetite Gabbro	Magnetite gabbro with layers of magnetite anorthosite, and olivine gabbro / Olivine gabbro			750	
Magnet Heights Gabbro-Norite	Main magnetite layer			250	
Mapoch Gabbro-Norite	Mostly homogeneous gabbo and norite / Pyroxenite marker	Pyramid Gabbro-Norite	Gabbro and norite with interlayered anorthosite	800	2 700 to 4 400
Leolo Mountain Gabbro-Norite				1 500	
Winnaarshoek Norite-Anorthosite	Upper mottled anorthosite / Main mottled anorthosite			1 200	
Winterveld Norite-Anorthosite	Alternating layers of chromitite pyroxenite norite and anorthosite / Giant mottled anorthosite / Bastard reef / Merensky reef / UG : Chromitite layer	Mathlagame Norite-Anorthosite	Alternating layers of leuconorite, anorthosite, pyroxenite and chromitite	1 000	450
Mooihoek Pyroxenite	Pyroxenite interlayered with chromitite and dunite / Steelpoort chromitite layer / Lowermost chromitite layer	Ruighoek Pyroxenite	Feldspathic pyroxenite with chromitite layers	500	480
Serokolo Bronzitite	Pyroxenite	Tweelaagte Bronzitite	Pyroxenite	300	50
Jagdlust Harzburgite	Harzburgite interlayered with pyroxenite and dunite	Groenfontein Harzburgite	Alternating layers of harzburgite and pyroxenite	500	400
Rostock Bronzitite	Pyroxenite	Makgope Bronzitite	Monomineralic pyroxenite	400	140
Clapham Bronzitite	Norite / Feldspathic pyroxenite / Harzburgite layer near base	Eerlyk Bronzitite	Feldspathic pyroxenite with discontinuous harzburgite and norite layers near base	400	380
Shelter Norite	Norite, feldspathic pyroxenite, quartz norite, anorthosite norite	Kolobeng Norite	Norite and quartz norite	up to 100	up to 240

Table 1.1   Lithostratigraphic subdivision of the Bushveld Complex (after SACS, 1980)

Formal subdivision			Radiometric ages	Informal subdivision	
Lebowa Granite Suite	Makhutso Granite		1 670±30 Ma [x]U-Pb		
	Nebo Granite Verena Porphyritic Granite Klipkloof Granite Bobbejaankop Granite Lease Granite Balmoral Granite		1 920±40 Ma [x]U-Pb		
Rashoop Granophyre Suite	Stavoren Granophyre Rooikop Granophyre Porphyry Zwartbank Pseudogranophyre	Rooikop Granophyre Porphyry	2 090±40 Ma [xx]U-Fb		
Rustenburg Layered Suite	Eastern Bushveld	Western Bushveld	2 095±24 Ma [xxx]Rb-Sr		
	Luipershoek Olivine Diorite Ironstone Magnetite Gabbro Magnet Heights Gabbro-Norite	Bierkraal Magnetite Gabbro		Upper zone	Subzone C Subzone B Subzone A
	Mapoch Gabbro-Norite Leolo Mountain Gabbro-Norite Winnaarshoek Norite-Anorthosite	Pyramid Gabbro-Norite		Main zone	Subzone C Subzone B Subzone A
	Winterveld Norite-Anorthosite Moolhoek Pyroxenite	Mathlagame Norite-Anorthosite Ruighoek Pyroxenite		Critical zone	Upper subzone Lower subzone
	Serokolo Bronzitite Jagdlust Harzburgite Rostock Bronzitite Clapham Bronzitite	Tweelaagte Bronzitite Groenfontein Harzburgite Makgope Bronzitite Eerlyk Bronzitite		Lower zone	Upper bronzitite subzone Harzburgite subzone Lower bronzitite subzone Basal subzone
	Shelter Norite	Kolobeng Norite		Marginal zone	

BUSHVELD COMPLEX

[x]Coertze et al. (in press)

[xx]Faurie (1977)

[xxx]Hamilton (1977)

Table 1.2   Lithostratigraphic subdivision of the Bushveld Complex
(after SACS, 1980)

therefore may be appropriately used as a lithostratigraphic boundary. It is also a prominent and well documented erosional disconformity (Kruger, 1990) or regressive paraconformity (Irvine, 1982) (See Chapter 4). It is not within the scope of this work to embark in detail on the reasons why the base of the Main Zone should be placed at the base of the Merensky Unit, and for further information the reader is referred to Irvine (1982) and in particular, to Kruger (1990, 1991).

The term `Bushveld Magmatic Province', as described by Irvine (1982), is taken here to include the marginal sills, the layered mafic and ultramafic succession, the granophyres, felsites and granites (the Bushveld Complex of SACS, 1980). As proposed by Kruger (1990), it ought also to include other Bushveld-related mafic and ultramafic intrusions such as the Losberg and Molopo Farms complexes. As suggested by Irvine (1982), the Bushveld Complex should consist only of the layered mafic and ultramafic succession (the Rustenburg Layered Suite of SACS, 1980), which is in keeping with similar complexes such as Stillwater, Duluth, Skaergaard, Rhum, Munni Munni, Jimberlana and the Great Dyke. It should also be noted that abundant literature describing these complexes all apply the zonal terminology, eg Naldrett (1989), Naldrett et al (1990), Boudreau & McCallum (1992), Nicholson & Mathez (1991), Mogessie et al (1991), Hoatson & Keays (1989), Barnes & Naldrett (1985), Kruger & Marsh (1985), Wilson et al (1989), Naldrett & Wilson (1990), Wilson (1992), Keays & Campbell (1981), Campbell et al (1983) and McBirney & Noyes (1979), to quote a few.

The best exposure of the Bushveld Complex occurs in the mountainous eastern Bushveld, where the complete succession is exposed. Consequently, initial formalisation of the lithostratigraphy by SACS (1980) was based on this succession. The northern and western lobes are situated in relatively flat-lying country where exposure is generally poor due to extensive soil cover. Despite the limitations of exposure, comprehensive drilling and mapping has not only confirmed the many similarities with the eastern Bushveld succession but also highlighted a number of differences. Lithostratigraphic columns for the eastern and western Bushveld are shown in Figures 1.2 and 1.3 respectively.

Diorite
9000
Olivine diorite
Magnetite layer 21
Magnetite layer 20
19
Magnetite layers 8
17
4500
Anorthosite
LUIPERSHOEK
OLIVINE DIORITE
(subzone C)
Olivine diorite
8500
Mottled anorthosite
Magnetite layer 15
Anorthosite
Norite and gabbro
Olivine diorite
4000
Mottled and spotted anorthosite
Feldspathic pyroxenite
Fine-grained norite
Magnetite gabbro
8000
WINNAARSHOEK
NORITE-ANORTHOSITE
(subzone A)
Main mottled anorthosite layer
'Porphyritic' norite
Mottled anorthosite
Fine-grained norite
Magnetite layer 14
Mottled anorthosite
Magnetite layer 13
IRONSTONE
MAGNETITE GABBRO
(subzone B)
Magnetite layer 12
Olivine gabbro
Magnetite layer 11
Magnetite layers 9 and 10
Magnetite layer 8
Banded norite
3500
'Porphyritic' norite
Troctolite
Olivine gabbro
7500
Fine-grained norite
Feldspathic pyroxenite
Fine-grained norite
Mottled and spotted anorthosite
Mottled anorthosite
Bastard Reef
Merensky Reef
Norite
Magnetite gabbro
3000
Anorthosite
Norite
MAGNET HEIGHTS
GABBRONORITE
(subzone A)
Magnetite layer 7
Magnetite layer 6
Feldspathic pyroxenite
Anorthosite, Anorthositic norite
UG-2 Chromitite Layer
Magnetite layers 1 to 5
Main Magnetite Layer
Mottled anorthosite
Lower Magnetite layers 2 & 3
Lower Magnetite layer 1
Fine-grained norite
7000
WINTERVELD
NORITE-ANORTHOSITE
(upper subzone)
Pyroxenite
UG-1 Chromitite Layer
Norite
Anorthosite
Gabbro
Norite
Pyroxenite
Norite
2500
Gabbronorite
MAPOCH
GABBRONORITE
(subzone C)
Mottled anorthosite
6500
MG-Chromitite Layers
Anorthosite
Pyroxenite
Norite and gabbro
'Porphyritic' norite
ZWARTKOPPIES
PYROXENITE
(lower subzone)
Steelpoort Chromitite Layer
Dunite
2000
Feldspathic pyroxenite
Thornhill Pyroxenite Layer
Harzburgite
Feldspathic pyroxenite
Fine-grained norite
6000
SEROKOLO
BRONZITITE
(upper bronzitite subzone)
Bronzitite
1500
Harzburgite
Dunite
LEOLO MOUNTAIN
GABBRONORITE
(subzone B)
JAGDLUST
HARZBURGITE
(harzburgite subzone)
Harzburgite
Bronzitite
Harzburgite
Dunite
Homogeneous gabbronorite
1000
ROSTOCK
BRONZITITE
(lower bronzitite subzone)
Bronzitite
5000
500
Norite
CLAPHAM
BRONZITITE
(basal subzone)
Feldspathic bronzitite
4500
Norite
Harzburgite
0
marginal
zone
SHELTER NORITE
Norite

upper zone
main zone
critical zone
lower zone
main zone

Figure 1.2   Lithostratigraphic column for the eastern Bushveld Complex
(after von Gruenewaldt et al, 1985)

Figure 1.3   Lithostratigraphic column for the western Bushveld Complex
(after SACS, 1980)

1.3 GEOLOGY OF THE RUSTENBURG AREA

1.3.1 GENERAL

The town of Rustenburg is mostly situated on soil-covered Marginal, Lower and Critical zone stratigraphy of the western Bushveld Complex. The Lower Zone is better developed to the west and east of the town. The southern limit of Rustenburg extends onto the Magaliesberg quartzite of the Transvaal Sequence, a formation which has been preserved as a prominent mountain range, while to the north there is extensive Main Zone development (Figure 1.4). The Merensky reef occurs at the contact between the Critical and Main zones, and crops out (largely beneath soil cover) immediately north of Rustenburg and continues on a strike of north-west and east. The Merensky reef occurrence of the western Bushveld has a strike length of approximately 160km, which is currently mined by five companies, namely, Rustenburg Platinum Mines (Rustenburg, Amandelbult and Union Sections), Impala Platinum Mines, Western Platinum Mines, Eastern Platinum Mines, and Northam Platinum Mines.

This study was conducted at Rustenburg Platinum Mines Ltd - Rustenburg Section, which consists of two adjacent mines, East Mine and West Mine, situated to the east and north of Rustenburg respectively (Figures 1.4 and 1.5). The mining lease area extends from the farm Boschfontein 268JQ in the west, to Brakspruit 299JQ in the east, a distance of about 30km, with the centre of the property measuring some 7 km across. The Merensky reef crops out continuously beneath soil cover along the southern lease boundary and dips in a northerly direction at an average of 10°. Data for this study have been collected at Frank Shaft, which is situated roughly in the centre of the lease area and constitutes the most westerly workings of the East Mine (Figure 1.5).

1.3.2 REGIONAL GEOLOGY AND STRATIGRAPHY

The lithostratigraphic succession of the western Bushveld Complex is best developed in the Rustenburg district where it attains a maximum thickness of approximately 7000m. In this area the floor of the complex abuts against the Magaliesberg quartzites of the Transvaal Sequence which consists of irregular and dismembered masses of quartzite and hornfels enclosed within diabase and hybrid igneous rocks (Viljoen & Hieber, 1986). These floor rocks are overlain by

EXPLANATION

A   Pilanesberg and other alkaline complexes

Granite & Felsite
Granophyre

Upper zone
Main zone   Bushveld
Critical zone   Complex
Lower zone
Marginal zone

Magnetitite layers
Merensky Reef

Quartzite   Pretoria Group
Shale
Dolomite   Chuniespoort Group   TRANSVAAL
Quartzite   Black Reef Group   SEQUENCE
Fault
R P M Rustenburg Platinum Mines

Main Towns & Cities
Mining Lease Areas

KILOMETRES

Figure 1.4   The western Bushveld Complex, showing the locality of
              RPM Rustenburg Section
              (modified after Viljoen & Hieber, 1986)
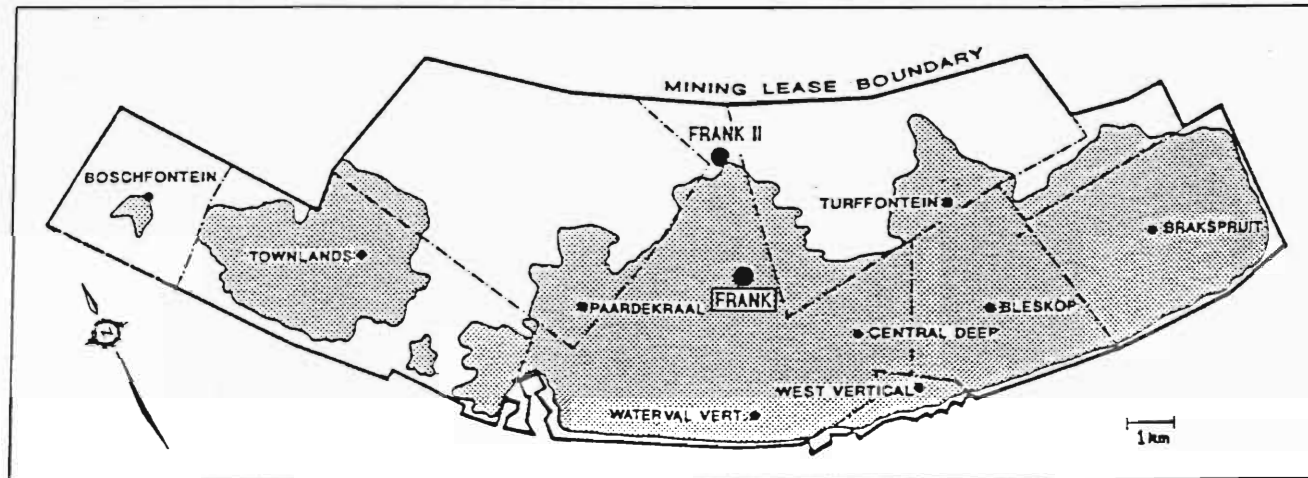
Figure 1.5   Rustenburg Platinum Mines Ltd - Rustenburg Section
lease area, showing the locality of Frank Shaft.
The shaded portion represents mined-out areas.
(E-W strike length = approx. 30km)

the Bushveld Complex. The basal lithology is undifferentiated norite of the Marginal Zone which reaches a maximum thickness of 240m. This is stratigraphically overlain by approximately 970m of alternating pyroxenite and harzburgite of the Lower Zone.

The Critical Zone consists of a ca. 830m thick succession consisting of a lower ± 480m thick pyroxenite subzone (the lower Critical Zone, or LCZ), and an upper ± 350m thick alternating norite and anorthosite subzone (the upper Critical Zone, or UCZ). The LCZ is host to the Lower Group 6 (LG6) chromitite layer which is widely exploited for its chromium content. The UCZ hosts the well known Upper Group 2 (UG2) chromitite layer. In all, the Critical Zone is host to 13 (14 where the LG6A occurs) well developed chromitite layers, numbered from the base upwards; these are the Lower Group (LG) 1 to 7, the Middle Group (MG) 1 to 4, and the Upper Group (UG) 1 and 2 (a UG3 layer is commonly only developed in the Eastern Bushveld). The contact between the LCZ and UCZ is placed at the MG2 horizon, at which point plagioclase becomes a cumulus phase within the rocks.

Overlying the Critical Zone is the approximately 3000m thick Main Zone, separated by a paraconformity (as defined by Irvine, 1982). The base of the Main Zone is marked by the base of the Merensky reef, which itself, forms the base of the ± 10m thick Merensky Unit. Overlying the Merensky Unit is the ca. 92m thick Bastard Unit. Together these two units form the basal transitional macrounit of the gabbronorite-dominated lower Main Zone (LMZ), a subzone characterised by magma mixing and influx (Kruger, 1990). The upper Main Zone (UMZ) consists mostly of homogeneous gabbronorite, which reflects almost continuous differentiation. The top of the Main Zone is marked by the base of the Pyroxenite marker (Kruger, 1990; Klemm et al, 1985; Sharpe, 1985).

The overlying Upper Zone is approximately 2000m thick and consists largely of the lower cumulate magnetite layers and overlying magnetite gabbro.

There are considerable local variations in the thickness of individual units and zones. In the extreme western part of the RPM Rustenburg Section lease area the lower units, particularly those of the Lower Zone, become substantially thinner, with the stratigraphic distance between the floor contact and the Merensky reef reduced to 280m. Over much of the remaining lease area this stratigraphic thickness is about 1700m.

A generalised lithostratigraphic column for the central portion of RPM Rustenburg Section lease area is shown in Figure 1.6. It shows the stratigraphy from the LG6 chromitite to the top of the Bastard Unit.

The UCZ consists of 5 major units, the base of each being defined by the chromitite and pyroxenite layers identified as the MG2, MG3, MG4, UG1 and UG2. The uppermost portion of the UG2 Unit consists of a dominantly norite package which is host to four prominent anorthosite layers (the Boulder Subunit). The close proximity of these layers to the Merensky reef and their lateral persistence renders them extremely useful markers from a mining point of view. This stratigraphic interval, extending from the base of the Boulder Bed marker to the base of the Merensky reef (the top of the UCZ), comprises the Boulder Subunit. The transitional macrounit of the LMZ consists of the overlying Merensky and Bastard units.

The Bushveld Complex is a major repository of several economic metals including the platinum-group elements (platinum (Pt), palladium (Pd), rhodium (Rh), osmium (Os), iridium (Ir) & ruthenium (Ru)), chromium (Cr) and vanadium (V), which are mined as primary products, and nickel (Ni), copper (Cu), cobalt (Co), gold (Au) and silver (Ag) as secondary by-products from the PGE and Cr mining operations. Economic chromium mineralisation occurs within the Lower Group (LG) chromitite layers of the lower Critical Zone, whereas the vanadium deposits occur within the titaniferous magnetite layers of the Main and Upper zones. The platinum-group element (PGE) deposits occur in a number of different lithologic settings:

a) Feldspathic orthopyroxenite and harzburgite (Merensky reef) of the lower Main Zone.

b) The Upper Group 2 (UG2) chromitite layer of the upper Critical Zone.

c) Basal feldspathic orthopyroxenite (Platreef) of the northern Bushveld.

d) Discordant dunite pipes of the eastern Bushveld.

All these occurrences have been mined at some stage or another, but present PGE mining operations are confined to the Merensky reef, UG2 chromitite reef and more recently, the basal Platreef of the northern Bushveld. Mining of the dunite pipes ceased in about 1930 (Naldrett, 1989).
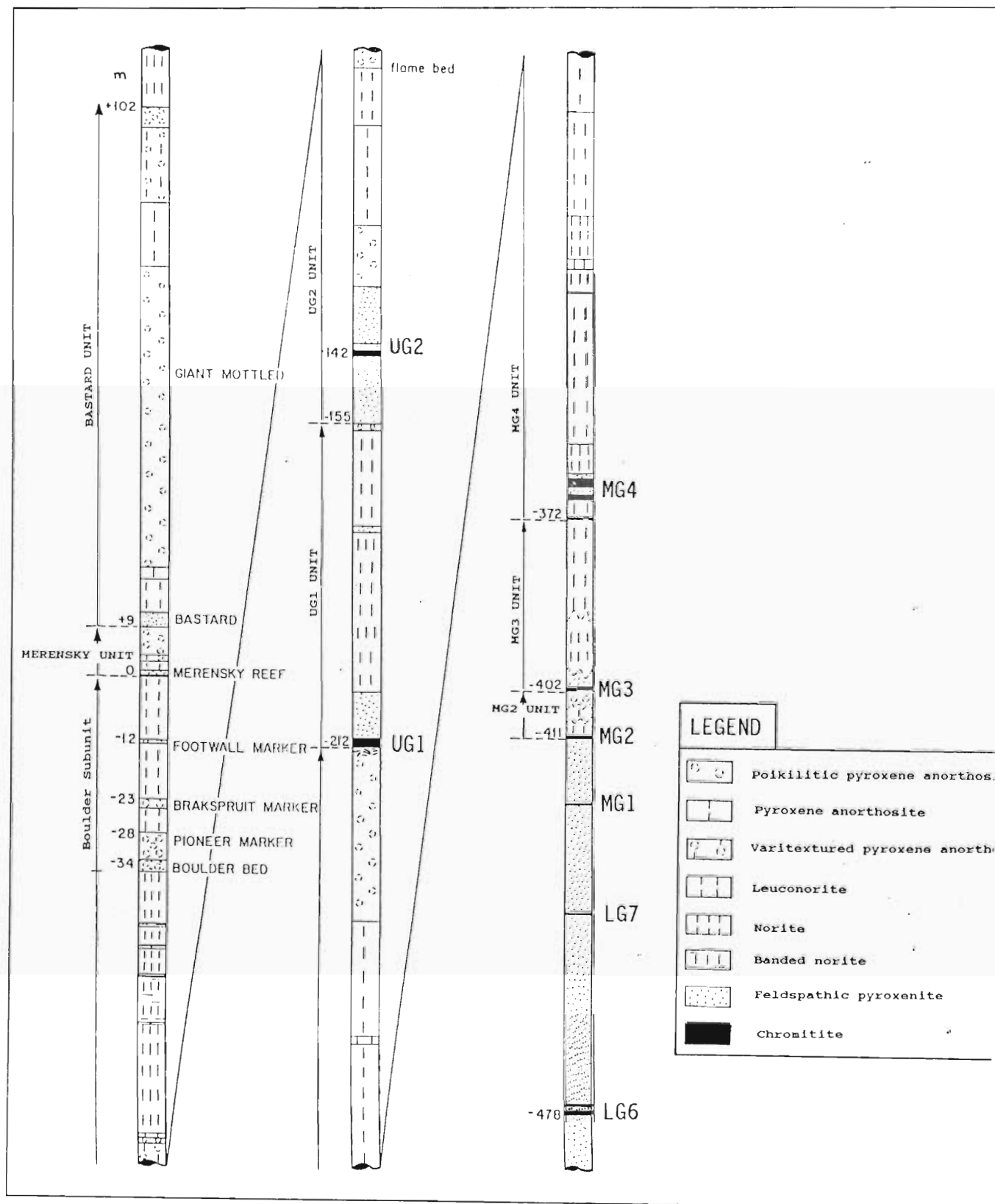
Figure 1.6   Generalised upper Critical and lower Main Zone
stratigraphy at RPM Rustenburg Section
(modified after Viljoen & Hieber, 1986)

This work is concerned with the stratiform PGE-enriched Merensky reef of the western Bushveld Complex. It has been the subject of much research and speculation over the years and as yet no complete consensus has been reached on its origin, petrogenesis and mineralisation controls.

1.3.3 <u>MINING HISTORY IN THE RUSTENBURG AREA</u>

The Merensky reef was discovered in the Rustenburg district by Dr Hans Merensky in June 1925, about 45km east of the present RPM Rustenburg Section (RPM-RS) lease area. Extensive soil cover made exploration difficult but nevertheless, shortly after, the Merensky reef was located by trenching in the present RPM-RS lease area. Potgietersrust Platinums Ltd commenced mining operations here at the end of 1929 under the administration of Johannesburg Consolidated Investment Company Limited, by this time an already powerful force in the platinum mining industry. JCI Ltd had already acquired Premier Rustenburg Platinum Company Ltd, Eerstegeluk Platinum Mines Ltd and Rustenburg Platinum Company in 1926. Rustenburg Platinum Mines Ltd was formed in 1931 by the amalgamation of the Rustenburg operations following a severe slump in the platinum market. Further deterioration then resulted in the closure of the mine. The market remained in a very fragile state until 1933 when a significant improvement saw the recommencement of operations, and later, their expansion. Since then the industry has grown despite numerous erratic market fluctuations, and today, shrouded in caution and secrecy, production is maintained at a consistently high level (Viljoen & Hieber, 1986).

REVIEW OF MERENSKY REEF EVOLUTION AND OBJECTIVES
OF PRESENT STUDY

2.1 MODELS FOR THE PETROGENESIS AND EVOLUTION OF MERENSKY TYPE OREBODIES

Many models and related contributions have been proposed to explain the petrogenesis of PGE-enriched sulphide orebodies in mafic and ultramafic layered intrusions. Very broadly, these models range from primary magmatic to hydrothermal. The primary magmatic/orthomagmatic models imply PGE concentration by magma unmixing, whereby an immiscible sulphide liquid unmixes from the magma, from which it then scavenges PGE before crystallising as a layer. Hydrothermal models, on the opposite side of the spectrum, propose that PGE transport and concentration occurred through the action of upward, downward or laterally migrating PGE and/or volatile-enriched fluids.

From a point of view of reviewing the historical evolution of models proposed for the evolution of the Merensky reef and similar orebodies, it is appropriate that a selection of some of the various contributions in this regard be chronologically summarised in the following section. In view of the subtle variations in many models pertaining to the origin of the Merensky reef and other magmatic PGE deposits, a chronologic list of the major contributions to the subject are summarised in some detail.

Stumpfl E.F. & Tarkian M.(1976) - believe that the evolution of the Merensky reef was the result of a complex polyphase process involving, *a)* magmatic crystallisation, *b)* alteration of silicates by late-magmatic solutions, *c)* partial redistribution of sulphides, and *d)* mobilisation and redeposition of platinum-group minerals (PGM). They find it difficult to advocate that the observed BMS and PGM intergrowths were the products of magma unmixing or exsolution, and rather support the theory of transport and redistribution by the later action of migrating chloride brines.

Vermaak C.F. & Hendriks L.P.(1976) - in a review rather than a petrogenetic study of the Merensky reef, this work supports a magmatic origin for the mineralisation. They go so far as

to say that 'the association of PGE with such elements as Bi, Te, Hg, Sn and Sb has led to erroneous speculations regarding a possible hydrothermal origin of the precious minerals in the reef or to postulations of possible additions of magma after the footwall rocks of the reef had crystallised.'

Naldrett A.J. & Cabri L.J.(1976) - suggest that the main criterion for the formation of a rich concentration of magmatic sulphides is that the host magma should be saturated in sulphur, and in addition contain a reasonably high proportion of immiscible sulphide droplets which can then then settle rapidly to form a continuous, thick sulphide blanket. They explain the genesis of PGE concentrations as occurring in four main steps: *1)* partial melting of the mantle, *2)* on rising into the crust, the silicate melt crystallises and the concentration of PGE in the residual melt changes through differentiation of the silicate melt, *3)* during crystallisation, droplets of liquid sulphide segregate from the melt and act as a collector of PGE before settling to form a layer, and *4)* redistribution of PGE by the action of hydrothermal solutions occurs after crystallisation.

Schwellnus J.S.I. et al (1976) - speculate that magmatic sulphide liquid acted as a PGE collector from the silicate magma, and on cooling, the PGM exsolved from the sulphides and were concentrated in the early differentiates during magmatic crystallisation. The Merensky reef chromitite layers crystallised before the sulphide and PGE mineralisation occurred and also acted as PGE collectors. The final remobilisation and concentration of BMS and associated PGE mineralisation was then induced by the action of subsolidus magmatic volatiles.

Hiemstra S.A.(1979) - explains the genesis of the Merensky reef (and UG2) as the result of magma unmixing, followed by the scavenging of PGE by various collectors (sulphide droplets, chromite grains and an iron alloy), which settled and accumulated under the influence of gravity. He suggests, because of the small amounts of sulphides and chromite, and the fact that they settled very slowly, that the main and most efficient collector of PGE was an iron alloy formed under exceptional conditions.

Keays R.R. & Campbell I.H.(1981) - in their study of the Jimberlana Intrusion, W Australia, suggest that the PGE content of sulphides is largely governed by the *R factor*, a measure of the amount of silicate liquid in equilibrium with the sulphide melt. They speculate that the sulphides of the Bushveld and Stillwater complexes were required to reach equilibrium with large volumes

of silicate liquid.   The Bushveld Complex received several pulses of magma, and during the early stages of crystallisation magma density decreased with fractionation.   Once plagioclase became a cumulus phase this trend reversed and eventually the resident magma became slightly more dense than the parent magma.   It was at this stage that the Merensky reef formed, where the parent magma rose as a turbulent plume, followed by rapid cooling and sulphur precipitation.   The rapid cooling of the upper magma cell caused an increase in its density, resulting in convective overturn which swept the PGE sulphide-rich cell to the bottom of the chamber.

Elliott W.C. et al (1982) - propose a link between redox equilibria and PGM petrogenesis, whereby a lowering of fO_2 and/or raising of fS_2 would trigger sulphide immiscibility and permit the stabilisation of a sulphide layer in a magma chamber.   They propose that the fS_2/fO_2 ratio of the magma was already very close to sulphide stabilisation, and that the final shift was induced by an injection of volatiles (H_2, CH_4 and /or H_2S).   The formation of a magmatic PGE enriched layer requires extraction of these elements from a large volume of magma, and the action of these volatiles would have secured this more efficiently than the action of a liquid.

Cameron E.N.(1982) - speculates that the genesis of the Merensky reef was not the product of progressive fractionation of the Bushveld magma, but rather a sudden and unique event, an event that altered the chemistry of the system and triggered the precipitation of sulphides.   The sudden event was probably an injection of new primitive magma enriched in sulphur, and/or on mixing with the residual magma it may have caused a change in fO_2 and fS_2.   Alternatively, a decrease in the solubility of sulphides may have been initiated by a change in total pressure.

Campbell I.H. et al (1983) - insist that if sulphides are to have a high PGE content they must have achieved equilibrium with a large column of silicate melt, *ie*, they must have attained a high *R factor*.   Temperature, rather than turbulent magma mixing, appears to have had the greater influence on sulphide precipitation.   A plume of primitive magma rising to an intermediate level in a density stratified chamber will lose heat rapidly to the overlying layer. Rapid cooling would result in the separation of an immiscible sulphide liquid, and gravitational instability as a consequence of the attendant density increase.   Turbulent convection would result, allowing for thorough mixing of sulphides and silicate melt and hence ensuring a high *R* value (≥ 100000).   Following convective overturn, the plume would eventually settle and spread out across the floor of the magma chamber, giving rise to the PGE reef.   The pegmatoidal

texture of the Merensky reef is believed to be the product of gravity settling of large crystals (*ie* true gravity cumulates which acted as traps for intercumulus volatiles and incompatible elements), while the adjacent finer grained rocks are believed to have formed by *in situ* crystallisation.

Irvine T.N. et al (1983) - argued that the Stillwater Complex is the product of two parent magmas, *viz* ultramafic and anorthositic, and that the J-M reef sulphides formed from immiscible sulphide liquid precipitated in response to mixing of the two parent magmas. The two magmas differed sufficiently in density to form separate layers which underwent double-diffusive convection, a process which controlled their mixing and crystallisation through both thermal and chemical exchange. The sulphide liquid is believed to have precipitated as part of a downdip cumulate accretion process, separating in response to temperature changes and mixing effects associated with the upward transfer of fractionated melt past particular diffusive interfaces along the crystallisation front. They postulate the same process for the Bushveld Complex and its Merensky reef. They speculate that the pegmatoidal texture of the Merensky reef is the product of postcumulus magmatic replacement (or metasomatism) of a peridotite layer during upward infiltration of intercumulus liquid related to compaction of the cumulate pile.

Lee C.A.(1983) - studied the trace and platinum-group element geochemistry of W Bushveld Merensky Unit exposures, in search of evidence pointing towards the development of the Merensky reef, and Merensky Unit as a whole. The following briefly summarises this contribution:

The Bushveld magma was close to, or at, sulphur saturation during its emplacement and crystallisation up to the Merensky reef event. Factors which may have resulted in increased S solubility are: raising any one of FeO content, S activity, pressure or temperature, or lowering fO_2 and αSiO_2. T-fS_2 relationships show that the ability of a PGE to form a PGE sulphide at a given temperature is dependent of the S activity. At low fS_2 PGE fractionation can occur.

The growth of the Bushveld Complex stratigraphic pile up to the level of the Merensky reef was dominated by magnesian orthopyroxene accumulation in the Lower Zone and lower Critical Zone, later joined and dominated by plagioclase. Both minerals are Fe-poor, so the Fe content of the residual lquid would increase. Any reduction in FeO or increase in SiO_2 would lead to S precipitation. Evidence points to internal control on the S mineralised sequences of the

Bushveld Complex in that:

a) Parallel but opposing chemical trends controlling S solubility as a consequence of normal fractionation of the initial magma.

b) Change in liquid structure and the decrease in its ability to carry sulphur.

c) Initial S saturation of the magma will influence the precipitation of sulphide.

The S and PGE accumulated in the residual liquid as incompatible elements through bottom growth and expulsion from the accumulating crystal pile, the S and PGE being accommodated in an increasingly Fe rich residual liquid. The mechanism for sulphide precipitation would in itself lead to a change in the liquid composition at the stage of the Merensky reef. A considerable volume of liquid would have been affected with immiscible sulphide liquating from the silicate liquid and settling under gravity, and also scavenging the overlying liquid of PGE.

Campbell I.H. & Barnes S.J.(1984) - suggest that the failure of previous models to adequately explain the very high concentrations of PGE in the Merensky reef, UG2 and J-M reef is attributed to the fact that they have used partition coefficients (D) which are too low, *eg* D_{Pt} = 1000 and D_{Pd} = 1500 (Naldrett, 1981), and their use was apparently successful only because the R value was less than D, making it difficult to distinguish between different D values. They propose that D_{Pt} and D_{Pd} be calculated from the Pt-Pd content of natural magmatic sulphides and the silicate liquids from which they are believed to have crystallised, *ie* from present day rock samples. As a result, D_{PGE} values of the order of 10^5 for immiscible sulphide - silicate liquid partitioning for all types of magmatic sulphide deposits, and a D value of $\geq 10^6$ for metal - silicate liquid partitioning are proposed.

Kruger F.J. & Marsh J.S.(1985) - propose that a new influx of slightly more siliceous magma mixed with the resident magma by turbulent convection. Some erosion and solution of the footwall occurred resulting in the disconformity at the base of the Merensky reef. The mixing led to the formation of dense immiscible sulphide droplets which scavenged PGE, Ni and Cu from the magma and were then deposited on the floor of the chamber. After mixing, a stable double diffusive convection system became operative as heat was lost from the top of the chamber. The basal convection layer (estimated to be 10 to 30m thick, despite mass balance considerations indicating that it ought to be much thicker) started bottom crystallisation of orthopyroxene and later, of plagioclase which sintered to form large, polygonal grains. Penecontemporaneous infiltration of fluid from the footwall modified the isotopic and chemical

character of the crystal pile by mixing with and displacing the preexisting interstitial fluid. The Merensky reef pegmatoid is believed to have formed as a result of trapping of final late-stage magmatic fluids expelled from the footwall rocks. This induced pegmatoidal growth of crystals by delaying the solidification process and redistributing the PGE, Ni and Cu sulphides.

Ballhaus C.G. & Stumpfl E.F.(1985) - proposed that late-magmatic volatile phases under conditions of low fO_2, dominated by compounds of the C-O-H-S + Cl system, played a major role in the modification of, and concentration of PGE in the Merensky reef. Evidence for late-magmatic volatile phases include the presence of chlorite-rimmed graphite, chlorine-rich hydrous silicates, magnetite, quartz and saussuritised plagioclase. The migration and action of chlorine-rich fluids are believed to be responsible for the precipitation of graphite, the pegmatoidal texture of the Merensky reef, and the transport and redistribution of PGE-enriched sulphides (via stratiform enrichment during magmatic differentiation).

Cawthorn R.G. & McCarthy T.S.(1985) - point out the usefulness of incompatible trace element geochemistry in determining the compositions of trapped liquid and estimations of magma addition. On a major scale there is an upward enrichment of P and Zr through the Critical Zone and including the Merensky reef, but is abruptly terminated by a drop in both element abundances in the Main Zone. This is consistent with a new magma injection above the Merensky reef, close to the floor of the magma chamber. The concentration of incompatible elements in the Merensky reef is consistent with the general fractionation trend of the underlying footwall rocks. The abrupt chemical change at the base of the Main Zone does not support a fluid infiltration metasomatic model for the genesis of the Merensky reef.

Naldrett A.J. et al (1986) - propose the following model: The sequence of cumulus phases and the compositional variation of the orthopyroxene within the pyroxenites and norites of the cyclic units is consistent with the lower parts of each of these units being the consequence of the fractional crystallisation of a given batch of magma. A fresh pulse of initial magma rose as a turbulent plume through the fractionated resident magma to its density level, and in the process entrained some resident magma. If both magmas were close to sulphur saturation, mixing would cause immiscible sulphide droplets to liquate and be swirled around in the magma (and in the process achieve a high R factor and high PGE tenor). As the new layer cooled, suspended crystals, sulphides and some entrained liquid sank to form a discrete orthocumulate layer which crystallised to form the Merensky reef. Small amounts of diffusion between the new

primitive magma and resident magma caused chromite to appear on the liquidus, which gave rise to the basal chromitite layer of the reef. The hybrid magma subsequently formed by mixing, underwent diffusion with the underlying Merensky reef, again causing chromite saturation and accounting for the upper chromitite layer. The pegmatoidal texture of the Merensky reef is accounted for by recrystallisation of the semi-solid layer by upward migration of volatiles and intercumulus liquid expelled by crystallisation of the footwall rocks. The authors believe that it was not possible for the PGE to be transported or concentrated by this process.

Boudreau A.E. et al (1986) - argue that PGE can be transported and concentrated by high-temperature subsolidus hydrothermal fluids. The pegmatoidal texture, and presence of anomalously large amounts of hydrous accessory minerals such as apatite, phlogopite and magmatic amphibole, indicate that fluids were at some stage an important factor in the petrogenesis of the Merensky reef. The authors found that the apatites, phlogopites and calcic amphiboles associated with the ore zones in both the Bushveld and Stillwater complexes are particularly Cl-rich. They argue that Cl-rich hydrothermal fluids exsolved during solidification of the cumulate sequence and acted as transporting agents for the PGE and REE. The high (Pt+Pd)/Ir ratios of these deposits is also believed to be consistent with a hydrothermal origin, as both Pt and Pd are more soluble in Cl-complexing fluids than Ir.

Hamlyn P.R. & Keays R.R.(1986) - propose a model for the genesis of Merensky-type orebodies by precipitation from S-deficient, PGE-rich, second stage magmas. First-stage basaltic magmas originating from undepleted or mildly depleted mantle sources are sulphur saturated at the time of segregation. During ascent, these magmas become depleted in PGE due to the coprecipitation of an immiscible sulphide phase. The large R-factor (the ratio of the mass of silicate liquid equilibrating with a given mass of sulphide liquid) would then promote strong fractionation of the PGE into the early sulphide phase. Emplacement and cooling of the magma will induce further sulphide fractional segregation. The resultant PGE tenor of these sulphides is too low to be consistent with the considerably higher values observed in Merensky reef type ores and certain mantle-derived peridotites residual from MORB magma genesis. To overcome this problem, the authors have proposed a second-stage magma model, where further melting of the depleted source causes complete dissolution of the residual PGE-rich sulphides. This melt separates from the mantle undersaturated in sulphur and enhanced in PGE. During early silicate fractionation, the PGE and other chalcophile elements will behave incompatibly and will concentrate until such time as the magma reaches sulphur saturation,

15

resulting in the observed PGE tenors.

Ballhaus C.G. & Stumpfl E.F.(1986) and Stumpfl E.F. & Ballhaus C.G.(1986) - in their studies of hydrous silicates and fluid inclusions within the Merensky reef, propose *in situ* sulphide unmixing during the intercumulus stage, followed by redistribution and concentration of the PGE by volatile-enriched, highly fractionated, intercumulus, Cl-rich fluid. *In situ* intercumulus sulphide unmixing is proposed to account for the interstitial textural status of the BMS and their close association with hydrous silicates, *eg* phlogopite. Prior to sulphide unmixing in a hydrous magma, S is likely to exist as H_2S. Subsequent S saturation then induces a reaction between H_2S and oxides of the silicate melt to produce sulphide melt plus H_2O. During the reaction the magma is enriched in water until a separate C-O-H-S-Cl rich fluid unmixes. The PGE are believed to have fractionated into the Cl-rich fluid rather than the sulphide melt, and subsequent upward migration and crystallisation concentrated the PGE and volatiles in the Merensky reef (as opposed to sulphides scavenging PGE from the hangingwall magma). During cooling of the fluid the PGE precipitated around the peripheries of the sulphide droplets.

Barnes S.J. & Campbell I.H.(1988) - argue that the abundant evidence for the action of late magmatic fluids, *eg* presence of: layered pegmatoids, intergrowths of BMS with hydrous minerals such as phlogopite, Cl-rich nature of phlogopite and apatite, fluid inclusions, graphite *etc* within the Merensky reef, do not refute or invalidate the magmatic hypothesis. They correctly point out that the presence of a pegmatoidal layer *eg* the Merensky reef of the western Bushveld Complex, and footwall to the UG2, does not infer any systematic association with PGE enrichment. They support the magmatic hypothesis and maintain that PGE-rich immiscible sulphide-oxide liquid unmixed as a cumulus phase at liquidus temperature, and that the secondary features supporting a hydrothermal model were superimposed at a late stage. Due to its much lower solidus, sulphides also crystallised during the final stages within trapped vapour-saturated intercumulus silicate melt, simultaneously with amphiboles, phlogopite, apatite *etc*. The pegmatoidal nature of the Merensky reef arises from interaction with late magmatic fluids and resultant recrystallisation. Local remobilisation of sulphides and PGE, deuteric alteration, precipitation of graphite *etc* resulted from lateral migration and cooling of the exsolved vapour phase.

Mathez E.A. et al (1989) - support the hydrothermal hypothesis, and in their study of carbon occurrence in the Bushveld and Stillwater complexes, propose a C-O-H-Cl rich fluid system. The first fluid to exsolve from the intercumulus melt was a mixture of CO_2, CO and HCl, with minor amounts of S and H_2O. Graphite began to precipitate from the fluid at supersolidus temperature and the system cooled down a T-fO_2 path parallel to and $\geq$ 2 log units below that of the Ni-NiO oxygen buffer. When graphite appeared the fluid evolved to a more hydrogen-rich composition (by graphite precipitation and loss of oxygen to the surrounding silicate-oxide assemblage). This resulted in a $\geq$ 70% reduction in fluid mass and as a consequence chlorine, sulphur and other residual species were concentrated in the intercumulus fluid and melt.

Hoatson D.M. & Keays R.R.(1989) - in their study of Merensky reef type mineralisation conducted on the Munni Munni Complex, propose the following models. Petrogenesis of this reef type is believed to have resulted from combined magmatic processes of crystal fractionation and magma mixing. Crystal fractionation was assumed from the observed increasing Cu/(Cu+Ni) ratios and incompatible element trends with stratigraphic height.

Model 1: A hot, buoyant, sulphide-saturated tholeiitic magma rose through the density stratified PGE-enriched, S-undersaturated resident ultramafic magma, and spreading out at its own density level. Crystallisation of plagioclase and subsequent Fe-enrichment of the melt resulted in increased magma density, leading to overturning and mixing with the PGE-enriched, fractionated portions. This mixing produced the main PGE ore layer.

Model 2: Involves the fractionation and internal mixing of one magma, where repeated injections of primitive magma mixed with the resident magma along the chamber floor. This formed a hybrid magma which displaced the remainder of the resident magma. Eventually the bottom layer on the chamber floor became S- saturated and formed the first PGE-poor sulphide unit (overlying layers still S-undersaturated). A new (and the last) batch of primitive magma then mixed with the S-saturated magma and S precipitation stopped (resident magma along the roof and upper walls of the chamber now became S-saturated). The system became gravitationally unstable leading to major overturn, mixing the upper S-saturated magma with the larger volume of fractionated, near S-saturated, PGE-rich magma in the remainder of the chamber, producing the main PGE ore layer.

In both models, magma mixing induced S-saturation in the hybrid magma and established a high R-factor. The chalcophile PGE were scavenged by immiscible sulphide droplets (due to their high sulphide/silicate partition coefficients) which were deposited to form the PGE ore layer. Evidence of hydrothermal activity was superimposed at a later stage and may have been responsible for local redistribution of sulphides.

Naldrett A.J. et al (1990) - describe a detailed unifying magmatic model (and its variations) to explain the different types of PGE deposits which occur in layered intrusions. Factors controlling the PGE content of a magmatic sulphide liquid include the PGE content of the silicate magma, the partition coefficients of the different PGE between coexisting sulphide liquid and silicate magma, and the silicate/sulphide ratio (R-factor) of the equilibrating liquids. The processes primarily responsible for the genesis of the PGE reefs are fractional crystallisation, magma mixing and constitutional zone refining.

The Merensky reef was formed as a consequence of inputs of fresh primitive magma which mixed with the resident magma, which by this stage was crystallising plagioclase. The sulphides segregated from their source magma in a batch that formed during turbulent plume magma mixing. The batch of sulphide liquid subsequently became well equilibrated with a large mass of this magma in a turbulently convecting layer. The sulphide liquid then settled from this layer, together with associated silicates and entrained magma to form the reef.

Amosse J. et al (1990) - Although not a comprehensive model explaining the petrogenesis of Merensky reef type deposits, this study demonstrates that PGE (in the form of complex ions in which the PGE is uncharged) can dissolve in, and precipitate out of, high temperature silicate melts in the absence of any associated fluid phase. The authors discriminate between the Ir-group PGE (Ir Ru Os) and the Pt-group PGE (Pt Pd Rh). An increase in fO_2 in equilibrium with the melt induces a considerable decrease in Ir solubility, which explains the early enrichment in the Ir-group PGE in ultramafic cumulates, while the Pt-group PGE remain in solution. An increase in fS_2 increases the solubility of this group further. At S-saturation BMS will precipitate (fS_2 buffered by BMS - Pt still highly soluble) along with the Pt-group PGE dissolved in them. This accounts for the abundance of Pt, Pd and Rh in nickel sulphide horizons of stratiform ultramafic deposits.

Lee C.A. & Butcher A.R.(1990) - based on the results of their Rb-Sr isotope study through the Merensky sequence at Atok Platinum Mine (E Bushveld), question the importance of a magma mixing event to Merensky reef mineralisation. Using continuous sampling, they found no significant isotopic variation from the gabbronorite/feldspathic pyroxenite footwall, through the Merensky reef, to its hangingwall norite. From the overlying leuconorites and anorthosites to the base of the Bastard Unit, a progressive increase in $^{87}Sr/^{86}Sr$ from 0,7064 ± 2 to 0,7074 ± 2 is noted. From just within the basal feldspathic pyroxenite of the Bastard Unit there is a major reversal in the initial $^{87}Sr/^{86}Sr$ profile, back to 0,7062 ± 2, the same as the gabbronorites, pyroxenites and norites of the underlying Merensky Unit. Whole rock geochemistry does not distinguish between the Merensky Unit pegmatoidal feldspathic pyroxenite and the Merensky and Bastard unit feldspathic pyroxenites. This suggests *in situ* isochemical recrystallisation may be responsible for the Merensky pegmatoid. There is no isotopic evidence of magma mixing in the PGE-enriched pyroxenites of either Atok-type or Rustenburg-type Merensky reef. Rather, the first evidence of magma mixing is seen in the plagioclase cumulates higher up in the unit. This is consistent with the model of Eales *et al* (1986), who suggest that the Merensky and Bastard pyroxenites are products of fresh mafic magma inputs into a previously fractionated magma column (producing norites and anorthosites). Hybridisation occurred through the mixing of the supernatant liquid with the lowermost portion of a major influx, emplaced hundreds of metres above the cumulate floor.

Alternatively, the authors suggest that the Merensky and Bastard pyroxenites may be the products of later sill intrusion, where the Merensky reef may represent the emplacement of a PGE + S-rich melt, derived from a magma chamber which became increasingly enriched in PGE as melt was removed to form the Critical Zone cumulates. This emplacement thus occurred as a unique event.

Wilson A.H. & Tredoux M.(1990) - The style of mineralisation in the P1 pyroxenite layer of the Great Dyke is not consistent with batch segregation of sulphide but rather indicates a process of progressive fractional precipitation. The occurrence of the mineralised layers towards the top of the ultramafic unit, rather than at the base, suggests that a major mixing event of residual magma with a new influx of primitive liquid was not the primary control on the mineralisation. Rather, the setting is more consistent with fractional segregation of sulphide, and repetition of the mineralisation is ascribed to periodic, relatively small pulses of new magma which overturned within the stratified chamber. The stratified character of the magma chamber was

sustained by new pulses entering as fountains. The maximum enrichment of PGE occurs at the first appearance of sulphide as a result of the high partitioning of these elements into sulphide liquid.

Naldrett A.J. & Wilson A.H.(1990) - in their work on the Great Dyke, propose a model for the origin of PGE mineralisation by fractional segregation of sulphide. A magma chamber consisting of a series of compositionally distinct layers is envisaged. Initially, crystallisation resulted in the lowermost of these layers becoming S-saturated, resulting in sulphides fractionally segregating and accumulating, along with bronzite, on the chamber floor. Segregation eventually ceased by which time the magma had become PGE depleted. Either a new pulse of PGE-enriched magma, or mixing with the overlying layer, initiated another mineralising cycle, a process which is believed to have repeated itself several times to account for the various pyroxenite-hosted sulphide zones. High bronzite Mg-number (Mg#) of orthopyroxene values preceed the onset of sulphide segregation, at which point, the Mg# decreases in value. This suggests that the replenishing magma was more primitive than the depleted magma. Bronzite crystallisation continued during replenishment and the net effect was an increasing Mg# up the pyroxenite cumulate asemblage. Once the input ceased the magma composition moved back to sulphide saturation point, where sulphide segregation and bronzite crystallisation occurred simultaneously (hence the decreased Mg#), until arrested by the next fresh magma input. The authors point out that the theory of a new pulse of light magma mixing with a dense resident magma with plagioclase on the liquidus (as proposed for the Merensky reef), cannot apply in the Great Dyke situation as its mineralisation is located within pure bronzitites.

Zientek M.L. et al (1990) - in their study of the incompatible element geochemistry of the Stillwater Complex J-M reef, argue that neither magma mixing nor fluid migration models readily explain why the minor quantities of sulphide minerals immediately adjacent to the sulphide-enriched reef have different element ratios from the sulphide minerals within the reef. They propose that the sulphides within the reef crystallised from a cumulus immiscible sulphide liquid which had become enriched in PGE during a magma mixing event, which then accumulated to form a layer. Evidence is strong that the J-M and Merensky reefs formed following an injection of new magma, and that the resulting cumulates show very little evidence of trapped liquid, with post-cumulus minerals compositionally looking like high-temperature cumulus minerals. Postcumulus processes efficiently remove all the incompatible and low-melting fractions,

leaving only a few percent trapped liquid. The latter is presented as evidence to suggest that the bulk of the sulphide mineralisation in the J-M (and presumably the Merensky reef) formed as a result of settling of an immiscible sulphide phase generated during magma mixing.

The sulphides which occur adjacent to the reef are believed to have formed as the last dregs of trapped intercumulus liquids reached S-saturation, a sulphide liquid unmixed and a sulphide was precipitated. The PGE tenor of these sulphides would be lower because they equilibrated with a much smaller volume of silicate liquid. Alternatively, it is proposed that some of the sulphides which formed as a result of magma mixing were trapped as inclusions in silicate minerals soon after they formed, reducing the amount of magma with which they could equilibrate, and therefore reducing their PGE tenor.

McCandless T.E. & Ruiz J.(1991) - studied Os isotope systematics in the UG1 and UG2 chromitites, and the Merensky reef, from both the eastern and western Bushveld Complex. ^{187}Re decays to ^{187}Os and because of the large Re/Os fractionation between crust and mantle, any crustal source should have a higher ^{187}Os/^{186}Os ratio than the mantle does. Neither hydrothermal or magmatic processes should fractionate Os isotopes. If minerals with very low Re/Os ratios are analysed, the ^{187}Os/^{186}Os ratio of the Os-bearing mineral should reflect the source value at the time of mineralisation. A mantle-source value of 0,9 (for 2 Gα) would be expected for large volumes of mafic and ultramafic magma. However, the authors have found ^{187}Os/^{186}Os ratios ranging from 1,28 and 1,60, significantly higher than those predicted for a mantle source. They have concluded that Os must have been added to the Bushveld Complex by assimilation of crustal material (adjacent country rocks), either by a tholeiitic A magma during emplacement, or by hydrothermal fluids. Evidence does suggest that some PGE were mantle derived, but the emphasis made here is that the mantle is not the only source for PGE and that crustal contamination and hydrothermal processes ought to be given serious consideration in this regard. In this respect the McCandless and Ruiz arguement is seriously flawed. ^{187}Os is completely decoupled from the other PGE. It is a very sensitive indicator of crustal contamination, but tells nothing about the provenance of the other PGE (or even non-radiogenic Os), which have completely different geochemical provenance.

Nicholson D.M. & Mathez E.A.(1991) - propose the following model for the petrogenesis of the Merensky reef based on the results of their work at Rustenburg Platinum Mines (Rustenburg Section). They envisage a protoreef consisting of partially molten pyroxenite underlain by a

partially molten norite containing a much higher proportion of intercumulus melt, and confined to the orthopyroxene-plagioclase cotectic. Volatiles were introduced to the melt-rich horizon via a series of high-angle fractures in the underlying rocks. Vapour concentrated in the melt horizon because of its inability to sustain fractures, and was therefore unable to propagate further upward in the sequence. This induced hydration and subsequent isothermal melting of the melt-rich protoreef. H_2O from the vapour was absorbed by the H_2O-undersaturated melt, leaving the residual vapour enriched in carbon. Hydration melting initially caused orthopyroxene resorption, followed by plagioclase melting as orthopyroxene diminished. Eventually the melt migrated to the chromite stability field with accompanying resorption of plagioclase. The stratigraphy downwards through the base of the reef, of pegmatoidal feldspathic pyroxenite - chromitite - anorthosite - norite, represents the sequence of stable mineral assemblages from high to low H_2O contents through the hydration/melting front. Experiments have shown that hydration melting of norite footwall and pyroxenite hangingwall produces a mixed melt that upon cooling, remains spinel saturated as it crystallises in the order olivine - orthopyroxene - plagioclase, and is now represented by the Merensky pegmatoid. The concentration of PGE was not dealt with in any detail by the authors but they ascribe it to either the accumulation of magmatic sulphides from the overlying magma into the protoreef, or the transport in and deposition of PGE by the vapour that initiated the hydration.

Schurmann L.W. & Von Gruenewaldt G.(1991) - speculate that the gradual cooling of the Lower Zone magma, accompanied by crystallisation of orthopyroxene, gradually increased the magmas S carrying capacity. Mixing with an influx of Critical Zone magma produced a hybrid from which the UG2 chromitite layer crystallised. Further cooling of the Lower Zone magma led to further S-saturation and unmixing of sulphide droplets which remained in suspension during the crystallisation of the UG2 to Merensky interval. An injection of Main Zone magma which then mixed with the Lower Zone/Critical Zone hybrid formed a further hybrid magma which caused some resorption of the footwall norite. This was followed by slumping due to cooling of the Lower Zone magma and the accumulation of orthopyroxene and sulphides at its base. Limited mixing of the Lower Zone magma with the Lower Zone/Main Zone hybrid resulted in the crystallisation of the Merensky reef basal chromitite layer. This was followed by settling of orthopyroxene and sulphides. This then caused the slumped Lower Zone magma to rise and mix with the Lower Zone/Main Zone hybrid, which produced the upper chromitite layer. Further cooling allowed the continued crystallisation and settling of orthopyroxene to form the Merensky pyroxenite, and later the crystallisation of cumulus plagioclase to form the

remainder of the unit. It is speculated that the pegmatoidal texture of the Merensky reef was the result of either postcumulus replacement, or recrystallisation between the chromitite layers in response to the presence of volatiles.

Boudreau A.E. & McCallum I.S.(1992) - based on their work on the Stillwater J-M reef propose a model for concentration of PGE by high-temperature, Cl-rich magmatic fluids. They propose that strata-bound orebodies, *eg* the J-M or Merensky reefs, may develop by a zone-refining or chromatographic process broadly analogous to a uranium roll-front. The Cl-rich fluids, which were exsolved from the footwall cumulate sequence, migrated upward and remobilised minor amounts of S and PGE present therein. This fluid then redissolved on encountering the higher and hotter intercumulus liquids which were not yet fluid saturated. This allowed the addition of sulphur and PGE to the silicate liquid and, due to their limited solubility in silicate liquid, induced sulphide precipitation. This 'front' continued to move upwards as the system cooled, followed by the fluid saturation front. Prior magma mixing which may have formed a stratigraphic discontinuity at which ore fluids were trapped, would have controlled the location of the reef.

The PGE-enriched reefs can form during the separation and migration of Cl-bearing fluids which mobilised the ore constituents originally held in sulphide precipitated as part of a cotectic cumulus assemblage. The high observed Pt and Pd concentrations (higher than can be accounted for by trapped liquid concentration alone), and the presence of sulphides as inclusions in cumulus oxides and silicates within the footwall cumulates appear to be consistent with the precipitation of sulphide as a PGE host as part of the cumulus assemblage. The low S concentrations in the footwall cumulates and the presence of PGE- and S-enriched pegmatoids beneath the J-M reef are consistent with a later loss of some PGE and S to a separating fluid. If a 0,1 to 0,5 wt % fluid were evolved during solidification of the footwall cumulate sequence (the amount of fluid exsolved by the crystallisation of 2 to 10% fluid-saturated intercumulus liquid) without completely resorbing the cumulus sulphide fraction, the fluid/silicate liquid distribution coefficients for Pt and Pd would need to be about as large as the sulphide liquid/silicate liquid coefficients in order to remove significant Pt and Pd. Much smaller fluid/liquid distribution coefficients are required if enough fluid is evolved to remove the cumulus sulphide completely. Isolation of some sulphide from the fluid, *eg* trapping in cumulus minerals, would require less fluid and allow some ore constituents to remain in the source cumulates.

As opposed to a magmatic model, which would require sulphide equilibration with up to 7 km of magma with 100% removal of PGE, the fluid concentration model suggests that the PGE are preconcentrated in footwall cumulates by the precipitation of cumulus sulphide. The Cl-rich assemblages in the footwall cumulates of the J-M reef may indicate the Cl-rich environment required for the efficient transport of PGE.

Coghill B.M. & Wilson A.H.(1993) - in their study of the upper P1 pyroxenite of the Great Dyke, found that the PGM are generally associated with base metal sulphides, and occur in three distinct textural environments: *1)* at the boundary of sulphides and silicates/hydrosilicates, *2)* entirely enclosed within sulphides, and *3)* entirely enclosed within silicate and hydrosilicate minerals. These phenomena are considered to have important genetic implications, and to explain these (and other) observations they propose a multi-process model, in which they envisage the genesis of the PGE mineralisation in terms of complexation and intermediate compound formation. Essentially this consists of primary orthomagmatic mineralisation followed by local remobilisation and crystallisation during a hydromagmatic stage. The term `*affinity factor*' is introduced to express the apparent distribution coefficient of an individual PGE between silicate and sulphide liquids.

Briefly, the model proposes very early-stage entrapment of high temperature PGM (laurite & cooperite) in cumulus silicates, and direct formation of sperrylite from PGE entrained in the magma. These phases comprise the relict high temperature orthomagmatic PGM. This was followed by direct partitioning of PGE into unmixed sulphide, and stabilised cluster formation with semi-metals (Te, Bi & As) entrapped by monosulphide solid solution. The subsequent dissociation and exsolution of PGM and semi-metals resulted in the formation of orthomagmatic solid solution PGM in sulphides. This was followed by the hydromagmatic / hydrothermal stage which was initiated by the exsolution of hydrous fluid from intercumulus silicate liquid. Interaction with the hydrous fluid resulted in: *1)* local redistribution of PGE, *2)* silicate inter-reactions and alteration, *3)* mobilisation of sulphides, and *4)* local redistribution of semi-metals. These processes collectively terminated in the low temperature crystallisation of hydromagmatic PGE arsenides and bismuthotellurides.

2.1.1 SYNOPSIS

It is clear from the above that a wide range of concepts exist on the petrogenesis of layered mafic and ultramafic PGE deposits, with models falling into categories of: *a)* Magmatic/magma mixing, *b)* Hydrothermal, *c)* Magmatic and hydrothermal, *d)* Hydrous fronts, *e)* Fractionation, and *f)* Crustal contamination.

While it is probably time that these models represent tangible processes, the difficulty comes in allocating their relative merits in each particular situation, and in this case, more specifically the Merensky reef. A common shortfall of many of the models is their intention to provide a universal mechanism for the occurrences of PGE. Due to its sheer uniqueness and number of fundamental contrasts with other PGE deposits (*eg* variation in grade with thickness), it seems clear that a simple universal model cannot be applied to the Merensky reef. A further exacerbating factor for the Merensky reef in particular is that there is currently no continuous, detailed and systematic geochemical data available in the literature, nor is there sufficient reference to and recognition of adequate field and observational data (*eg* the high degree of variability). It is these limitations which have stimulated a more detailed study of some of the basic and fundamental characteristics of the Merensky reef.

2.2 <u>AIMS AND OBJECTIVES OF THE PRESENT STUDY</u>

Various aspects of the Merensky reef, and similar orebodies of other layered intrusions, have been the subject of much research and speculation over the past few decades, as outlined above. Early research largely focused on descriptive geology and petrography. With the subsequent advent of increasingly sophisticated analytical instrumentation and techniques, research became more concentrated towards isotopic, geochemical and petrogenetic modelling aspects. More recently, attention has tended to focus on combining observational geology, *eg* macro- and microtexture, structure and mineralogy, with detailed geochemistry, aimed towards more sophisticated petrogenetic modelling.

The broad objectives of this study have been to document the nature and variability of normal undisturbed Merensky reef in more detail, to obtain basic and systematic geochemical data which is presently not available, and to assess the processes that were mainly responsible for the observed petrological and geochemical characteristics. The study is based on continuous borehole core sampling through four different Merensky reef successions. Such data will assist in modelling the origin of the PGE enrichment in the Merensky reef, in the evaluation of models

published from time to time, and may be used to place constraints on the primary controls on the PGE mineralisation and the compositions of the silicates. Merensky reef abnormalities and complications such as potholes, koppies, metasomatic replacement, alteration and structural disturbance have been specifically excluded in this study.

2.3 METHODOLOGY

2.3.1 GENERAL

Considering the variability of the Merensky reef and the fact that this criterion ought to be taken into account in a study of this nature, RPM Frank Shaft was considered to be an ideal study location. Frank Shaft is situated roughly in the centre of RPM Rustenburg Section 30km strike lease area (see Fig. 1.5), and exposes the transition from predominantly thin, high grade Merensky reef in RPM-RS East Mine, to predominantly thick, lower grade Merensky reef in RPM-RS West Mine. The Frank Shaft west longwalls are host to the thicker reef facies, and the east longwalls host to the thinner facies.

2.3.2 SAMPLING

Sampling was carried out by underground diamond drilling upwards from development crosscuts up into the Merensky reef succession ahead of the longwall mining faces. The idea was to obtain a reasonably representative spread of Merensky reef facies types across the shaft. However this was not entirely successful due to logistic problems associated with mining activity, drillsite accessibility and some deviation in the nature of the Merensky reef from what was observed in the approaching longwall. Five sites were selected on the following criteria:

a) The then current reef facies being mined in the respective longwalls.

b) It was essential that the reef intersections be normal, *ie* drilling sites were located as remotely as possible from known disturbances such as potholes, koppies, faults, dykes, replacement pegmatite bodies, altered and densely jointed areas.

The drilled stratigraphic section in each case extended from within the norite immediately below the Footwall marker, through to the Bastard pyroxenite, *ie* approximately 15m of stratigraphy above and below the Merensky reef. Three AXT size (core diameter = 32,51mm) holes were drilled within centimetres of one another at each site, one intersection for geochemical analysis, one for thin sections and one spare.

Drilling was carried out at the following sites (Figure 2.1):

a) Boreholes R23B, R23C & R23D in F30-19 interlevel crosscut north at survey peg F26035 - 24,8m, drilled ahead of A Longwall West (not shown in Figure 2.1).

b) Boreholes R24A, R24B & R24C in F3E-23 interlevel crosscut north at peg F23374 + 28,4m, drilled ahead of C Longwall East.

c) Boreholes R25A, R25B & R25C in F2-25 level crosscut north at peg F26998 + 2,3m, drilled ahead of D Longwall East.

d) Boreholes R26A, R26B & R26C in F3E-22 interlevel crosscut north at peg F26908 + 14m, drilled ahead of C Longwall East.

e) Boreholes R27A, R27B & R27C in F24-21 level crosscut north at peg F26043 + 23,8m, drilled ahead of B Longwall West.

Subsequent advance of the longwalls through the drilling positions allowed for detailed investigation and documentation of the *in situ* exposures, prior to any geochemical study.

Details of borehole core continuous sampling for geochemical analyses are as follows:

a) *Borehole R24A:* Hangingwall: 12 samples (total 1,25m)
Merensky reef: 7 samples (total 0,33m)
Footwall: 13 samples (total 1,24m)
Total R24A samples = 32
Sampled section = 2,82m

Figure 2.1 Underground plan of Frank Shaft showing the localities of the boreholes drilled for this work (R24 to R27).
(A to E = A to E longwalls east & west)

SCALE 1 : 13850
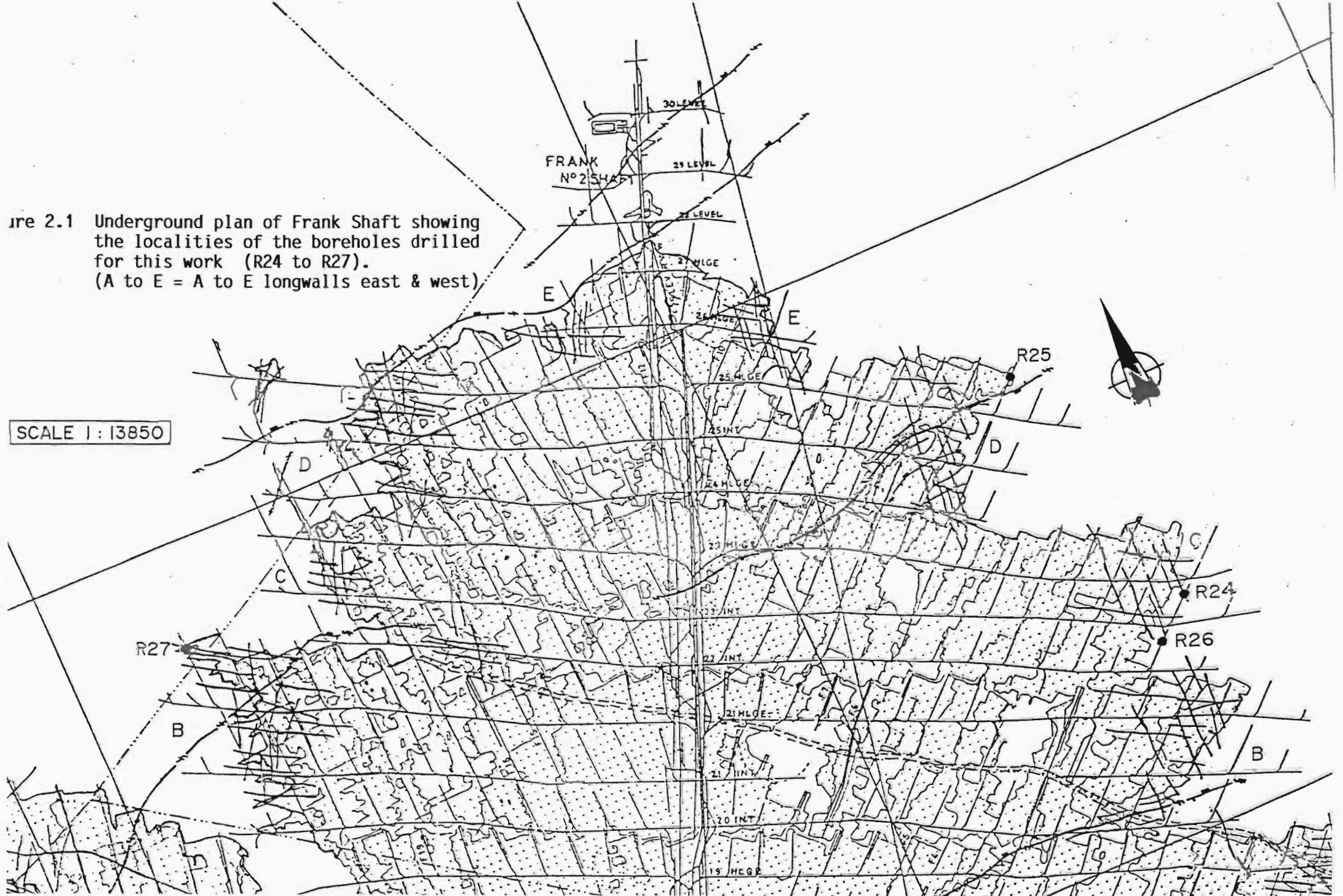
b) *Borehole R25A:* Hangingwall: 12 samples (total 1,49m)

Merensky reef: 5 samples (total 0,28m)

Footwall: 13 samples (total 1,595m)

Total R25A samples = 30

Sampled section = 3,365m

c) *Borehole R26A:* Hangingwall: 15 samples (total 2,45m)

Merensky reef: 3 samples (total 0,15m)

Footwall: 17 samples (total 2,53m)

Total R26A samples = 35

Sampled section = 5,13m

d) *Borehole R27A:* Hangingwall: 15 samples (total 2,55m)

Merensky reef: 21 samples (total 1,92m)

Footwall: 16 samples (total 2,60m)

Total R27A samples = 52

Sampled section = 7,07m

NB A complete detailed listing of borehole sampling is presented in Appendix I.

For ease of plotting geochemical data against the stratigraphic sections (see Chapter 6) all samples have been given equal interval status in the vertical section. This has the desirable effect of artificially expanding the Merensky reef interval to a small extent relative to its hangingwall and footwall, as sample widths within the Merensky reef are smaller and become progressively wider away from the reef (see Appendix I). This apparent distortion does not unrealistically alter the observed geochemical patterns, or interpretations, in any way and aids continuity of the profiles.

Boreholes R24B, R25B, R26B and R27B were correspondingly sampled for thin section preparation. Boreholes R23B and R23C were retained for comparative purposes and were not sampled.

2.3.3 <u>GEOCHEMICAL ANALYSES</u>

The sample section from borehole R27A was analysed for whole-rock major and trace element composition by X-Ray Fluorescence spectrometry (XRF) at the University of Natal, Pietermaritzburg (see Appendix I for details). Correction programs were written by A.H. Wilson. Samples were analysed for the following elements:

Major elements: SiO_2, Al_2O_3, Fe_2O_3, MnO, MgO, CaO, Na_2O, K_2O, TiO_2, P_2O_5, Cr_2O_3 and NiO.

Trace elements: Nb, Y, Rb, Zr, Sr, Pb, Ga, Co, As, Zn, Cu, Ni, Ba, Sc, V, La and S.

Sample sections from boreholes R24A, R25A and R26A were analysed only for the following trace elements: Zr, Sr, Nb, Y, Rb, Zn, Cu, Ni, Ba, S and P.

The R27A whole-rock samples were also analysed for the platinum- group elements (PGE); Pt, Pd, Rh, Ir, Os and Ru, and Au, by Neutron Activation Analysis (NAA) at University College, London. The R27A thick Merensky reef section was selected to obtain greater resolution and detail through the reef, which would show more clearly the PGE + Au distribution, variation and behaviour. A portion of the R25A section was analysed locally by the fire assay method for Pt, Pd, Rh, Ir, Ru and Au, by JCI Minerals Process Research Laboratories (MPRL).

The R27A section was further analysed for orthopyroxene and plagioclase mineral separate major element content by XRF. The samples were analysed for the following major elements: SiO_2, Al_2O_3, Fe_2O_3, FeO, MnO, MgO, CaO, Na_2O, K_2O, TiO_2, P_2O_5, Cr_2O_3 and NiO.

The mineral separate method (developed by A.H. Wilson) was used in preference to electron microprobe for determination of orthopyroxene and plagioclase compositions because of the heterogeneous compositions of these minerals, due to the effects of minor zoning, subsolidus exsolution and alteration. These effects are overcome by bulk sampling as individual crystals differ in these respects. A relatively large quantity of crystals (as opposed to a select few in microprobe analysis) is likely to yield reliable average compositions.

Clinopyroxene occurs in low abundance ($\leq 5\%$) in the rocks studied, and has not been collected or analysed as a separate mineral in this study.

(See Appendix I for details on sampling, methods and analytical/processing equipment).

CHAPTER 3

TERMINOLOGY

3.1 PYROXENES

The pyroxene classification and nomenclature used in this work is that recommended by the IUGS Subcommittee on Pyroxenes (Morimoto, 1988).

The 50% rule is applied to complete solid solution series between two end members. These are the Mg-Fe pyroxenes (enstatite-ferrosilite and clinoenstatite-clinoferrosilite series) and Ca pyroxenes (diopside-hedenbergite series). Subdivision names of the intermediate solid solution ranges, such as bronzite, hypersthene and eulite of the enstatite-ferrosilite series, and salite and ferrosalite of the diopside-hedenbergite series, have been discarded. However the 50% rule is not applied rigorously to the Ca-Mg-Fe pyroxenes and the Na-Ca pyroxenes. The widely accepted terms such as augite and pigeonite have been retained (Morimoto, 1988, p240-241). The intermediate and well known solid solution component, bronzite, constitutes the greater proportion of pyroxenes in this study. However, as suggested above, this term is not used, and rather the equivalent composition, according to the 50% rule, between En_{80} and En_{90} is adopted. This is consistent with commonly used plagioclase terminology, where composition is expressed as % anorthite (An) in the anorthite-albite solid solution series.

3.2 ROCK TYPES

The classification and nomenclature of the mafic and ultramafic plutonic rocks referred to in this study is broadly consistent with the recommendations laid down by the IUGS Subcommission on the Systematics of Igneous Rocks (Streckeisen, 1976; Le Bas & Streckeisen, 1991; Middlemost, 1991). However, it is not always possible, or practical, especially from mining and communication points of view, to classify Bushveld rocks on modal proportions alone. Textural considerations must also be taken into account, in particular, the recognition of cumulus, intercumulus, postcumulus and heteradcumulus phases. The rock naming system which has

evolved for the Bushveld rocks is somewhat inconsistent and haphazard. Rocks have been named on both modal mineralogy, *eg* norite and leuconorite, and on texture, *eg* spotted anorthosite and mottled anorthosite. The terms *spotted anorthosite* and *mottled anorthosite* constitute colloquialisms and do not adequately reflect either the mineralogy or texture of the rocks, and have therefore been discarded in this work (see below).

The following definitions are considered appropriate for this work:

Anorthosite - a plagioclase cumulate, containing very little, or no macroscopically visible pyroxene.

Poikilitic pyroxene anorthosite (previously 'mottled' or poikilitic anorthosite) - a plagioclase cumulate containing abundant, large (several cm across), irregularly shaped heteradcumulus pyroxene oikocrysts. The oikocrysts give the rock its characteristic 'mottled' appearance. On a macro-scale, the pyroxene content of this rock type commonly exceeds the recommended maximum modal 10% for anorthosite (Streckeisen, 1976), but it is suggested here that the insertion of the word *pyroxene* in the name would allow for this variant.

Pyroxene anorthosite (previously 'spotted' anorthosite) - a plagioclase-orthopyroxene (+ minor clinopyroxene) cumulate, where aggregates of cumulus pyroxene crystals are tightly concentrated into 'spots' of ≤ 1cm across, distributed within a matrix of cumulus plagioclase. The pyroxene content of this rock is commonly ≥ 10%, and less frequently ≤ 10%. It is recommended here that the prefix *spotted* be abandoned in favour of the prefix *pyroxene*, thereby retaining the status of the rock as an anorthosite, and also allowing for a pyroxene content which may be in excess of the IUGS recommended 10%.

Varietextured pyroxene anorthosite - (previously 'spotted' and 'mottled' anorthosite) - a rock with the characteristics of both the two rock types.

Norite - a plagioclase-orthopyroxene (+ minor clinopyroxene) cumulate, where the plagioclase content is between 35 and 65% The pyroxene occurs as discrete cumulus crystals dispersed within a matrix of cumulus plagioclase throughout the rock. However, norite is texturally diverse at RPM-RS, where a variety commonly referred to here as 'corona norite' typically occurs in the Boulder Subunit. Dispersed throughout the normally textured norite, to variable extent, are small pyroxene crystal aggregates completely surrounded by rims of pure white

plagioclase (coronas). The rims are generally of approximately equal thickness to the diameters of the aggregates (≤ 1cm).

Leuconorite - a variety of norite where the plagioclase content lies between 65 and 90%. The corona variety is also common.

Melanorite - a variety of norite where the plagioclase content lies between 10 and 35%. The corona variety is not commonly observed.

Feldspathic orthopyroxenite - an orthopyroxene (+ minor clinopyroxene) cumulate, containing texturally interstitial, or intercumulus, plagioclase. The plagioclase content varies from about 5 to 20%, and in a recent study (Nicholson & Mathez, 1991), was measured at 17%. Although the latter falls within the modal range of melanorite, the rock is texturally distinct as a feldspathic (*ie* plagioclase-bearing) pyroxenite. It commonly contains scattered, elongate clinopyroxene oikocrysts which enclose cumulus orthopyroxene (and also some BMS, but not plagioclase), and which vary in length from 1 to 7cm. When oikocrysts are present the rock is referred to as a *poikilitic feldspathic pyroxenite*. The most common Merensky reef lithology is the coarsely crystalline variety of this rock type, known as *pegmatoidal feldspathic pyroxenite*. Its textural habit is granular orthopyroxene with interstitial plagioclase. Crystal size, however, is very variable (0,5 to 6cm) but is most commonly between 1 and 2cm. The plagioclase content is typically higher (and more variable) than its medium-grained equivalent, at between 10 and 35%.

Pegmatoidal feldspathic harzburgite - a rock similar in all respects to pegmatoidal feldspathic pyroxenite, except for the olivine content of between 35 and 60%. The olivine typically exists as rounded, relict crystals (≤ 1cm) surrounded by peritectic rims of orthopyroxene.

Merensky reef - this term, as used in this thesis, refers specifically to the PGE-enriched pegmatoidal feldspathic pyroxenite layer and its associated chromitite layers. The term *reef*, more specifically, refers only to the fact that the layer is of current economic value. It is a strictly informal geological term which, when used in isolation, has no specific petrological or stratigraphic connotation, and is therefore uncapitalised. The terms *Bastard Reef* and *Bastard reef* still commonly appear in the literature, and in both instances are incorrect. The basal feldspathic pyroxenite layer of the Bastard Unit has no economic value and thus should simply

be referred to as the *Bastard pyroxenite.*

3.3 CUMULATE TERMINOLOGY OF LAYERED INTRUSIONS

The igneous terminology used in this work essentially conforms with that defined by Irvine (1982), with some expansion of layered intrusion subdivision terms as defined by Kruger (1990). Some terms have been redefined or modified by Wilson (1992, p614-617) for application to the Great Dyke, but are also considered appropriate for this work. These are:

Parent liquid - that liquid which constitutes the main body of magma giving rise to the cumulates in question. The composition of the parent liquid does not vary on a small scale but will continuously change in response to bulk crystallisation.

Cumulus crystals - granular crystals which constitute the framework of the rock and which may be euhedral, subhedral or anhedral. Cumulus crystals are readily identified texturally but no inferences can be drawn regarding their origin.

Intercumulus liquid - the liquid occupying the interstices of the cumulus crystals either as an open system connected to the overlying body of magma, or as a closed system within the network of cumulus crystals. In the latter situation the intercumulus liquid is called the trapped liquid.

Adcumulus component - that part (usually early) of the cumulus crystal which grew in equilibrium with the parent liquid. In some cases the entire cumulus crystal network may have formed by adcumulus growth; in other cases, the adcumulus component of the crystals may be obscured by overgrowth of lower temperature compositions or by reaction with the more evolved trapped liquid.

Orthocumulus component - that part of the cumulus crystal as well as additional late-stage phases which grew from the trapped liquid between the cumulus grains in a closed system or evolved infiltrating liquid. Orthocumulus overgrowth may take place on crystals which initially formed by adcumulus growth.

33

Porosity - This is the proportion of melt in a solid-melt association and is essentially related to the entrapment of liquid. In the early stages of nucleation and crystal growth the porosity will be very high (approaching 1). Where the liquid is not trapped but is part of an open system linked to the overlying body of parent magma the porosity would be called the initial porosity. As a consequence of continued crystal growth the initial porosity will be reduced. When the system becomes closed the porosity is called the residual porosity and the liquid contained in the pore spaces is the trapped liquid. In perfect adcumulates the residual porosity is zero. In the final rock the proportion of trapped liquid would be represented by postcumulus overgrowth on the original cumulus crystals as well as additional later phases. The residual porosity cannot be determined by direct observation.

Oikocryst - one or more mineral phases which are texturally interstitial to the discrete cumulus phases and therefore assumed to have grown later, but which developed in an open system with the parent magma, and therefore effectively would constitute an adcumulate phase. It is also possible that they grew at the same time as the cumulus phases but at a slower rate. Oikocryst minerals do not occur as an evenly distributed mesostasis on a small scale, but as discrete single phases, sometimes with well developed crystal form. These may contain a smaller proportion of cumulus crystals than outside the enclosing oikocryst. Where these phases grew in equilibrium with the parent magma they may be regarded as having adcumulus status. In such cases, all the intercumulus liquid would have been excluded by the growing network of cumulus crystals and oikocrysts, and the oikocrysts may be regarded as heteradcumulus phases as defined by Wager & Brown (1968). In practice, the liquid from which the oikocrysts grew must be slightly more evolved than the parent magma but this may be a steady-state situation dominated by replenishment of parent magma in the open crystal-liquid system. In this case, a component of the oikocryst may be regarded as being heteradcumulus. The initial shape and compositions of the oikocrysts may be obscured by orthocumulus overgrowth of lower temperature compositions of the same phase during solidification of the trapped liquid.

Discrete postcumulus phases - this is a textural term and refers to those mineral phases which surround and sometimes enclose the cumulus phases. They include both the late-stage phases which grew from the trapped liquid as well as heteradcumulus (oikocryst) mineral phases. The proportion of discrete postcumulus phases may be determined by direct observation.

Postcumulus material - this would include the discrete postcumulus phases as defined above, as well as the orthocumulus overgrowth on the original cumulus crystals. This term has genetic connotations cannot be quantified without an estimate of the overgrowth.

The above terminology deviates from previous classifications in that it is not the amount of discrete postcumulus phases that defines the type of cumulate, as suggested by Irvine (1982), but rather the relative contributions of the end-member types, *ie* the orthocumulus and adcumulus components, the latter including the heteradcumulus component of the oikocryst phases. The terminology does not imply crystal settling but relates to processes rather than observational characteristics, which is consistent with the genetic aims of cumulus terminology.' (Wilson, 1992)

CHAPTER 4

THE VARIABILITY OF THE MERENSKY REEF AND THE INTER-RELATIONSHIP WITH THE ADJACENT STRATIGRAPHY

4.1 INTRODUCTION

Over the years, mining at Frank Shaft has exposed noticeable stratigraphic variation within the Boulder Subunit footwall succession to the Merensky reef. The lithostratigraphic sequence itself remains unchanged, the variation rather being one of thickness of individual layers within the succession. In this sense, the Boulder Subunit and its relationship with the similarly variable Merensky reef has been investigated in some detail.

Normal Merensky reef is highly variable in nature, the primary and most obvious variation being reef thickness. Closely associated with this are numerous other variations which are largely characteristic of the particular reef variety. These include physical variation such as texture, fabric, presence of chromitite layers, proportions of base metal sulphide (BMS) mineralisation and presence of footwall anorthosite. Uncertainty exists as to the origin and relationship of the immediate footwall anorthosite layer, and therefore this rock type has also been studied. Variation in layer thickness of the Boulder Subunit footwall is independent of Merensky reef variation. However, variation of the immediate footwall anorthosite layer appears to be highly dependent on Merensky reef variation.

4.2 LOCAL STRATIGRAPHY

4.2.1 THE BOULDER SUBUNIT

The Boulder Subunit constitutes the uppermost portion of the UG2 Unit and also the upper Critical Zone. At Frank Shaft it consists of an approximately 34m thick package consisting of norite with subordinate anorthosite interlayers. A stratigraphic section showing the Boulder Subunit and its variability is shown in Figure 4.1 (see Figure 4.2 for lithological legend).

The base of the Boulder Subunit is defined by the Boulder Bed marker. This is a 1,6m thick layer of poikilitic pyroxene anorthosite or pyroxene anorthosite, which hosts abundant oblate spheroidal feldspathic orthopyroxenite boulders (long axis ± 15cm), mostly of pegmatoidal texture. A thin discontinuous chromitite layer (a few mm thick) commonly occurs at or near the basal contact, and rarely, a thin pegmatoidal feldspathic pyroxenite layer (± 10cm thick) which overlies it. The Boulder Bed is overlain by a 2m thick layer of very coarse poikilitic pyroxene anorthosite.

The remainder of the subunit is composed of norite packages of variable thickness which separate the remaining markers (Figure 4.1). Pyroxene anorthosite layers however often occur between the coarse poikilitic pyroxene anorthosite and the Pioneer marker. The Pioneer marker itself consists of two orthopyroxene-rich bands a few centimetres apart, occurring towards the top of a 1,4m thick alternating sequence of pyroxene anorthosite and poikilitic pyroxene anorthosite, about 28m below the Merensky reef. The overlying Brakspruit marker is a 1,4m thick package of poikilitic pyroxene anorthosite which occurs at ± 21m below the Merensky reef. The uppermost of the traditional markers is the Footwall marker which consists of a 0,8m thick poikilitic pyroxene anorthosite layer which occurs ± 12m below the Merensky reef.

A fifth, less well defined but laterally persistent marker, colloquially termed the 'streepies', occurs between the Footwall marker and the Merensky reef. It is variable both in thickness and internal lithostratigraphy. It is a well layered and commonly lightly banded leuconorite layer, which may have one or more melanorite bands developed at or near the top contact, and thinner anorthosite bands towards the middle and bottom. It may occur directly beneath the Merensky reef, to as much as 6m below it.

4.2.2 THE MERENSKY UNIT

The Merensky Unit is an approximately 10 to 11 metre thick unit consisting of a differentiated sequence of feldspathic orthopyroxenite, norite and anorthosite. It forms the base of the transitional macrounit of the lower Main Zone (Kruger, 1990), and rests on the transgressive paraconformity at the top of the Boulder Subunit.
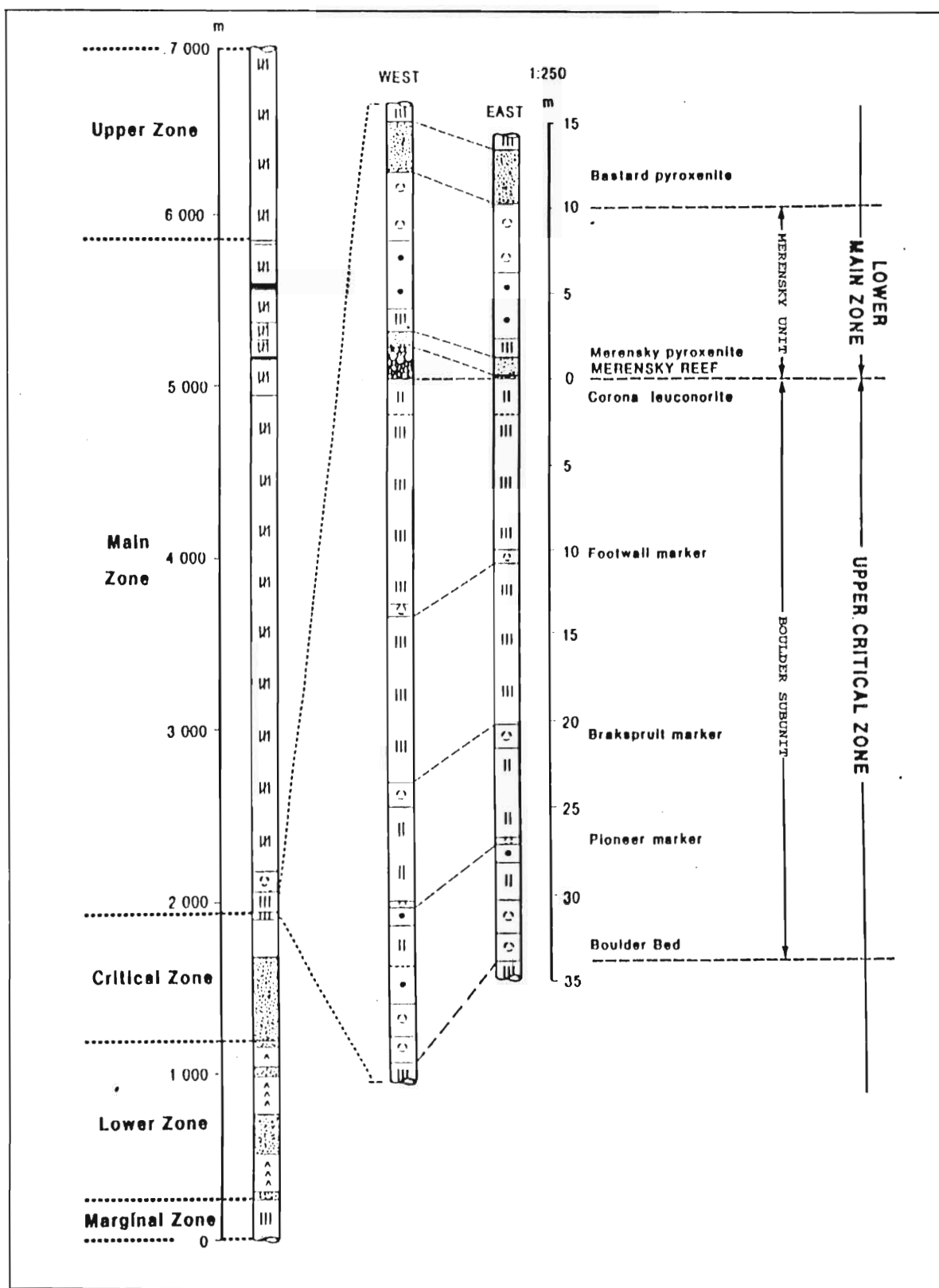
Figure **4.1** Generalised stratigraphic column for the western Bushveld **Complex, and the** detailed upper Critical Zone and lower Main Zone stratigraphy at Frank Shaft, RPM Rustenburg Section.
(see Figure **4.2 for legend)**

LITHOLOGICAL LEGEND
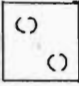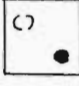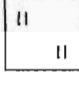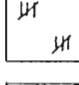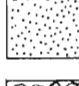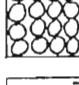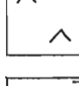
- Anorthosite
- Poikilitic pyroxene anorthosite
- Pyroxene anorthosite
- Varitextured pyroxene anorthosite
- Leuconorite
- Norite
- Melanorite
- Gabbronorite
- Feldspathic orthopyroxenite
- Pegmatoidal feldspathic orthopyroxenite
- Feldspathic harzburgite
- Pegmatoidal feldspathic harzburgite
- Chromitite
- Magnetite

Figure 4.2   Lithological legend

The Merensky reef, which displays considerable variation in thickness, occurs at the base of the unit. It is typically a pegmatoidal plagioclase-bearing (feldspathic) orthopyroxenite bounded top and bottom by thin chromitite layers. It is often, but not always, underlain by a highly variable, but generally conformable, anorthosite layer which is believed to form part of the Merensky Unit (Nicholson & Mathez, 1991). This layer varies in thickness, often markedly over short distances, between 0,5 and 30cm, and may consist of either anorthosite, pyroxene anorthosite and/or poikilitic pyroxene anorthosite. Its basal contact is characteristically highly undulatory. This anorthosite is present regardless of footwall composition. and is consistently present irrespective of the depth of Merensky reef transgression of the footwall.

The Merensky reef is overlain by a 1m thick layer of medium to locally coarse-grained poikilitic feldspathic pyroxenite (the Merensky pyroxenite). The term poikilitic refers to the fact that the rock contains elongate (2 - 7cm long), randomly orientated and distributed clinopyroxene oikocrysts poikilitically enclosing orthopyroxene (opx) and base metal sulphide (BMS) grains. Plagioclase is not observed to be enclosed by the oikocrysts. The medium-grained feldspathic pyroxenite grades upwards over a few cm into a ± 1m thick norite and leuconorite layer. This in turn is overlain by a 4m thick pyroxene anorthosite layer and finally by a 4m thick poikilitic pyroxene anorthosite layer. The latter directly underlies the Bastard pyroxenite and marks the top of the Merensky Unit (Figure 4.1).

Figure 4.3 shows the stratigraphy revealed in the drilling program for this work. Five holes were drilled from beneath the Footwall marker up to the Bastard pyroxenite; R25A, R24A and R26A on the east of Frank Shaft, and R27A and R23B on the west. The variation commonly encountered between the Footwall marker and the Merensky reef is clearly illustrated. So too is the variation in the thickness of the Merensky reef. It should be noted that the Merensky pyroxenite maintains a thickness of about 1m irrespective of Merensky reef thickness (Vermaak, 1976). The overlying norite is rather more variable while the overlying anorthosite layers also exhibit constant thickness. The thickness of the Merensky Unit therefore shows a dependence on the variation in thickness of the Merensky reef and hangingwall norite.
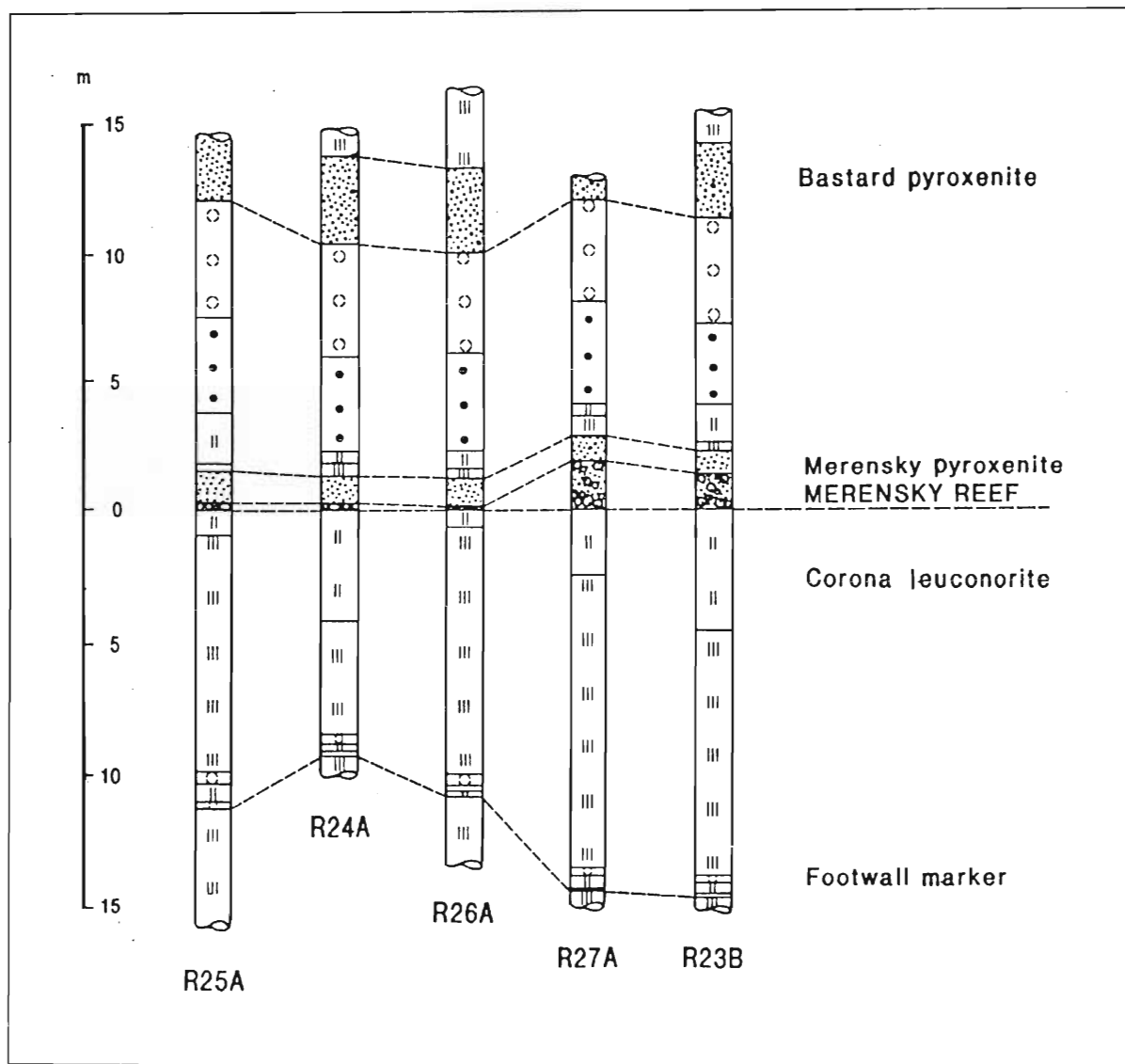
Figure 4.3   The stratigraphic variation, revealed by underground
boreholes R23 to R27, between the Footwall marker
and the Bastard pyroxenite at Frank Shaft, RPM
Rustenburg Section.
(see Figure 4.2 for legend, and Figure 2.1 for
borehole localities)

4.3 RELATIONSHIP BETWEEN THE MERENSKY REEF AND THE FOOTWALL LITHOLOGIES

It is well established in the literature that the Merensky reef rests on a regressive discontinuity developed at the top of the Boulder Subunit. Kruger (1990) and others refer to this as an erosional disconformity or unconformity, but the term *paraconformity*, defined by Irvine (1982), would seem to be more appropriate. A paraconformity, as the term is modified to suit the Merensky situation, may be defined as a magmatic regressive discontinuity, where, on a large scale the contact is apparently conformable, but locally demonstrates erosion of, or regression in the underlying cumulate succession.

4.3.1 THE MERENSKY REEF BASAL CONTACT

On a large scale the Merensky reef is conformable with the Boulder Subunit footwall stratigraphy. On a smaller scale, however, it is observed in both conformable and transgressive relationships with the footwall. Mapped examples of such undulatory transgressive relationships with footwall are shown in Figures 4.4a and b. Figure 4.4a shows the Merensky reef assuming a lower elevation over a distance of 1,5m with its lower contact transgressing the streepies. Note that the thin, discontinuous anorthosite layer is still developed at the lower elevation. Figure 4.4b shows an example of relatively large-scale reef undulation where again the footwall leuconorite is transgressed and the anorthosite layer is present.

A widespread, commonly observed phenomenon is the dimpled Merensky reef basal contact. Dimples are best developed in the thin Merensky reef facies (4 to 20cm), an example of which is shown in Figure 4.5. The depth of dimpling varies from a few cm to about 20cm. These are small-scale features which are manifested as sharp, frequently recurring, transgressive basal contact undulations. They vary in shape from rounded, pointed or elongate, to totally irregular. Chromitite occurrence within dimples also varies. Smaller dimples of a few cm in depth are often filled with chromitite, while larger ones may be lined with a continuous chromitite layer, a locally thickened layer, thinned or discontinuous chromitite layer. In some cases chromitite may be locally absent. Most dimples host normal reef pegmatoidal feldspathic pyroxenite but in some, pegmatoid is only patchily developed within medium-grained feldspathic pyroxenite.
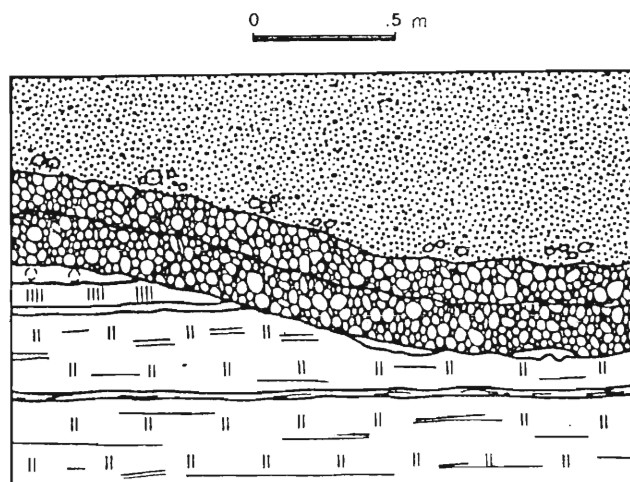
Figure 4.4a   The Merensky reef basal contact transgressing
               the 'streepies' marker (see Fig. 4.2 for legend)
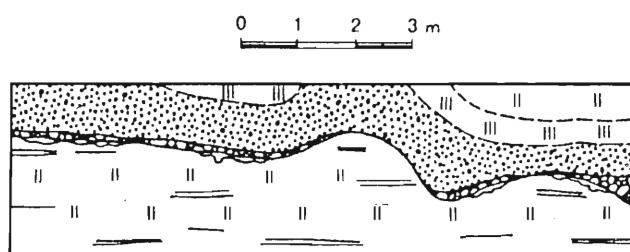
Figure 4.4b   Merensky reef small-scale transgressive
               undulation
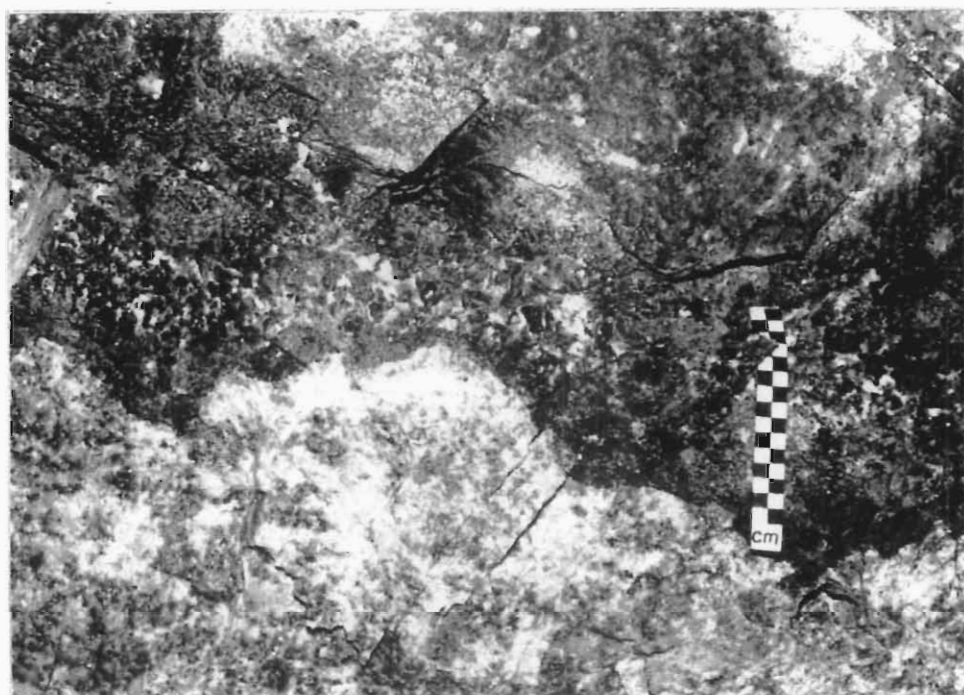
Figure 4.5   Examples of dimpled Merensky reef basal contact.

In dimpled Merensky reef the top contact does not show the sharp undulations of the basal contact, but does follow the larger, more gentle undulations.

In the thicker Merensky reef facies basal contact dimpling is less pronounced and in some cases may not occur at all.

4.3.2 THE IMMEDIATE FOOTWALL ANORTHOSITE LAYER

Where it occurs, this layer is developed directly beneath the Merensky reef basal contact and is of a highly variable nature. It has been noted by a number of authors in their descriptions of the Merensky reef, *eg* Vermaak (1976), Viljoen & Hieber (1986), Viljoen *et al* (1986), Leeb-du Toit (1986) and Nicholson & Mathez (1991). It is best developed in the thin reef facies where it commonly reaches thicknesses of 30cm + (often 2 to 3 times the thickness of the Merensky reef) and is usually continuous (Figure 4.6). In such cases it invariably occurs as a poikilitic pyroxene anorthosite but may also occur as a pyroxene anorthosite. Its basal contact with footwall leuconorite is usually well defined but is frequently very jagged and sharply undulatory, with long fingers which penetrate deeply (up to 1m) into the leuconorite (Figure 4.7). In the medium thickness reef facies this layer is thinner (0,5 - 7cm), frequently discontinuous and occurs as pure white anorthosite (simply referred to as anorthosite). Its basal contact is generally very sharp and far less undulatory. In the thick reef facies it is not developed at all. Generally, the thicker the Merensky reef, the thinner the anorthosite layer (Figure 4.8), and the thicker the anorthosite layer the more `spotted' (pyroxene anorthosite) or poikilitic (poikilitic pyroxene anorthosite) it becomes.

The anorthosite displays remarkable conformability with the Merensky reef (Vermaak, 1976). It is developed irrespective of the relative elevation of the Merensky reef, and closely follows it where the relationship between the Merensky reef and Boulder Subunit footwall is transgressive. This occurs to the point of even remaining parallel with individual dimples. Although there are some exposures which show thinning (Figure 4.9) or even absence of anorthosite beneath dimples, there are many where it follows dimples to near perfection. This, and the fact that it closely follows the Merensky reef irrespective of its relative elevation to footwall layers, suggests that it formed as part of the Merensky Unit. This is consistent with the interpretation of Nicholson & Mathez (1991).

40
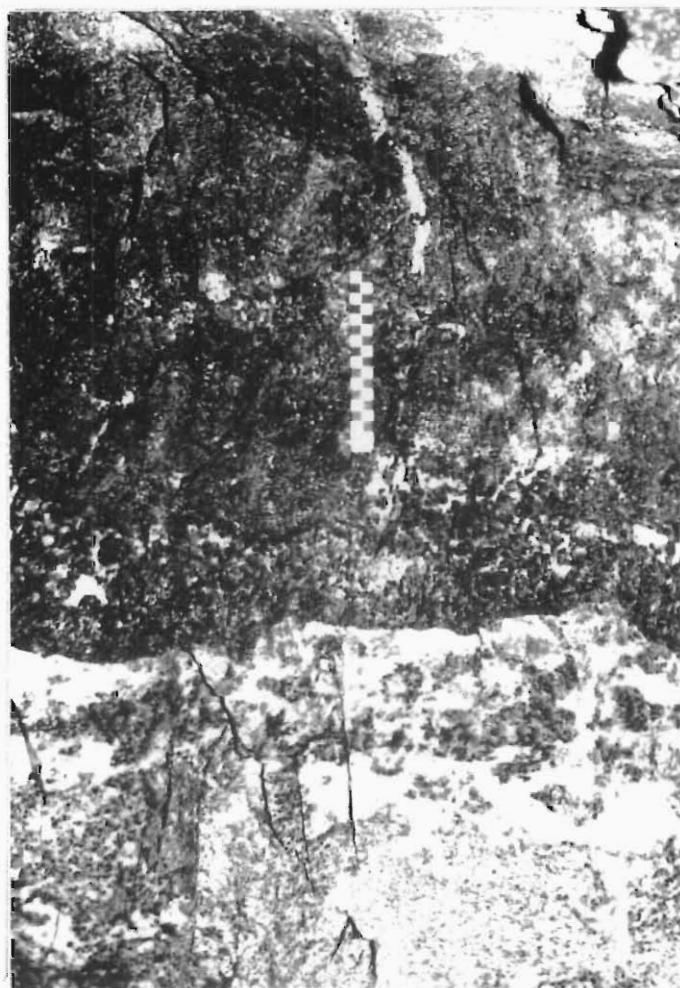
Figure 4.6   Immediate footwall poikilitic pyroxene anorthosite
as it commonly occurs beneath thin Merensky reef.
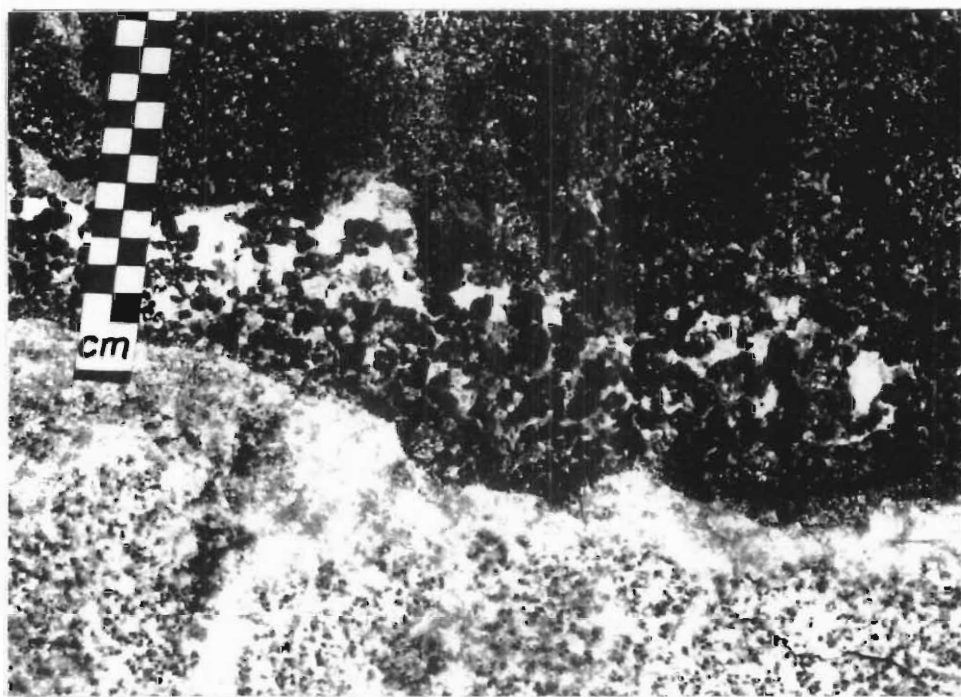
Figure 4.7   An example of irregular and sharply undulatory
immediate footwall anorthosite underlying thin
Merensky reef.   Note some undulations are
sympathetic with the Merensky reef basal contact.
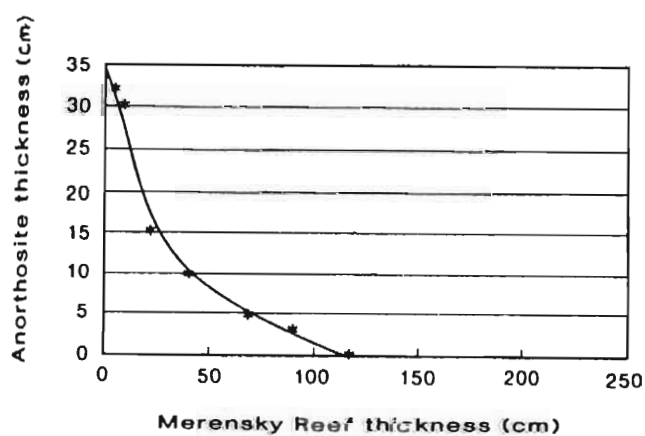
Figure 4.8   Approximate variation in footwall anorthosite
thickness with Merensky reef thickness
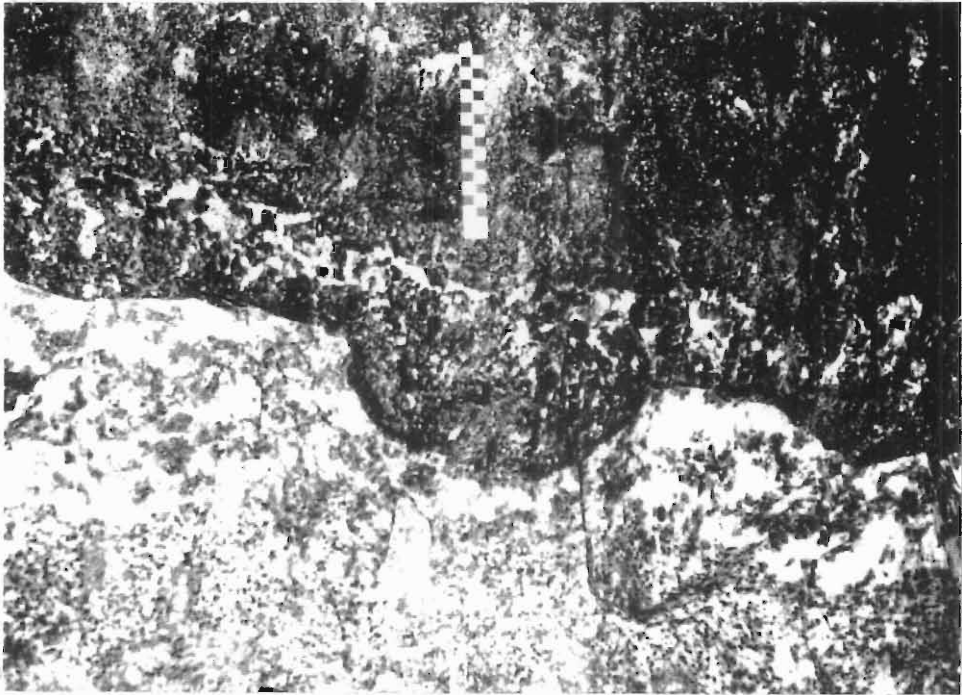
Figure 4.9   An example of the footwall anorthosite showing thinning beneath a prominent Merensky reef basal contact dimple.

Base metal sulphide (BMS) mineralisation occurs within the anorthosite layer, but this again is very variable in terms of distribution and frequency. Where the layer is thick (*ie* beneath thin Merensky reef), visible BMS mineralisation is relatively abundant. The BMS are almost exclusively associated with orthopyroxene crystals, aggregates of pyroxene crystals or pyroxene oikocrysts. However, where the anorthosite layer is thin, and devoid of pyroxene, BMS mineralisation is absent.

4.3.3 STRATIGRAPHIC VARIATION IN THE BOULDER SUBUNIT

Variation in stratigraphic distance between the Boulder Subunit markers and the Merensky reef has been recognised for some time (Viljoen & Hieber, 1986). In order to understand more clearly the nature and magnitude of this variation, and to what extent the regressive paraconformity influenced this, a total of 63 crosscuts throughout the Frank Shaft underground area were mapped in detail under the author's supervision (D.Crabb, *pers comm*, 1990 & 1991). Figure 4.10 shows graphically the mapped stratigraphic variation in the east and west areas of Frank Shaft underground workings respectively. The Boulder Bed marker (BB) was used as the datum and the other markers, the Pioneer (PM), Brakspruit (BK), Footwall (FW), Streepies (ST) and Merensky reef (MR) measured relative to it.

A number of trends are apparent and are detailed as follows:

a) Higher up the Boulder Subunit stratigraphy, the undulatory nature of the markers, relative to the BB, increases in intensity. The BB is known to be a relatively consistent, non-undulatory layer.

b) Despite this, individual layers essentially remain conformable with one another, including the ST and MR.

c) The Boulder Subunit is thicker in the west, where the mean stratigraphic distance between the BB and MR is 37m. On the east this distance is 32m and the mean for Frank shaft as a whole is 34m.

d) The distance between the FW and MR is greater in the west.
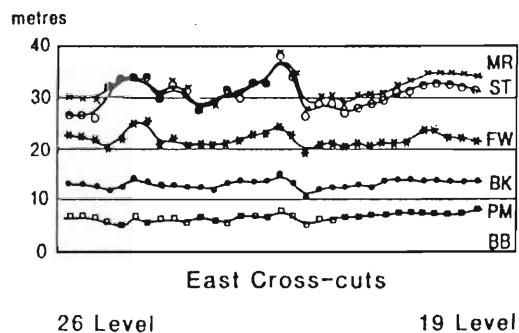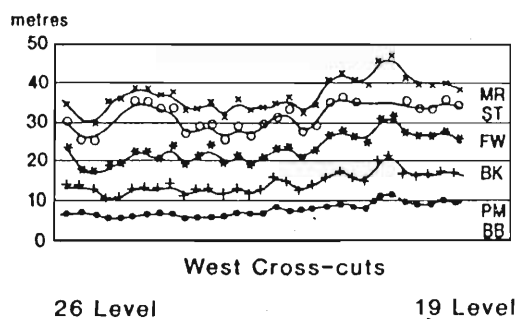
41

metres
West Cross-cuts
26 Level   19 Level

MR
ST
FW
BK
PM
BB

metres
East Cross-cuts
26 Level   19 Level

MR
ST
FW
BK
PM
BB

MR – Merensky reef   BK – Brakspruit marker
ST – Streepies   PM – Pioneer marker
FW – Footwall marker   BB – Boulder Bed marker

Figure 4.10   Boulder Subunit stratigraphic variation across Frank Shaft

metres
26 level   West Crosscuts   19 level
MR
FW

metres
26 level   East Crosscuts   19 level
MR
FW
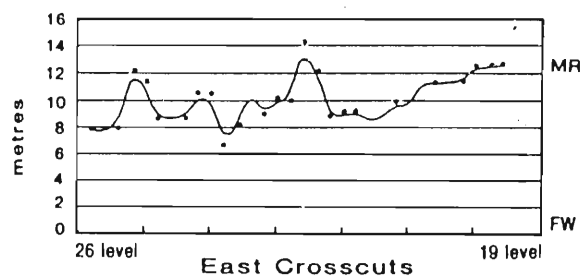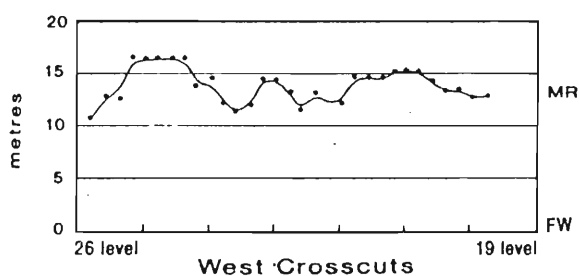
Figure 4.11   Variation in Footwall marker to Merensky reef stratigraphic distance across Frank Shaft

metres
0 2 4 6 8 10 12 14
26 level   19 level
West Levels
MR
ST

metres
0 2 4 6 8 10 12 14
26 level   19 level
East Levels
MR
ST
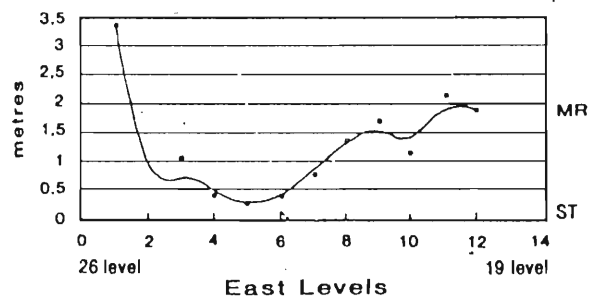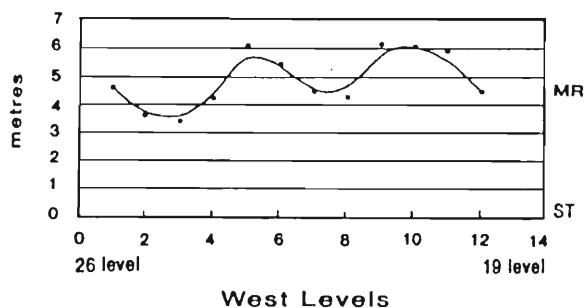
Figure 4.12   Variation in 'streepies' to Merensky reef stratigraphic distance across Frank Shaft

e) The distance between the ST and MR in the east is very variable but remains small, while in the west it is greater and remains fairly constant.

Figure 4.11 shows in finer detail the variation in stratigraphic distance between the FW and MR. In the east this averages about 10m and in the west about 13,5m. Similar information with regards the ST to MR distance is shown in Figure 4.12.

These observations bear implications for the nature of the paraconformable contact between the Boulder Subunit and Merensky Unit. They confirm the apparent conformability of the Merensky reef to its footwall lithologies. More important however, is the sympathetic and stronger than anticipated undulatory nature of the Boulder Subunit layers. This serves to confirm that the large scale Merensky reef undulations may not be as trangressive as originally envisaged (Brown, 1991).

4.4 MERENSKY REEF VARIATION

The extreme variability of the Merensky reef at RPM Rustenburg Section is a well known phenomenon and has been reported on at various levels by a number of authors, *eg* Viljoen & Hieber (1986), Allen (1986), Chunnett (1987), Kinloch & Peyerl (1990) and Nicholson & Mathez (1991). Merensky reef variablility exists in terms of numerous deviations from so-called normal or idealised status (which may vary from author to author), and it is this aspect which has received most attention in the literature. However, there is very little detailed description and interpretations on the variability of *normal* Merensky reef, and it is this issue which is addressed in the present work. Normal Merensky reef shows a number of variations, the most obvious of these being its variation in thickness. Associated with this are a number of other variations, such as the number and position of associated chromitite layers, texture, mineralogy, BMS & PGE mineralisation, occurrence and nature of the immediate footwall anorthosite layer.

4.4.1 THE QUESTION OF NORMAL MERENSKY REEF

No universally acceptable definition of normal Merensky reef is available in the literature. 'Normal' Merensky reef of the eastern Bushveld, for instance, is quite different from 'normal' Merensky reef of the western Bushveld, which immediately complicates any universal definition. In the eastern Bushveld, *eg* at Atok Platinum Mine (Mossom, 1986; Lee & Butcher, 1990), normal Merensky reef consists of a layer of medium-grained poikilitic feldspathic pyroxenite resting on an unmineralised pegmatoidal feldspathic pyroxenite footwall, and bound top and bottom by thin chromitite layers. As Lee and Butcher (1990) point out, the initial ratios of both the Atok and Rustenburg Merensky reef types are the same (0,7064 ± 1) and, their $^{87}Sr/^{86}Sr$ ratios are almost identical. As they suggest, this would indicate that the greater extent of inferred postliquidus modification to the Rustenburg Merensky reef (and Atok Merensky reef footwall), did not significantly disrupt the Rb-Sr systematics. The isotopic similarity between the texturally distinct Atok and Rustenburg Merensky reefs would appear not to be due to their similar BMS and PGE mineralisation however. Lee and Butcher (1990) found not only the reef to be isotopically identical, but also the unmineralised pegmatoidal footwall to the Atok reef, Merensky pyroxenite hangingwall to the Merensky reef, and Bastard pyroxenite (the latter two at both Atok and Rustenburg). Rationalisation of this phenomenon remains problematic.

Despite this enigma, a concise description of western Bushveld Merensky reef (Rustenburg type), as it occurs most commonly within the framework of normal, undisturbed circumstances, for the purposes of this work is as follows:

'The economic base metal sulphide (BMS) and platinum-group element (PGE) enriched, texturally variable, plagioclase-bearing (feldspathic) orthopyroxenite, olivine orthopyroxenite, or less commonly, harzburgite layer, which is situated at the base of the Merensky Unit. Considerable variation exists in layer thickness, texture, and to a lesser extent, style, grade and location of the BMS and PGE mineralisation. Texturally it is either pegmatoidal, partially pegmatoidal or, less commonly, medium-grained, and has one or more thin chromitite layers associated with it (commonly two, but up to four). It is overlain by medium, to locally coarse-grained, commonly poikilitic, feldspathic orthopyroxenite of the Merensky pyroxenite, which in contrast, maintains relatively constant layer thickness. The Merensky reef paraconformably overlies the uppermost leuconorite-norite of the Boulder Subunit, and may be directly underlain by a conformable late reaction anorthosite layer of highly variable thickness.'

4.4.2 <u>MERENSKY REEF CHROMITITE LAYERS AND ANORTHOSITE OCCURRENCE</u>

Nicholson & Mathez (1991), suggest that a relationship exists between the nature and occurrence of the Merensky reef basal chromitite layer, and that of the underlying anorthosite layer. The number of chromitite layers associated with the Merensky reef vary between one and four, and occur at the upper and lower contacts, within it and within the overlying medium-grained Merensky pyroxenite. In the latter case, patchy discontinuous pegmatoid is frequently developed in contact with the chromitite. The thickness of the chromitite layers ranges from a grain- thickness to nearly 4cm. The layers may be `flat-lying' and conformable to highly undulatory and locally discordant, and continuous or discontinuous. The chromite grains vary from being very densely packed to loosely packed and even disseminated, from coarse grained, sometimes platey, to very fine grained. The dominant interstitial mineral in the basal chromitite layer is plagioclase, whereas in the overlying chromitite layers it is orthopyroxene.

4.4.2.1 <u>Thin Merensky reef facies (4 - 20cm)</u>

In this facies type the pegmatoidal feldspathic pyroxenite is normally enveloped by two well developed chromitite layers. The upper chromitite layer seldom exceeds 1cm in thickness and undulates gently in sympathy with the often far sharper undulations of the basal chromitite. Patchy pegmatoid is sometimes developed immediately above it, extending a few cm into the overlying Merensky pyroxenite. The basal chromitite varies in thickness from ≤ 1 to nearly 4cm and is frequently very undulatory, giving rise to pronounced footwall dimpling (Figures 4.13a & b). Rarely the lower chromitite layer may be situated about 3 to 4 cm above the Merensky reef basal contact. In this instance only a few sparse grains of chromite occur along the basal contact, with little or no footwall anorthosite developed. The footwall anorthosite layer is however generally well developed beneath the basal chromitite layer in the thin reef facies. It varies in thickness from about 10 to 35cm and within this size range mostly occurs as poikilitic pyroxene anorthosite. In some instances poikilitic pyroxene anorthosite also extends in the form of long tongues down to about 1m below the basal chromitite. At this depth below the Merensky reef visible BMS are still associated with the pyroxene oikocrysts. The variation in thickness can be largely attributed to the sharp undulatory nature of its basal contact with
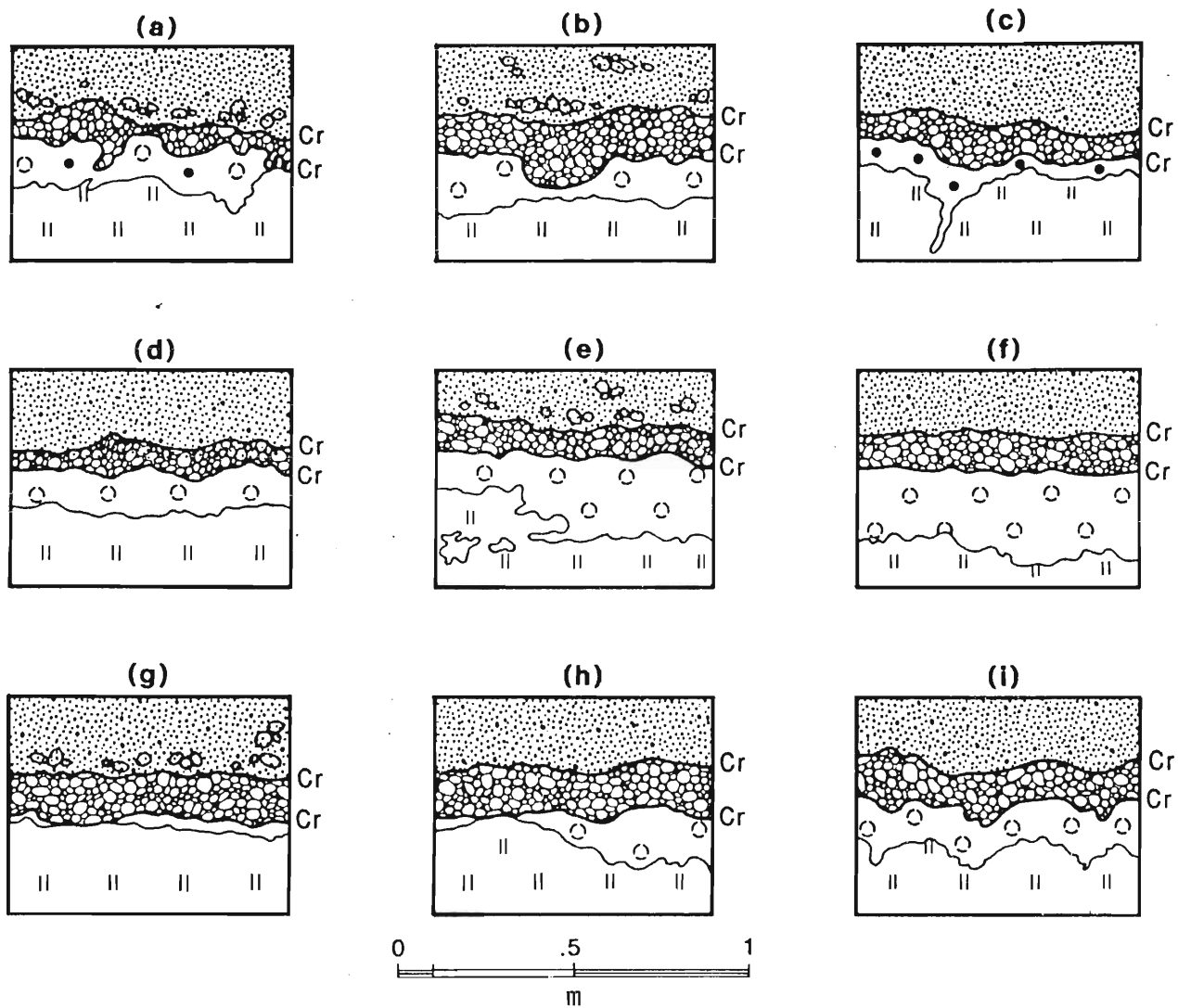
Figure 4.13   Variation in Merensky reef basal contact and underlying
              anorthosite layer in the thin reef facies
              (Cr = chromitite layer)
              (see Figure 4.2 for legend)

leuconorite, one which may often be diffuse, wispy and ill-defined (Figures 4.13c to f). Less commonly the anorthosite layer may be thinner than 10cm, in which case it occurs as a pyroxene anorthosite (Figure 4.13c), and in some cases even thinner, where below about 5cm it occurs as a pure anorthosite (Figure 4.13g). Although generally well developed in the thin reef environment, the anorthosite layer sometimes appears to be intermittently discontinuous, whereas, microscopically there is always a very thin pure plagioclase layer separating chromite from leuconorite. Where the basal chromitite layer is dimpled the anorthosite layer behaves in a variety of ways, from following the dimples to near perfection (Figure 4.13i), to thinning considerably under dimples (Figures 4.13a & b). At the same time it may be thickened under local Merensky reef topographic highs. Such variations generally occur over relatively short distances.

4.4.2.2 Medium Merensky reef facies (20 - 40cm)

In this facies, three chromitite layers are commonly developed, two of them typically enveloping the pegmatoid, with the third either situated within the pegmatoidal layer, or within the overlying Merensky pyroxenite (Figures 4.14a to c). The thickness of the basal chromitite layer rarely exceeds 1cm in this facies, and although often undulatory, is seldom sharply dimpled. The anorthosite occurrence in the medium reef facies is again highly variable, from periodic but infrequent absence (Figure 4.14a), to a thin anorthosite layer (Figure 4.14c), to a 30cm thick poikilitic pyroxene anorthosite layer (Figure 4.14b). In this facies in particular, it is noted that the thinner the anorthosite layer, the sharper and less undulatory is its basal contact with leuconorite, the lower its pyroxene content, and the less well developed (or thinner) is the Merensky reef basal chromitite layer.

4.4.2.3 Medium-thick Merensky reef facies (40cm - 1m)

In this facies, either two or three chromitite layers are commonly developed, the variable being the sporadic absence of the basal chromitite layer. This chromitite layer is usually very thin, varying from grain-thickness to about 5mm. The basal contact of the Merensky reef, whether identified by a basal chromitite layer or not, is often gently undulatory but not dimpled to the extent seen in the thinner reef facies. Larger wavelength undulations are also common, in

(a)

Cr
Cr
Cr

(b)

Cr
Cr
Cr

(c)

Cr
Cr

Cr

0   .5

Figure 4.14   Merensky reef and underlying anorthosite layer
variation in the medium reef facies
(Cr = chromitite layer)
(see Figure 4.2 for legend)
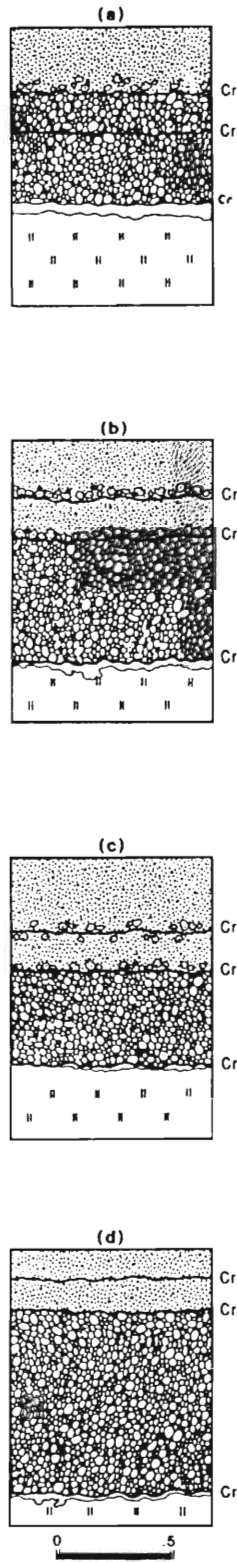
Figure 4.15   Merensky reef and underlying anorthosite layer
                variation in the medium-thick reef facies
                (Cr = chromitite layer)
                (see Figure 4.2 for legend)

which case transgressive relationships with the footwall leuconorite are frequently noted. The anorthosite layer, also sporadically absent, seldom exceeds 5cm in thickness and consists exclusively of anorthosite (with no macroscopically visible pyroxene). This anorthosite exhibits a sharp, well defined and seldom undulatory contact with the underlying leuconorite (Figures 4.15a to d), and remains consistently parallel with the Merensky reef basal contact.

4.4.2.4 Thick Merensky reef facies (1 - 2m)

In the thick Merensky reef facies up to three chromitite layers are developed. The basal chromitite layer is frequently absent (thin sections of the basal contact area show only disseminated chromite grains, sometimes quite abundant and extending tens of cm up into the reef). The most readily recognised chromitite layers occur at, near or above the top contact of the pegmatoid (Figure 4.16). The undulatory nature of the basal contact is generally confined to gentle, relatively low amplitude, long wavelength undulations. The anorthosite layer is not developed at all, with the Merensky reef basal contact simply being one between pegmatoidal feldspathic pyroxenite and leuconorite.

4.4.3 VARIATION IN TEXTURE AND BMS MINERALISATION

The Merensky reef consists essentially of a pegmatoidal feldspathic pyroxenite layer. It consists of a cumulate framework of subhedral to euhedral coarse-grained orthopyroxene crystals with interstitial plagioclase (with subordinate interstitial clinopyroxene). The plagioclase content commonly constitutes about 30% of the rock. Olivine is present in relatively small quantities (less than 5%) as a relict cumulus mineral poikilitically enclosed in orthopyroxene. The rock contains accessory interstitial phlogopite and BMS, and may, in addition to chromitite layers, contain some disseminated chromite. The BMS, with which the majority of the PGE mineralisation is associated, occur as irregular interstitial blebs of highly variable size. In order of decreasing abundance, the BMS consist of pyrrhotite, pentlandite, chalcopyrite and pyrite (Viljoen & Hieber, 1986). The different Merensky reef facies commonly show differences in texture and BMS abundance and distribution.

Figure 4.16   Thick Merensky reef facies variety.   Note
there is no basal chromitite layer developed.
(Cr = chromitite layer)
(see Figure 4.2 for legend)

4.4.3.1 Thin to Medium Merensky reef facies (4 - 40cm)

This Merensky reef facies is texturally consistent and comprises a framework of subhedral to euhedral orthopyroxene crystals of grain size 1 to 2cm. Plagioclase crystals are of similar size and occupy interstices between the orthopyroxene crystals (Figures 4.17 & 4.18). In some areas extensive but often patchy pegmatoid is developed immediately above the upper chromitite layer, extending up to about 10cm into the Merensky pyroxenite (Figure 4.19). Coarse olivine crystals (approx 1cm across), occurring as relict rounded cores surrounded by peritectic rims of orthopyroxene, are occasionally observed in the medium reef facies (Figure 4.20), but seldom in thin reef facies (the paint lines which appear in Figure 4.20, and a few others which follow, are mining-related and are of no consequence to this work). In localised areas a serpentinised pegmatoidal feldspathic harzburgite layer about 10cm thick may be developed at the base of the medium facies reef, separated from the remaining pegmatoidal feldspathic pyroxenite by a thin chromitite layer. In these cases interstitial plagioclase crystals commonly display dense layering-parallel expansion fractures filled with serpentine minerals such as antigorite. Figures 4.21, 4.22, 4.23 & 4.24 show a typical examples of medium facies Merensky reef. In Figure 4.21 three chromitite layers are developed, with the reef underlain by a thick anorthosite layer resting on the 'streepies' marker.

Visible accessory BMS are common in this reef facies. They occur as irregularly shaped blebs competing with plagioclase for interstitial space. The sulphides comprise a net-textured distribution through the pegmatoidal layer, with individual associations ranging in size from a few mm to 3cm across, and may be up to 7cm (excluding the rarely encountered abnormal BMS concentrations which may be tens of cm across). They are invariably in contact with orthopyroxene crystals and are rarely enclosed in plagioclase. Accessory phlogopite is also commonly in direct contact with the BMS blebs. BMS mineralisation also occurs within the chromitite layers (to a lesser extent and individual grains very much smaller than in the pyroxenite portions), and extends well into the hangingwall and footwall. In the hangingwall medium grained Merensky pyroxenite BMS occur in decreasing abundance up throughout the entire 1m thick layer but not into the overlying norite. It is most abundant closest to the Merensky reef top contact where it commonly occupies all the interstitial space between orthopyroxene crystals in small patches, to the total exclusion of plagioclase. Scattered accessory phlogopite occurs throughout the Merensky pyroxenite, much of it in contact with BMS occurrences.
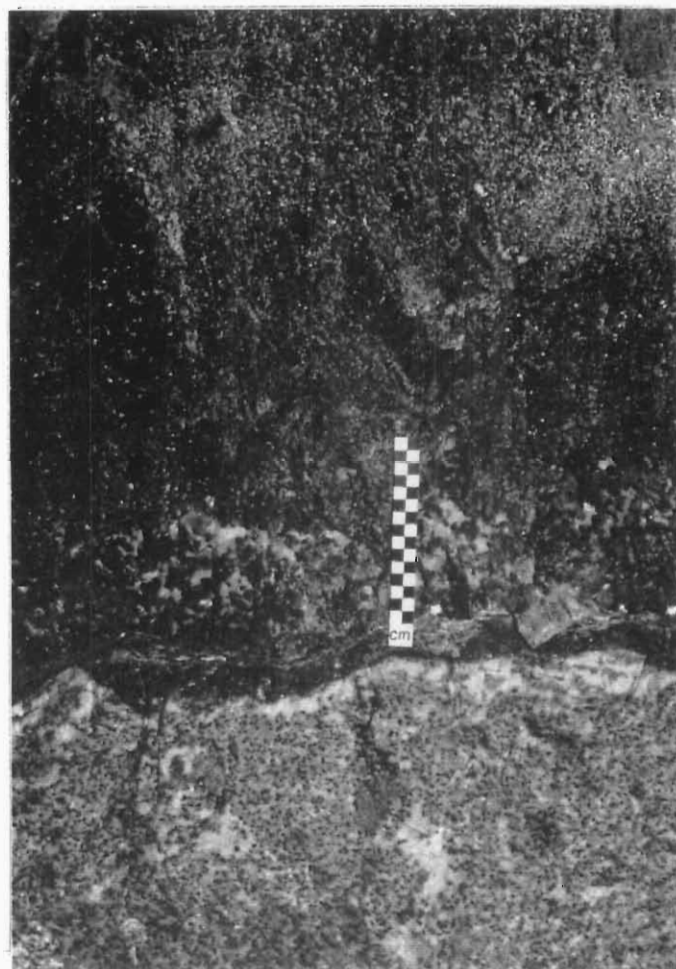
Figure 4.17   Typical thin Merensky reef showing top and bottom
chromitite layers, pegmatoidal texture, and
dimpled basal contact.   In this case the footwall
anorthosite is thin and patchy.
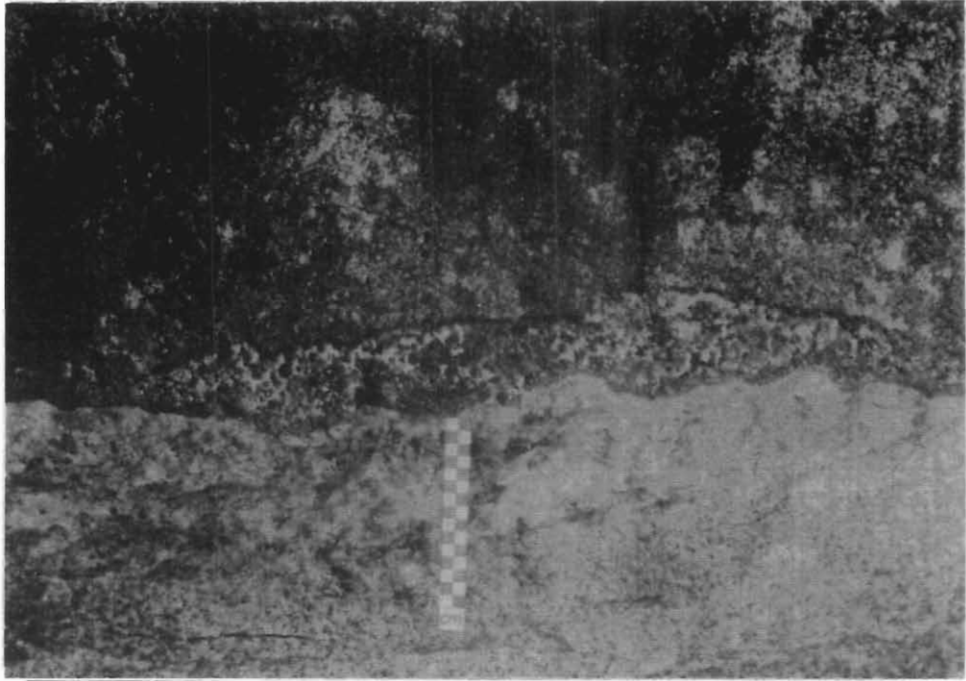
Figure 4.18   Thin Merensky reef showing typical pegmatoidal
               texture, well developed chromitite layers,
               closely spaced variation in thickness, undulatory
               top contact, dimpled basal contact, and thick,
               relatively uniform footwall anorthosite.
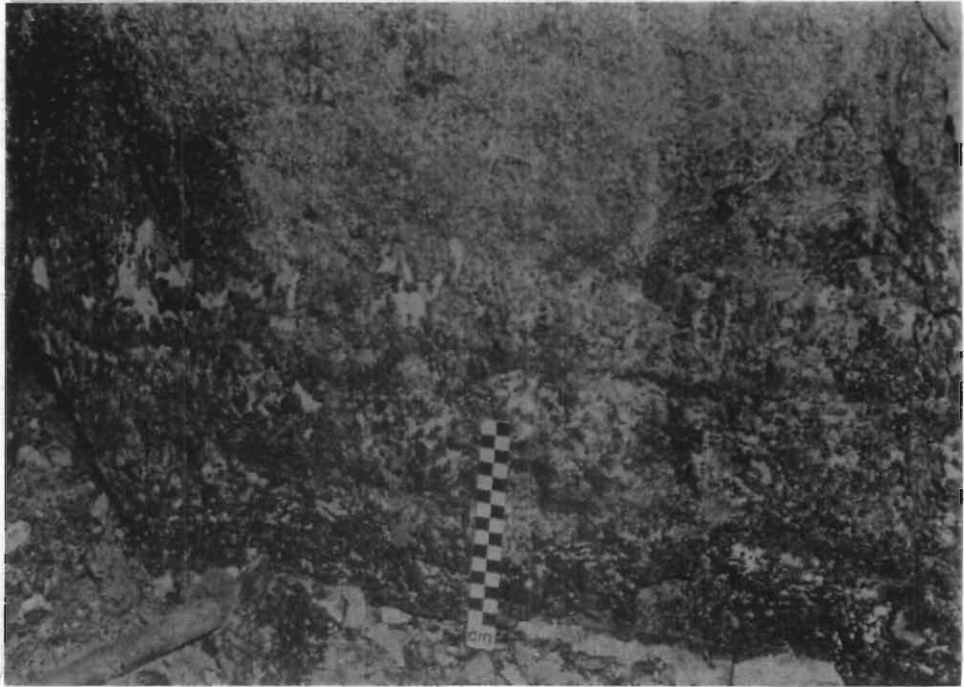
Figure 4.19   Medium Merensky reef with three chromitite layers
developed.   Patchy pegmatoidal feldspathic
pyroxenite occurs above the uppermost chromitite
layer, within the overlying Merensky pyroxenite.
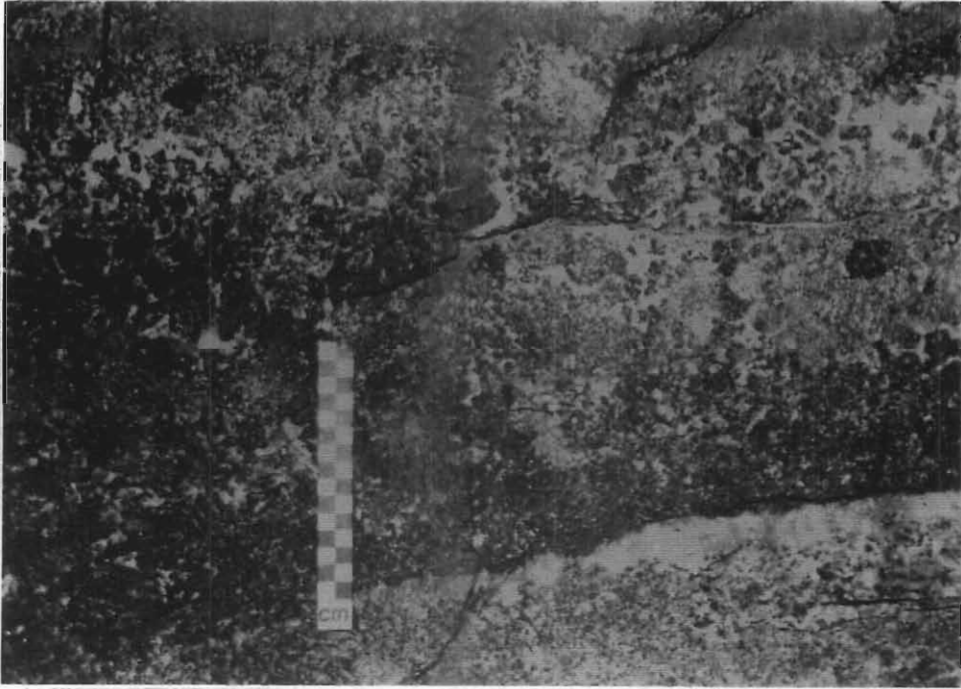
Figure 4.20   Medium Merensky reef with a 5cm thick layer of
               pegmatoidal feldspathic harzburgite developed at
               the base.   The olivine crystals in this layer
               are typically rounded and often rimmed by
               orthopyroxene.   The olivine is also invariably
               very dark green to black in colour as a result of
               exsolved magnetite occurring as a by-product of
               serpentinisation.
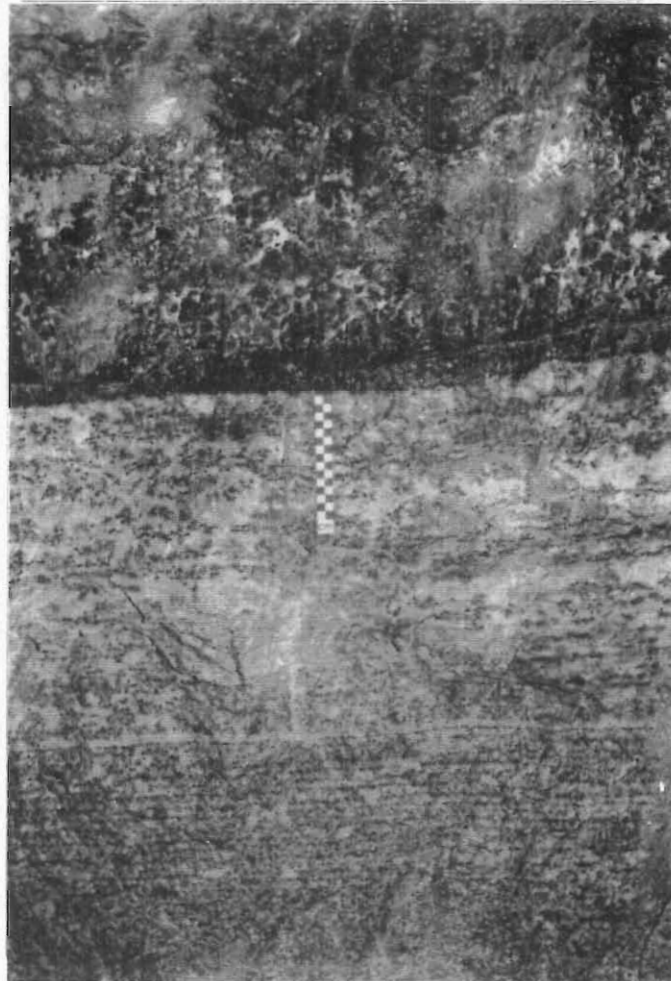
Figure 4.21   Medium Merensky reef with three well developed
chromitite layers, underlain by a thick footwall
anorthosite resting on the 'streepies' marker.
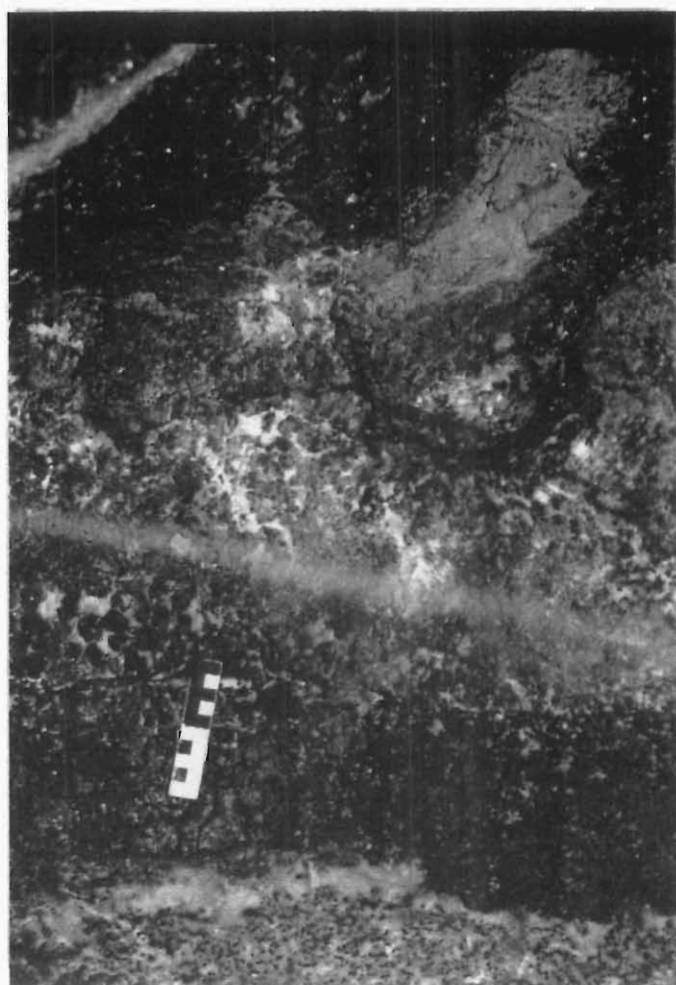
Figure 4.22   Medium Merensky reef, the bottom 15cm of which
                consists of serpentinised pegmatoidal feldspathic
                harzburgite.   Note the thin footwall anorthosite
                layer and the patchy pegmatoid above the upper
                reef contact.
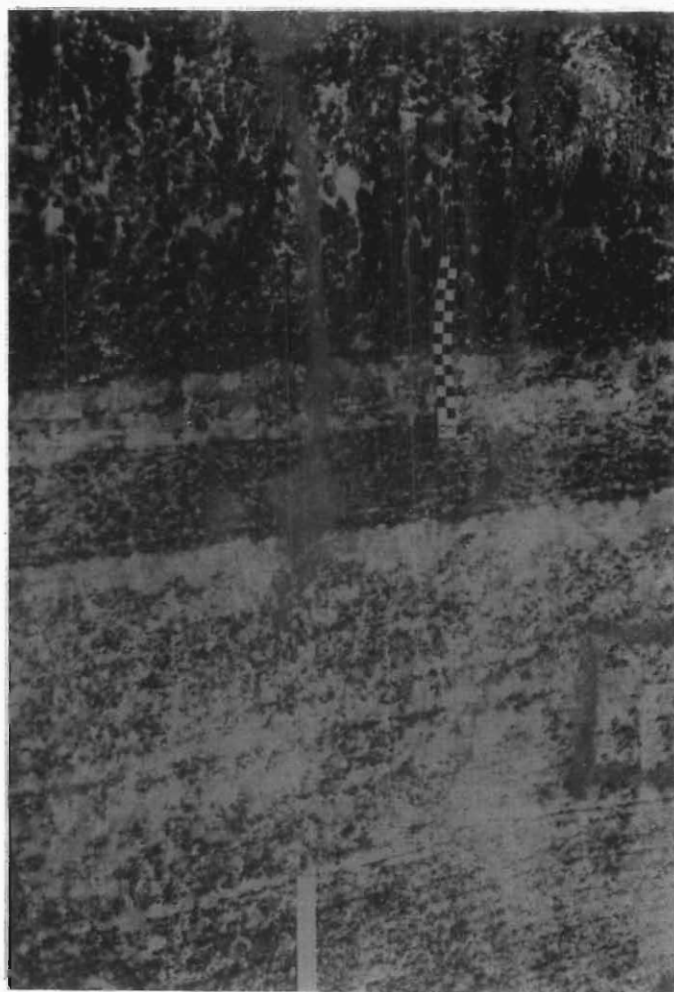
Figure 4.23   Medium Merensky reef with large pegmatoidal crystals, resting directly on the 'streepies' marker.
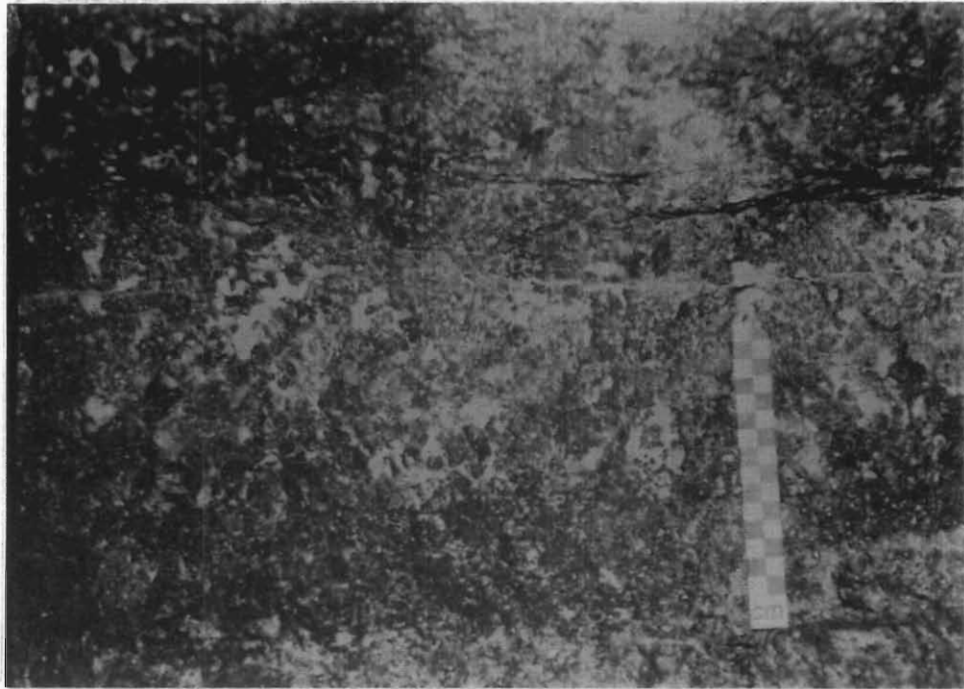
Figure 4.24   Medium Merensky reef showing a variety of crystal
sizes and some patchy pegmatoid development.

BMS occurrence in the footwall rocks is slightly more variable. Where an immediate footwall anorthosite layer is developed, and where it is thick and consists of poikilitic pyroxene anorthosite, BMS occurrences are most abundant. Here BMS commonly occur as dense concentrations of very small grains associated with the oikocrystic pyroxene. BMS grains are not hosted by the pure plagioclase portions of the rock. Similarly, where the anorthosite layer occurs as a pyroxene anorthosite, less abundant BMS grain concentrations are exclusively associated with the pyroxene grain concentrations. Where the anorthosite is thin and consists only of pure plagioclase there is no visible BMS mineralisation.

Below the anorthosite layer, BMS mineralisation (and accompanying economic PGE mineralisation) within the leuconorite is common down to a depth of about 50cm below the Merensky reef, and less frequently, occurs to about 1m below the Merensky reef. These BMS grains are generally ≤ 1mm across and are associated with pyroxene crystals.

The BMS concentration and distribution throughout these reef successions is a fairly accurate estimation of the accompanying PGE concentration and distribution. PGE grades are invariably high in this reef facies.

4.4.3.2 Medium-thick Merensky reef facies (40cm - 1m)

This reef facies is slightly more texturally variable than the thinner facies. The basic cumulate-type structure of the rock remains similar but grain size, of the pegmatoid in particular, is more variable. Crystal size ranges from 1 to 7cm with the average about 1,5 to 2cm. Where crystal size is as large as 7cm, both the orthopyroxene and interstitial plagioclase crystals are of similar size. Orthopyroxene crystals are commonly subhedral but may be euhedral, whereas the plagioclase crystals are generally subhedral and of irregular shape because of their interstitial nature. Patchy pegmatoid development immediately above the upper chromitite layer is commonly observed, and less commonly within the reef itself. Figure 4.25 shows an example of the latter texture developed in a 1m thick Merensky reef exposure. Rounded, partially replaced olivine crystals are sometimes observed, particularly towards the base of the pegmatoid. Small, scattered flakes of phlogopite constitute a common accessory mineral.
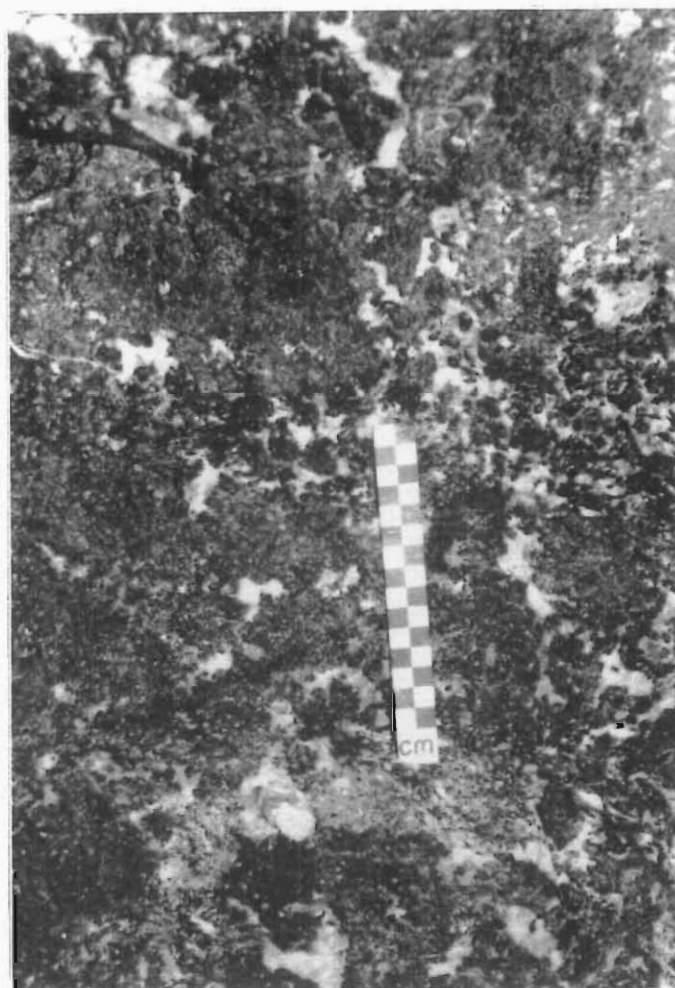
Figure 4.25   Medium-thick Merensky reef showing extensive
               patchy pegmatoidal development and large
               variety in grain size.

Visible interstitial BMS blebs generally become smaller and more sparse as reef thickness increases, and particularly where reef thickness exceeds 60cm visible BMS are significantly more concentrated towards the top portion of the pegmatoid where the chromitite layers are best developed. This pattern is also reflected in the PGE distribution, with the exception of where the basal chromitite layer is developed, in which economic PGE values are situated. As with the thinner reef facies, BMS mineralisation extends well into the overlying Merensky pyroxenite. The footwall leuconorite mineralisation however decreases sharply as the Merensky reef becomes thicker, and generally where reef thickness exceeds 60cm, visible leuconorite footwall BMS mineralisation is sparse and PGE values are invariably subeconomic. Where the immediate footwall anorthosite layer shows reduced pyroxene content as it becomes thinner, so too is there an accompanying reduction in BMS and PGE mineralisation. The medium-thick Merensky reef facies is invariably of lower PGE grade than the thinner reef facies (but of equal total metal content).

4.4.3.3 Thick Merensky reef facies (1- 2m)

The thick Merensky reef facies is texturally diverse compared to the thinner reef facies. Here the reef is commonly of partially pegmatoidal texture, with numerous, irregular patches of fine to medium-grained feldspathic pyroxenite dispersed randomly throughout the lower and middle portions (Figures 4.26, 4.27, 4.28 & 4.29). These non-pegmatoidal areas commonly host numerous, elongate, randomly orientated clinopyroxene (augite) oikocrysts. The upper ± 40cm, in close proximity to the chromitite layers, is most commonly pegmatoidal. Patchy pegmatoid development is commonly observed immediately above the upper chromitite layer, seldom extending more than about 7cm into the Merensky pyroxenite (Figures 4.30 & 4.31). More rarely, small, irregular, isolated patches of pegmatoid may be developed a few cm above the upper chromitite layer, within the Merensky pyroxenite. Crystal size of the pegmatoid generally ranges between 1 and 3cm, but crystals as large as 5cm are not uncommon. In any given exposure, crystal size, within these limits, may vary considerably and, occasionally, plagioclase crystals may exceed this. Examples of this have been noted where plagioclase forms long (up to approx 50cm), continuous, subvertical to vertical interstitial channel-like structures, which suggest sites of fluid movement (Figures 4.32 & 4.33). Olivine is a relatively common mineral in this reef facies. It occurs as rounded relict crystals of ± 1cm diameter, surrounded by peritectic rims of orthopyroxene, and is essentially confined to the bottom ± 20cm of the reef,
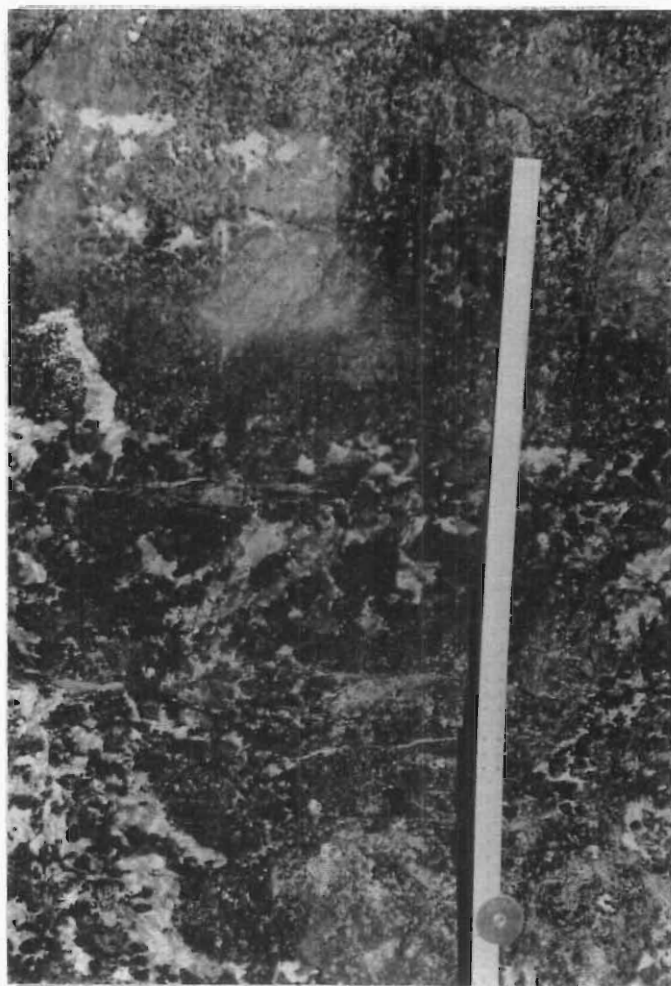
Figure 4.26   Upper portion of thick Merensky reef showing
                typical partial pegmatoidal development and large
                interstitial plagioclase crystals.
                (top half of 1m clinorule used as scale)

Figure 4.27   Middle portion of thick Merensky reef showing
               a partially pegmatoidal texture.   Note the
               large plagioclase crystals and the rimming of
               orthopyroxene crystals.

Figure 4.28   Thick Merensky reef showing typical scattered
partially pegmatoidal texture.

Figure 4.29   Close-up view of thick Merensky reef showing the
               partially pegmatoidal texture and large variation
               in crystal size.

Figure 4.30   Top contact of thick Merensky reef (upper chromitite
layer at 10cm down from top of scale) showing
patchy pegmatoidal development associated with
the upper chromitite layer.

Figure 4.31   Top contact of thick Merensky reef (at 5cm up
                from base of scale) showing patchy pegmatoid,
                where in this case is largely confined to
                immediately beneath the uppermost chromitite
                layer.

Figure 4.32   Upper portion of thick Merensky reef showing
               long vertically orientated channel-like
               plagioclase occurrences.

Figure 4.33   Close-up view of thick Merensky reef showing
              channel-like plagioclase occurrences.

or concentrated along the basal contact. A basal chromitite layer is rarely developed in this facies (Figure 4.34) but disseminated chromite is common in the lower 10 to 20cm (Figures 4.35 & 4.36), and also in the vicinity of the upper chromitite layers. Accessory phlogopite occurs as scattered flakes throughout the reef. The patchy, randomly interspersed pegmatoidal and fine to medium-grained textures observed in this facies is strong evidence to suggest that submagmatic *in situ* recrystallisation of the Merensky reef occurred.

Most BMS mineralisation occurs towards the top of the reef, especially in the vicinity of the chromitite layers. The mineralisation occurs as interstitial blebs very variable in size. The visible concentration of BMS mineralisation decreases rapidly further down the reef and is rare in most cases within the bottom 10 to 20cm. This becomes more evident as the reef becomes thicker *ie* approaching 2m. The PGE mineralisation follows a similar trend, and in mining operations at RPM Rustenburg Section the bottom ± 10cm of the reef is commonly left *in situ* as footwall waste. As with the other facies, BMS mineralisation frequently extends up throughout the ± 1m thick Merensky pyroxenite hangingwall, however not necessarily implying that economic PGE mineralisation occurs throughout. Visible BMS mineralisation in the footwall leuconorite is rare and is of no economic importance.

4.5 SUMMARY AND CONCLUSIONS

The following points summarise the important observations of this section:

a) The thickness of individual layers within the Boulder Subunit demonstrate considerable variability. This results in the observed thickness differences of the subunit. In the east the mean thickness of the Boulder Subunit is 32m, in the west it is 37m, while the mean for Frank Shaft is 34m. This suggests that mechanisms that gave rise to the Boulder Subunit were variable and progressive, arising from lateral changes in liquidus conditions.

b) Up through the Boulder Subunit stratigraphy, the large-scale undulatory nature of the marker layers increases in intensity relative to the Boulder Bed marker. Despite this, the layering is conformable due to sympathetic undulation. It may thus be concluded that fundamental controls existed in local domains giving rise to layers of variable thickness within a conformable
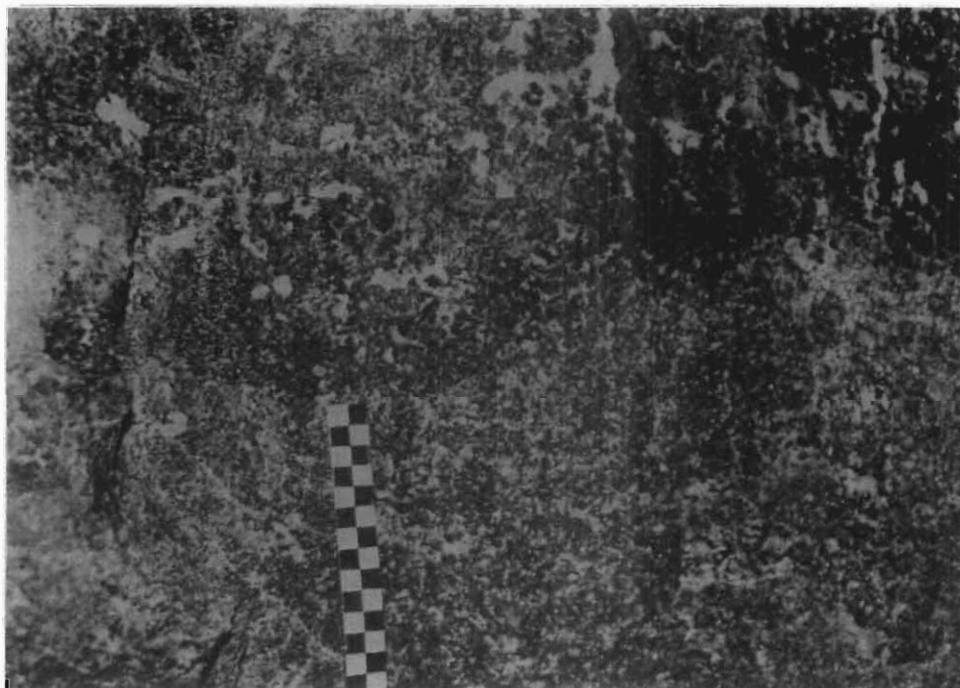
Figure 4.34   Basal contact of thick Merensky reef (top of cm
scale on contact).   Note there is no basal
chromitite or footwall anorthosite layers
developed.   Note too in this case the
undulatory nature of the contact.
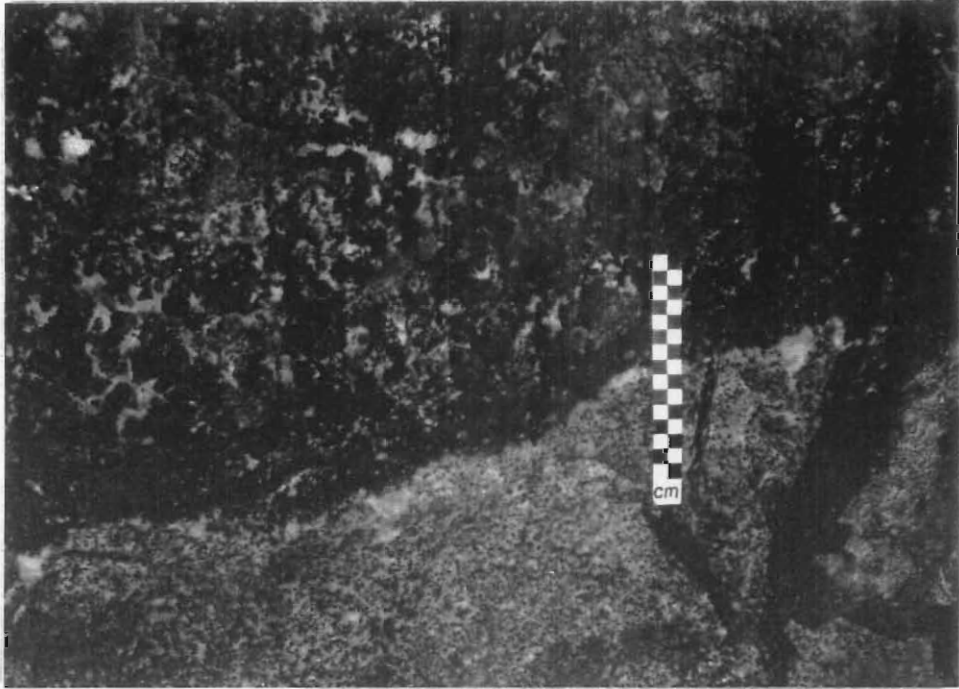
Figure 4.35   Basal contact of thick Merensky reef.   In this
               case there is some disseminated chromite
               concentrated in places along the contact,
               hence the thin localised footwall anorthosite
               layer.

Figure 4.36   Basal contact of thick Merensky reef with some
disseminated chromite along contact, and the
resultant, in this case very thin, footwall
anorthosite layer.

succession.

c) The `streepies', and the Merensky reef, compare well with this conformability, and demonstrate that the commonly observed stratigraphic variation is not a result of Merensky reef transgression alone.

d) The Merensky reef basal contact demonstrates a strong small-scale transgressive relationship with its Boulder Subunit footwall. This suggests that the Merensky reef may have been emplaced as a separate event from the footwall stratigraphy.

e) Both the apparent conformability and the regressive nature of the Merensky reef basal contact have been shown. This demonstrates that the discontinuity between the Merensky and Boulder units may more appropriately be described as a paraconformity, rather than an unconformity or disconformity.

f) Together with thickness the Merensky reef varies considerably in texture, basal contact dimpling, BMS (& PGE) distribution and grade and, occurrence, number, position and thickness of chromitite layers. The nature of the variation is largely characteristic of the different reef facies.

In general the following aspects show greater development in thick Merensky reef facies:

i) there is greater textural diversity, which suggests increasingly incomplete recrystallisation.

ii) the basal contact dimpling is less well developed. This may be a function of the absence of a basal chromitite layer and limited reaction with the footwall.

iii) the BMS and PGE grade is greater towards the top of the reef. In the latter part of this chapter this is shown to be a function of the constant metal content of the Merensky reef and late-stage recrystallisation and redistribution of the reef components.

iv) the BMS are finer grained and increasingly disseminated. This is also consistent with constant metal and associated sulphide content of the Merensky reef.

v) the PGE grade is lower (as expressed in gt^{-1} or ppm). This is evidence for constant metal content of the   Merensky reef, irrespective of thickness.

vi) as the number of chromitite layers increases towards the top of the reef they also

become correspondingly thinner.

vii) the basal chromitite layer is absent or poorly developed.

- Thin MR generally has two chromitite layers which envelope the pegmatoid. The thickest chromitite layers are also most common in this facies.
- Medium MR commonly has both two or three chromitite layers, the third layer developed within the reef, the other two enveloping it.
- Medium-thick MR commonly has two well developed upper chromitite layers, while the basal chromitite layer is usually less well, or poorly, developed.
- Thick MR most commonly has either two or three upper chromitite layers, and no basal chromitite layer (disseminated chromite however is common towards the base).

g) Observations relating to the immediate footwall anorthosite layer associated with the Merensky reef are:

i) Persistent conformability with the Merensky reef, irrespective of its transgressive nature, including its occurrence in potholes and koppies.

ii) Highly irregular nature of its basal contact.

iii) Paucity of BMS and PGE mineralisation relative to the underlying leuconorite.

iv) Lithological changes (from anorthosite to poikilitic pyroxene anorthosite) associated with its variation in thickness.

v) Sympathetic occurrence and variation in thickness with the occurrence and variation of the reef basal chromitite layer. This and other evidence suggests that the anorthosite layer is a late-stage product of reaction between the Merensky reef basal chromitite layer and the underlying Boulder Subunit leuconorite (see later discussion).

vi) Discontinuous nature and periodic absence where no noticeable change in Merensky reef elevation has occurred.

This evidence strongly suggests that the immediate footwall anorthosite layer constitutes part of the Merensky Unit, as a late-stage reaction layer, which is difficult to explain by any known process, or by the physical removal of the pyroxene component as a result of re-equilibration in the subsolidus stage, a process suggested by Hunter (1987).

h) The partially pegmatoidal texture, most commonly observed in the medium-thick and thick

Merensky reef facies, provides some evidence that the Merensky reef underwent late-stage *in situ* recrystallisation. The channel-like plagioclase occurrences occasionally observed in the thick facies suggest late-stage fluid movement associated with the recrystallisation.

CHAPTER 5

PETROGRAPHY OF THE MERENSKY REEF SUCCESSION

5.1 INTRODUCTION

The four study sections comprise Merensky reef of 2,82m to 7,07m in thickness, and between ± 1,5 and ± 2,5m of the immediate hangingwall and footwall. Although thicknesses of individual layers vary, the basic stratigraphy from the base upwards comprises; norite to leuconorite - pegmatoidal feldspathic pyroxenite - medium grained feldspathic pyroxenite - norite - leuconorite - pyroxene anorthosite.

The rock types are characterised by a mineral assemblage in which orthopyroxene, plagioclase and clinopyroxene are the major constituents, with chromite in cases where chromitite layers are developed. Base metal sulphides and phlogopite are prominent accessory minerals within the pyroxenites. Olivine may occur as a subordinate mineral being variably peritectically replaced by orthopyroxene. It infrequently occurs as a relict essential mineral where, uncommonly, a thin (up to ± 10cm thick) pegmatoidal feldspathic harzburgite layer forms the basal portion of thin to medium Merensky reef facies, usually separated from the remainder of the reef by a chromitite layer.

5.2 PETROGRAPHIC DESCRIPTIONS

Petrography is not the main emphasis of this study, and therefore only simple observatory work has been carried out on normal thin sections for the silicates and chromitite layers. The base metal sulphides (BMS) and their relationships with the silicates and chromitite layers were observed using conventional polished sections and large polished slabs prepared from samples of thick and thin Merensky reef facies. No microprobe work was carried out. Due to the economic significance of the BMS, their mode of occurrence, lithostratigraphic location and identification are discussed separately for each lithology.

Previous work on Merensky reef BMS in the Rustenburg area, *eg* Mostert *et al* (1982) and Viljoen & Hieber (1986), indicates that the most abundant BMS is pyrrhotite ($Fe_{1-x}S$: hexagonal

± Fe_9S_{10}, monoclinic ± Fe_7S_8), followed by pentlandite (($Fe,Ni)_9S_8$), chalcopyrite ($CuFeS_2$) and pyrite (FeS_2) in order of decreasing abundance. Mostert *et al* (1982) in their study at Impala Platinum Mines (adjacent to RPM Rustenburg) determined the BMS abundances as: 41% pyrrhotite, 37% pentlandite, 18% chalcopyrite and 4% pyrite. In addition, accessory amounts of cubanite ($CuFe_2S_3$), valleriite (($Fe,Cu)S_2$), bornite (Cu_5FeS_4), galena (PbS), molybdenite (MoS_2), nickel-mackinawite (($Fe_{1+x},Ni)S$), sphalerite (($Zn,Fe)S$), bismuthinite (Bi_2S_3), niccolite (NiAs) and nickel-skutterudite (($Ni,Co)As_{2-3}$) have been identified (Viljoen & Hieber, 1986).

5.2.1 FOOTWALL LEUCONORITE

5.2.1.1 Silicates

The footwall leuconorite is an orthocumulate rock consisting of a cumulus framework of subhedral to euhedral plagioclase and limited orthopyroxene. The majority of orthopyroxene and the minor amount of clinopyroxene which occurs (Figures 5.1 & 5.2) is intercumulus. Plagioclase typically makes up between 60 and 65% of the rock, orthopyroxene between 30 and 35%, and clinopyroxene always less than 5%. Grain size ranges from 0,1 to 3mm, with the greater proportion of crystals occurring between the range of 0,5 to 1,5mm (medium-grained). The plagioclase is strongly twinned, showing abundant Carlsbad and albite twinning, and minor pericline twinning. Orthopyroxene typically shows strong cleavage traces (Figures 5.1 & 5.2) and occasionally displays clinopyroxene (augite) exsolution lamellae which occur parallel to the (100) crystallographic axis (Figure 5.3). The late-stage intercumulus mineral content of footwall leuconorite, consisting dominantly of base metal sulphides and phlogopite, is generally low, with the greatest proportion of readily visible intercumulus mineralisation occurring within ± 1m of the overlying Merensky reef. Figure 5.4 shows examples of this, where relatively abundant interstitial accessory phlogopite is developed together with minor BMS grains.
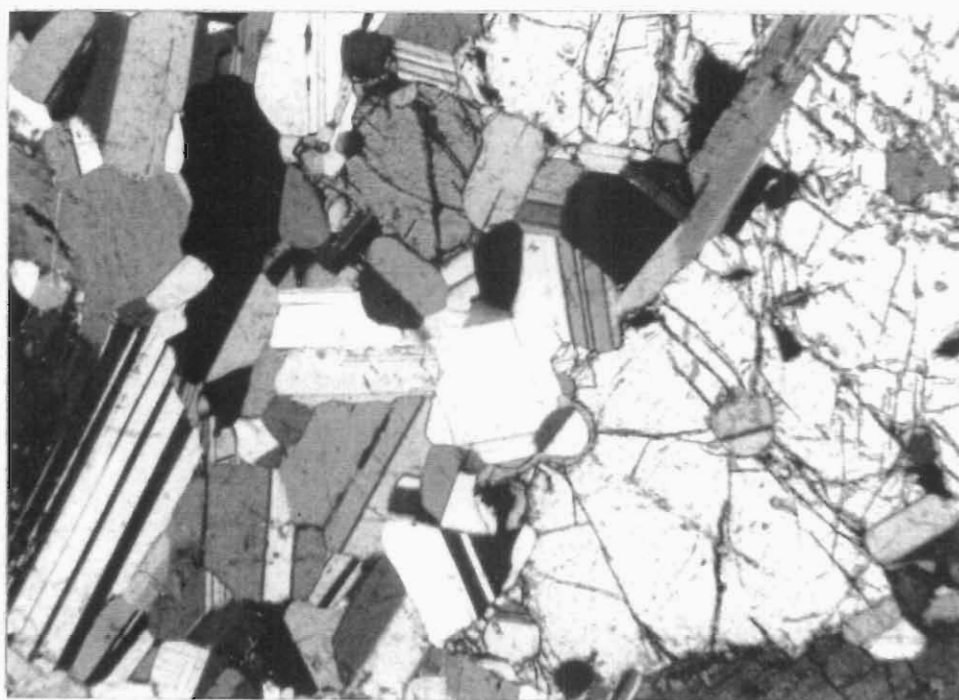
1mm

Figure 5.1   Photomicrograph of footwall leuconorite showing the
cumulus plagioclase and intercumulus orthopyroxene.
Note the Carlsbad and albite twinning in the
plagioclase.   (crossed nicols)

1mm
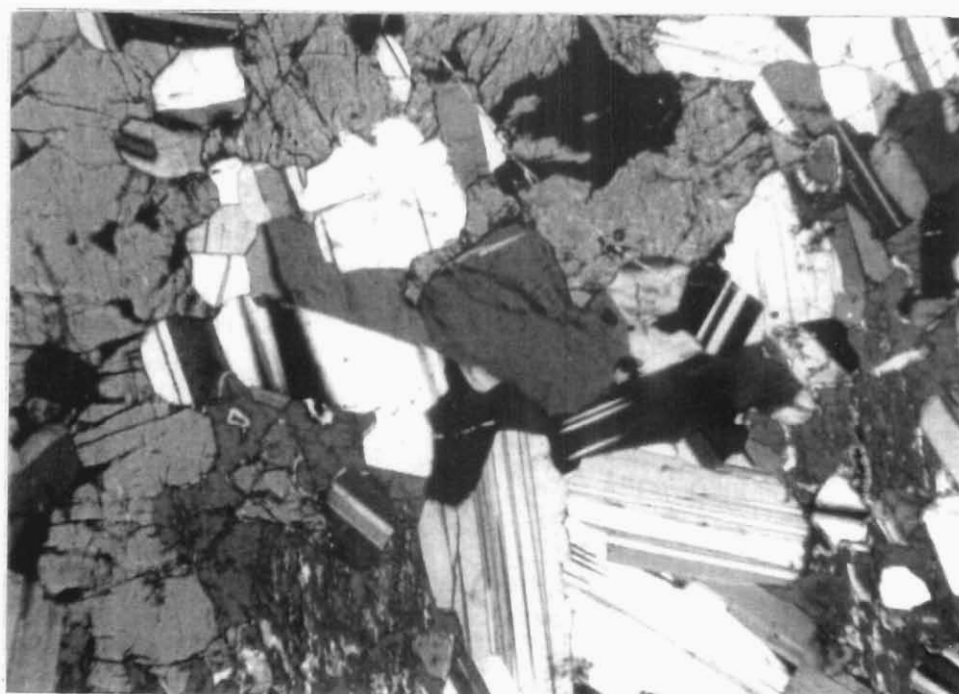
Figure 5.2   Footwall leuconorite showing typical textural
relationships between cumulus plagioclase and
intercumulus orthopyroxene and clinopyroxene.
(crossed nicols)

1mm

Figure 5.3   Footwall leuconorite with intercumulus orthopyroxene
             showing bleby clinopyroxene exsolution lamellae
             parallel to the 100 crystallographic axis.
             (crossed nicols)

1mm
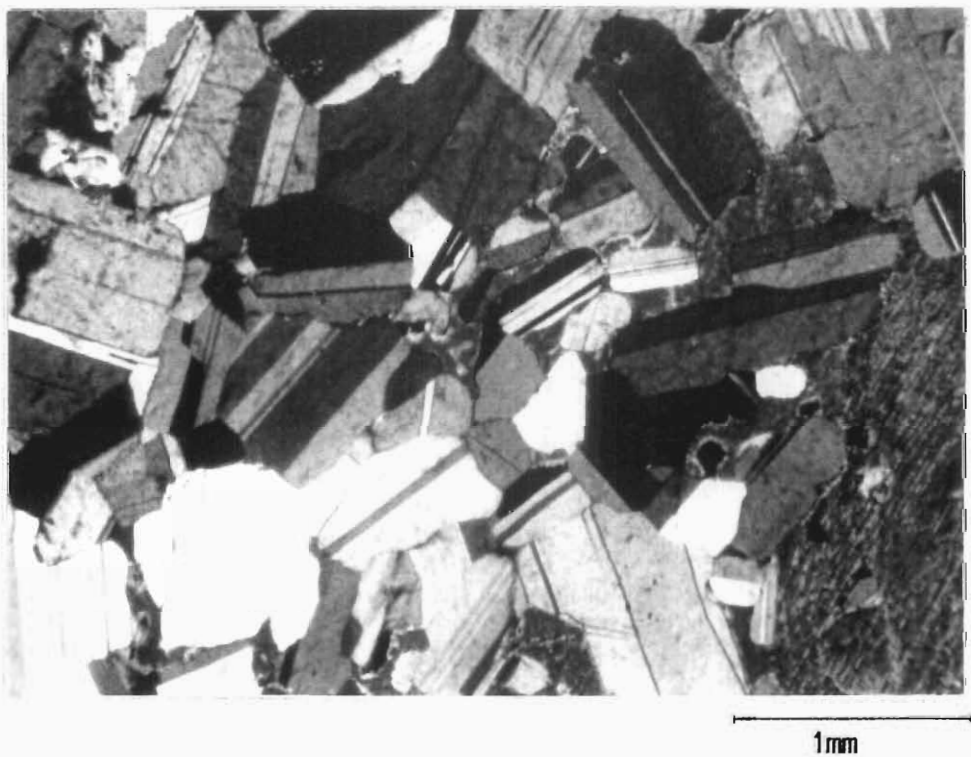
Figure 5.4   Footwall leucomorite showing a local abundance of
             interstitial phlogopite.   (crossed nicols)

5.2.1.2 Base Metal Sulphides

The frequency of BMS occurrence within the footwall leuconorite is variable, depending largely on the Merensky reef type (see Chapter 4). Except for the frequency and size of individual BMS grains, no differences have been found between BMS in thin Merensky reef footwall and BMS in thick Merensky reef footwall. Sulphide grains are generally small (≤ 2mm across) and occur as interstitial, anhedral grains and blebs. They are invariably in contact with pyroxene crystals and do not occur in the monomineralic cumulus plagioclase areas of either the leuconorite or immediate footwall anorthosite layer. Generally, the footwall anorthosite shows a paucity of BMS relative to the immediate underlying leuconorite. BMS are only observed in the anorthosite where pyroxene is present, *ie* in pyroxene anorthosite and more commonly, in poikilitic pyroxene anorthosite, where grains are very small and always in direct contact with intercumulus pyroxene. The association of phlogopite with BMS in the footwall leuconorite does occur (Figure 5.4), but far less frequently than in the overlying pyroxenites.

Pyrrhotite and chalcopyrite were identified as the main sulphide phases, pyrrhotite being the more abundant. Minor amounts of accessory bornite occur in replacement and exsolution relationships with chalcopyrite. No pentlandite or pyrite was identified. However, pentlandite usually occurs as granular veinlets, flames or lamellae in pyrrhotite and is easily identified by the fact that it is isotropic under crossed nicols (Craig & Vaughan, 1981). Pyrrhotite and chalcopyrite occur most commonly as complex bimineralic intergrowths and less frequently as discrete minerals. This texture is illustrated in Figure 5.5 in which interstitial pyrrhotite grains, in contact with orthopyroxene crystals, show minor caries-type replacement by chalcopyrite. Caries and island textures are common where chalcopyrite has replaced pyrrhotite as a subsequent phase (V.Daltry, *pers comm*). This phenomenon would appear to be in contradiction with Mostert *et al* (1982), who propose that chalcopyrite (as Cu-rich sulphide melt) was the first sulphide to unmix from the silicate magma, followed by pyrrhotite and pentlandite. They did however observe similar textures where pyrrhotite grains are rimmed by chalcopyrite.
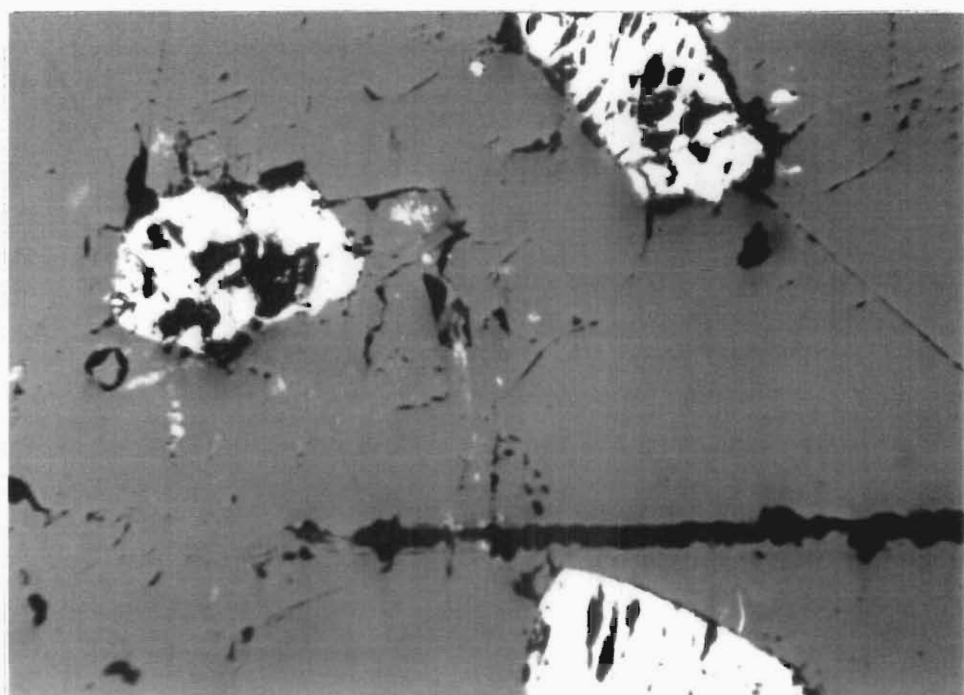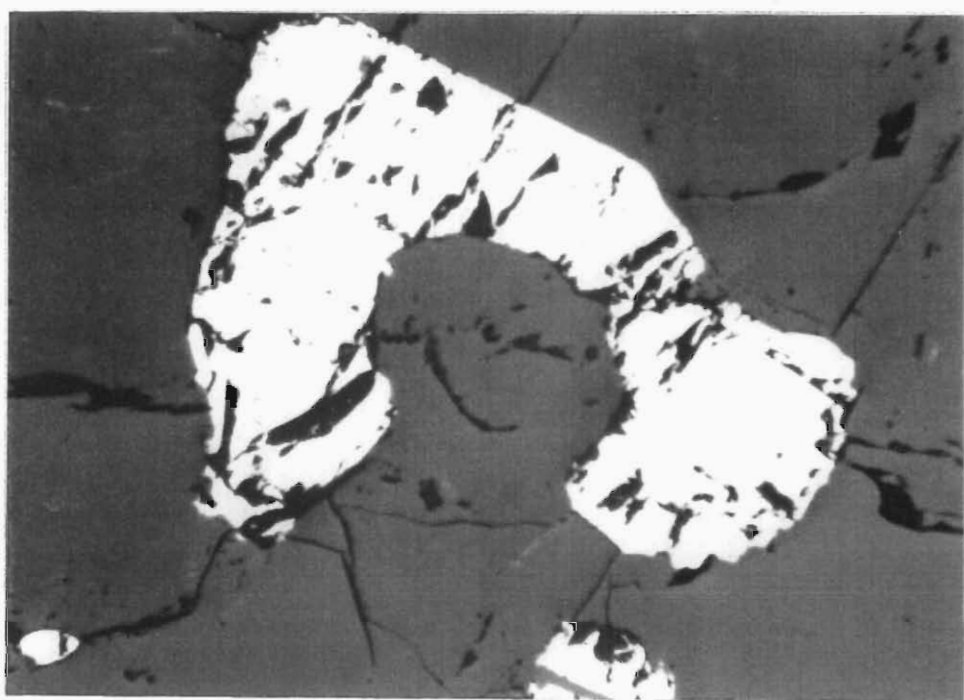
Figure 5.5   Examples of intergrown pyrrhotite and chalcopyrite, where
chalcopyrite has partially replaced pyrrhotite in footwall
leuconorite.   (plane polarised light)

5.2.2 MERENSKY REEF

5.2.2.1 Silicates

The Merensky reef is an orthocumulate consisting of a framework of very coarse-grained (pegmatoidal) cumulus subhedral to euhedral orthopyroxene crystals (with minor clinopyroxene), constituting 70 to 90% of the rock. Plagioclase, which may comprise up to 30% of the rock, occurs as an intercumulus mineral (Figures 5.6, 5.7 & 5.8). The plagioclase is invariably twinned, with albite and minor pericline twinning being the most common in the rocks studied. Orthopyroxene typically displays strong cleavage traces and expansion fractures, which are commonly occupied by serpentine and antigorite alteration veinlets (Figure 5.7). Blebby clinopyroxene exsolution lamellae developed parallel to the (100) crystallographic axis are also common. Plagioclase is also affected by local alteration as veins along expansion fractures and cleavage traces. Figure 5.9 shows alteration veinlets extending through an orthopyroxene crystal into an adjacent plagioclase crystal, suggesting that this type of alteration occurred as the result of late-stage hydration.

Abundant accessory minerals occur together with plagioclase as interstitial phases within the Merensky reef. The most abundant of these are base metal sulphides and phlogopite. Figure 5.10 shows large interstitial phlogopite occurrences, some of which are closely associated with base metal sulphides.

5.2.2.2 Chromitite Layers

The Merensky reef chromitite layers consist predominantly of cumulus anhedral to subhedral chromite grains of highly variable size (0,1 to 3mm), with both orthopyroxene and plagioclase occurring as the main interstitial minerals. Orthopyroxene tends to be the dominant interstitial mineral in the upper chromitite layers (Figure 5.11), while plagioclase is the dominant interstitial mineral in the basal chromitite layers (Figure 5.12). Textures indicate that chromite grains underwent late-stage growth. Figure 5.13 shows a basal chromitite layer in which the chromite grains have assumed amoeboid shapes and are observed in various stages of psuedoenclosure of interstitial plagioclase. Figure 5.14 shows a similar phenomenon as viewed in a polished section, where chromite grains have psuedoenclosed portions of the
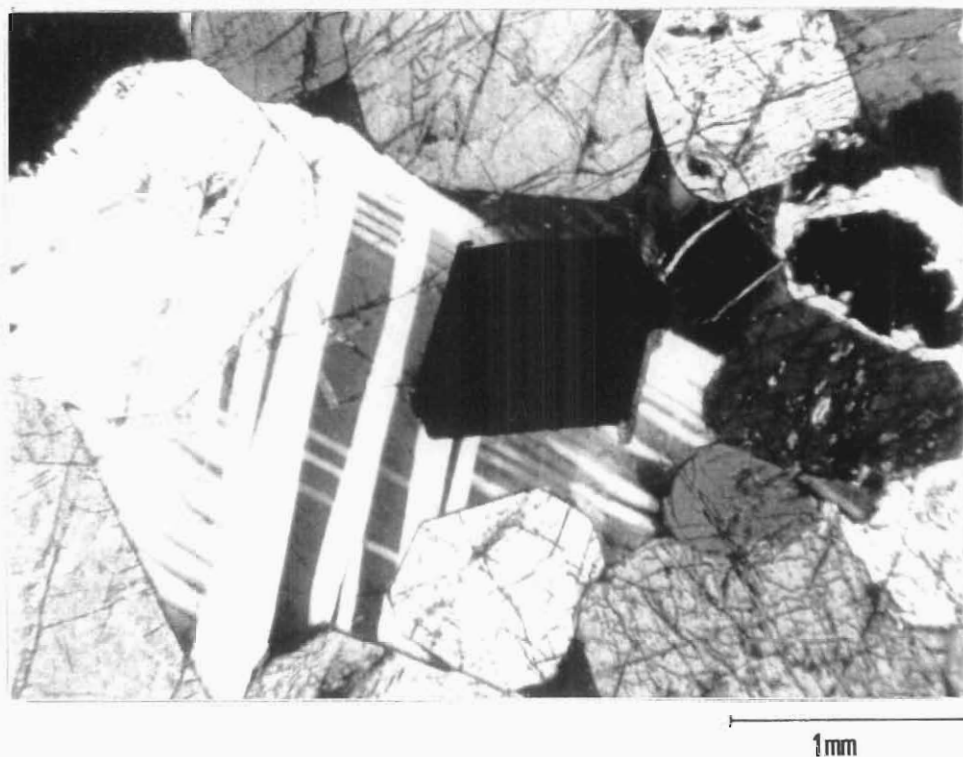
1mm

Figure 5.6   Merensky reef showing cumulus subhedral to euhedral
orthopyroxene crystals with intercumulus plagioclase
displaying both albite and pericline twinning.   Note
the interstitial euhedral BMS grain in the plagioclase.
(crossed nicols)

1mm
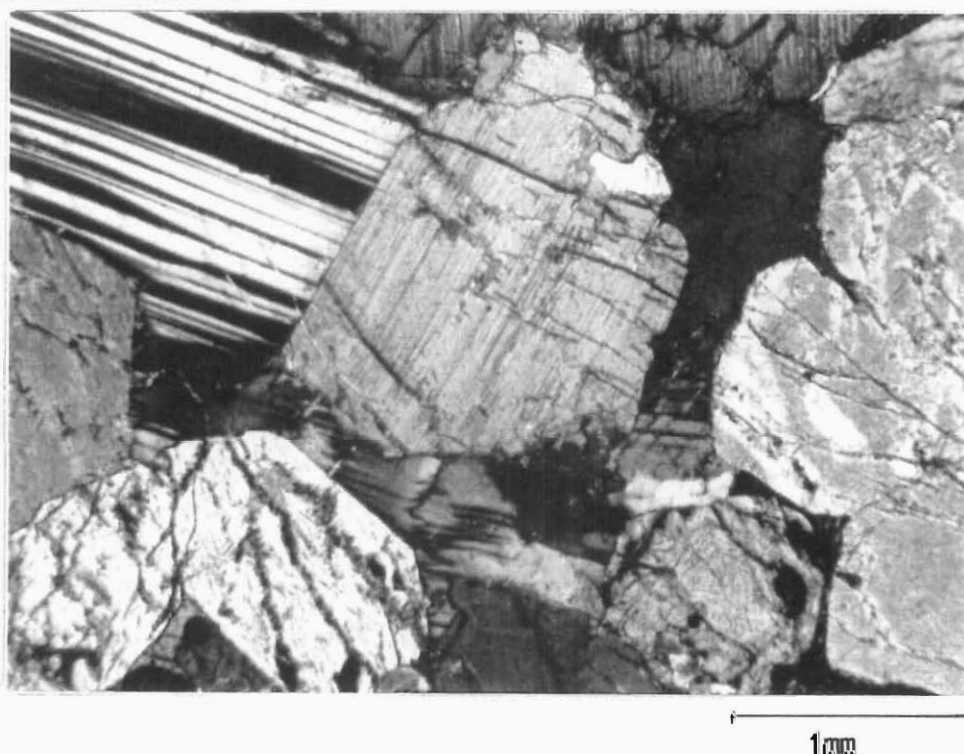
Figure 5.7   Merensky reef orthopyroxene and intercumulus plagioclase.
Note the incipient exsolution in the central orthopyroxene
crystal, the albite twinning in the plagioclase, and the
alteration veinlets in the bottom left orthopyroxene
crystals.   (crossed nicols)
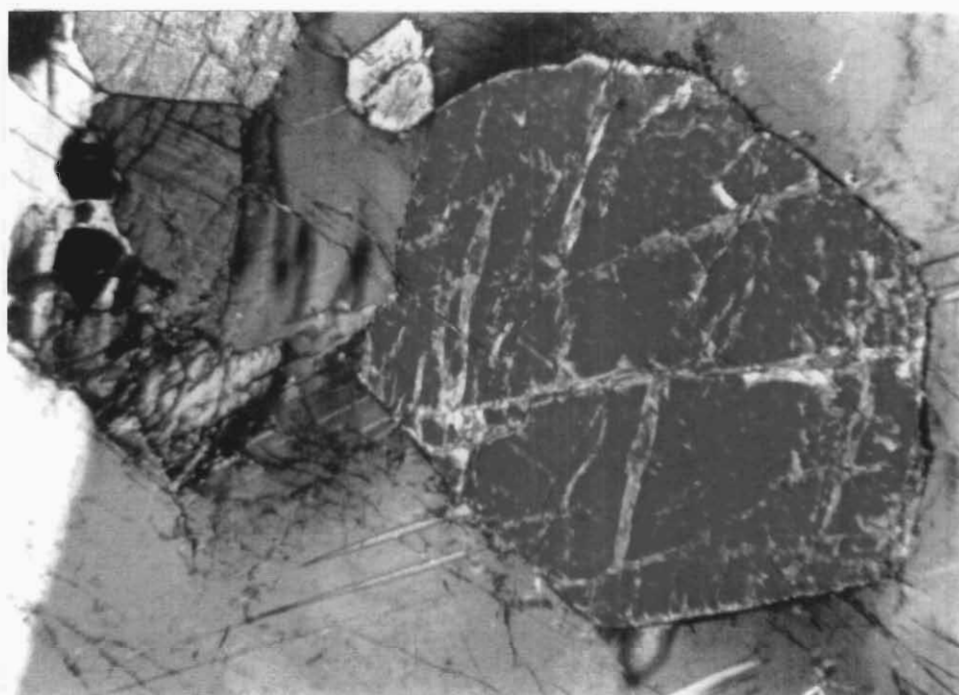
Figure 5.8   Merensky reef euhedral clinopyroxene crystal enclosed
             in intercumulus plagioclase.   (crossed nicols)
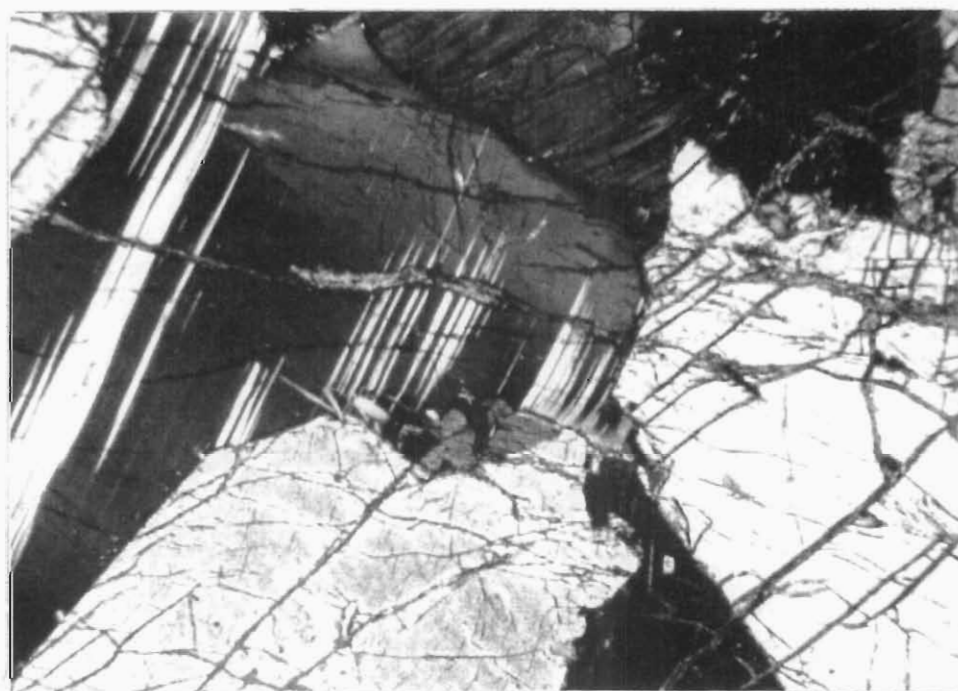
Figure 5.9   Serpentine/antigorite veinlets in plagioclase extending
             into adjacent orthopyroxene crystal.
             (crossed nicols)
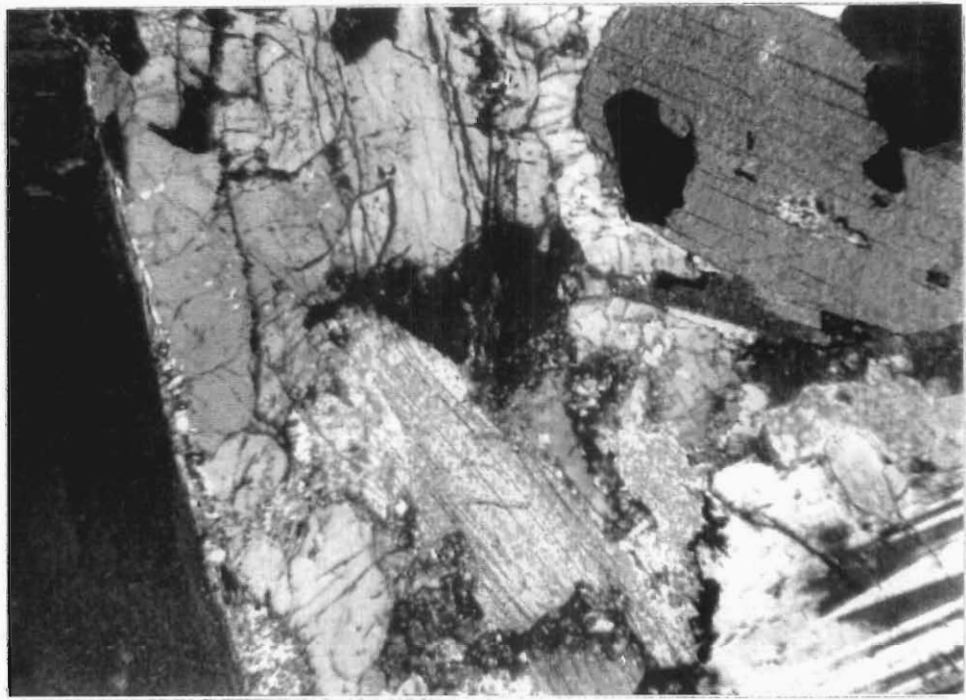
Figure 5.10   Abundant local interstitial phlogopite occurrence in the
               Merensky reef.   (crossed nicols)
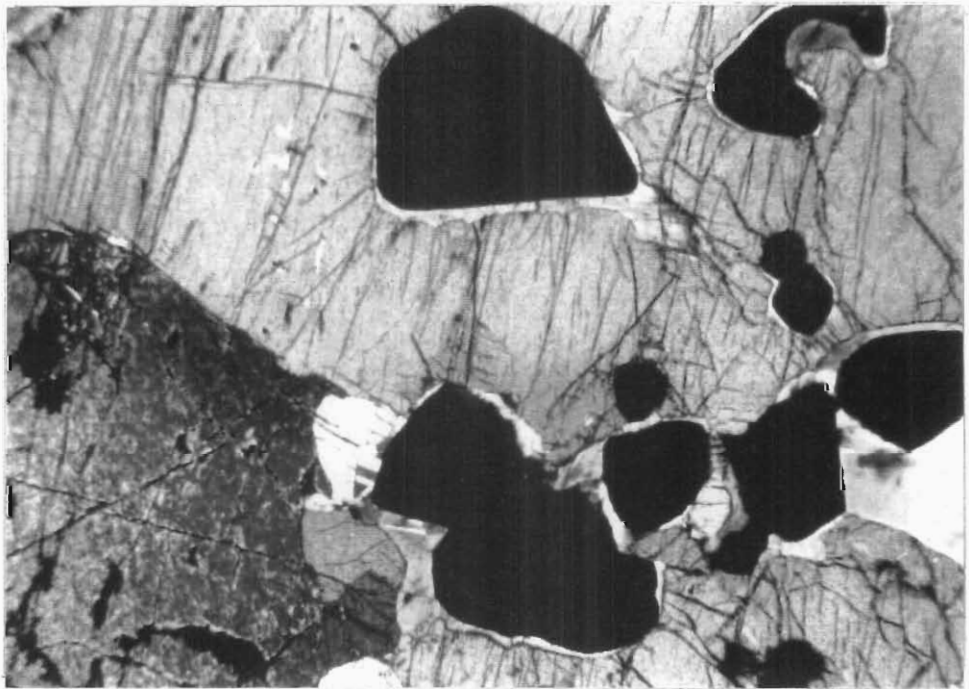
Figure 5.11   Subhedral chromite grains of a Merensky reef upper
               chromitite layer, where orthopyroxene is the dominant
               interstitial mineral.   Note the plagioclase reaction
               rims around the chromite grains.   (crossed nicols)
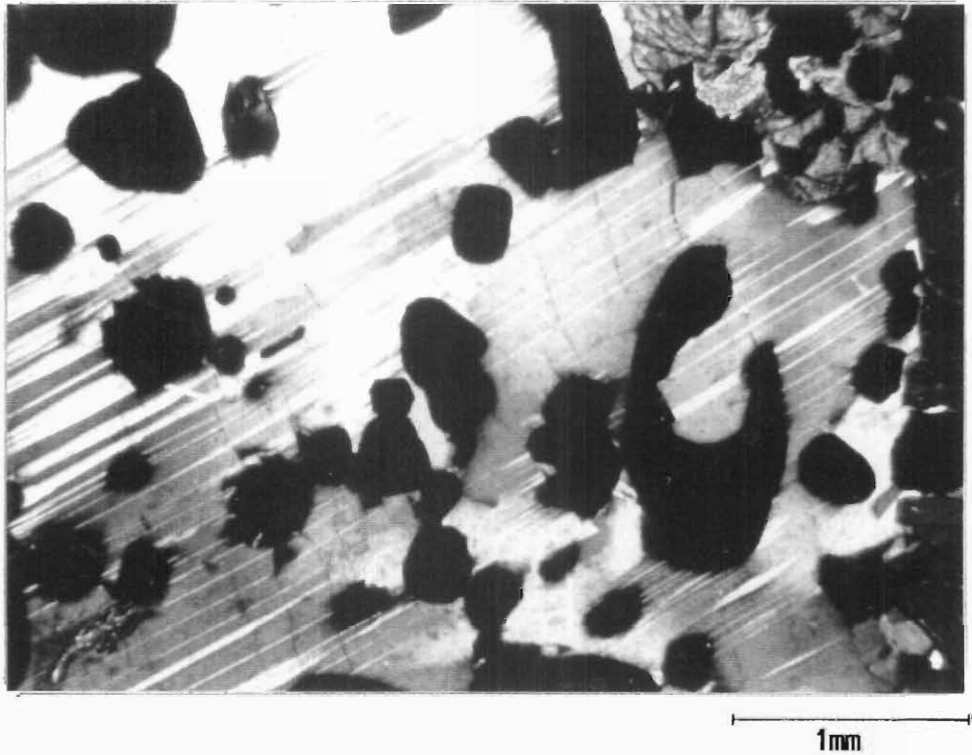
Figure 5.12   Chromite grains of a thin Merensky reef facies basal
                chromitite layer, where plagioclase is the dominant
                interstitial mineral.   (crossed nicols)
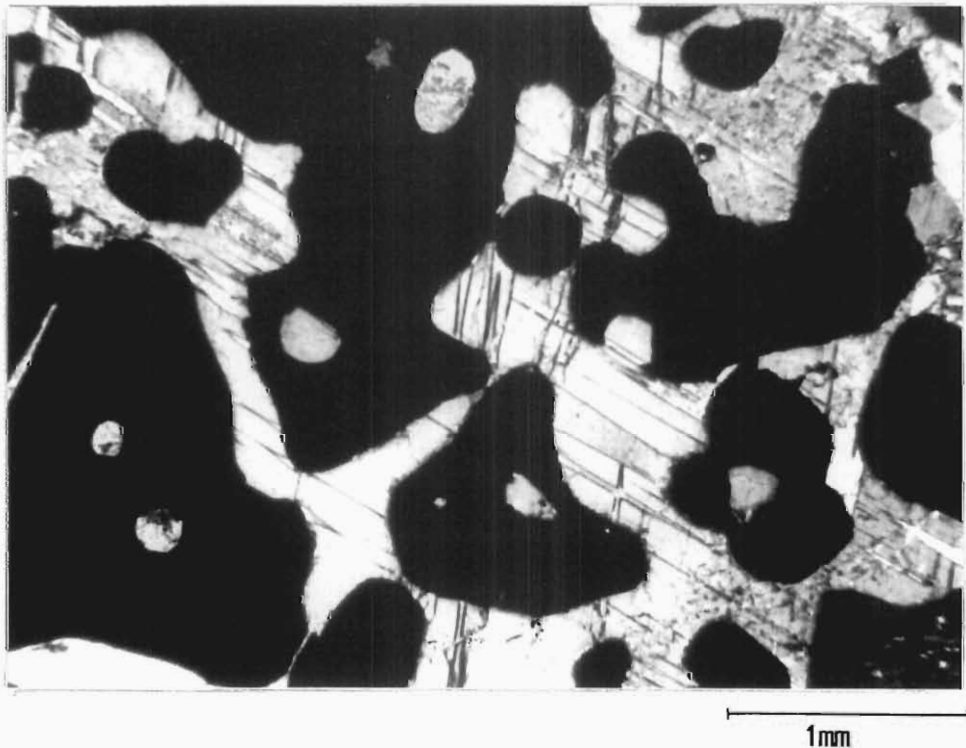
Figure 5.13   A Merensky reef basal chromitite layer showing amoeboid
                shaped chromite grains which show various stages of
                psuedoenclosure of the surrounding plagioclase.
                (crossed nicols)
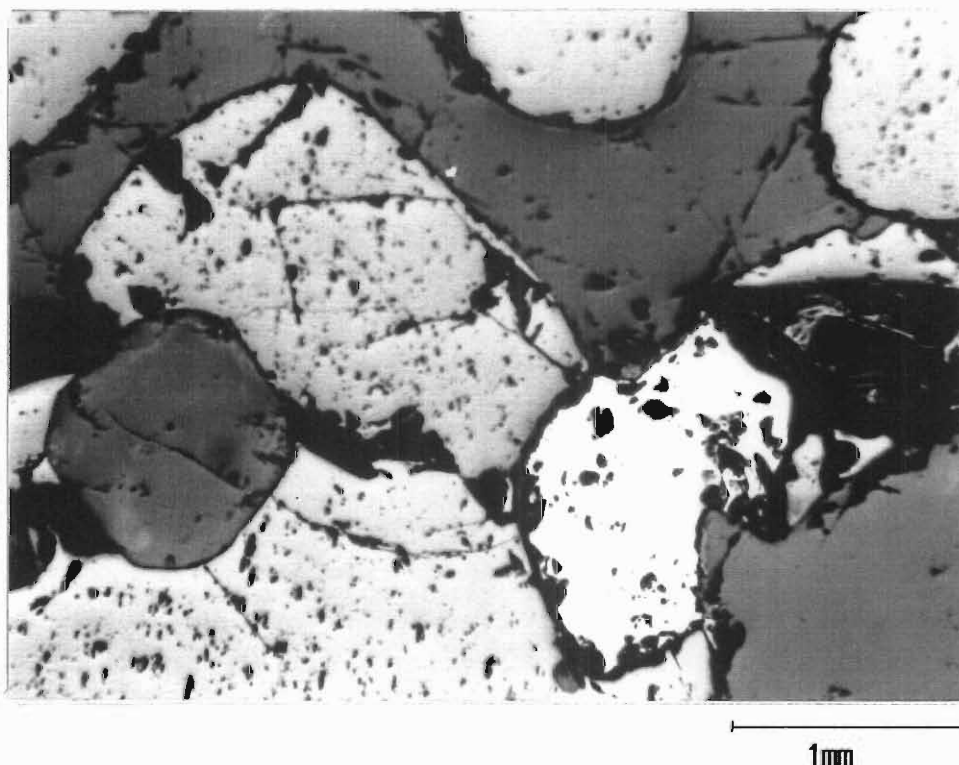
Figure 5.14   Psuedoenclosure of plagioclase (dark grey) by chromite
               (light grey).   Note the interstitial pyrrhotite grain
               (light yellow).   (plane polarised light)
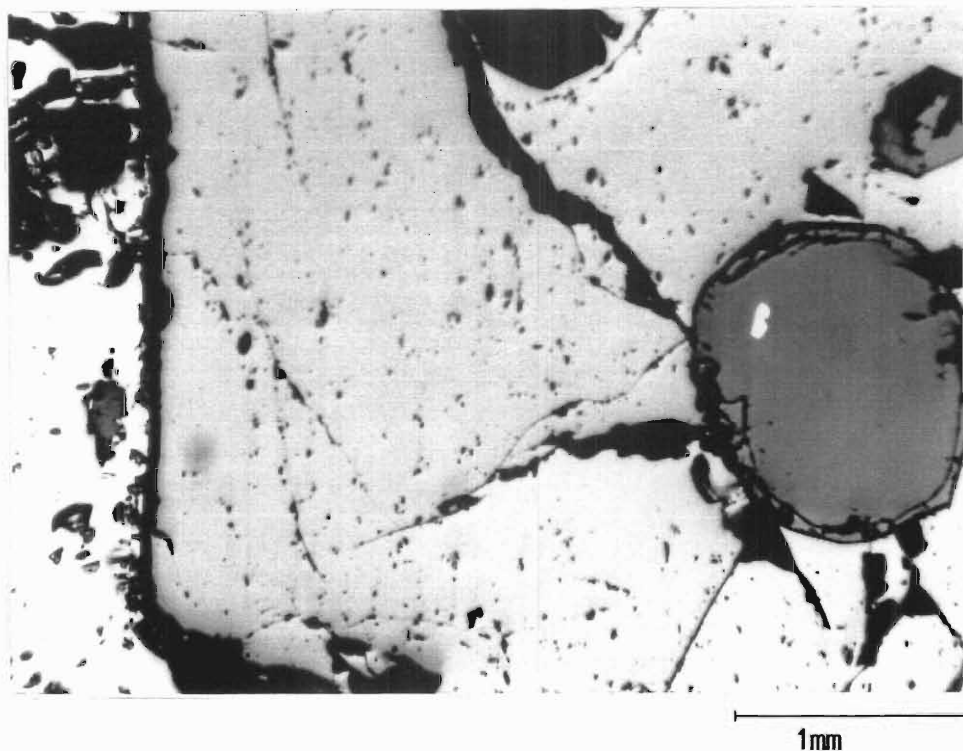
Figure 5.15   An example of total psuedoenclosure of plagioclase by
               chromite in a Merensky reef basal chromitite layer.
               Note the large pyrrhotite grain to the left of the
               chromite.   (plane polarised light)

adjacent silicate grains. Figure 5.15 shows an example of total psuedoenclosure of silicate by chromite.

5.2.2.3 Base Metal Sulphides

Base metal sulphides are variably abundant in the Merensky reef and occur throughout, irrespective of reef thickness. They range greatly in size from $\leq 0,005mm$ to about 7cm and occur as anhedral grains, blebs or masses. The spatial and textural mode of occurrence is variable.

The most common and volumetrically significant occurrence of BMS is one in which the sulphide minerals are interstitial to the cumulus pyroxenes. In this situation the BMS are in spatial competition with intercumulus plagioclase and various late-stage phases (Figures 5.16 & 5.17). Here the BMS are either in contact with both pyroxene and plagioclase, or they are wholly enclosed in plagioclase. The interstitial BMS comprise the larger grain-size occurrences. The close spatial association between interstitial BMS and phlogopite is typical of the Merensky reef throughout the Bushveld Complex (Figures 5.18 & 5.19).

The Merensky reef base metal sulphides identified in this study consist only of pyrrhotite and chalcopyrite and show a wide variety of textures including exsolution and various replacement phenomena. Figure 5.20 shows an interstitial pyrrhotite grain with well developed twinning parallel to the (100) crystallographic axis, and lamellar replacement by chalcopyrite. Figure 5.21 shows typical caries and island texture replacement of pyrrhotite by chalcopyrite. Lamellar exsolution of monoclinic pyrrhotite in hexagonal pyrrhotite is also common (Figure 5.22). Lamellar exsolution of chalcopyrite also occurs in pyrrhotite (Figure 5.23). Spectacular examples of almost total replacement of pyrrhotite by chalcopyrite are common, where only relict islands of pyrrhotite remain within the chalcopyrite (Figures 5.24 & 5.25).

To a lesser extent, BMS are also hosted by the chromitite layers. BMS grain size is typically much smaller and they are about as much interstitial to the typically amoeboid chromite grains as they are psuedoenclosed by them. Both plagioclase and orthopyroxene are commonly enclosed along with BMS grains. Figure 5.26 shows a chalcopyrite grain psuedoenclosed in chromite, while the adjacent orthopyroxene crystal contains an intergrowth of pyrrhotite and
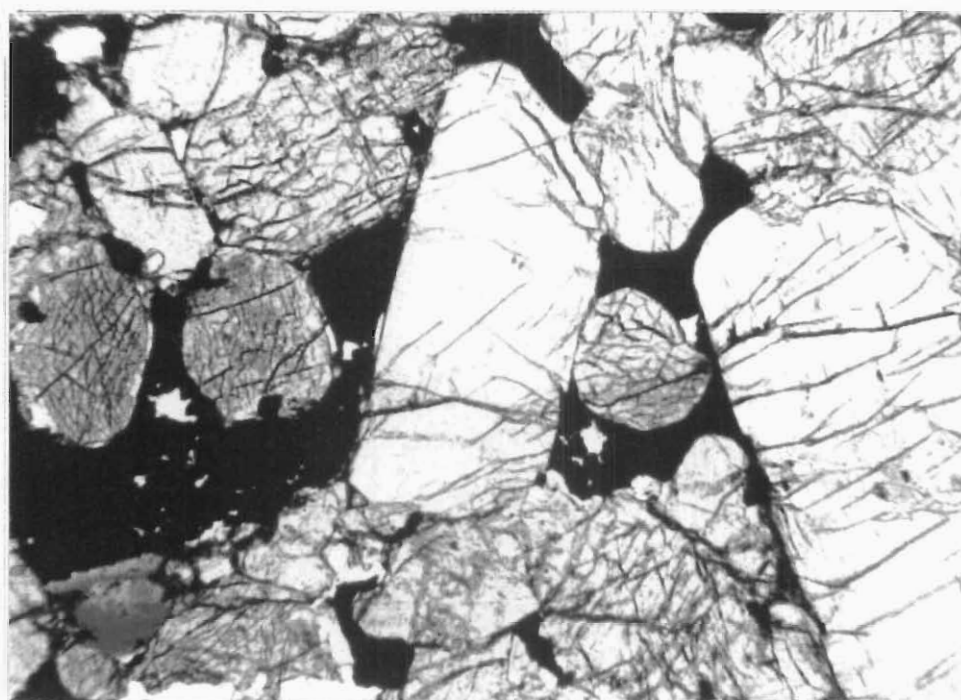
(plane polarised light)   1mm
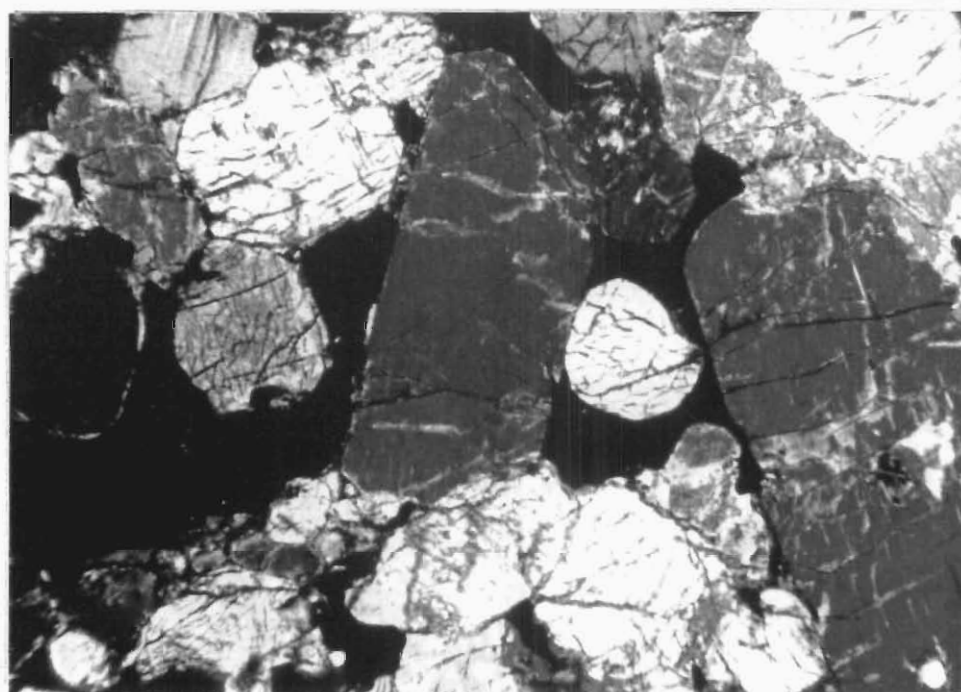
(crossed nicols)   1mm

Figure 5.16   Base metal sulphide occupying interstitial space between cumulus orthopyroxene and clinopyroxene crystals of the Merensky reef.
(BMS isotropic)
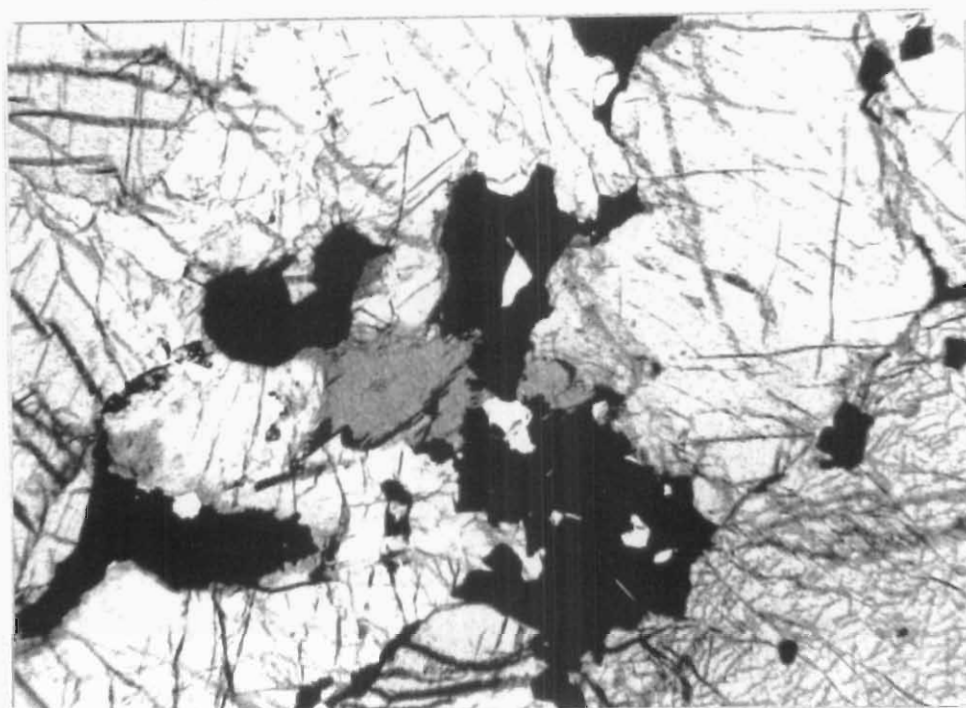
(plane polarised light)   1mm
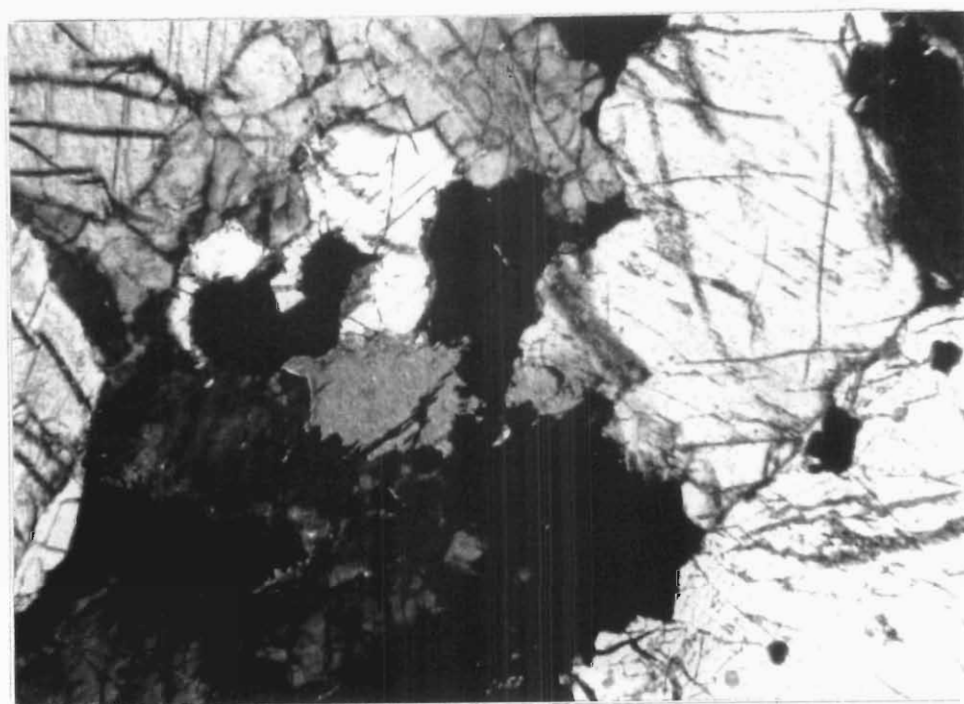
(crossed nicols)   1mm

Figure 5.17   Base metal sulphide and phlogopite occupying interstitial
               space between cumulus orthopyroxene of the Merensky reef.
               (BMS isotropic)
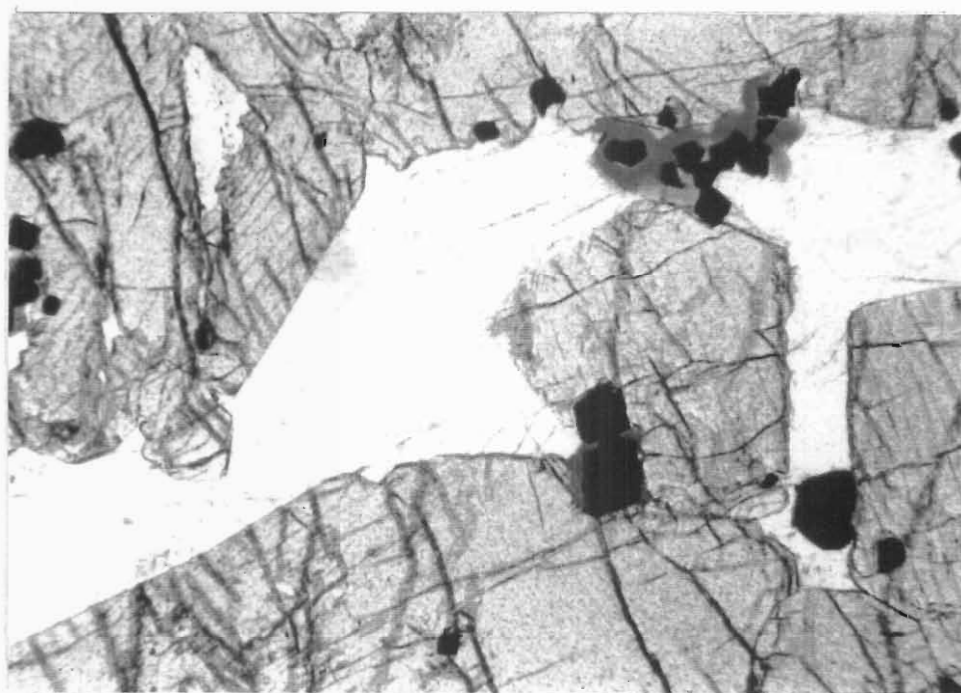
(plane polarised light)   1mm
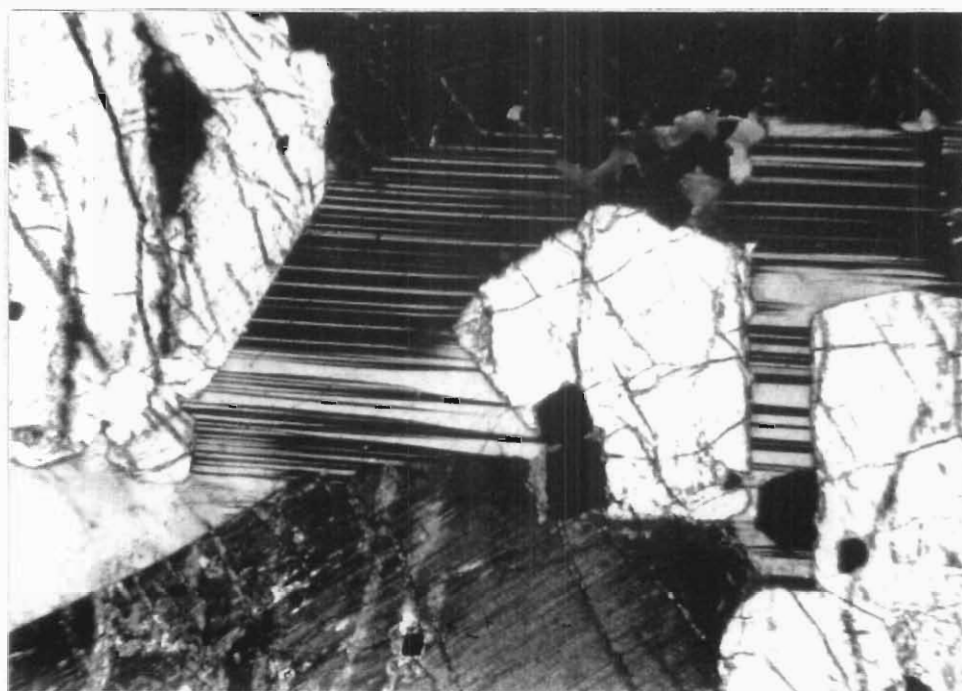
(crossed nicols)   1mm

Figure 5.18   Interstitial BMS grains associated with phlogopite.
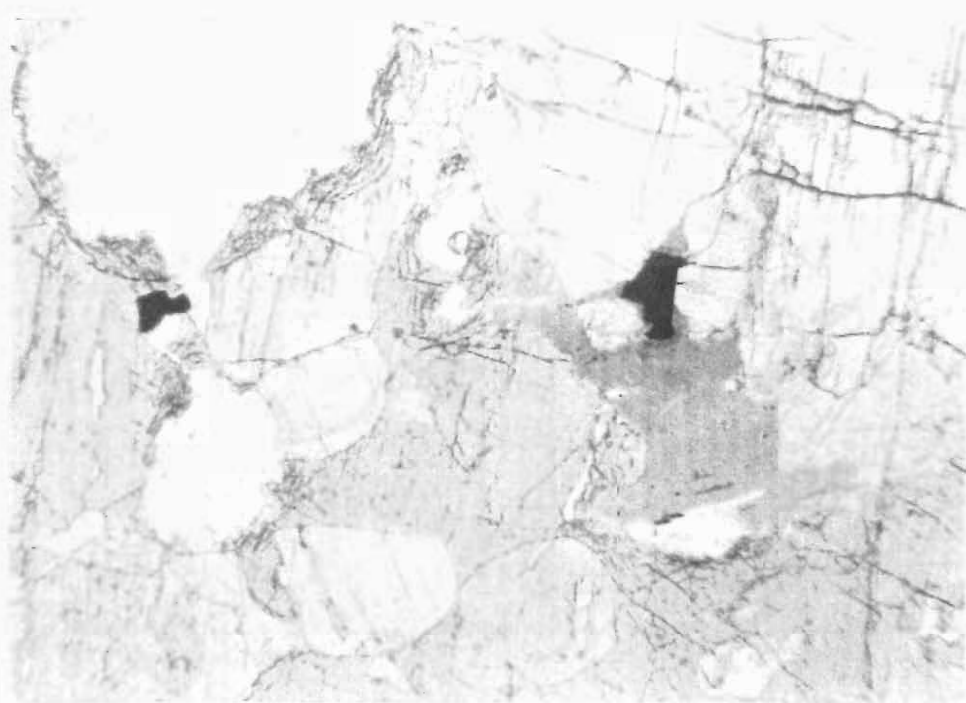
(plane polarised light)   1mm
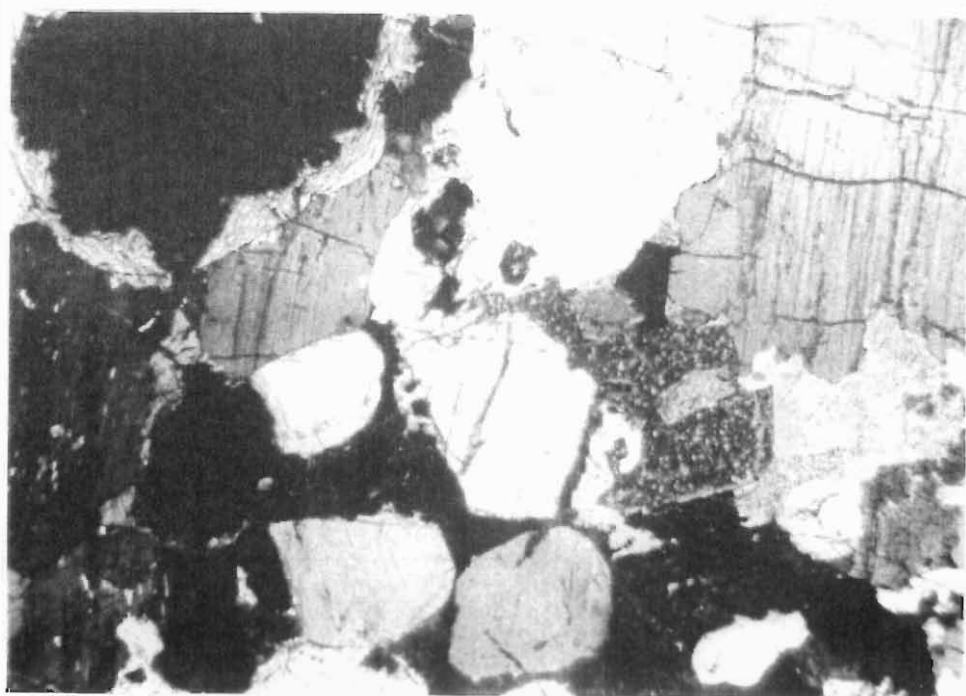
(crossed nicols)   1mm

Figure 5.19   An example of the commonly observed close spatial
               association between BMS and phlogopite in the
               Merensky reef.

1mm
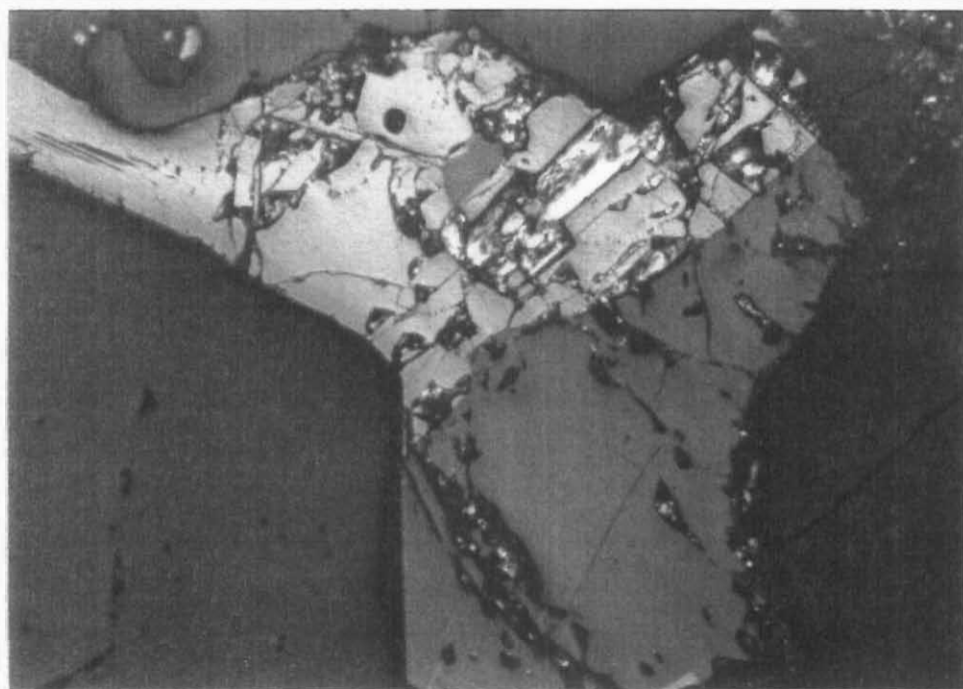
Figure 5.20   Interstitial pyrrhotite grain showing twinning parallel
to the (100) crystallographic axis, and some minor
replacement by chalcopyrite.   (crossed nicols)

1mm
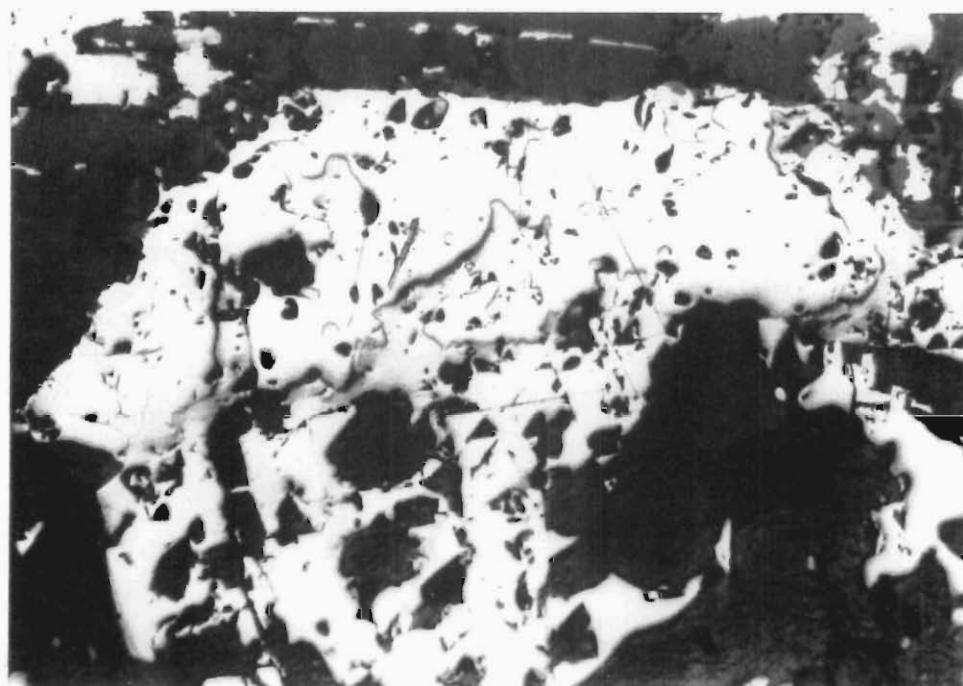
Figure 5.21   Replacement intergrowth of pyrrhotite (light yellow)
and chalcopyrite (darker yellow).
(plane polarised light)
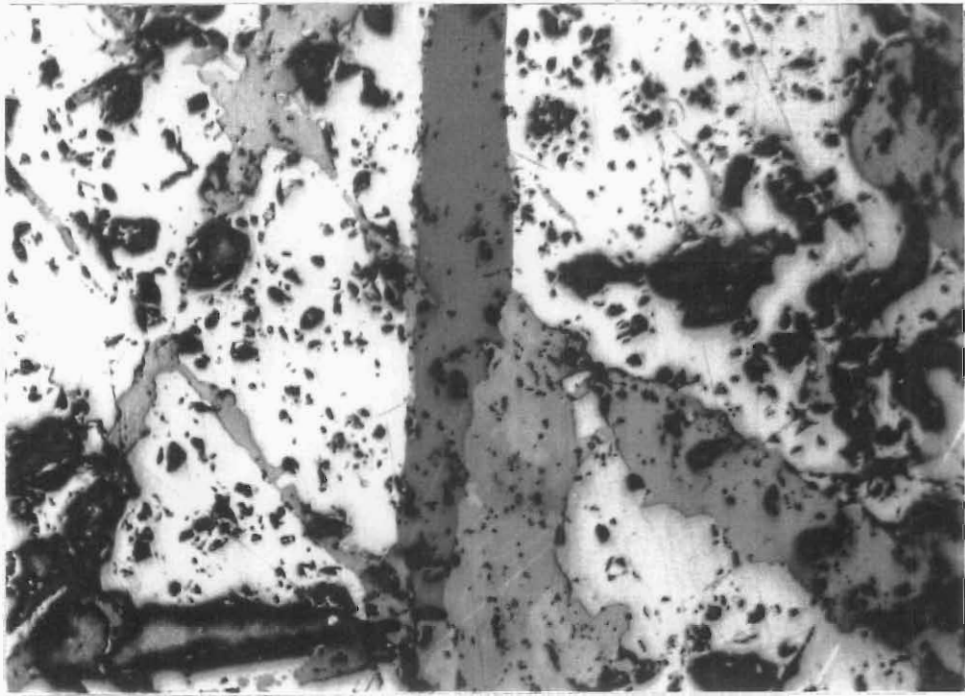
1mm

Figure 5.22   Lamellar exsolution of monoclinic pyrrhotite (brown
               pleochroism) in hexagonal pyrrhotite (light yellow
               pleochroism).   The red-brown pleochroic mineral is
               chalcopyrite.   (crossed nicols)
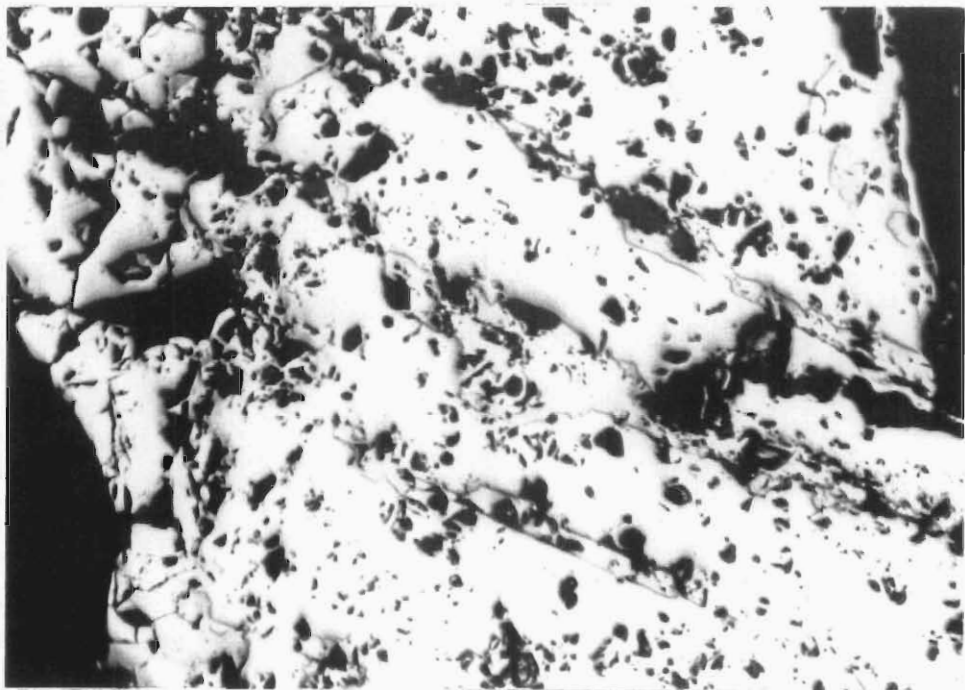
1mm

Figure 5.23   Lamellar replacement of pyrrhotite (light yellow) by
               chalcopyrite (darker yellow).
               (plane polarised light)
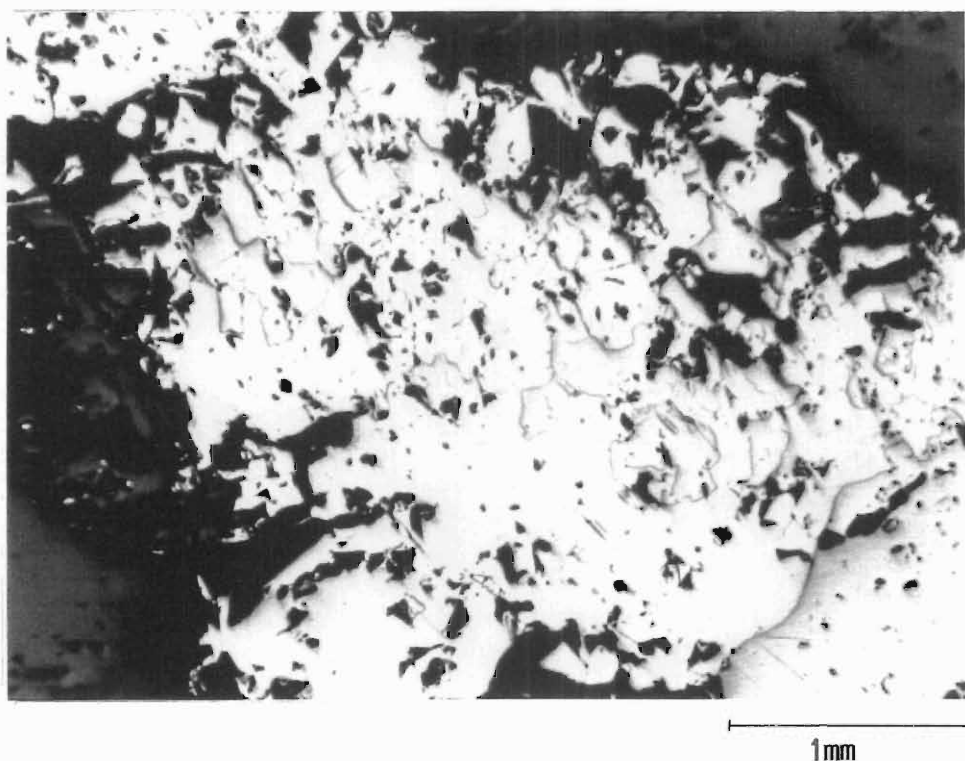
1mm

Figure 5.24   An example of almost total replacement of pyrrhotite
               by chalcopyrite, resulting in relict islands of
               pyrrhotite.   (plane polarised light)
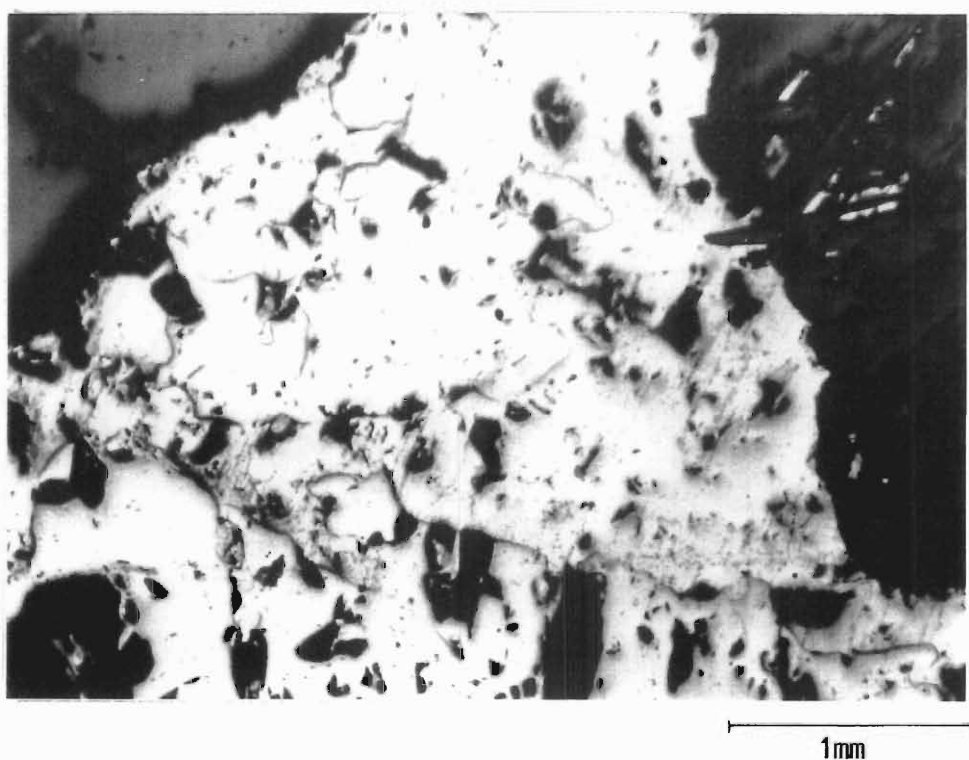
1mm

Figure 5.25   Another example of near complete replacement of
               pyrrhotite by chalcopyrite.   Remnant islands of
               pyrrhotite remain scattered throughout the
               chalcopyrite.   (plane polarised light)

1mm
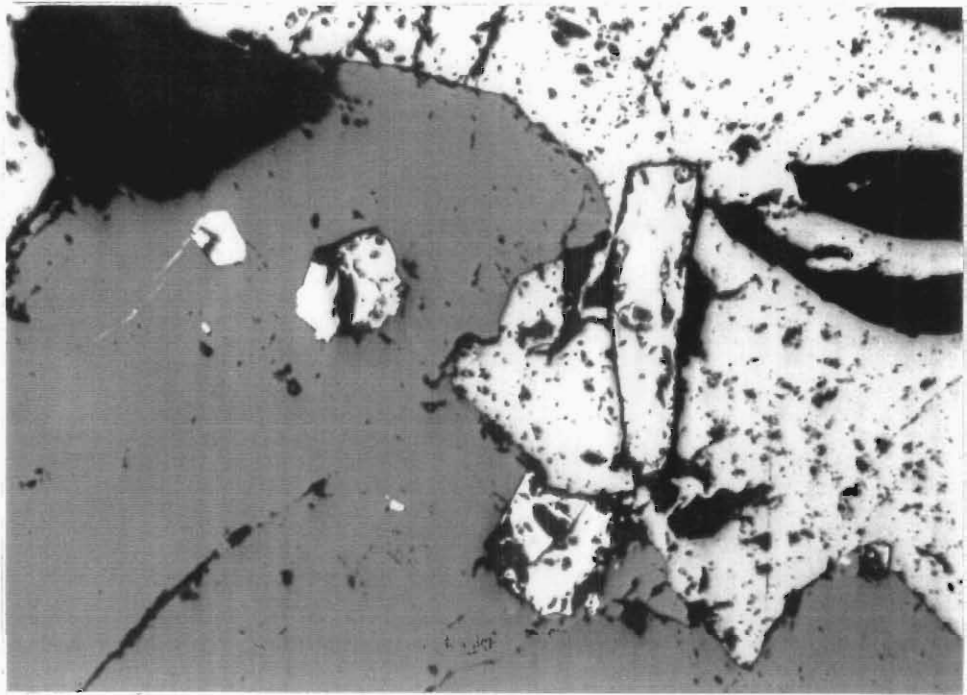
Figure 5.26   Rectangular-shaped chalcopyrite grain enclosed in a
              chromite grain (light grey-brown) of a Merensky reef
              basal chromitite layer.   The adjacent plagioclase
              crystal encloses pyrrhotite and chalcopyrite
              intergrowths.   (plane polarised light)
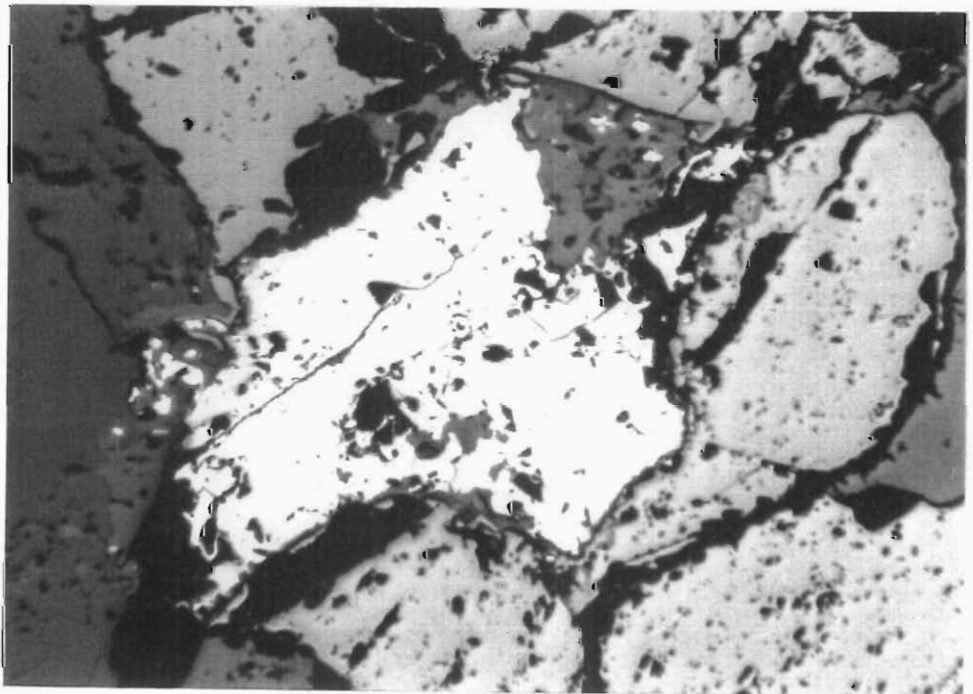
1mm

Figure 5.27   Interstitial chalcopyrite-pyrrhotite intergrowth in a
              Merensky reef basal chromitite layer.
              (plane polarised light)

chalcopyrite. Figures 5.27 and 5.28 show interstitial intergrowths of pyrrhotite and chalcopyrite in chromitite layers.

Less frequently still, small BMS grains are wholly enclosed within cumulus orthopyroxene. They occur either as lone anhedral to subhedral grains or blebs, or with small amounts of plagioclase which presumably crystallised from intercumulus liquid trapped during adcumulus orthopyroxene crystallisation (Figure 5.29, 5.30 & 5.31). These observations would appear to be in direct conflict with those of Ballhaus & Stumpfl (1986, p202), who state that, 'nowhere in the normal Reef have early separated sulfides been found as inclusions in cumulus orthopyroxene'.

BMS also occur as elongate blebs (similar in appearance to exsolution lamellae) developed along orthopyroxene cleavage planes (Figures 5.32 & 5.33). It is likely that this texture represents a late-stage phenomenon involving remobilised BMS. This phenomenon has also been noted in the mineralised rocks of the Great Dyke (Coghill & Wilson, 1993).

5.2.3 MERENSKY PYROXENITE

5.2.3.1 Silicates

The typically medium-grained, relatively homogeneous feldspathic orthopyroxenite which comprises the orthocumulus Merensky pyroxenite, consists of a framework of subhedral to euhedral cumulus orthopyroxene crystals (Figure 5.34). Plagioclase occurs interstitially to the pyroxene, where it shares space with base metal sulphides and late-stage phases such as phlogopite (Figures 5.34 & 5.35).

5.2.3.2 Base Metal Sulphides

Base metal sulphide occurrence within the Merensky pyroxenite is similar to that of the Merensky reef, in that grains consist of intercumulus, anhedral blebs which compete with plagioclase and late-stage accessory minerals for interstitial space, often to the total exclusion of plagioclase (Figure 5.36). However, BMS grain size is generally smaller than that of the
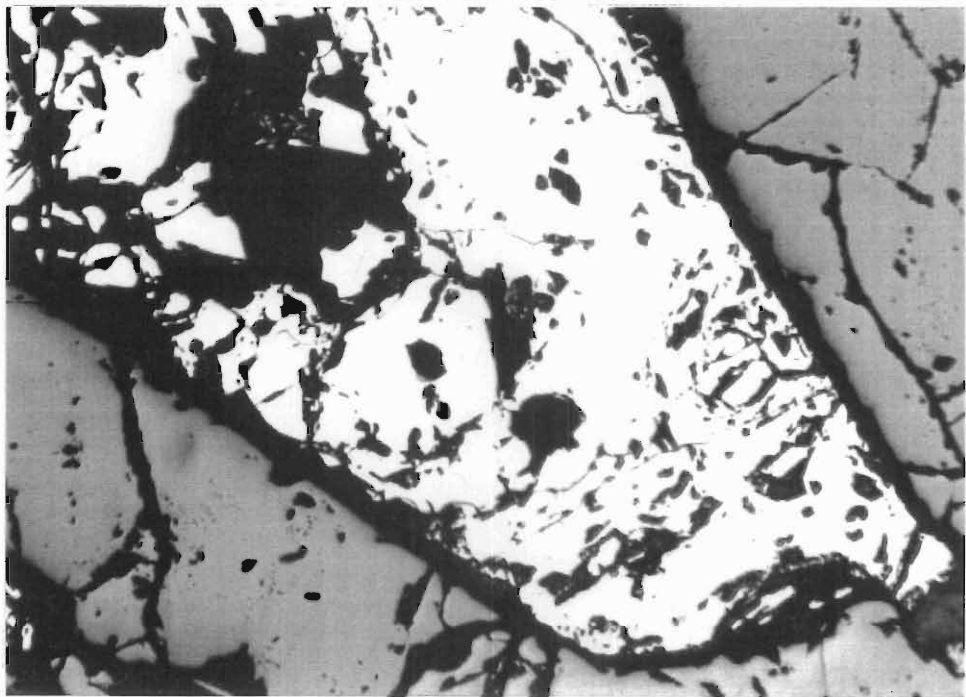
0,5mm

Figure 5.28   Intergrowth of pyrrhotite (pink-yellow) and chalcopyrite
                (yellow) interstitial to chromite grains of a Merensky
                reef basal chromitite layer.
                (plane polarised light)
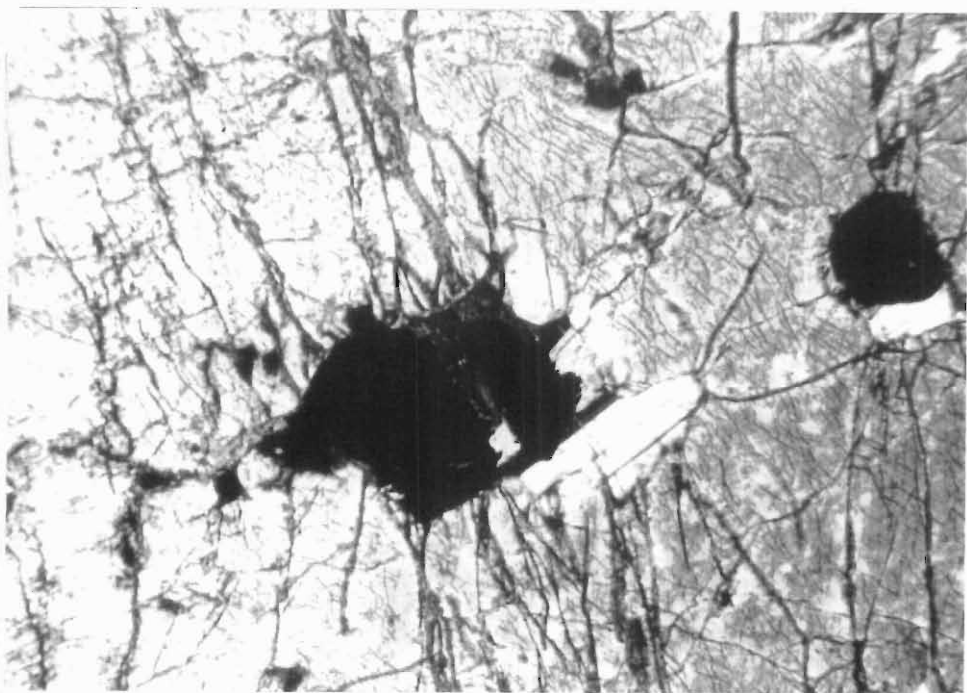
1mm

Figure 5.29   Base metal sulphide grains, plus minor plagioclase and
                phlogopite, enclosed within a cumulus pegmatoidal
                orthopyroxene crystal of the Merensky reef.
                (crossed nicols)
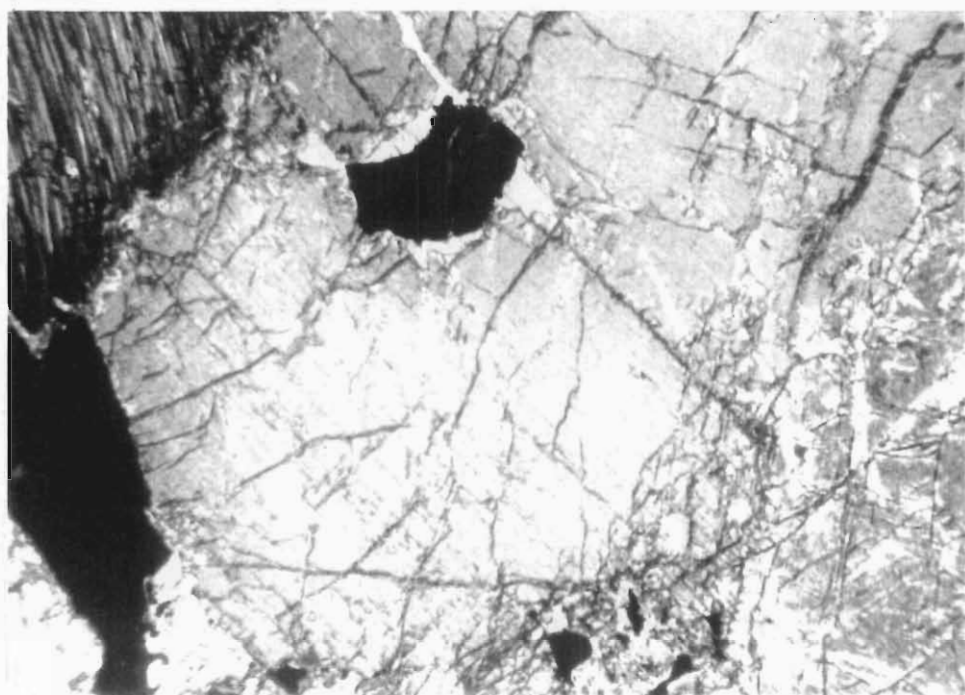
1mm

Figure 5.30   A base metal sulphide grain and some associated phlogopite
enclosed within a cumulus pegmatoidal orthopyroxene
crystal of the Merensky reef.   (crossed nicols)
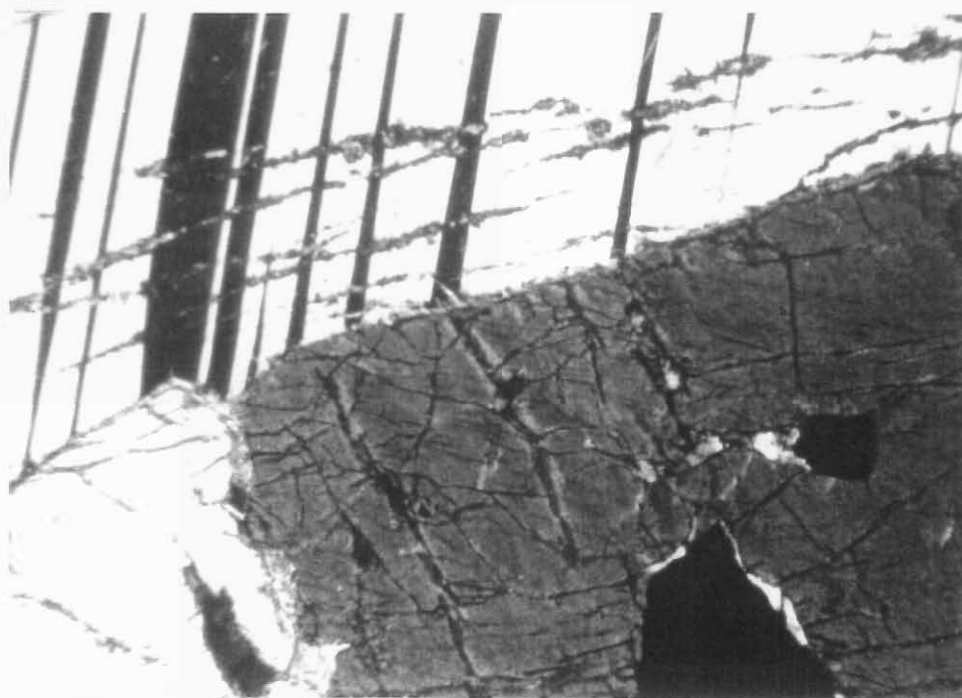
1mm

Figure 5.31   A base metal sulphide grain with a small amount of
plagioclase enclosed in a pegmatoidal orthopyroxene
crystal of the Merensky reef.   Note the alteration
in the orthopyroxene and particularly the adjacent
plagioclase crystal.   (crossed nicols)
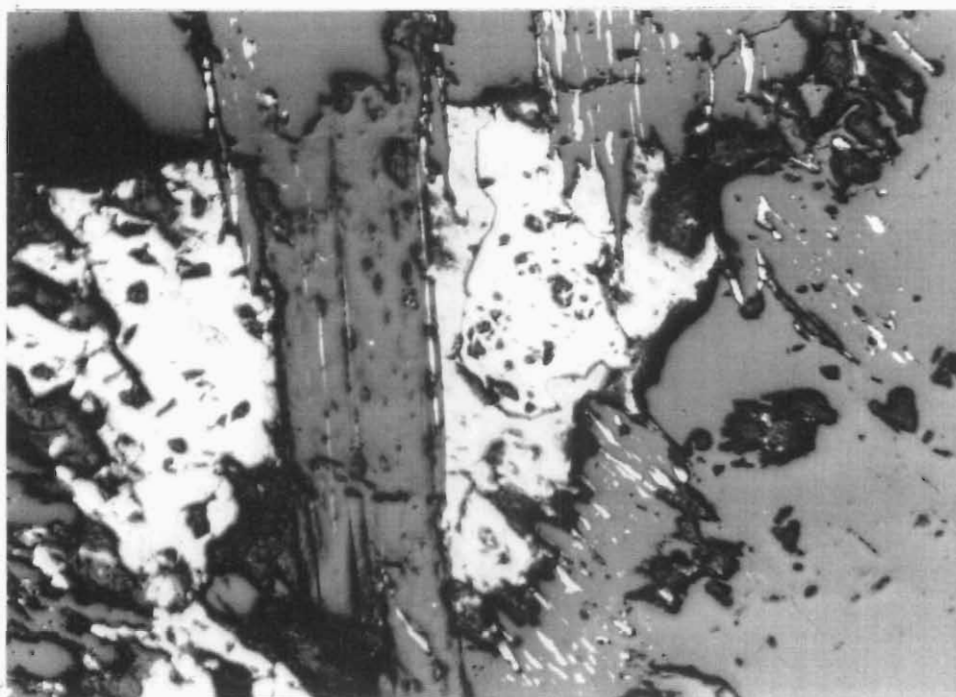
Figure 5.32   Interstitial pyrrhotite grains showing advanced caries
               replacement by chalcopyrite.   Note the small, elongate
               remobilised? chalcopyrite grains developed along cleavage
               planes in the adjacent orthopyroxene crystals.
               (plane polarised light)

Figure 5.33   Large interstitial pyrrhotite grain showing some caries
               replacement by chalcopyrite.   The adjacent orthopyroxene
               crystal contains secondary? elongate blebs of
               chalcopyrite developed along cleavage planes.
               (plane polarised light)
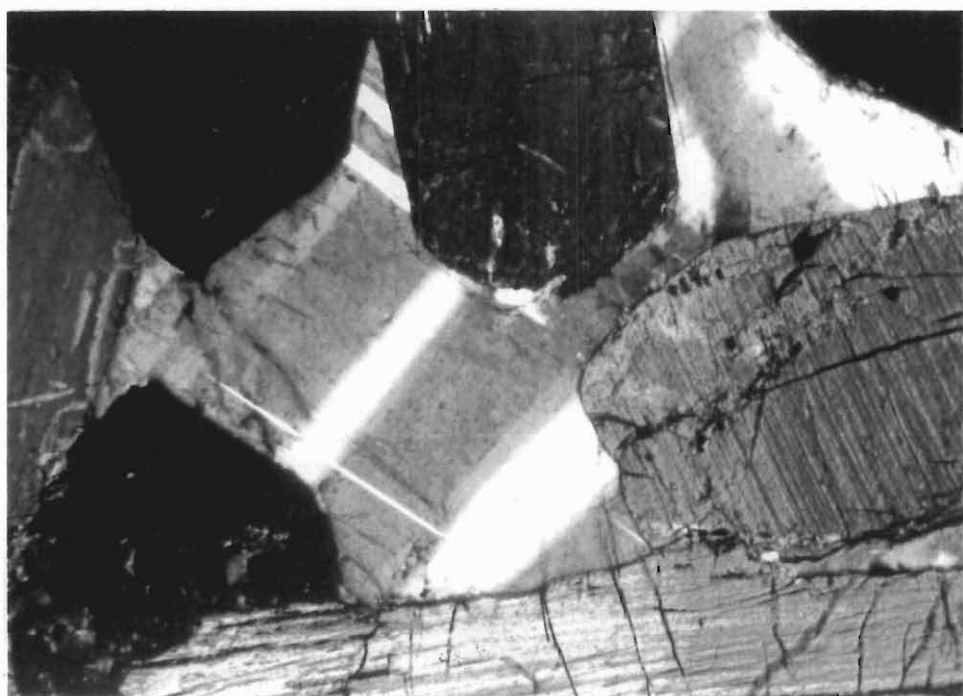
1mm

Figure 5.34   Subhedral to euhedral cumulus orthopyroxene and
               intercumulus plagioclase crystals of the Merensky
               pyroxenite.   Note the albite and pericline twinning
               in the plagioclase.   (crossed nicols)

1mm
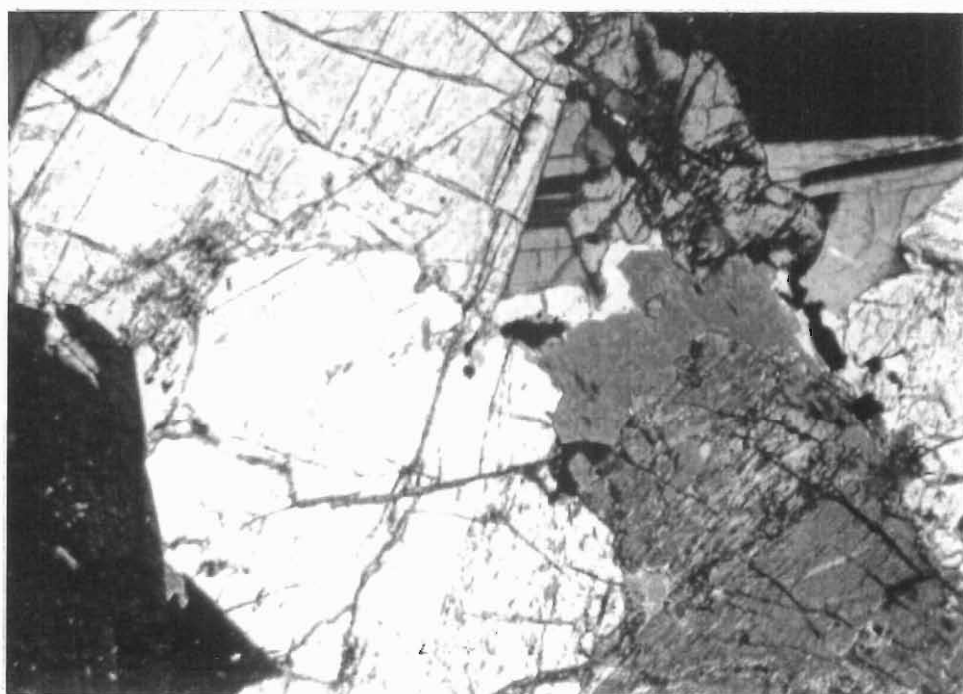
Figure 5.35   Subhedral cumulus orthopyroxene and intercumulus
               plagioclase and phlogopite of the Merensky pyroxenite.
               (crossed nicols)
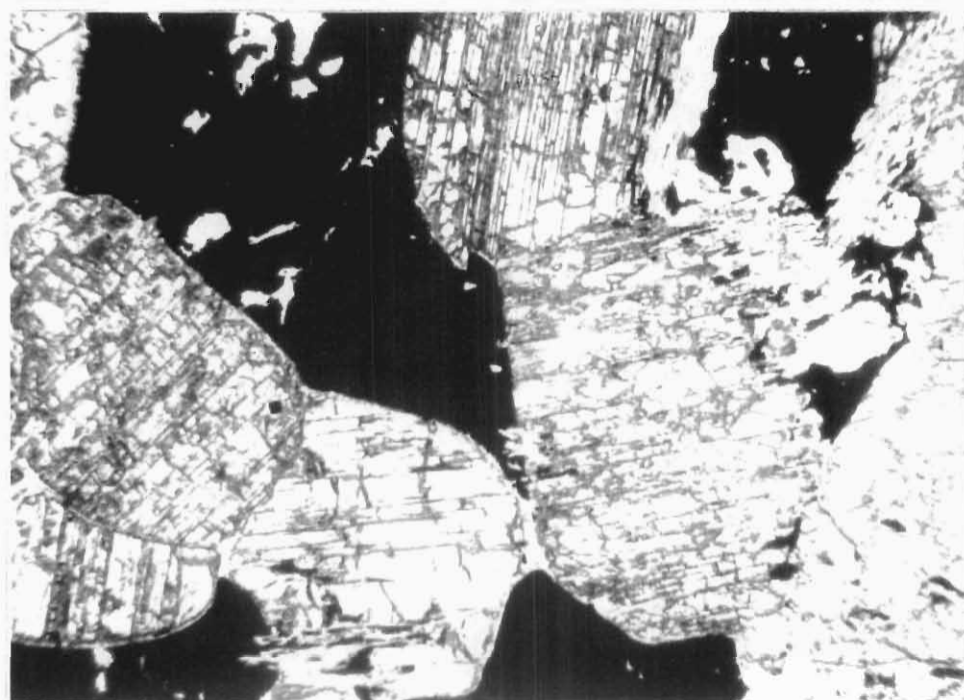
(plane polarised light)　　　　　　　　　　1mm
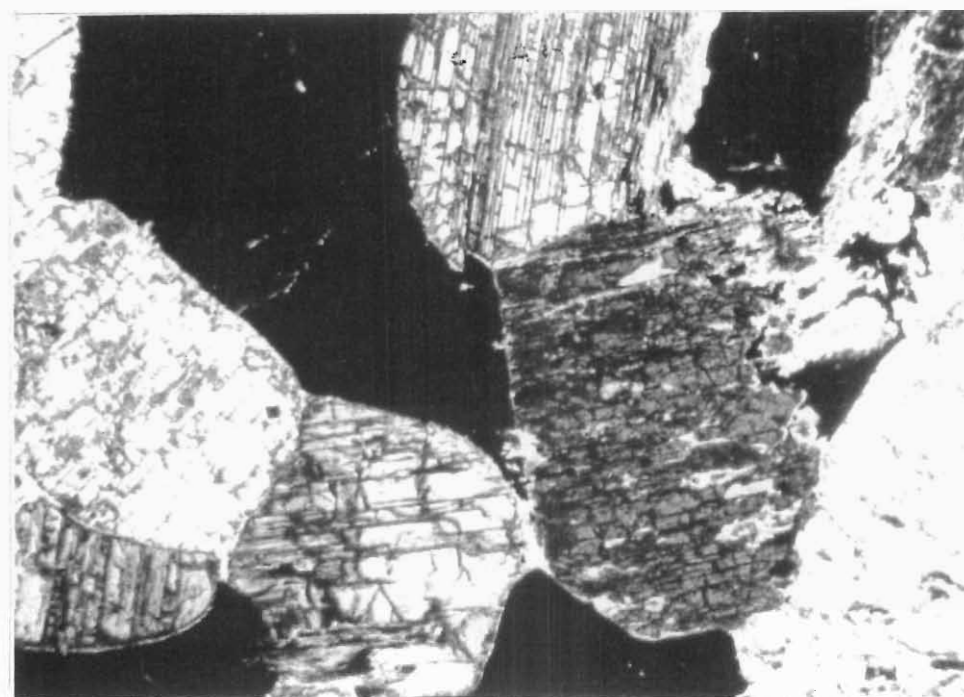
(crossed nicols)　　　　　　　　　　　　1mm

Figure 5.36　　Merensky pyroxenite cumulus orthopyroxene with
　　　　　　　　interstitial base metal sulphide developed to the
　　　　　　　　total exclusion of plagioclase.

underlying Merensky reef due to the more restricted interstitial space. In this study, only pyrrhotite and chalcopyrite were identified in the Merensky pyroxenite. Similarly to the Merensky reef, the BMS show a variety of textures involving the replacement of pyrrhotite by chalcopyrite. Figure 5.37 shows an interstitial chalcopyrite grain in plagioclase containing relict islands of pyrrhotite. Caries texture replacement of pyrrhotite by chalcopyrite is also commonly observed (Figure 5.38). Figures 5.39 and 5.40 show examples of small, irregularly shaped chalcopyrite grains enclosed in intercumulus plagioclase.

5.2.4 HANGINGWALL NORITE/LEUCONORITE/PYROXENE ANORTHOSITE

The hangingwall norite, which, over a very short vertical distance grades into leuconorite, is microtexturally very similar to the footwall leuconorite, except for the fact that no BMS are observed, as is shown in Figure 5.41. The overlying pyroxene anorthosite is a medium-grained plagioclase orthocumulate typically containing less than 10% combined intercumulus orthopyroxene and clinopyroxene (Figure 5.42). Plagioclase crystals are twinned, with Carlsbad and albite twinning being the most common. No BMS have been observed in the hangingwall pyroxene anorthosite.

5.3 CONCLUSIONS

The rocks of the Merensky Unit studied here all consist of differing proportions of a limited range of minerals, primarily orthopyroxene and plagioclase, with subordinate clinopyroxene. The norites and leuconorites are composed primarily of cumulus plagioclase and a lesser amounts of both cumulus and intercumulus pyroxene. Other interstitial phases include minor quantities of phlogopite and base metal sulphides, which are generally situated within ± 1m of the Merensky reef in the case of the footwall leuconorite. No base metal sulphides have been observed in the hangingwall norites and overlying pyroxene anorthosite.

The Merensky reef is a pegmatoidal orthopyroxene cumulate containing abundant BMS, the majority of which is interstitial. Minor amounts of BMS have been observed to be enclosed in cumulus orthopyroxene and remobilised into orthopyroxene cleavage planes. Both the silicate minerals and BMS minerals show abundant evidence for submagmatic and hydromagmatic
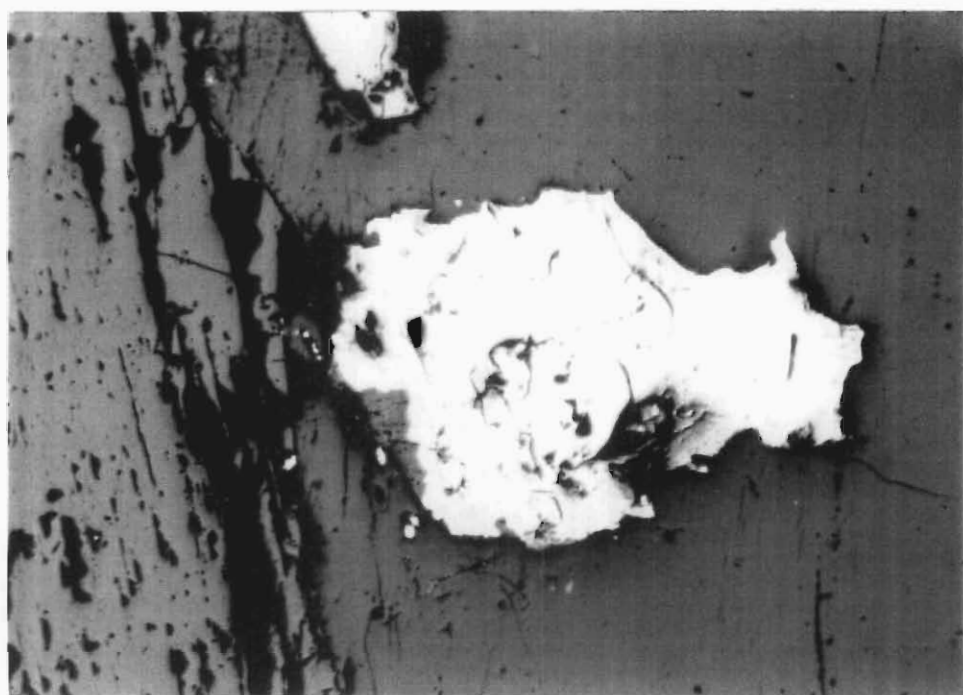
1mm

Figure 5.37   Intergrown pyrrhotite and chalcopyrite grain in
                intercumulus plagioclase, and in contact with cumulus
                orthopyroxene crystal to the left.   Note the remnant
                islands of pyrrhotite within the chalcopyrite.
                (plane polarised light)
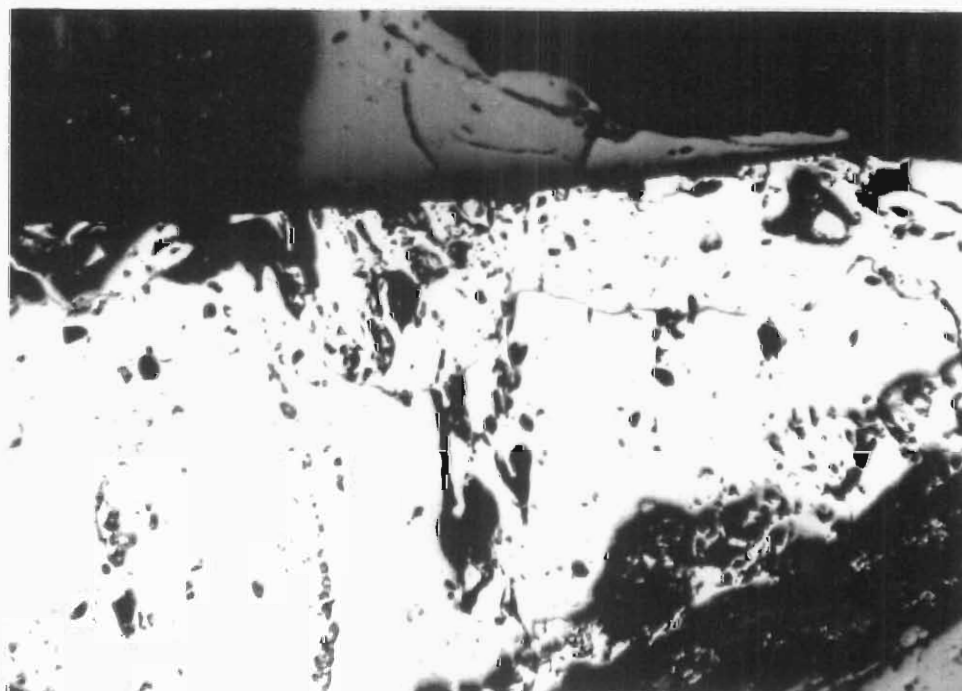
1mm

Figure 5.38   Chalcopyrite replacing large pyrrhotite grain.   The
                replacement front shows the typical caries texture.
                (plane polarised light)
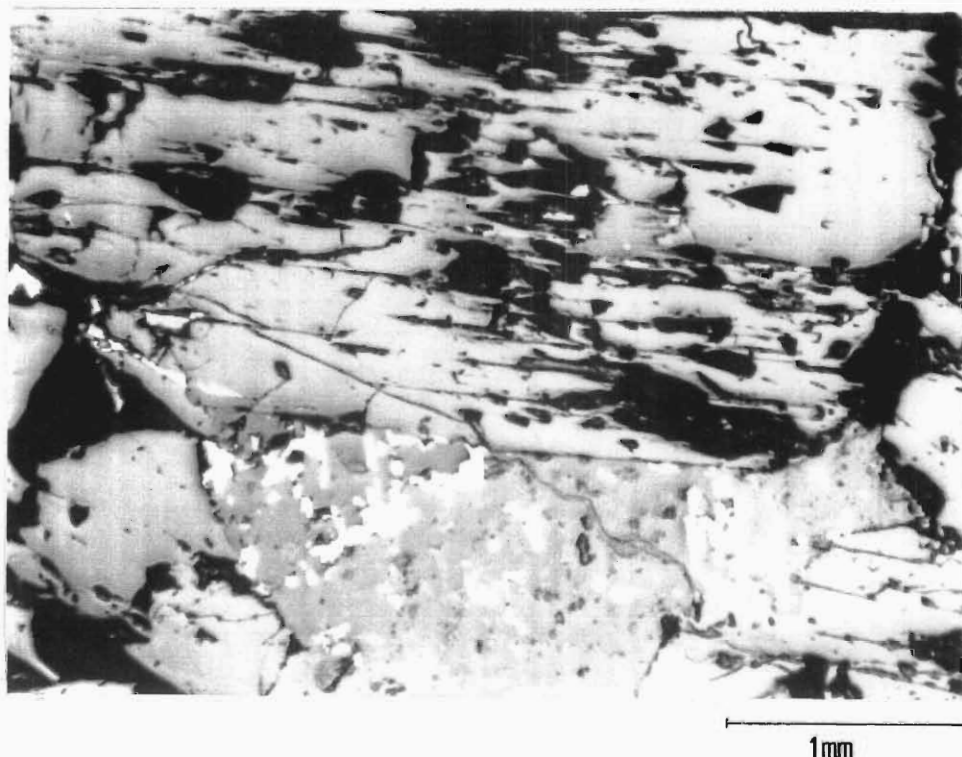
1mm

Figure 5.39   Numerous small chalcopyrite grains enclosed in
                intercumulus plagioclase, with a few elongate grains
                occupying cleavage planes of the adjacent cumulus
                orthopyroxene crystal.   (plane polarised light)

1mm
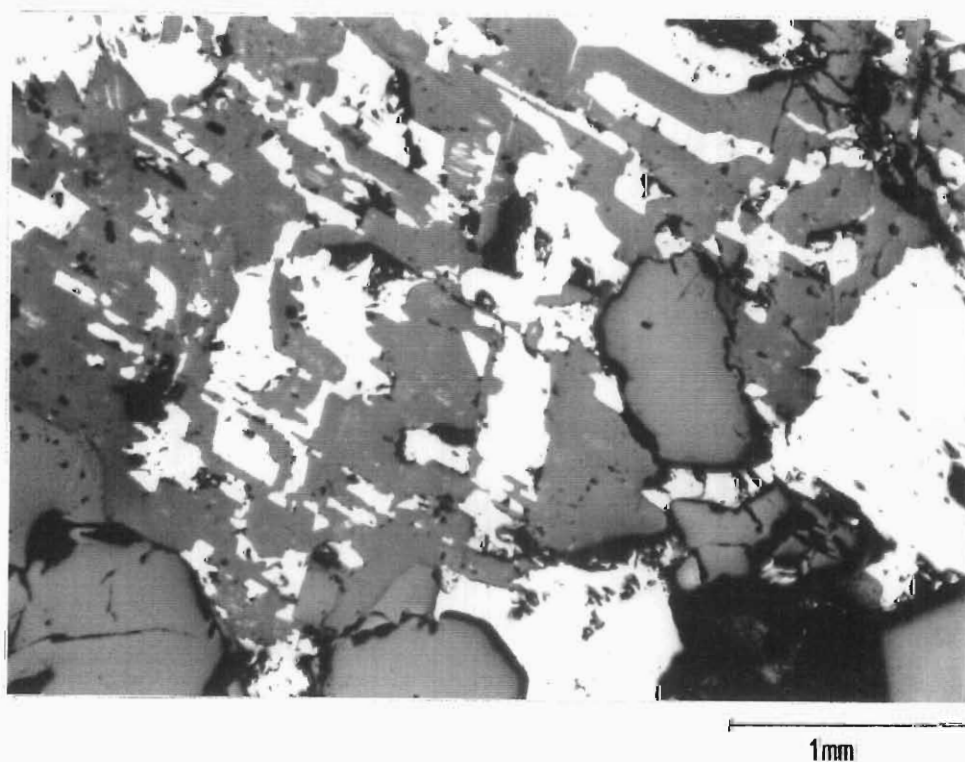
Figure 5.40   Numerous irregularly-shaped chalcopyrite grains enclosed
                by intercumulus plagioclase.
                (plane polarised light)

1mm

Figure 5.41   Cumulus plagioclase and intercumulus orthopyroxene and
                clinopyroxene of the hangingwall leuconorite.   Note
                the albite and Carlsbad twinning in the plagioclase.
                (crossed nicols)
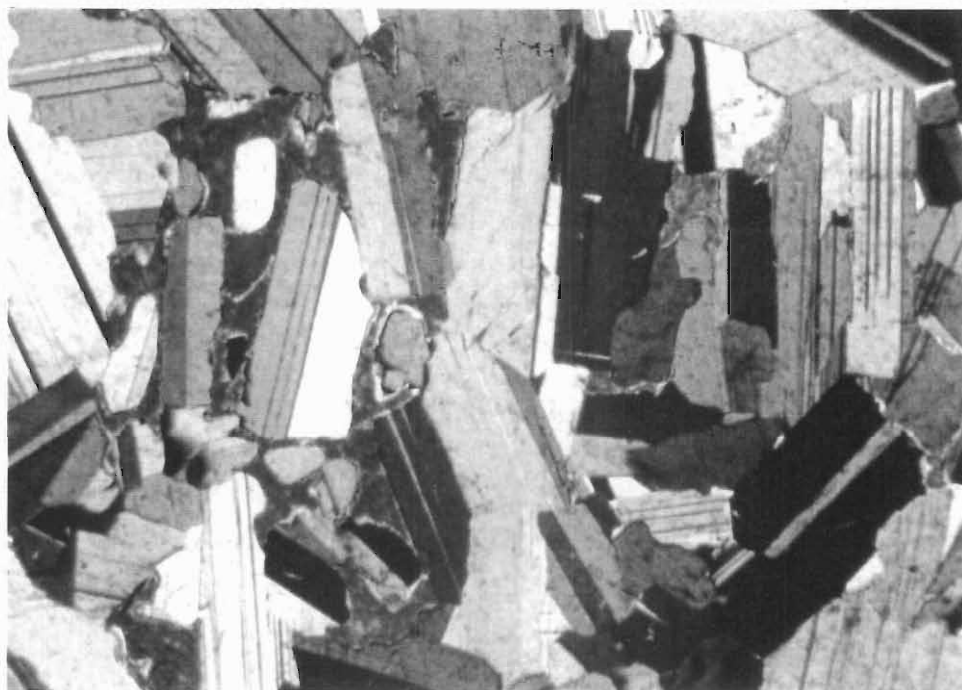
1mm

Figure 5.42   Cumulus plagioclase and intercumulus clinopyroxene
                observed in the hangingwall pyroxene anorthosite.
                Carlsbad and albite twinning of the plagioclase is
                universal.   (crossed nicols)

alteration, including recrystallisation, remobilisation, serpentinisation and, specifically in the case of the BMS, abundant replacement of pyrrhotite by chalcopyrite. The overlying Merensky pyroxenite is petrographically similar to the Merensky reef, the only essential differences being the relatively homogeneous medium-grained texture and the less abundant BMS occurrence.

CHAPTER 6

GEOCHEMISTRY OF THE MERENSKY SUCCESSION

6.1 INTRODUCTION

Geochemical studies have been conducted on four closely sampled normal Merensky reef sections from Frank Shaft, Rustenburg Platinum Mines - Rustenburg Section. Frank Shaft is ideally suited for the present study in that the Merensky reef is relatively undisturbed, and the transition from the texturally variable thicker Merensky reef facies in the west to the thinner facies in the east is exposed.

This study was undertaken to obtain geochemical data for the Merensky reef, which is currently not available, and which will constrain the origin of the PGE enrichment in the Merensky reef. The data can also be used for future studies as a reference section from which to determine regional and local geochemical changes which may occur in potholed Merensky reef.

High precision, low level X-Ray Fluorescence (XRF), Neutron Activation Analysis (NAA) and standard fire assay whole-rock and mineral separate geochemical analyses were performed on the four continuously sampled Merensky successions (Figure 6.1). The samples were analysed for a range of major elements, trace elements, PGE and Au.

The thick Merensky reef facies of borehole section R27A was selected for detailed whole-rock and mineral major and trace element geochemistry. Sampling problems would have limited the resolution of compositional variations in the thinner reef facies owing to the inherently coarse-grained nature of the Merensky reef. Intersections of the thinner reef facies (R24A, R25A and R26A) were only analysed for trace elements. In addition, R27A and R25A were analysed for PGE and Au by NAA and standard fire assay respectively. In all cases the same sample split was used for each analysis type and for the mineral separations.

The 7,07m R27A borehole section, containing a 1,92m thick Merensky reef (MR), was sampled on a continuous basis as 52 consecutive samples and analysed for the following elements: SiO_2, Al_2O_3, Fe_2O_3, MnO, MgO, CaO, Na_2O, K_2O, TiO_2, P_2O_5, Cr_2O_3, NiO, Nb, Y, Rb, Sr, Pb, Ga, Co, As, Zn, Cu, Ni, Ba, Sc, V, La, S, Rh, Pd, Pt, Ir, Os, Ru and Au.

Figure 6.1   The four continuously sampled Merensky successions used in this study.
(refer to text for explanation of lithological symbols)

Boreholes R24A (2,82m thick section, 32 consecutive samples, 0,33m thick MR), R25A (3,365m thick section, 30 consecutive samples, 0,28m thick MR), and R26A (5,13m thick section, 35 consecutive samples, 0,15m thick MR) were analysed for the following elements: Zr, Sr, Nb, Y, Rb, Zn, Cu, Ni, Ba, S and P. R25A was also analysed for Pt, Pd, Rh, Ir, Ru and Au.

For convenient readability and presentation of geochemical plots, each rock type has been assigned a letter symbol as follows:

W = hangingwall pyroxene anorthosite.

N = hangingwall norite/leuconorite.

X = Merensky pyroxenite (± medium-grained feldspathic pyroxenite).

C = chromitite layer.

M = Merensky reef pegmatoidal (or partially pegmatoidal) feldspathic pyroxenite enclosed by chromitite layers.

R = other Merensky reef pegmatoidal feldspathic pyroxenite not enclosed by chromitite layers.

H = Merensky reef pegmatoidal feldspathic harzburgite.

A = immediate footwall anorthosite.

L = footwall leuconorite/norite.

Although many geochemical trends are evident, major and trace element profiles fundamentally serve to distinguish the combined Merensky reef/Merensky pyroxenite (MR/MP) package from the underlying and overlying norites. The Merensky reef (MR) and overlying Merensky pyroxenite (MP) are usually easily distinguishable on the basis of texture and late-stage alteration. However, on the basis of major and trace element chemistry these two lithologies are virtually indistinguishable from one another. With few exceptions, the pyroxenite package as a whole displays either sharply enriched, or depleted `sawtooth' element profiles relative to the adjacent norites. In contrast, the geochemical patterns become noticeably smoother, at the top and bottom of the MR/MP package, ie from above the upper chromitite layer up through the MP, and the lower ± 0,4m of the MR (R27A section). The MR/MP pyroxenite package may thus be subdivided into three domains. The PGE geochemical profiles provide the only chemical way of clearly distinguishing the Merensky reef from the overlying Merensky pyroxenite. A notable feature is that the zone of elevated PGE values coincides exactly with the geochemically erratic middle MR/MP domain.

6.2 WHOLE-ROCK GEOCHEMISTRY

6.2.1 MAJOR ELEMENTS

Major element profiles for intersection R27A are presented in Figure 6.2, and average whole-rock major element abundances in Table 6.1. Whole-rock major element data is presented in Appendix II.

With the exception of K_2O and P_2O_5, the major elements reflect the silicate modal mineralogy, the major controls being exercised by plagioclase, pyroxene and chromite.

The major element profiles show either strong enrichment or strong depletion within the MR/MP package relative to the footwall and hangingwall norites. Throughout all the profiles to a greater or lesser extent, consistent patterns of variation exist in that:

a) Profiles are less variable within the footwall and hangingwall norites relative to the pyroxenite layers.

b) The change in element abundance from the footwall norite into the Merensky reef is accompanied by smooth profiles which extend 0,3m to 0,5m into the Merensky reef.

c) The upper ± 1,5m of the Merensky reef is characterised by highly variable `sawtooth' shaped element profiles.

d) The overlying Merensky pyroxenite is characterised firstly by element abundances, and also, by smoother element profiles than the upper part of the Merensky reef.

Major element variations show consistent patterns of depletion or enrichment through the Merensky reef. SiO_2, MgO and Fe_2O_3 essentially show the same pattern. Fe_2O_3 (as total Fe) shows a sharp increase at the base of the Merensky reef compared to the underlying leuconorite, and thereafter a gradual increase up through the Merensky reef and Merensky pyroxenite. There is a more gentle decrease in Fe_2O_3 from the Merensky pyroxenite into the overlying norite. This is consistent with the gradational contact between these layers. The

SiO2
R27A whole rock
Wt%

MgO
R27A whole rock
Wt%

Fe2O3
R27A whole rock
Wt%

CaO
R27A whole rock
Wt%

Na2O
R27A whole rock
Wt%

Al2O3
R27A whole rock
Wt%
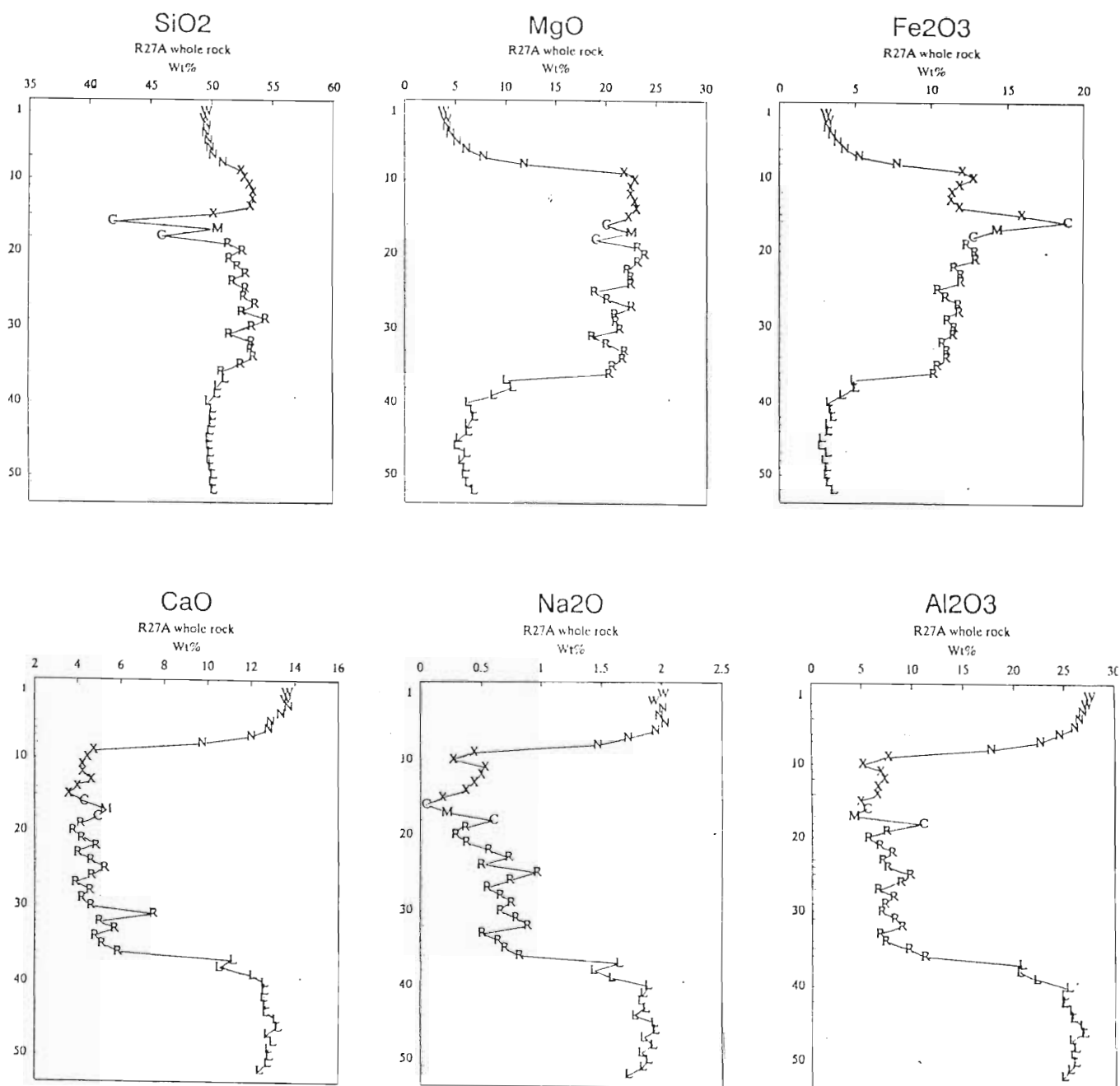
Figure 6.2a   R27A whole-rock Merensky succession major element profiles.
(refer to text for lithological symbols)
(sample numbers on y-axis)
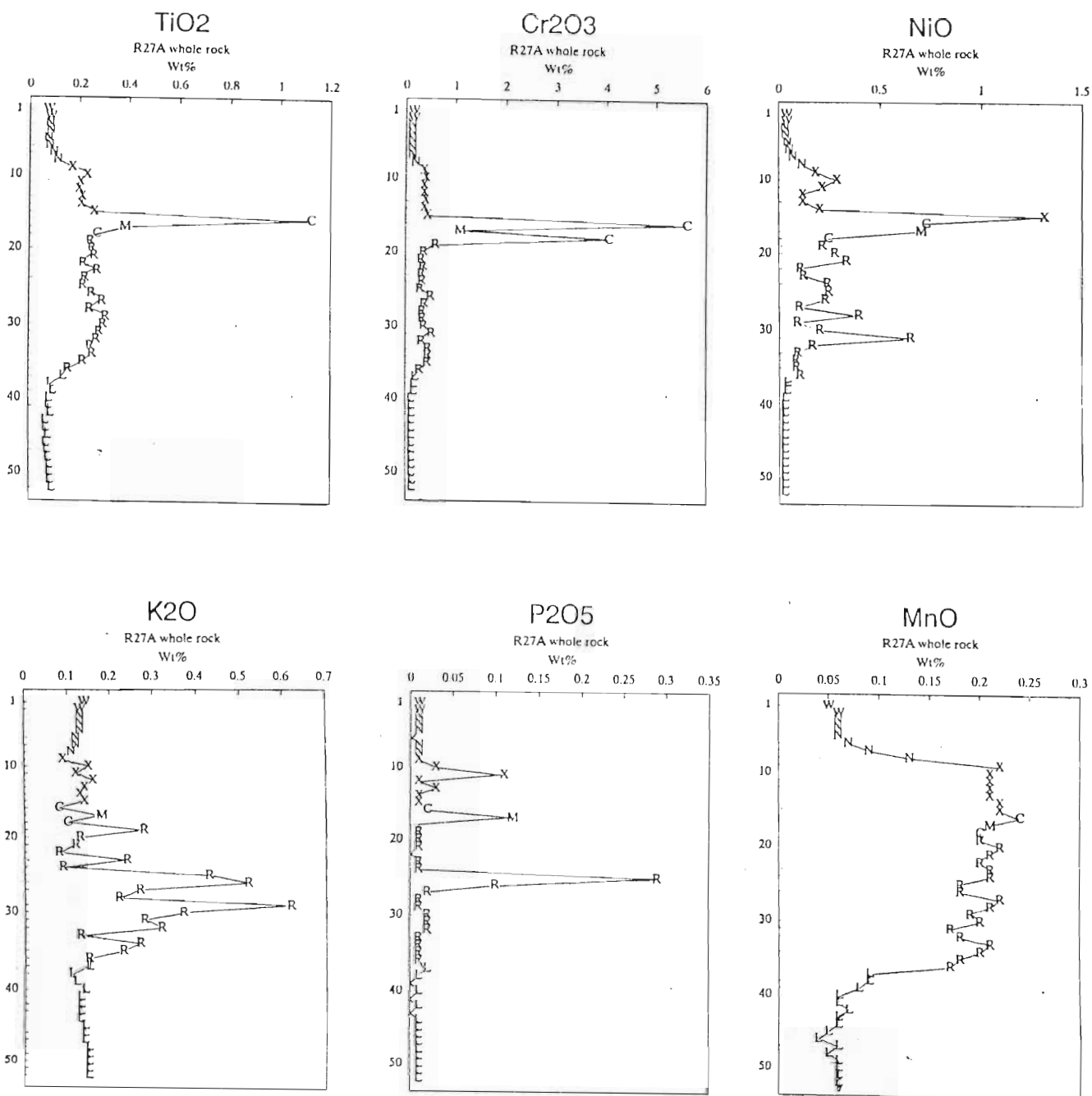
Figure 6.2b   R27A Merensky succession whole-rock major element profiles.
(refer to text for lithological symbols)

	W (2)	N (6)	X (7)	C (2)	M (1)	R (18)	L (8)
SiO_2 wt%	49,48	49,98	52,67	43,92	50,56	52,61	50,28
Al_2O_3	27,36	24,02	6,42	8,27	4,22	7,91	23,80
Fe_2O_3	3,11	4,64	12,43	15,83	14,28	11,41	3,81
MnO	0,06	0,08	0,21	0,22	0,21	0,20	0,07
MgO	3,89	6,57	22,38	19,48	22,51	21,38	7,67
CaO	13,59	12,41	4,28	4,62	5,32	4,83	12,11
Na_2O	1,97	1,86	0,39	0,32	0,22	0,64	1,74
K_2O	0,14	0,12	0,13	0,09	0,1	0,26	0,13
TiO_2	0,08	0,09	0,21	0,70	0,39	0,25	0,09
P_2O_5	0,01	0,01	0,03	0,01	0,12	0,03	0,008
Cr_2O_3	0,06	0,11	0,39	4,84	1,10	0,38	0,13
NiO	0,03	0,06	0,35	0,49	0,70	0,21	0,03
Y ppm	4,15	4,27	8,70	8,00	13,50	9,48	4,13
Zr	7,3	6,25	18,37	11,95	26,30	26,95	7,01
As	1,12	0,80	2,51	4,07	4,22	2,17	1,11
Zn	24,50	32,83	81,43	165,00	90,00	80,22	31,00
Cu	64,00	205,83	1211,7	1828,5	2182,0	573,22	23,50
Ni	185,50	429,00	2601,3	3708,5	5301,0	1565,8	205,0
Co	17,00	33,33	172,71	181,00	219,00	148,94	30,13
S	626,0	1488,7	9041,3	13021	19655	3898,6	108,0
Sr	404,35	356,82	87,16	86,45	46,60	111,06	359,1
Rb	1,10	1,03	4,56	2,35	7,70	10,02	1,03
Au	0,0032	0,0086	0,090	0,292	0,218	0,141	,0004
Rh	BD	BD	0,06	1,09	0,38	0,15	BD
Pd	BD	BD	0,32	2,75	2,35	1,20	BD
Pt	BD	0,018	1,38	16,76	8,42	2,13	BD
Ir	BD	,00003	0,036	0,40	0,164	0,045	BD
Os	BD	BD	0,027	0,333	0,177	0,032	BD
Ru	BD	BD	0,223	2,61	1,153	0,256	BD

Table 6.1   Average R27A Merensky succession whole-rock major element, trace element and platinum-group element compositions for each rock type through the succession.
(figures in parentheses indicate the number of samples in each case)

(BD = Analyses at detection limit)
(PGE Detection Limits: Pt = 6ppb   Pd = 25ppb   Rh = 0,6ppb   Ir = 0,1ppb
                        Os = 2ppb   Ru = 19ppb   Au = 0,1ppb)

chromitite layers show a specific increase in Fe_2O_3, with a corresponding general upward decrease in MgO and SiO_2 abundances in the whole rock.

Na_2O, CaO and Al_2O_3 are depleted within the Merensky reef and Merensky pyroxenite relative to the adjacent norites, being the major components of plagioclase, and all show variable upward depletion through the MR/MP succession.

The minor elements TiO_2, Cr_2O_3 and NiO show slight increases in the MR/MP package. TiO_2 and Cr_2O_3 are major components of chromitite and show sharply increased abundances at the chromitite layers. TiO_2 is marginally enriched in the pyroxenite layers. The trend, however deviates slightly in that the enrichment commences within the footwall leuconorite and continues up through the Merensky reef basal contact, maintaining a smooth profile 0,8m up into the reef. The remainder of the reef shows the typical `sawtooth' profile, with the uppermost chromitite layer most highly enriched in TiO_2, while the underlying chromitite layer shows no greater enrichment than the enclosing pyroxenite. NiO is a component of pyroxene, but primarily reflects the sulphide content of the MR/MP pyroxenite layers and shows a highly variable profile throughout.

K_2O and P_2O_5 show an erratic increase within the MR/MP pyroxenite package but, unlike the other elements, do not distinguish well between the pyroxenites and norites. These elements fundamentally reflect the presence of late-stage phases such as phlogopite and apatite. MnO occurs at low abundance and shows a similar profile to Fe_2O_3.

Whole-rock magnesium number (Mg# = molecular ratio of $MgO/(MgO+Fe_2O_3)$) and calcium number (Ca# = molecular ratio of $CaO/(CaO+Na_2O)$) show contrasting profiles through the sequence (Figure 6.3). Mg# decreases upwards through the sequence with a sharp upward decrease taking place at the hangingwall norite. In contrast, the Ca# shows an upward increase through the MR/MP pyroxenite package. Both patterns show erratic or `sawtooth' profiles in the pyroxenites but not in the norites. It is also noticeable that some peaks and depressions show contrasting behaviour with higher values of Mg# corresponding to lower Ca# values. The observed upward decrease in Mg# may reflect normal fractionation but this is not supported by the variation in Ca#. The reason for these differences is not clear. However, calcium may be influenced by the increased abundance of clinopyroxene up through the pyroxenite layers, *eg* the relatively high observed abundance of clinopyroxene (augite)

Mg# and Ca#
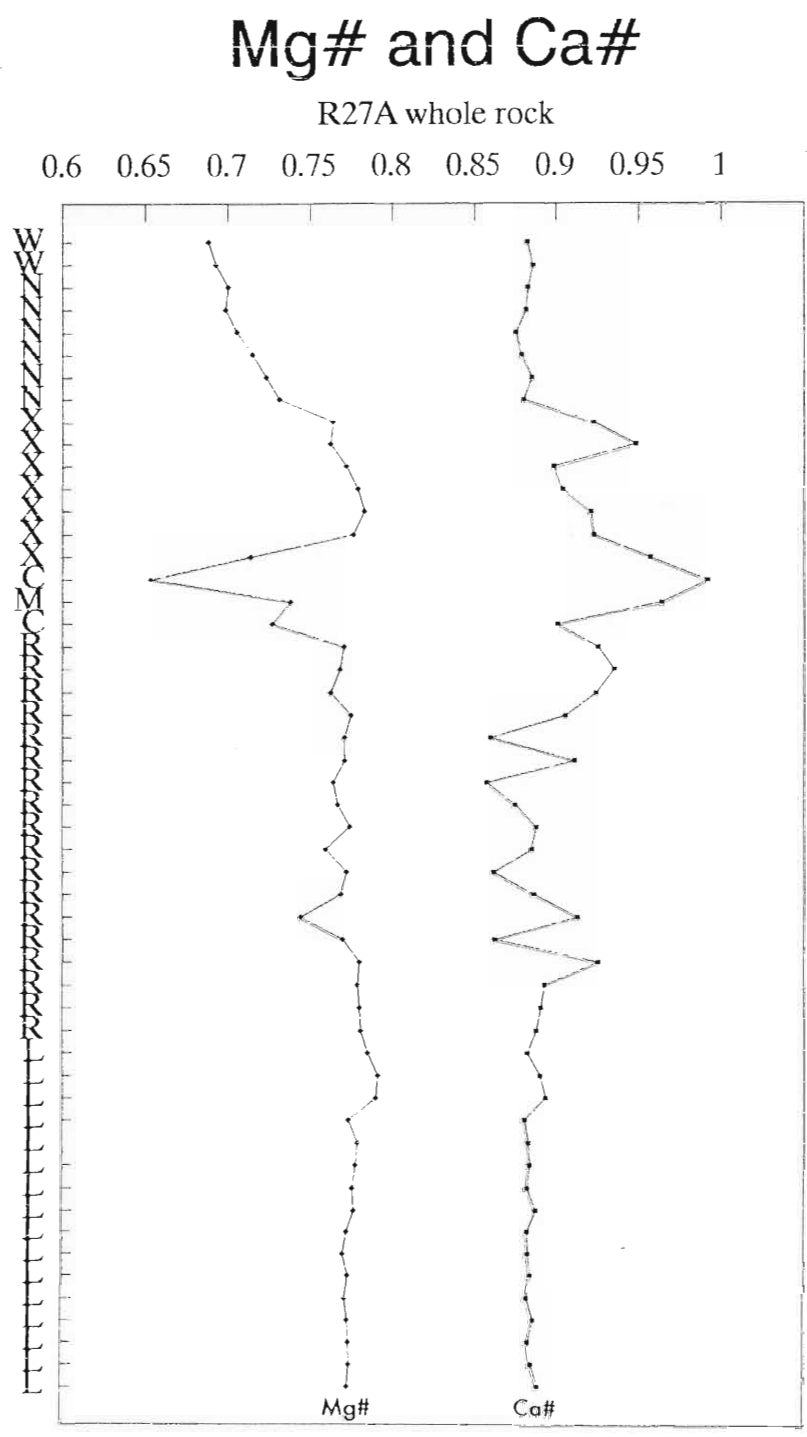
R27A whole rock

Figure 6.3   R27A whole-rock magnesium and calcium number profiles.

oikocrysts within the Merensky pyroxenite. The plagioclase is interstitial and it may also have undergone reaction with trapped liquid, which was in turn, in open-system connection with the overlying body of magma. Authors such as Lee (1983) and Cawthorne & McCarthy (1985) have pointed out that intercumulus plagioclase is subject to late-stage re-equilibration and therefore cannot be used as a fractionation monitor.

The Ca# increase is confined to the MR/MP package. Both the footwall and hangingwall norites show slightly decreasing Ca# trends which is consistent with a normal fractionation pattern. The footwall leuconorite Ca# trend can be extrapolated through the MR and MP to coincide exactly with the start of the hangingwall norite trend. This is consistent with the postcumulus status of plagioclase but may also be suggestive of late-stage plagioclase alteration within the MR/MP package. It may also be suggestive of decoupling of the MR/MP package from the norites.

6.2.2 TRACE ELEMENTS

Trace element profiles for the R27A section are shown in Figure 6.4 and the average whole-rock trace element abundances in Table 6.1. Whole-rock trace element data is presented in Appendix II. The values in Table 6.1 are for convenience shown to two significant figures in some cases, but are not intended to reflect any greater level of precision. Although the discussion is centred on the R27A section, trace element profiles for the R24A, R25A and R26A intersections are presented in Figures 6.5, 6.6 and 6.7 for comparison.

The trace element profiles fall into three broad groups:

a) Those controlled largely by sulphide distribution, *eg* S, Ni and Cu.

b) Those controlled by the dominant mineral phases (excluding sulphide) plagioclase, pyroxene and chromite, *eg* Sr, Co, Zn, Sc, V and Ga.

c) Those which are essentially incompatible with the major element phases, *eg* Nb, Zr, Y, Ba, Pb, La, As and Rb.
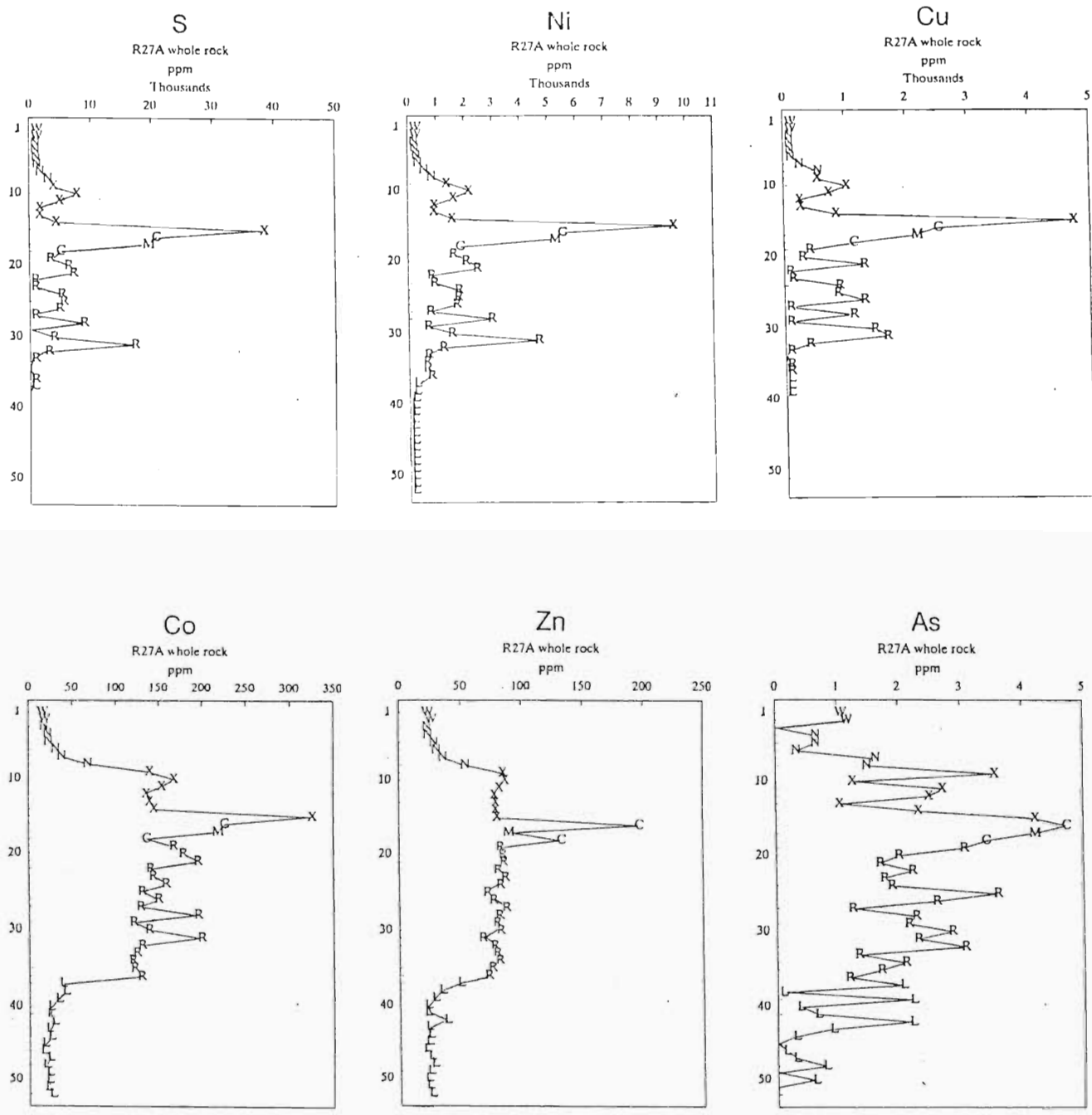
Figure 6.4a   R27A Merensky succession whole-rock trace element profiles.
(refer to text for lithological symbols)
(sample numbers on y-axis)
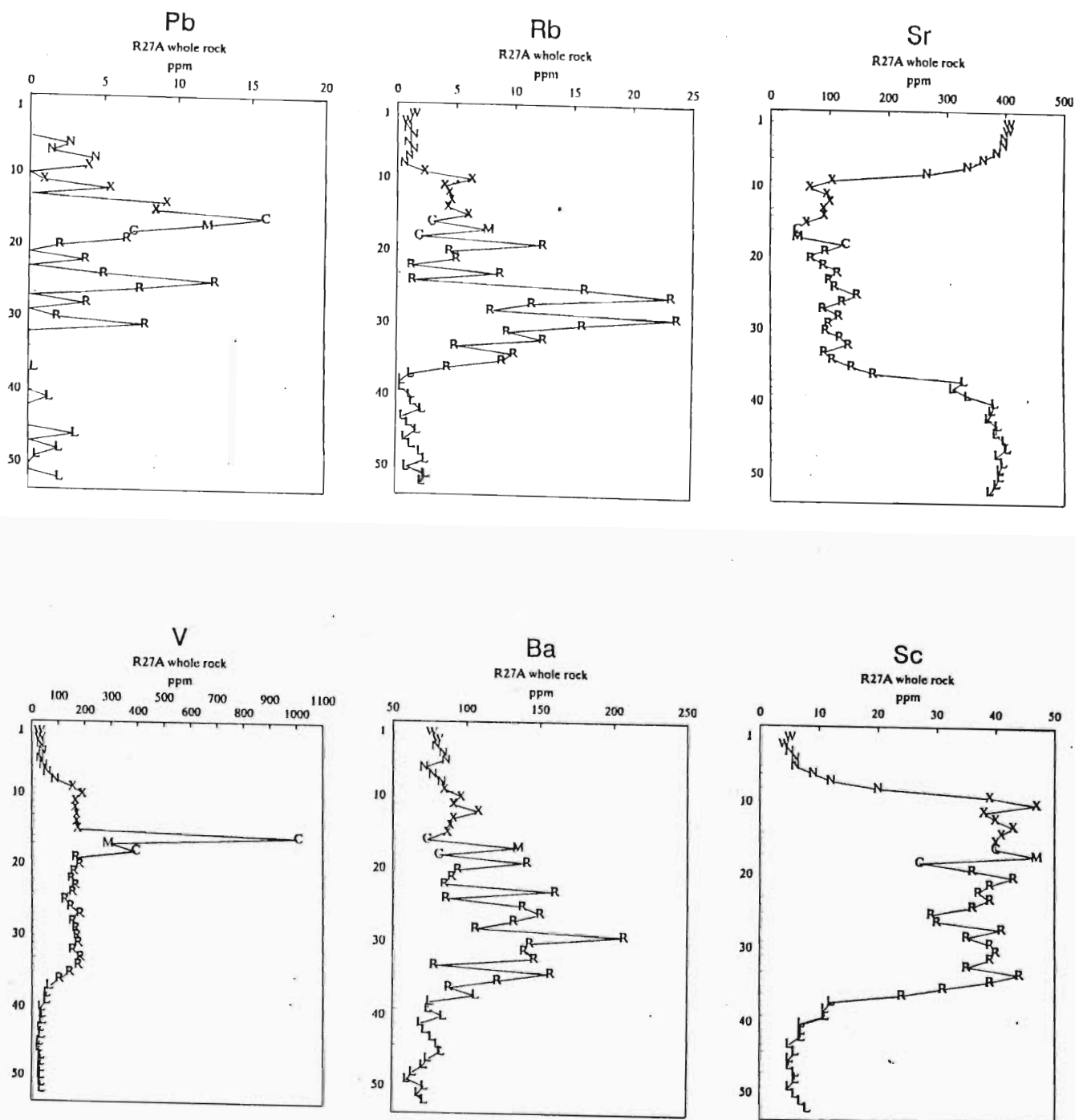
Figure 6.4b   R27A Merensky succession whole-rock trace element profiles.
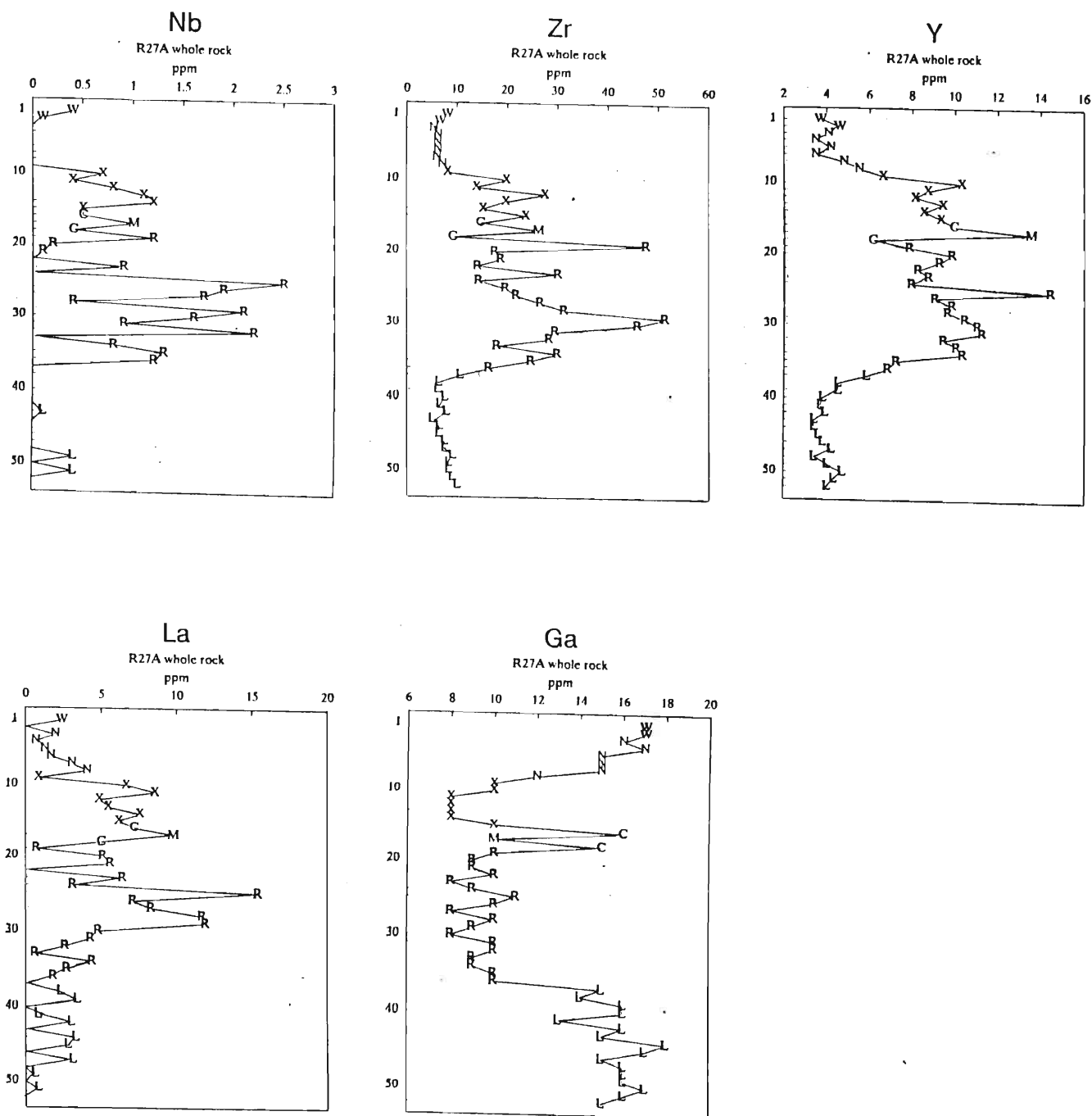
Figure 6.4c   R27A Merensky succession whole-rock trace element profiles.
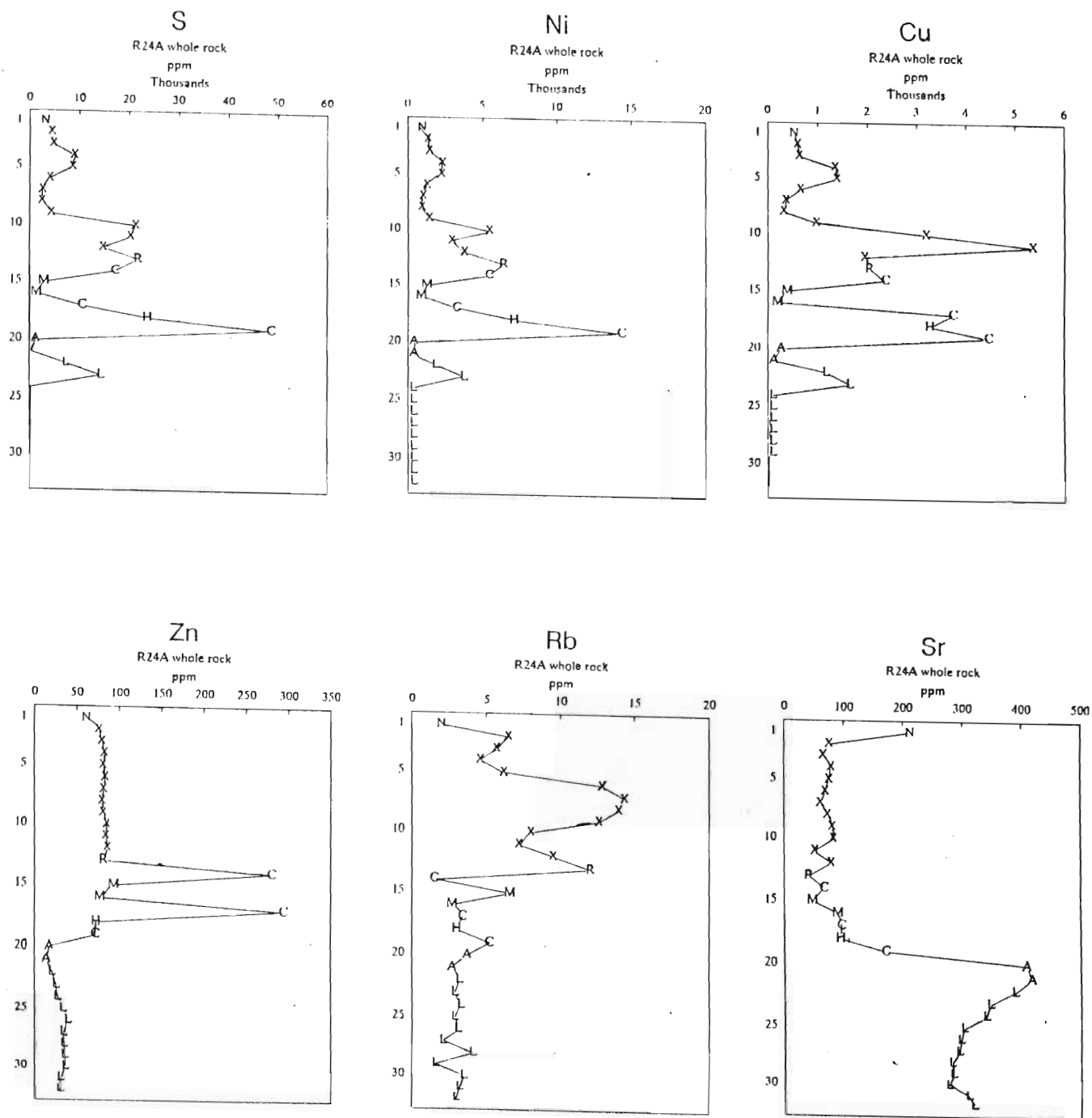
Figure 6.5a   R24A Merensky succession whole-rock trace element profiles.
               (see text for lithological symbols)
               (sample numbers on y-axis)
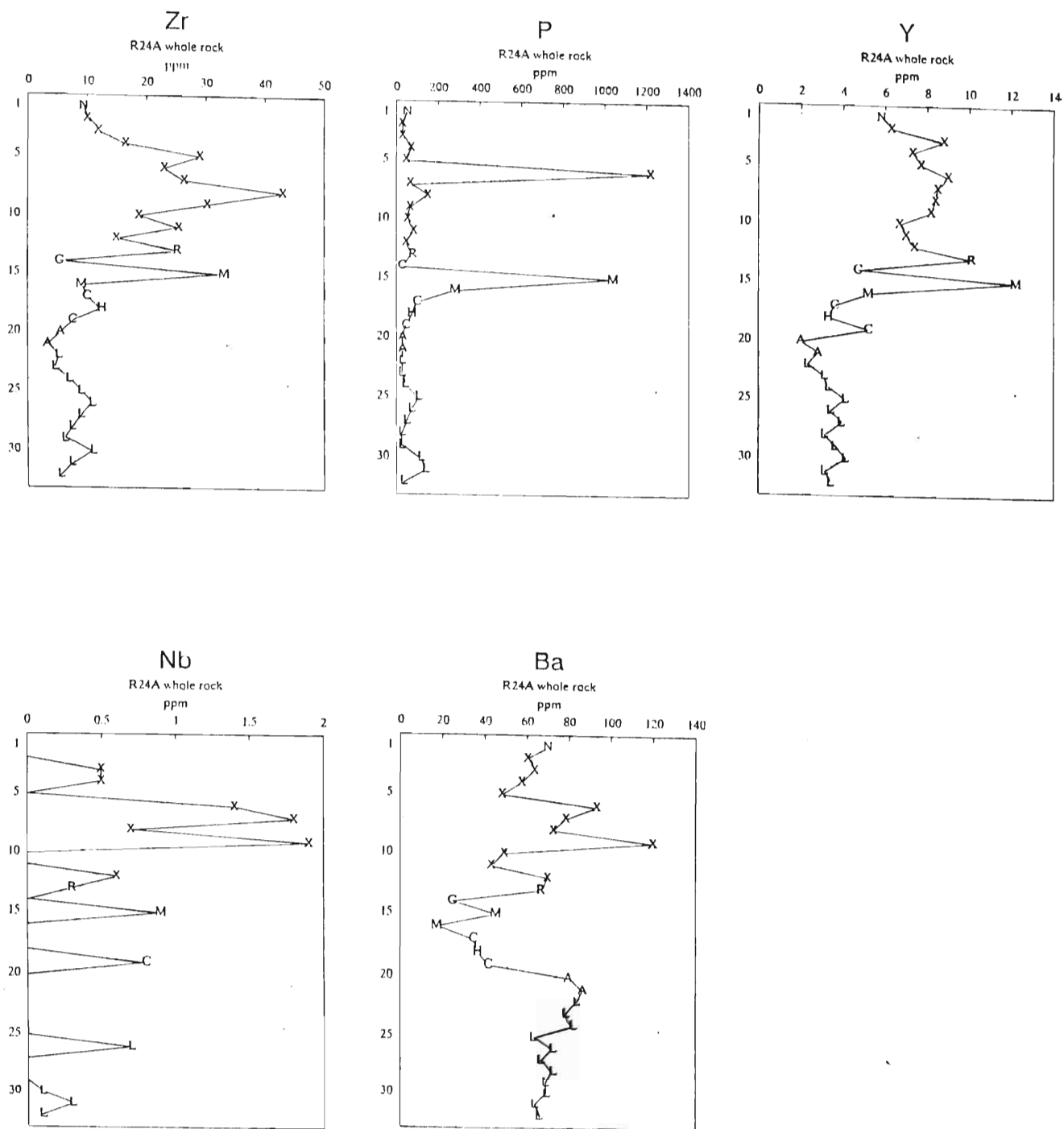
Figure 6.5b   R24A Merensky succession whole-rock trace element profiles.
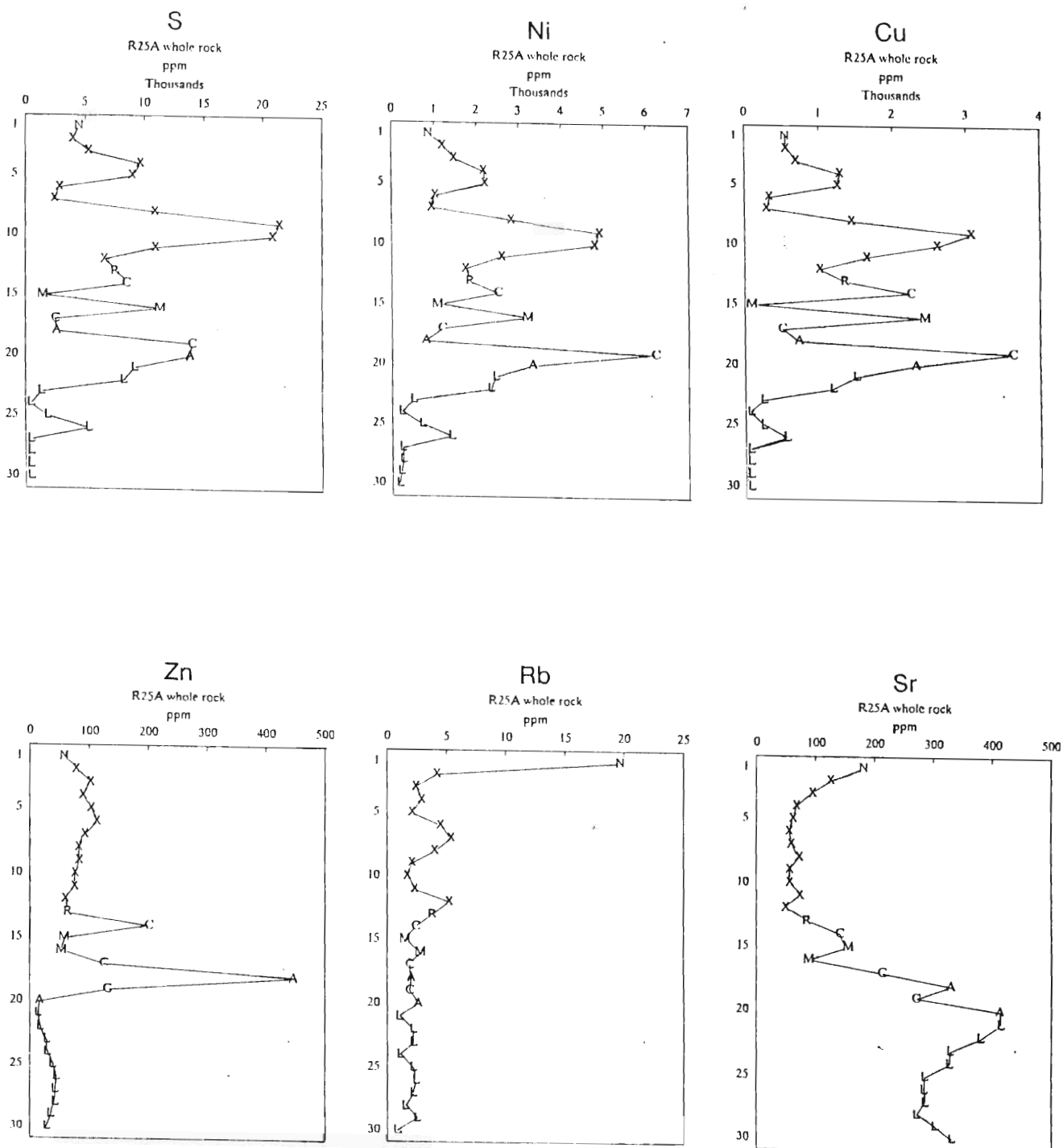
Figure 6.6a   R25A Merensky succession whole-rock trace element profiles.
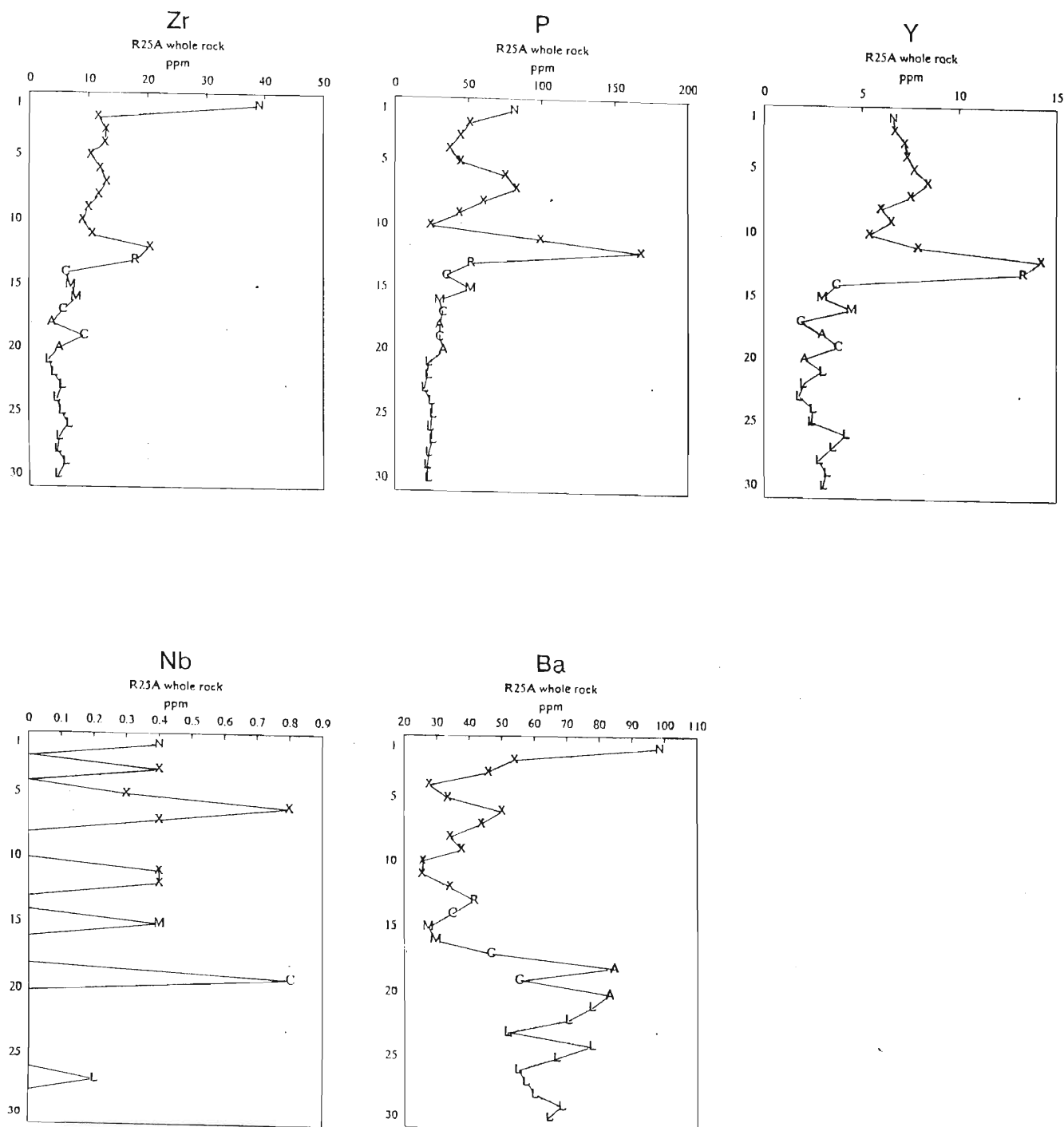
Figure 6.6b   R25A Merensky succession whole-rock trace element profiles.
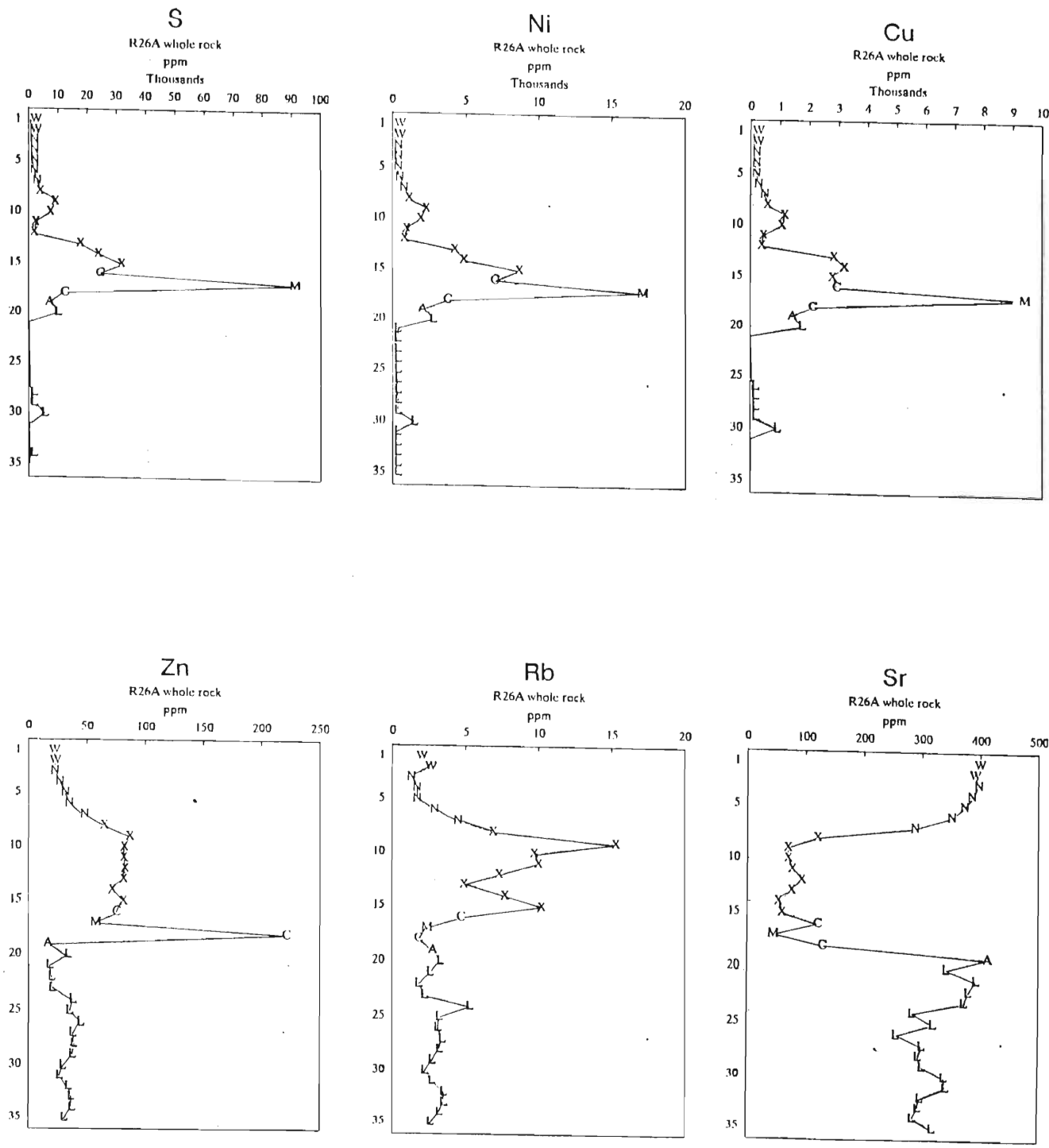
Figure 6.7a   R26A Merensky succession whole-rock trace element profiles.
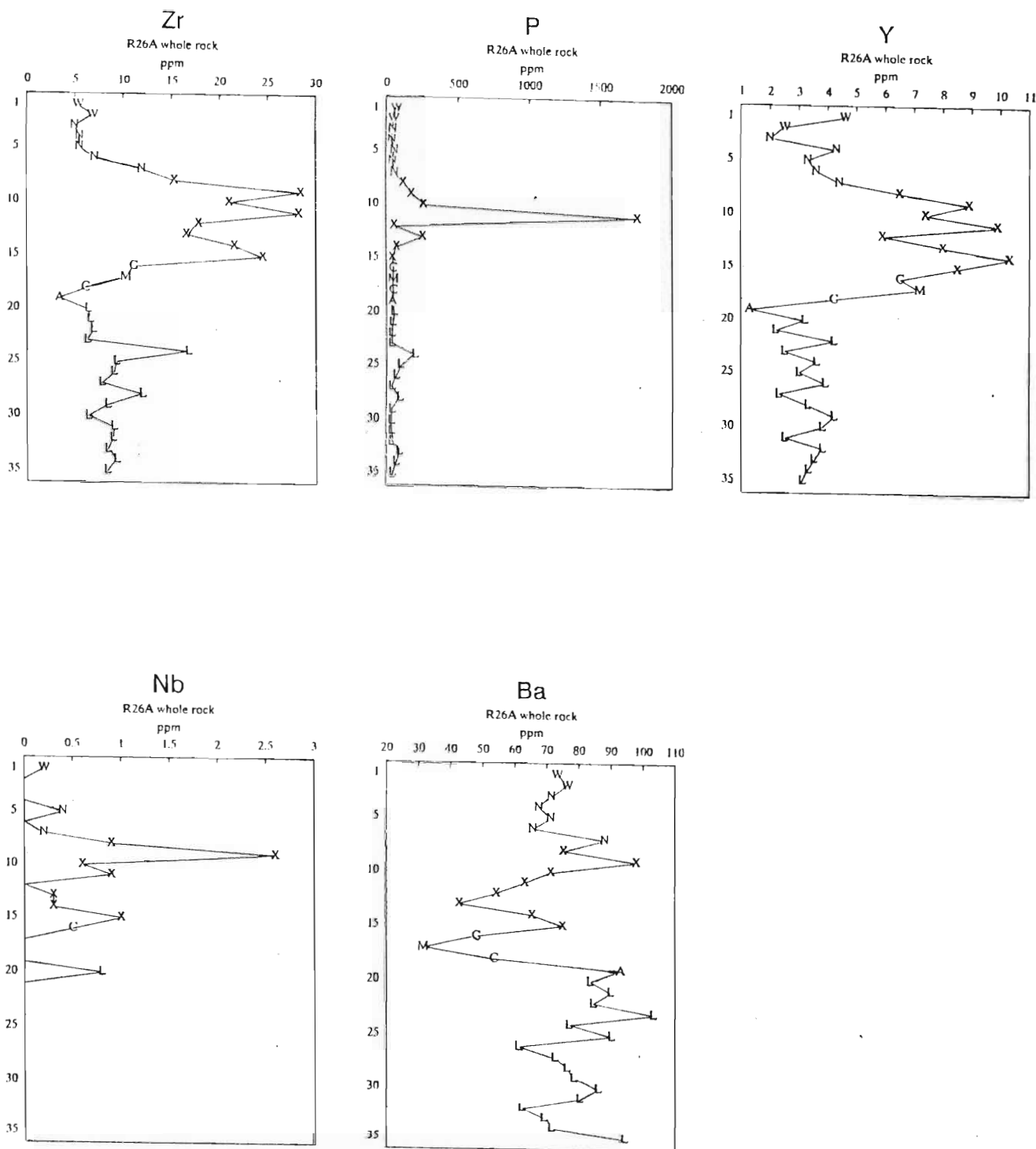
Figure 6.7b   R26A Merensky succession whole-rock trace element profiles.

S, Ni, Cu, follow similar profiles through the sequence with high, but variable, values occurring within the MR/MP pyroxenite package. These elements are the major constituents of, and fundamentally reflect the distribution of the base metal sulphides. The highest S, Ni and Cu values occur at the top of the Merensky reef, with peak values immediately above the uppermost chromitite layer, and lower, variable values towards the base of the reef. In the thinner Merensky reef sections R24A, R25A and R26A, high values are dispersed from the Merensky pyroxenite, through the Merensky reef where the highest values generally occur, to the footwall leuconorite. In each case the immediate footwall anorthosite layer shows depleted values relative to the overlying Merensky reef and immediately underlying leuconorite. This is consistent with the observation that the footwall anorthosite is commonly relatively devoid of visible base metal sulphides.

Zn, Co, Sc and V to a lesser extent, show similar sharp increases within the MR/MP package, where they reflect the increased pyroxene content, and, in the case of Zn and V, also the chromitite layers.

Ga and Sr reflect the amount of plagioclase present and illustrate the sharp drop in plagioclase abundance, and its variable composition, within the MR/MP package. Ga is also sensitive to chromite. In the R24A, R25A and R26A sections, peak Sr values are coincident with the immediate footwall anorthosite layer.

Nb, Zr, Y, Ba, Pb, La, As and Rb all show variable enrichment patterns within the MR/MP package. The level of data precision however, is variable, with the La data known to be of unavoidably poorer precision. These elements are incompatible with the major mineral phases and reflect the increased abundance of accessory late-stage mineral phases which have accumulated in the pyroxenite sequence. In the thinner reef R24A, R25A and R26A sections, Ba in particular, consistently shows depleted values within the Merensky reef, with higher values associated with the Merensky pyroxenite and footwall anorthosite/leuconorite. Elevated rare earth element (REE) contents are documented for the Atok Merensky reef pyroxenite, far in excess of that anticipated from partition modelling as cumulates. This has been interpreted as a late-stage alteration effect (Mathez, 1994). The high incompatible element concentrations observed in the present study accord with this observation, but there is no convincing evidence to suggest that it is a result of late-stage alteration.

Correlation coefficients based on linear regression at 95% confidence limits have been calculated for selected R27A trace element pairs. Coefficients have been separately calculated for individual rock units within the sequence and for the whole sequence (Tables 6.2a to e). Table 6.3 gives a summary of the degrees of correlation between selected trace elements, subdivided into good inter-element correlations (>0,9), medium correlations (0,75-0,9), and low correlations (0,5-0,75) grouped together for the different rock units of the sequence. Poor inter-element correlation coefficients of <0,5 have not been included. Specific attention may be drawn to the following correlations:

a) Zr may be used as a measure of trapped material in a cumulate rock. Correlations between S and Zr are poor throughout the sequence, with a whole-sequence average of 0,27. The highest coefficient of 0,53 occurs in the footwall leuconorite, which may be consistent with the fact that it is probably the least evolved part of the sequence, and in some way may reflect the presence of primary or submagmatic sulphide. Conversely, the coefficient of 0,15 for the Merensky reef suggests total decoupling between Zr in trapped liquid and sulphide.

b) Zn is a constituent of pyroxene, chromite and BMS. The S-Zn correlation analysis shows high correlations in the footwall and hangingwall norites (>0,9), where pyroxene and BMS concentrations are low, but very poor correlations in the pyroxenite layers. The latter may be due to the increased abundance of all three minerals, late-stage decoupling of sulphides, and alteration to the pyroxene chemistry.

c) The S-Ni-Cu-Co intercorrelations are high ($\geq$ 0,9) throughout the complete succession, being the major constituents of the BMS. The highest of these correlations occur in the Merensky pyroxenite ($\geq$ 0,99), and the lowest in the footwall leuconorite (0,7 to 0,8).

Throughout the Critical Zone cumulate sequence Ni abundance exceeds Cu (C.A.Lee, *pers comm*). This same pattern is observed in the four Merensky successions in this study, with the example of the R27A section presented in Figure 6.8. The variance is small within the footwall and hangingwall norites, whereas in the MR/MP package the variance is high. A few samples within the reef sequence have higher Cu/Ni ratios, and in two cases Cu exceeds Ni (Figure 6.9). The Cu and Ni profiles for the R27A section and the three other Merensky reef sequences show this same variation. This pattern is in fundamental contrast to sequences such as the Munni Munni (Barnes & Keays, 1992) and Great Dyke (Wilson & Tredoux, 1990). The Munni

	As	S	Ni	Cu	Zn	Co	Pb	Zr	Y
As	1,000	,5493	,5937	,5931	,5825	,5348	,3520	,5281	,6821
S	,5493	1,000	,9925	,9821	,9911	,9933	,8974	,1490	,7570
Ni	,5937	,9925	1,000	,9753	,9777	,9829	,8809	,1262	,7646
Cu	,5931	,9821	,9753	1,000	,9829	,9877	,8653	,2265	,8037
Zn	,5825	,9911	,9777	,9829	1,000	,9898	,9040	,2177	,7959
Co	,5348	,9933	,9829	,9877	,9898	1,000	,9236	,1893	,7379
Pb	,3520	,8974	,8809	,8653	,9040	,9236	1,000	,2017	,5293
Zr	,5281	,1490	,1262	,2265	,2177	,1893	,2017	1,000	,0902
Y	,6821	,7570	,7646	,8037	,7959	,7379	,5293	,0902	1,000

Table 6.2a   Correlation coefficients for trace element pairs,
             Borehole R27A hangingwall norite (WN)
             (linear regression at 95% confidence, n = 8)

	As	S	Ni	Cu	Zn	Co	Pb	Zr	Y
As	1,000	,6376	,6410	,6378	-,064	,6045	,6334	-,130	-,520
S	,6376	1,000	,9997	,9982	-,057	,9983	,4697	,3211	,2861
Ni	,6410	,9997	1,000	,9983	-,079	,9981	,4827	,3273	,2796
Cu	,6378	,9982	,9983	1,000	-,070	,9953	,5020	,3028	,2880
Zn	-,064	-,057	-,079	-,070	1,000	-,072	-,483	-,494	,0585
Co	,6045	,9983	,9981	,9953	-,072	1,000	,4372	,3542	,3282
Pb	,6334	,4697	,4827	,5020	-,483	,4372	1,000	,1502	-,304
Zr	-,130	,3211	,3273	,3028	-,494	,3542	,1502	1,000	,5067
Y	-,520	,2861	,2796	,2880	,0585	,3282	-,304	,5067	1,000

Table 6.2b   Correlation coefficients for trace element pairs,
             Borehole R27A Merensky pyroxenite (X).
             (linear regression at 95% confidence, n = 7)

	As	S	Ni	Cu	Zn	Co	Pb	Zr	Y
As	1,000	,6790	,6613	,7249	,5963	,4790	,8408	,0039	,3952
S	,6790	1,000	,9979	,9044	,4963	,9013	,7790	,1509	,4308
Ni	,6613	,9979	1,000	,8994	,4995	,9182	,7644	,1349	,4100
Cu	,7249	,9044	,8994	1,000	,5238	,7917	,7718	,1240	,3701
Zn	,5963	,4963	,4995	,5238	1,000	,4224	,5334	-,311	-,124
Co	,4790	,9013	,9182	,7917	,4224	1,000	,5993	-,117	,2571
Pb	,8408	,7790	,7644	,7718	,5334	,5993	1,000	-,229	,4044
Zr	,0039	,1509	,1349	,1240	-,311	-,117	-,229	1,000	,2331
Y	,3952	,4308	,4100	,3701	-,124	,2571	,4044	,2331	1,000

Table 6.2c   Correlation coefficients for trace element pairs,
Borehole R27A Merensky reef (CMR)
(linear regression at 95% confidence, n = 21)

	As	S	Ni	Cu	Zn	Co	Pb	Zr	Y
As	1,000	,7076	,4813	,6285	,6641	,4731	-,244	,0522	,4004
S	,7076	1,000	,8185	,8286	,8964	,7338	-,169	,5263	,7932
Ni	,4813	,8185	1,000	,9184	,8126	,9632	-,300	,1974	,7612
Cu	,6285	,8286	,9184	1,000	,7887	,8441	-,270	,1225	,7507
Zn	,6641	,8964	,8126	,7887	1,000	,7541	-,240	,4035	,6787
Co	,4731	,7338	,9632	,8441	,7541	1,000	-,394	,0819	,6727
Pb	-,244	-,169	-,300	-,270	-,240	-,394	1,000	,2795	-,277
Zr	,0522	,5263	,1974	,1225	,4035	,0819	,2795	1,000	,5041
Y	,4004	,7932	,7612	,7507	,6787	,6727	-,277	,5041	1,000

Table 6.2d   Correlation coefficients for trace element pairs,
Borehole R27A footwall leuconorite (L).
(linear regression at 95% confidence, n = 16)

	As	S	Ni	Cu	Zn	Co	Pb	Zr	Y
As	1,000	,6484	,7034	,6890	,7833	,7812	,7095	,5045	,7084
S	,6484	1,000	,9901	,9655	,5084	,7657	,6706	,2667	,5046
Ni	,7034	,9901	1,000	,9638	,5979	,8430	,6853	,3640	,5941
Cu	,6890	,9655	,9638	1,000	,5549	,7810	,6849	,3077	,5301
Zn	,7833	,5084	,5979	,5549	1,000	,8266	,5932	,5273	,7240
Co	,7812	,7657	,8430	,7810	,8266	1,000	,5880	,6351	,8377
Pb	,7095	,6706	,6853	,6849	,5932	,5880	1,000	,2168	,5122
Zr	,5045	,2667	,3640	,3077	,5273	,6351	,2168	1,000	,7342
Y	,7084	,5046	,5941	,5301	,7240	,8377	,5122	,7342	1,000

Table 6.2e   Correlation coefficients for trace element pairs,
Borehole R27A whole sequence.
(linear regression at 95% confidence, n = 52)
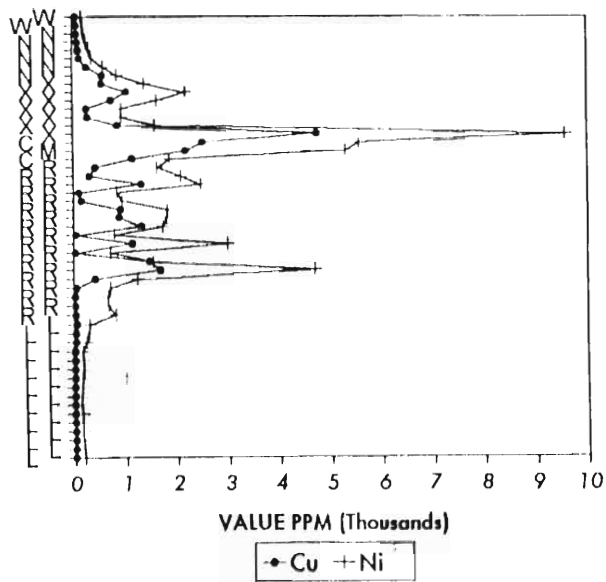
Figure 6.8   R27A whole-rock Cu and Ni profiles.
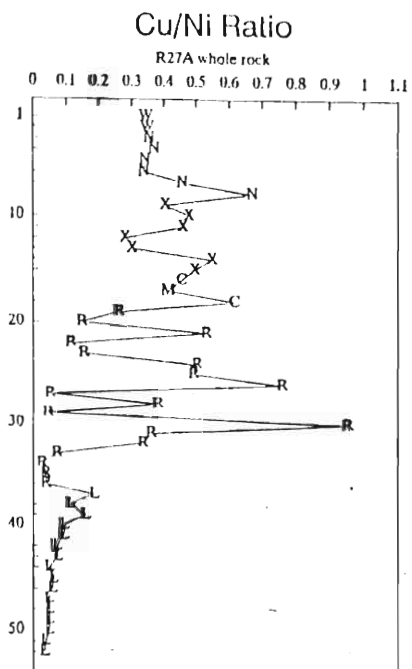
Figure 6.9   R27A whole-rock Cu/Ni ratio
profile.

Munni Complex is Cu-dominant and there is a three to four-fold increase in Cu abundance within its profiles, offset from the PGE peaks. In the case of the Great Dyke there is little variation in the Cu/Ni ratio, but there is a gradual increase in this ratio with the peaks offset from the PGE peaks, as is also the case in the Munni Munni Complex. Within the Merensky sequences there is an upward increase in the Cu/Ni ratio as a whole, with the greatest variation being in the pyroxenite package. This trend is shown in the R27A Cu/Ni ratio (Figure 6.9), where a strong upward-increasing trend exists with a zone of highly variable values coinciding with the MR/MP pyroxenite package and the base of the overlying norite. The less variable values within the footwall leuconorite are coincident with a virtual straight line, upward-increasing trend which may be extrapolated through the MR/MP pyroxenites exactly to the point where the smooth trend resumes within the hangingwall norite. This would suggest late-stage modification to the background Cu/Ni values within the mineralised MR/MP package.

The Cu/Ni ratio in the pyroxenite is partly influenced by the abundance of orthopyroxene (Ni in orthopyroxene lattice) and the composition of the base metal sulphides (BMS). Some higher Cu/Ni (and Cu/Cu+Ni) ratios correlate with higher plagioclase (*ie* lower silicate Ni), but in the sulphide dominant part of the sequence this control in minimal, and is overwhelmed by the BMS composition and abundance.

Cu, Ni and S follow very similar profiles with sympathetic peaks, which is consistent with the high correlation coefficients obtained for these elements. However, there is a distinct offset of the Zr (and P) peaks compared with the Cu, Ni and S peaks. This indicates late-stage decoupling of sulphides and incompatible elements. This could have been the result of an intercumulus space problem, with intercumulus plagioclase, BMS, late-stage accessories and trapped fluid all competing for the same space.

The incompatible element abundance may be used as a measure of trapped liquid in the cumulate pile. If sulphide originated as an immiscible phase and collected together with trapped silicate melt in the interstices between the cumulus pyroxene crystals in the Merensky reef and overlying Merensky pyroxenite, then there should be a strong correlation between S and the incompatible elements, *eg* Zr and P. Where sulphide is particularly abundant, *eg* in the Merensky reef itself, then dense immiscible sulphide liquid percolating through the cumulate pile may have physically displaced the trapped silicate liquid. This effect may then obscure any original correlation between the sulphide occupying available space with the trapped silicate
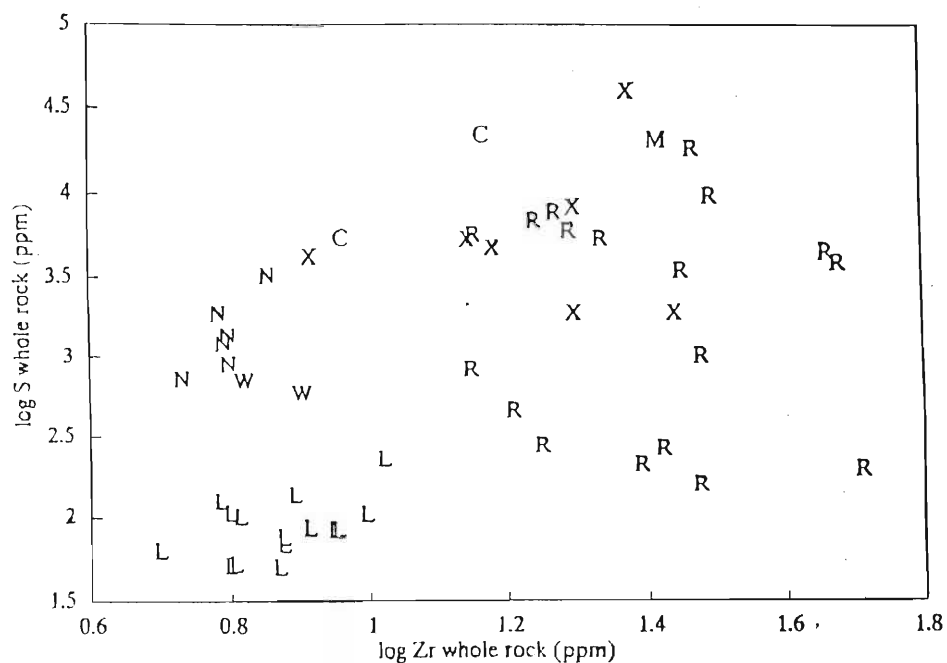
Figure 6.10   Log S v log Zr for profile R27A.   No linear trends
are evident.
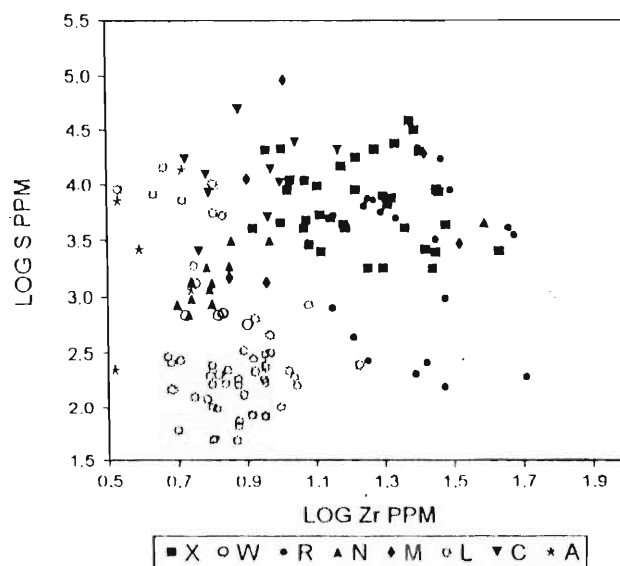
Figure 6.11   Log S v log Zr plot for profiles R24A to R27A combined.
No linear trends are evident.

liquid, and therefore also the incompatible elements. Further relationships are summarised in the log S v log Zr plot for R27A shown in Figure 6.10, and in the earlier correlation analyses. Two sulphide populations are evident, one population belonging to the footwall and hangingwall norites, in which positive Zr-S correlations exist on a rough basis, and the other belonging to the MR/MP pyroxenites, which shows a wide scatter and no Zr-S correlation. A straight line Zr-S trend indicates the presence of trapped primary or submagmatic sulphide, as in the norites, and more consistently, in the footwall leuconorites. The R25A section shows a negative Zr-S correlation in the footwall leuconorite, and in R26A a positive correlation is noted in the Merensky pyroxenite. Therefore, to some extent, each sequence has its own geochemical character, however, sharing the basic common features of positive correlations in the footwall leuconorite and poor correlations in the MR/MP package. Where there is suggestion of positive correlations this would indicate that zones of high porosity would act as traps for downward percolating sulphides. The negative correlations may indicate extensive displacement of the trapped liquid by sulphide liquid. Notwithstanding these small differences and possible Zr-S correlations in two of the sequences, as a group of 150 data points (Figure 6.11), the R27A Merensky reef and Merensky pyroxenite are higher in Zr and S, and no inter-relationship exists to suggest co-entrapment. The Zr-S correlations in the footwall leuconorite would suggest an earlier submagmatic process as being primarily responsible for the BMS and PGE accumulation, which was relatively unaffected by the late-stage hydromagmatic modification to the overlying pyroxenite package. The extent and relative intensity of immediate footwall mineralisation is dependent on Merensky reef thickness, with sub-economic values occurring in the footwall of the thick reef facies, and invariably highly economic values occurring in the footwall of the thin reef facies. This is a function of the fixed metal content of the Merensky package and the controls on sulphide migration.

6.3 MINERAL GEOCHEMISTRY

6.3.1 ORTHOPYROXENE

The major element profiles for the R27A orthopyroxene mineral separates are shown in Figure 6.12, and the orthopyroxene major element data presented in Appendix III. Similarly with the whole-rock profiles, the most variable element abundances occur in the MR/MP pyroxenite package. The three pyroxenite domains identified in the whole-rock profiles are not obvious

MgO

R27A opx
Wt%

FeO

R27A opx
Wt%

Mg#

R27A opx

Fe2O3

R27A opx
Wt%

SiO2

R27A opx
Wt%

Cr2O3

R27A opx
Wt%
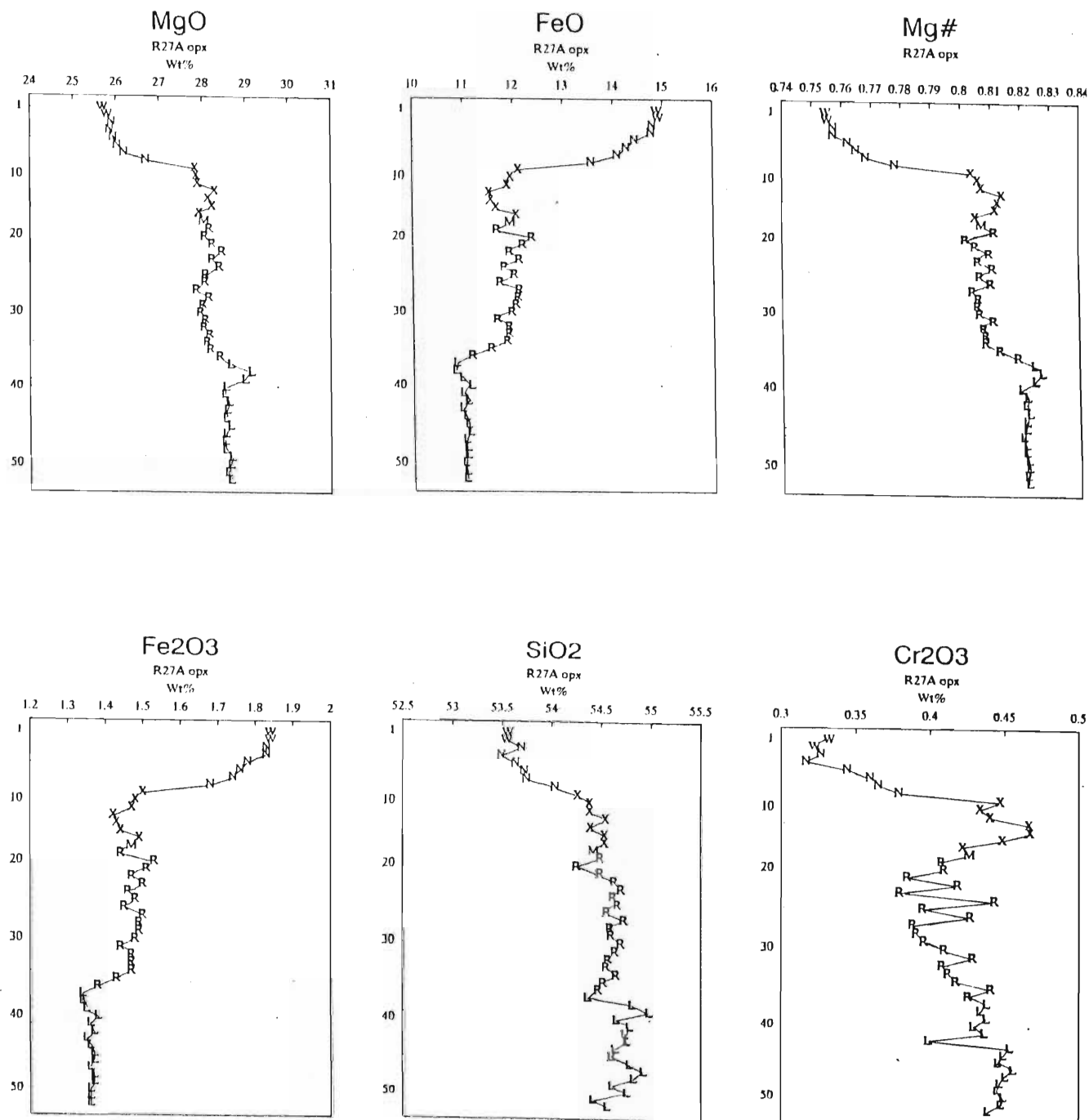
Figure 6.12a   R27A orthopyroxene major element profiles.
(refer to text for explanation of lithological symbols)
(sample numbers on y-axis)
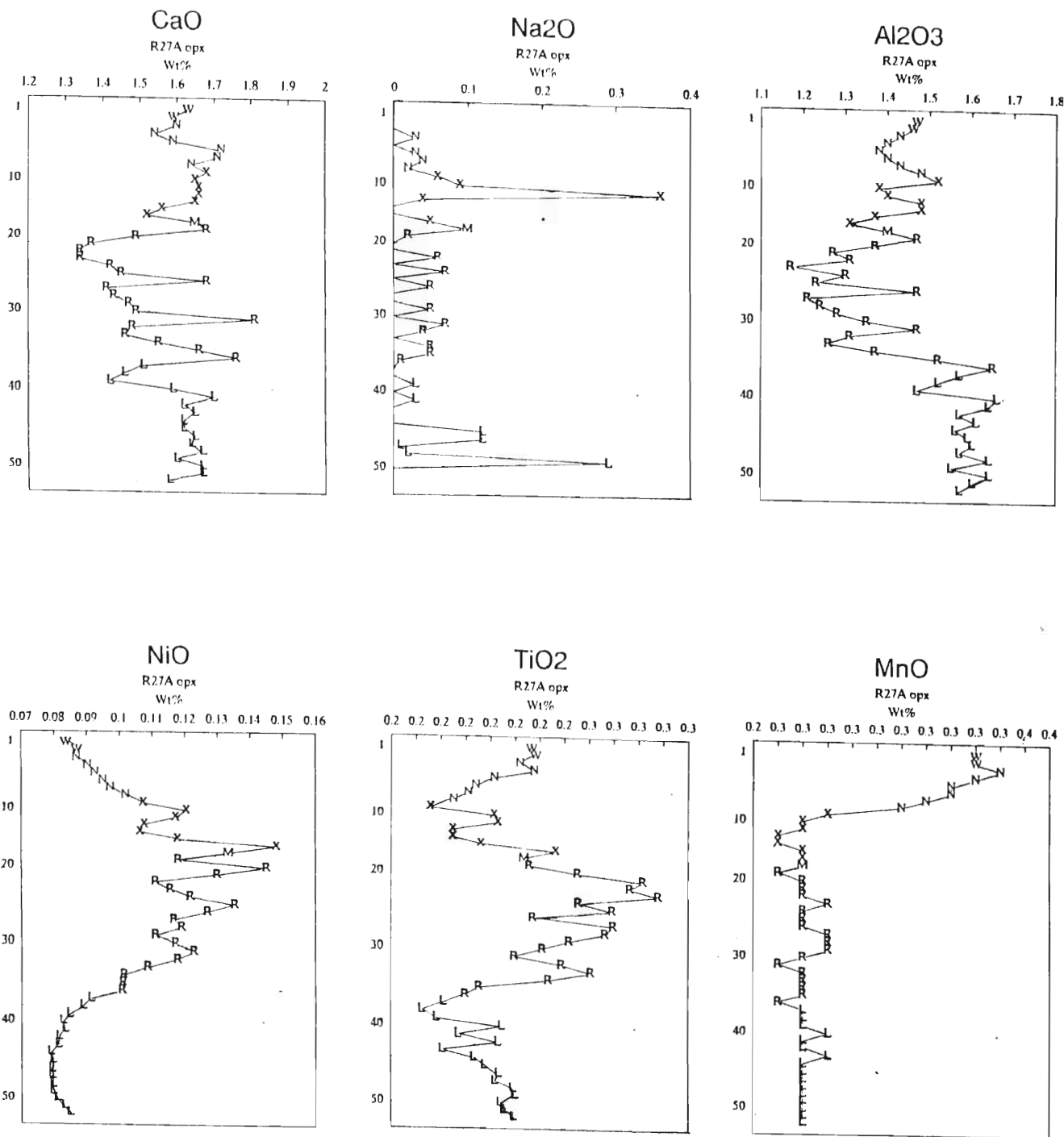
Figure 6.12b   R27A orthopyroxene major element profiles.

	W (2)	N (6)	X (7)	M (1)	R (18)	L (8)
SiO_2 wt%	53,55	53,72	54,43	54,42	54,58	54,71
Al_2O_3	1,47	1,42	1,42	1,40	1,35	1,58
Fe_2O_3	1,84	1,77	1,46	1,47	1,47	1,36
FeO	14,90	14,33	11,82	11,94	11,90	10,99
MnO	0,33	0,32	0,26	0,26	0,26	0,26
MgO	25,73	26,10	28,03	28,05	28,15	28,71
CaO	1,61	1,63	1,63	1,65	1,52	1,57
Na_2O	0,00	0,02	0,09	0,10	0,03	0,008
K_2O	0,00	0,00	0,00	0,00	0,00	0,00
TiO_2	0,2272	0,2103	0,2061	0,2238	0,2421	0,1975
Cr_2O_3	0,3268	0,3482	0,4461	0,4261	0,4097	0,4340
NiO	0,0852	0,0939	0,1178	0,1334	0,1178	0,0840
ZnO	0,00	0,00	0,00	0,00	0,00	0,00
Mg#	0,7548	0,7645	0,8086	0,8072	0,8083	0,8232

Table 6.4   Average R27A orthopyroxene major element compositions for
each rock type through the succession.
(figures in parentheses indicate the number of samples in
each case)

in the orthopyroxene chemistry. The average, lithologically grouped major element abundances calculated for the R27A orthopyroxene separates are presented in Table 6.4. The variable number of significant figures presented are simply a function of the calculations and are not intended to suggest differing degrees of data precision. The table is useful in that average trends through the succession are immediately obvious, eg orthopyroxene SiO_2 shows a progressive decrease from the footwall leuconorite (L) through to the hangingwall norite (N), which reflects the bulk composition of the pyroxene. The upward increase in FeO shows relatively little change in any compositional parameters. The orthopyroxene Mg# shows a general upward decrease through the lithologies, with some variation to this pattern observed within the MR/MP package (RMX).

The major element components of orthopyroxene (SiO_2, MgO and FeO/Fe_2O_3) reflect the stoichiometric relations (Fe^{3+} is calculated as 10% of total Fe). As expected, there is a very strong antipathetic variation between MgO and FeO, with SiO_2 following the variations of MgO, with sharp decreases and increases respectively into the hangingwall norite. The variations in orthopyroxene Mg# follow those of MgO. Cr_2O_3 also follows Mg# but shows exaggerated variations. Generally Mg# (and Cr_2O_3) show an overall decrease upwards through the succession with a significant reversal occurring in the Merensky pyroxenite.

The orthopyroxene magnesium number (opx Mg#) profile (Figure 6.12a) shows a stepwise upward decrease from the footwall leuconorite, through the MR/MP pyroxenite, to the hangingwall norite, also with a significant decrease from the Merensky pyroxenite into the overlying norite. The compositional variation within these three subdivisions is small but significantly different between the three. Average orthopyroxene composition varies from En_{82} in the footwall leuconorite, to En_{81} in the pyroxenite package, to En_{76} in the hangingwall norite-leuconorite-pyroxene anorthosite (Table 6.4).

The three-way lithology related grouping is emphasised in the plots of orthopyroxene Mg# v orthopyroxene Al_2O_3 and orthopyroxene TiO_2 v orthopyroxene Al_2O_3 (Figure 6.13). Orthopyroxene in the footwall leuconorite has the highest Mg# and shows an inverse relationship with Al_2O_3. Orthopyroxene in pyroxenite shows a weak positive trend between Mg# and Al_2O_3 and also shows the greatest range in Al_2O_3 (Figure 6.13b). Orthopyroxene in the hangingwall norites have the lowest Mg# and Al_2O_3 and a positive Mg#-Al_2O_3 trend. Inverse relationships between Al_2O_3 and TiO_2 exist in the pyroxenites and in the norites,
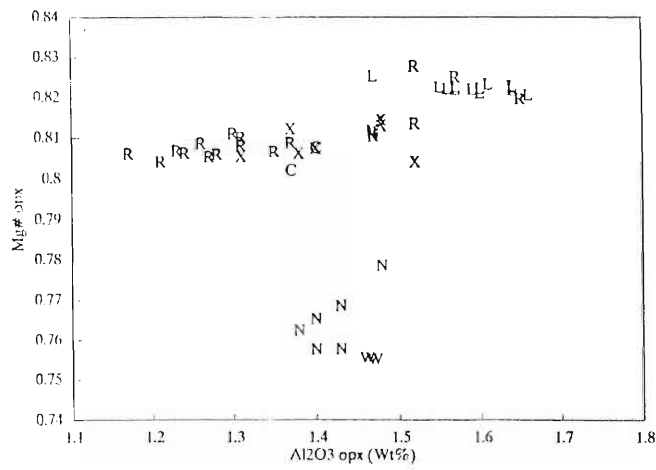
Figure 6.13a   Plot of orthopyroxene Mg number
v orthopyroxene Al_2O_3
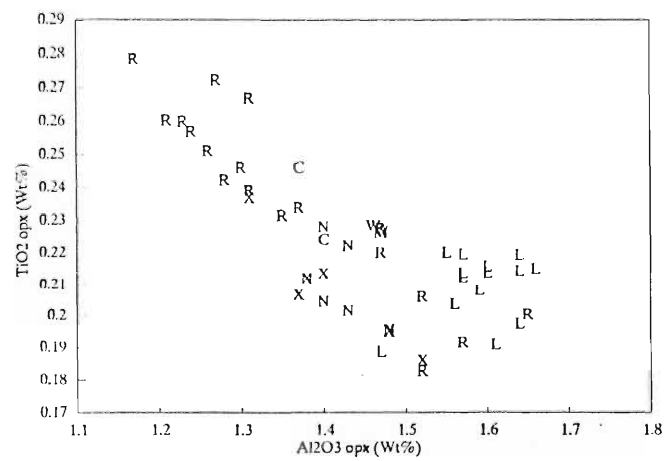
Figure 6.13b   Plot of orthopyroxene TiO_2 v
orthopyroxene Al_2O_3

whereas in the footwall leuconorite no compositional relationship is observed. Similar relationships exist in Critical Zone pyroxenites studied by Eales *et al* (1993), who discuss the control of plagioclase compositions on pyroxene chemistry.

NiO shows a completely different trend, with pyroxene in the footwall norites being particularly depleted in this component. NiO in orthopyroxene is highest in the pyroxenites, where a negative relationship exists with the orthopyroxene Mg# (Figure 6.14a). Levels of NiO are lower in the footwall and hangingwall norites where a positive relationship exists, with the high Mg# footwall leuconorite trend less well defined. Again the strong lithology related three way grouping is demonstrated. There is a broadly positive correlation between orthopyroxene NiO and whole-rock NiO (Figure 6.14b). This is indicative of late-stage Ni exchange or re-equilibration between base metal sulphides and orthopyroxene in this part of the sequence.

The CaO, Na_2O and Al_2O_3 profiles are more variable and erratic. Al_2O_3 in orthopyroxene shows general depletion in the Merensky reef, where TiO_2 is enriched. CaO is also generally depleted in the reef but with some erratically high values. Both the orthopyroxene CaO and Al_2O_3 show highly variable profiles through the pyroxene cumulate sequence. This would suggest late-stage modification of the orthopyroxene composition, a concept further supported by the relatively smooth trends in the adjacent norites. The general trends defined by the footwall leuconorite may be extrapolated to coincide with the commencement of the smooth profiles within the hangingwall norite. Na_2O is generally less than 0,1 wt% and thus samples with higher than this value may be slightly altered.

Studies on the Great Dyke pyroxene cumulates (Wilson, 1992) have revealed a fine-scale relationship between Mg# and whole-rock incompatible elements such as P and Zr. P v Mg# plots were found to define offset arrays which represent individual cryptorythmic units derived from discrete coherent liquid packages. Wilson (1992) interprets these patterns as a progressively decreasing Mg# for orthopyroxene with increasing P content in the whole rock, where the variation in orthopyroxene Mg# in each of the cryptorythmic units is related to the amount of trapped intercumulus liquid which reacted with the pyroxene (determined from the P concentration). Each of the cryptorythmic units represents a crystallisation episode from a discrete magma layer. The slope of each array is dependent on the relative P content of the magma (the steeper the slope the greater the P content), and the compositional intercepts, at zero P content, reflect the original liquidus composition of the pyroxenes. Later interaction with
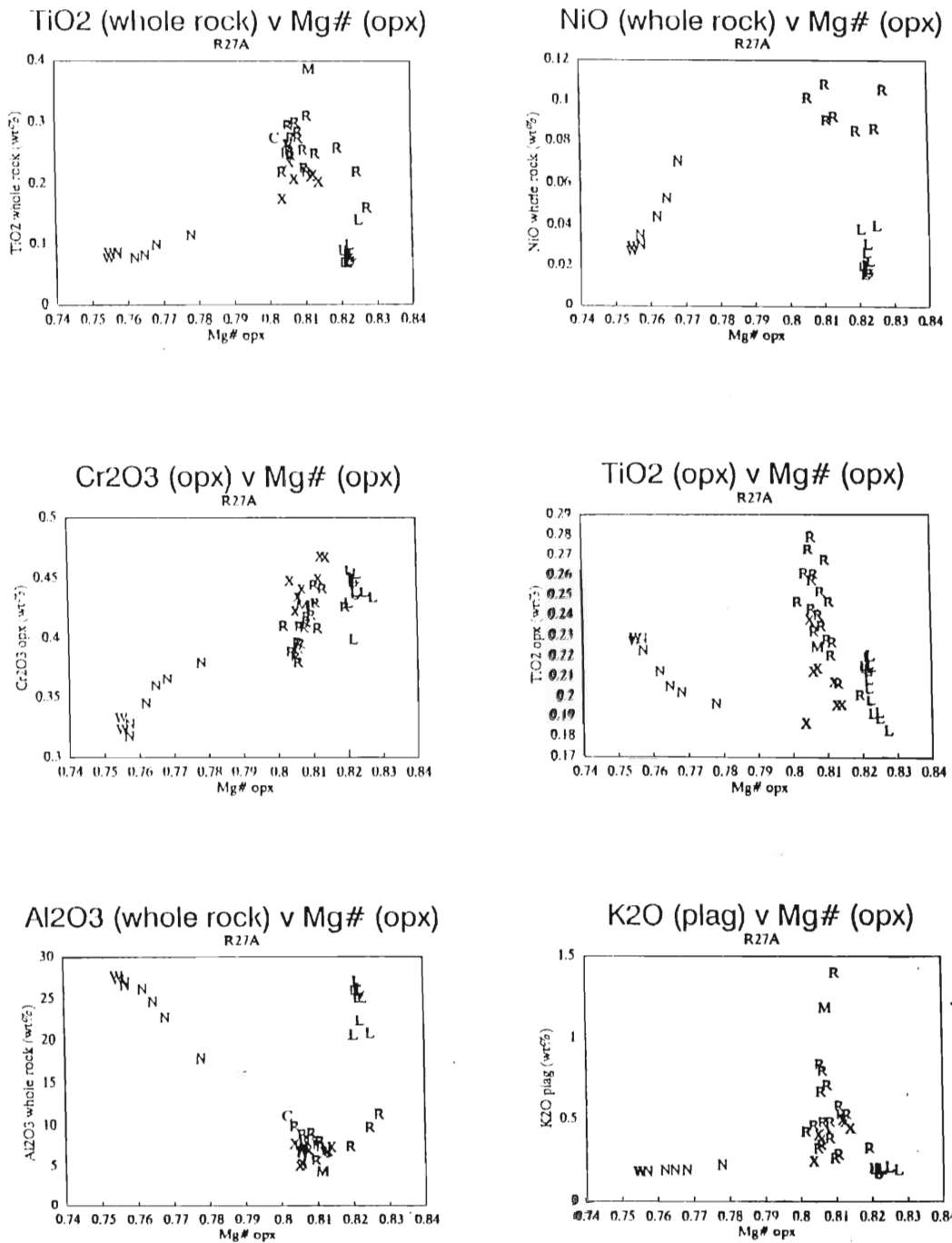
Figure 6.15a   A variety of plots with orthopyroxene magnesium
                number showing the three-way lithological
                grouping.
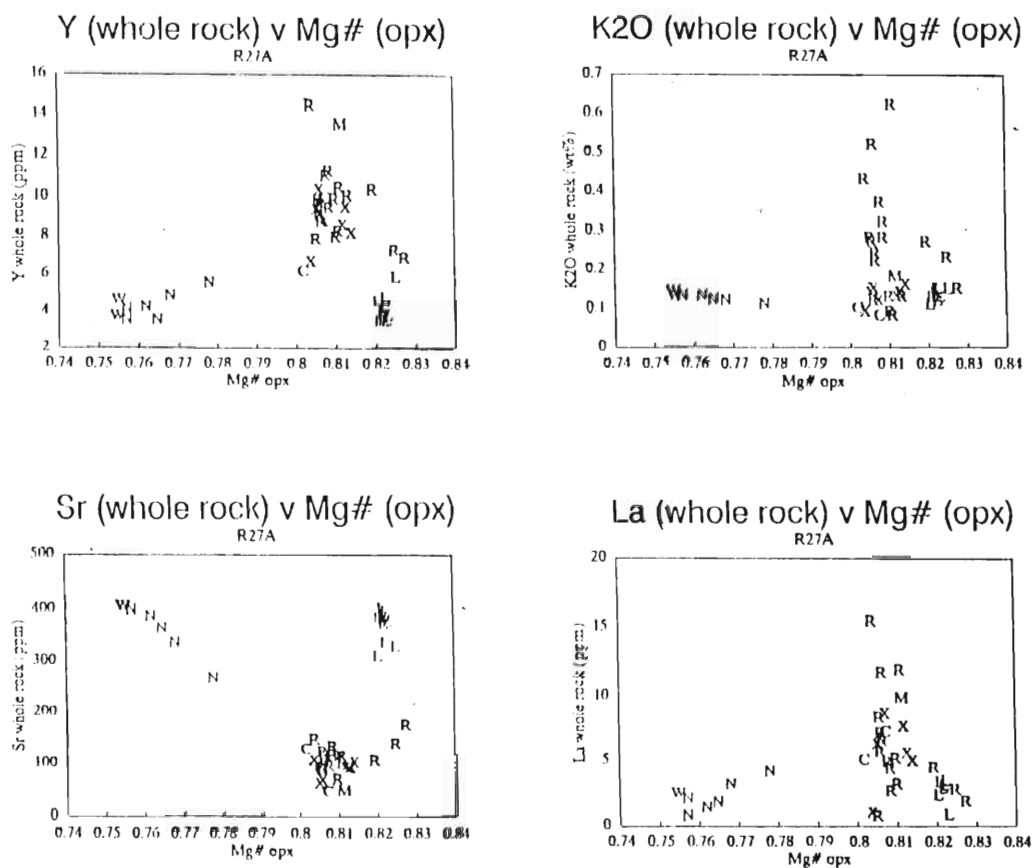
Figure 6.15b   A variety of plots with orthopyroxene magnesium
                number showing the three-way lithological
                grouping.

trapped liquid subsequently altered the composition of the orthopyroxenes (Wilson, 1992).

Similar plots, using Zr instead of P, were investigated for the R27A Merenksy section (Figure 6.14c). Unlike the Great Dyke, no offset cyclic arrays were found, but rather a scatter of points defining a lithology-related three-way grouping. The pyroxenite group shows the greatest scatter of points, and any trend extrapolated to zero Zr shows no significant change in Mg#. The footwall leuconorites have low Zr and high Mg#, and lie on an extension of the weak negative trend shown in the pyroxenite group. The third group consists of the hangingwall norites, which show evolved Mg# and low Zr, but no distinct trend. This pattern is similar to that shown by the higher variability Al_2O_3 v Zr plot, where there is evidence of late-stage interaction between these elements. It must therefore be deduced that the controls observed for the Great Dyke do not apply to the Merensky reef studied in this work.

Remarkably similar distributions emphasising the lithology related three-way grouping is repeated in the relationships between orthopyroxene Mg# and elements such as whole-rock Sr, La, Y, Zn, K_2O and Al_2O_3 (Figure 6.15a & b). These elements all show almost identical distribution patterns with respect to orthopyroxene Mg#.

6.3.2 PLAGIOCLASE

Average plagioclase compositions for the R27A section are presented in Table 6.5, and the major element stratigraphic profiles in Figure 6.16. The plagioclase major element data is presented in Appendix III. In most cases prominent element enrichments or depletions define the MR/MP pyroxenite package, in which there is the greatest variation in abundance. Similar to the whole-rock element profiles where the pyroxenite is subdivided into three domains, the bottom ± 0,3m of the Merensky reef is characterised by smooth profiles, leading into the more 'sawtooth' shaped profiles of the upper reef, then smoothing off slightly into the Merensky pyroxenite.

As expected, plagioclase CaO and Na_2O show mirror image trends. Stoichiometric requirements require that SiO_2 and CaO show almost perfect mirror image variations, whereas Al_2O_3 and SiO_2 show identical patterns. Plagioclase MgO is uniformly low (<0,4 wt%) but an anomalous zone of high values occurs in the upper Merensky reef. There is no obvious sign
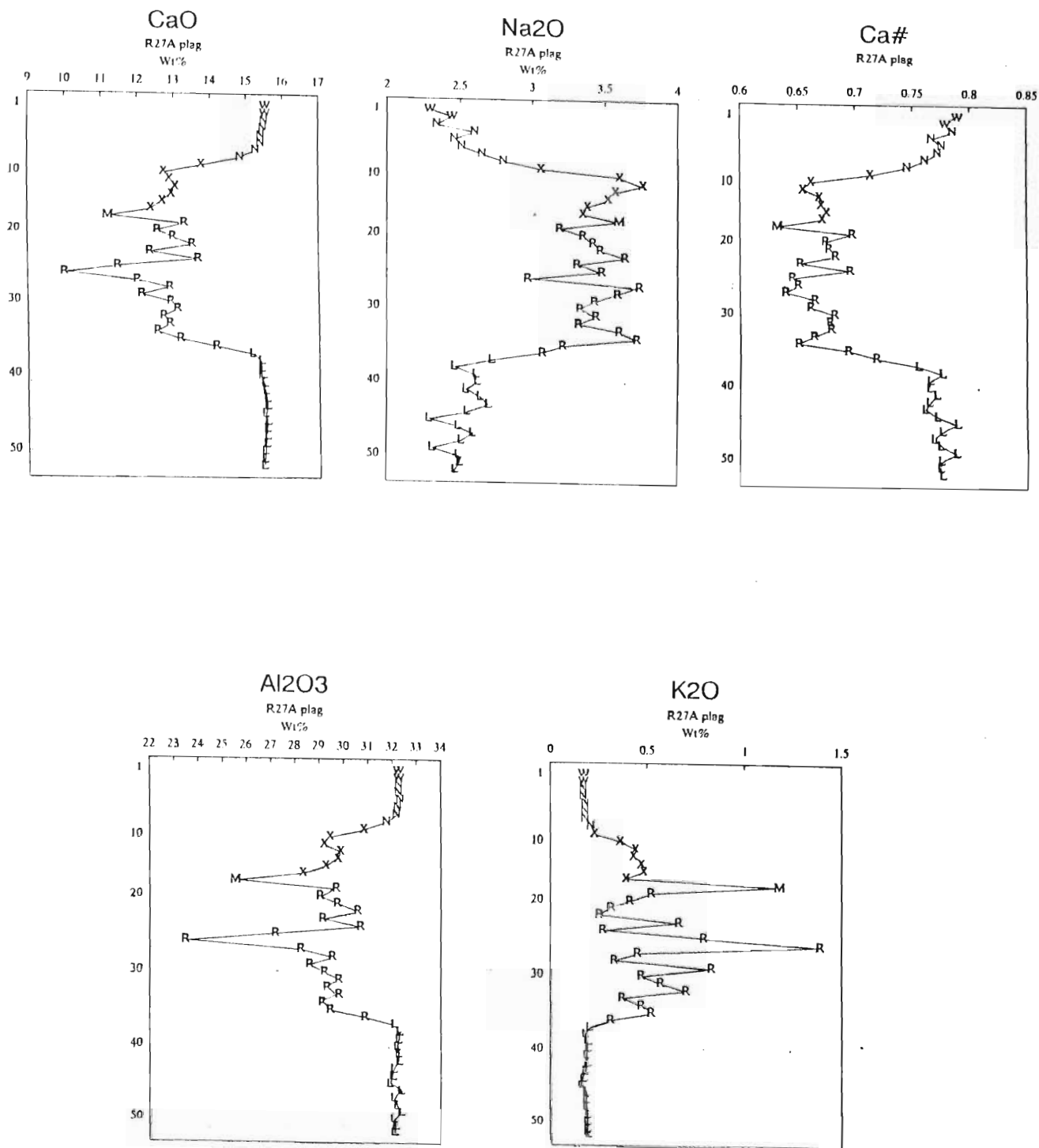
Figure 6.16a   R27A plagioclase major element profiles.
(refer to text for explanation of
lithological symbols)
(sample numbers on y-axis)
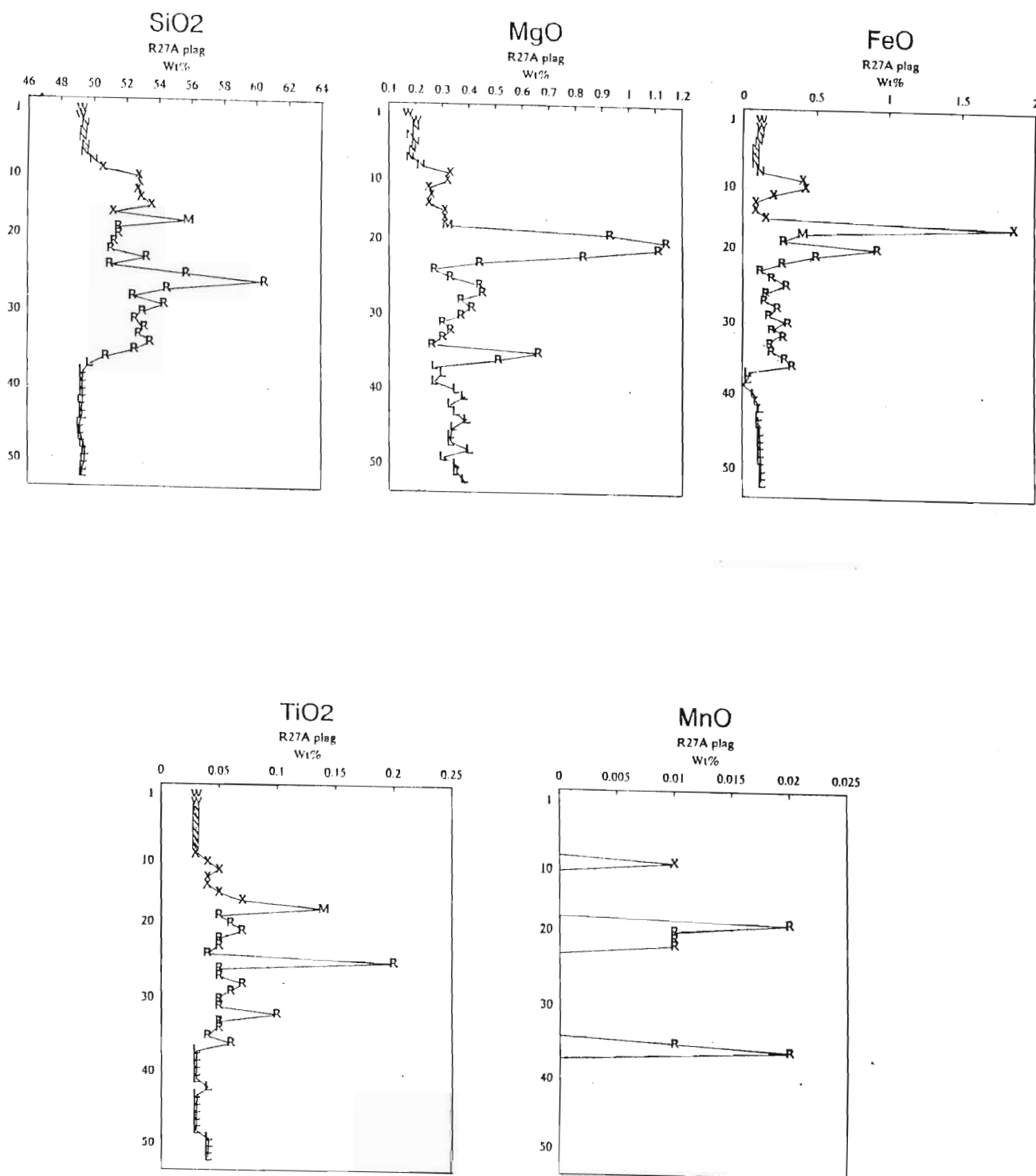
Figure 6.16b   R27A plagioclase major element profiles.

	W (2)	N (6)	X (7)	M (1)	R (18)	L (8)
SiO_2	49,22	49,54	52,40	55,87	53,10	49,38
Al_2O_3	32,26	32,17	29,53	25,54	20,09	32,18
Fe_2O_3	0,00	0,00	0,00	0,00	0,00	0,00
FeO	0,12	0,10	0,46	0,41	0,29	0,07
MnO	0,00	0,00	0,001	0,00	0,004	0,00
MgO	0,19	0,20	0,29	0,32	0,53	0,33
CaO	15,52	15,33	12,94	11,21	12,70	15,44
Na_2O	2,37	2,56	3,46	3,60	3,40	2,61
K_2O	0,17	0,18	0,40	1,18	0,53	0,19
TiO_2	0,03	0,03	0,05	0,14	0,34	0,03
Cr_2O_3	0,00	0,00	0,00	0,00	0,00	0,00
NiO	0,00	0,00	0,00	0,00	0,00	0,00
ZnO	0,00	0,00	0,00	0,00	0,00	0,00
Ca#	0,7840	0,7680	0,6738	0,6325	0,6729	0,7662

Table 6.5   Average R27A plagioclase major element compositions
for each rock type through the succession.
(figures in parentheses indicate the number of
samples in each case)

of contamination of plagioclase in the separates and the distribution can probably be explained by minor chloritisation and other alteration. TiO_2 and MnO occur in very low abundances. TiO_2 shows an erratic decrease up through the footwall leuconorite, followed by a highly erratic increase through the Merensky reef, subsiding into the Merensky pyroxenite. Abundances again increase sharply into the hangingwall norite. MnO shows a low, constant abundance through the sequence, and only shows a sharp increase at the top of the Merensky pyroxenite, which continues into the hangingwall norite.

Compositional profiles for plagioclase separates define two broad lithological groupings in calcium number (Ca#), FeO and K_2O contents, amongst others. Plagioclase in the footwall and hangingwall norites have very similar compositions, whereas pyroxenite plagioclase has a considerably lower, evolved Ca# and higher K_2O and FeO abundances, all with high variability.

There is the expected dense grouping and curvilinear relationship between CaO and Na_2O in plagioclase (Figure 6.17). This arises from stoichiometric controls, but also highlights the broad differences in composition of plagioclase between the norites and the pyroxenite unit.

Average plagioclase compositions range from An_{77} in the footwall leuconorite, to An_{67} in the MR/MP pyroxenites, to An_{77} in the hangingwall norite/pyroxene anorthosite (Table 6.5). The plagioclase Ca# profile (Figure 6.16a) shows a variable but systematic upward decrease through the footwall leuconorite, followed by a sharp drop into the overlying pyroxenite, where a constant to weakly increasing trend commences, followed by a strong increasing trend into the hangingwall norite and pyroxene anorthosite. The low Ca# of plagioclase in the pyroxenite together with the transitional compositions of the hangingwall norite trends would appear to be the result of late-stage influence on the plagioclase chemistry. The relationship between incompatible element chemistry and that of the cumulus and dominant intercumulus minerals is of importance. The plagioclase Ca# profile is broadly comparable to the profiles of the incompatible elements (Figure 6.4), which suggests some late-stage influence, particularly within the pyroxenite interval. The interaction of trapped intercumulus liquid and late-stage reaction and re-equilibration with cumulus orthopyroxene is known to have compositional effects on both the cumulus pyroxenes and the intercumulus plagioclase (Cawthorn & McCarthy, 1985; Barnes, 1986; Wilson, 1992). However, it cannot be assumed that the plagioclase crystallised entirely from the trapped liquid, as further compositional controls still need to be assessed.
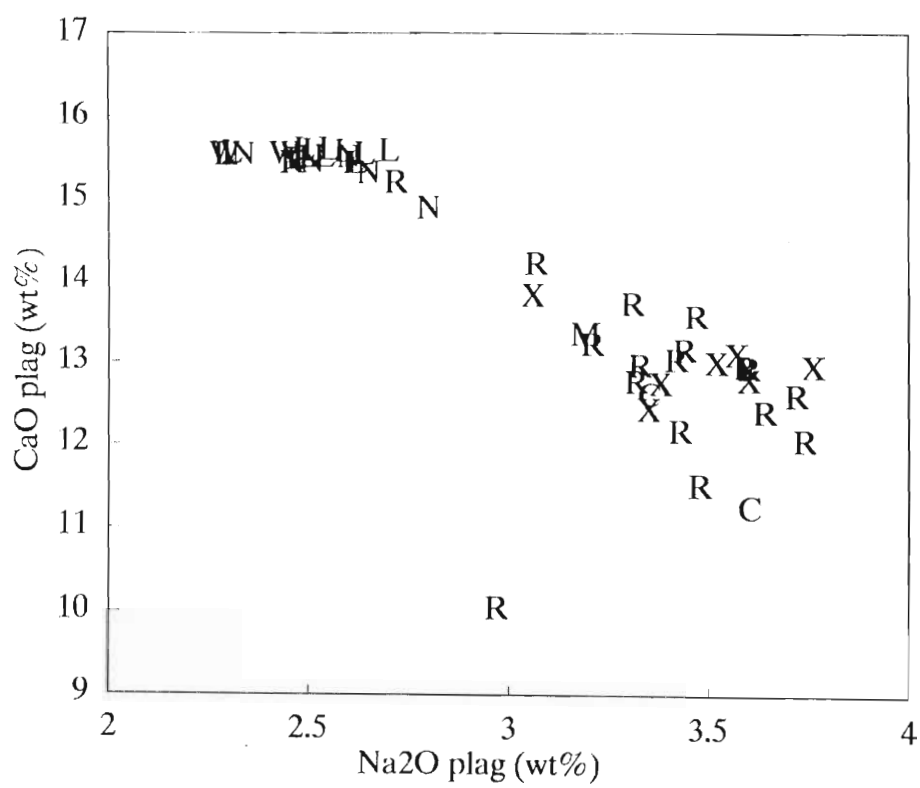
Figure 6.17   Plot of plagioclase CaO v plagioclase Na_2O

Binary plots of plagioclase components against whole-rock trace elements which may be controlled by plagioclase, *eg* Rb, Sr and K_2O, show contrasted patterns. A very crude positive relationship exists for plagioclase K_2O v whole-rock Rb in the pyroxenites, but not in the norites, which form a tight cluster with low abundances of these elements (Figure 6.18a). The plagioclase CaO v whole-rock Sr plot (Figure 6.18b) defines two groups, the first consisting of the pyroxenites, and the second of the footwall and hangingwall norites, both with rough positive trends. The pyroxenites show a steep, rough positive trend and somewhat lower abundances than the norites. The latter define a group with higher CaO-Sr abundances and a rough positive trend. The plagioclase CaO v whole-rock Rb relationship (Figure 6.18c) is the expected mirror image opposite of the plagioclase K_2O v whole-rock Rb, in which a rough negative relationship is observed within the pyroxenites. The footwall and hangingwall norites form a tight cluster with higher CaO and low Rb.

The plagioclase Ca# v orthopyroxene Mg# binary plot (Figure 6.19a) illustrates convincingly the three lithologically defined groups. The footwall plagioclase cumulates fall into a tight, high Mg#-Ca# group but do not show evidence of any geochemical trend. The pyroxene cumulates have evolved plagioclase Ca# and orthopyroxene Mg# and show a weak positive relationship. The hangingwall plagioclase cumulates form the third group, and show the most evolved orthopyroxene Mg#, but high plagioclase Ca#, and a clear negative trend. There is a close inter-relationship between plagioclase and pyroxene mineral chemistry. This is demonstrated in the plagioclase Ca# v orthopyroxene TiO_2 plot (Figure 6.19b), which shows two trends, with all samples from the footwall and hangingwall norites lying on the same positive trend. In the plagioclase cumulates the positive relationship would reflect primary liquidus conditions, with TiO_2 being partitioned into orthopyroxene at high temperature, thereby establishing the relationship with plagioclase Ca#. Orthopyroxene and postcumulus plagioclase have a trend of decreasing TiO_2 with increasing Ca# as a result of the two phases forming at different times. Low TiO_2 in pyroxene indicates restricted interaction of this mineral with trapped liquid at close to magmatic temperatures, when the plagioclase Ca# is also high. Greater interaction at lower temperatures is indicated by high TiO_2 and low Ca#. Thus in the feldspathic pyroxenites a systematic interaction with trapped liquid may be inferred from the increasing TiO_2 trend.
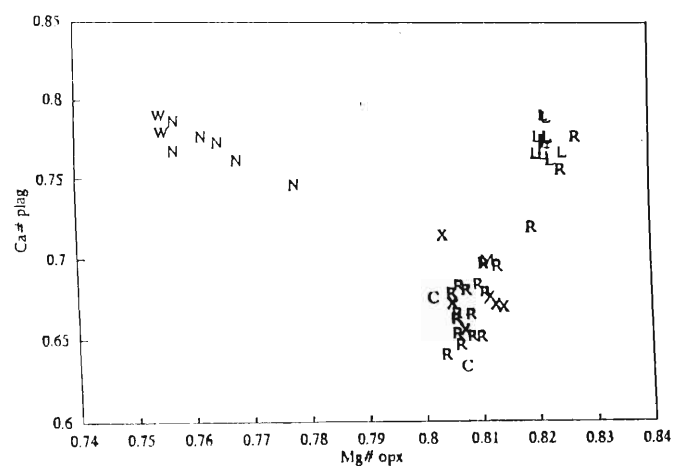
Figure 6.19a   Plot of plagioclase Ca number v orthopyroxene Mg number.
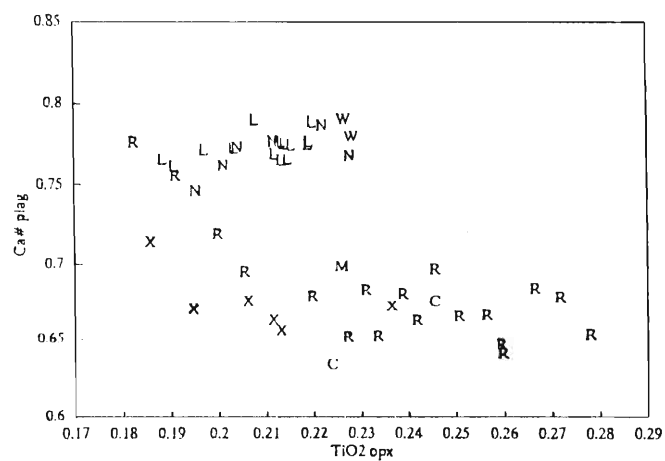
Figure 6.19b   Plot of plagioclase Ca number v orthopyroxene TiO$_2$

6.4 PLATINUM-GROUP ELEMENT GEOCHEMISTRY

6.4.1 GENERAL

Platinum-group elements (PGE) and gold (Au) occur with sulphides in several lithological environments, each with a particular geochemical characteristic. This feature has complicated efforts to produce an overall model for PGE concentration in the Merensky reef, and even more so, any universal model for PGE deposits in general. Table 6.6 shows a comparison of some selected PGE deposits as an example of inter-complex variability. The metal content of the Great Dyke (Wilson *et al*, 1989; Wilson & Tredoux, 1990; Coghill & Wilson, 1993), Munni Munni (Barnes & Keays, 1992), Penikat and Platreef (C.A.Lee, *pers comm*) deposits is variable and PGE grade varies little, if at all, with width of the mineralised zones. It is important here to draw attention to the fact that the Merensky reef metal content (cmgt^{-1} or cmppm) is constant irrespective of reef thickness, and therefore PGE (and base metal) grade (gt^{-1} or ppm) varies with reef thickness (*ie* the thicker the reef the lower the grade). This is a long-established phenomenon, which constitutes a fundamental contrast between the Merensky reef and other PGE-mineralised sequences, and one which must be incorporated into interpretations. To date this has not been done.

Many layered mafic and ultramafic complexes, in particular those which host economic PGE occurrences, are PGE-bearing throughout. The PGE occur at very low levels and exhibit a lithologically controlled pattern to the abundances. Studies in the Bushveld Complex show chromite > feldspathic pyroxenite > norite > anorthosite to be the decreasing order of PGE abundance in 'non-mineralised' rocks (Lee, 1989). In mineralised complexes, the PGE-sulphide enriched rocks have no geochemical footwall indicator to suggest or predict the overlying PGE-carrier. The Great Dyke has < 1ppm Pt and Pd (with Pt/Pd < 1) in the footwall, and then an abrupt 2 to 6-fold increase in both elements and a change in the Pt/Pd ratio to > 1, after which abundances decrease sharply into the hangingwall (Wilson & Tredoux, 1990). The Munni Munni Complex is Pd-dominant. Here the geochemical profiles show a gradual increase in Pd relative to Pt below the mineralised zone and a sharp decrease in both elements above the sequence (Barnes & Keays, 1992). Both the Great Dyke and the Munni Munni complexes have hangingwall offset Cu-Ni peaks, which are decoupled from the underlying precious metal peaks. These differ from the Merensky reef and Platreef patterns.

DEPOSIT	WIDTH (m)	Cu/Ni	Pt/Pd	METAL CONTENT RELATIVE TO WIDTH
Great Dyke	1-3	≥ 1	≥ 1	Variable
Munni Munni	3-7	$>->1$	<1	Variable
Penikat	1-20	$>->1$	>1	Variable
Platreef	1->20	≤ 1	≤ 1	Variable
Merensky reef	0,4-16	<1	>1	Constant

Table 6.6   Some fundamental contrasts between selected PGE-bearing layered intrusions.

In most cases the overall Pt/Pd ratio reflects the overall Pt-dominant or Pd-dominant character of the silicate host rocks, provided they are not extreme adcumulates (*ie* no interstitial material), and will have PGE ratios with the same characteristics as the mineralised zones. An exception is the Great Dyke where there is a change from Pd-dominance in the cumulates to Pt-dominance in the mineralised zones. In a PGE study of the Lower Group (LG) and Middle Group (MG) chromitites of the Bushveld Complex (Lee & Parry, 1988), a correlation between high modal chromite and depleted PGE has been documented. Anorthosite and leuconorite in the Rustenburg layered sequence are generally PGE-depleted relative to the feldspathic pyroxenites. These rocks tend to exhibit lithology-specific Pt/Pd ratios, with pyroxenite > 1 and plagioclase cumulates < 1. Thus there is some evidence of lithological and textural influence on the element abundances and ratios. This feature is demonstrated by the generally higher noble metal contents in chromitite, or rock containing accessory chromite (Lee, 1989).

The geochemical patterns for PGE and related chalcophile elements differ according to overall abundance. The geochemical inter-relationships are best displayed in mineralised sequences. In rocks with trace amounts of these elements, inter-relationships are poor to non-existent, which may reflect sampling problems using borehole core. Furthermore, each mineralised sequence has particular and unique geochemical patterns, and metal contents, which have to be accounted for. Contrasted PGE patterns in various Bushveld rocks are part of the interpretive approach in understanding PGE mineralisation. Geochemical inter-relationships in the PGE may be a function of overall abundance. An example of this is the Great Dyke, where the ratios of the PGE are dependent on the levels of abundance. This however, does not appear to be a fundamental characteristic of the Merensky reef.

6.4.2 PGE DISTRIBUTION AND RELATIONSHIPS

Stratigraphic profiles for the R27A section whole-rock platinum-group elements (PGE) and Au are presented in Figure 6.20, and average PGE abundances in Table 6.1. The PGE data for sections R27A and R25A are presented in Appendix IV. As is typical of Merensky reef PGE abundances;

Platinum (Pt) > Palladium (Pd) > Ruthenium (Ru) > Rhodium (Rh) > Gold (Au) > Iridium (Ir) > Osmium (Os).
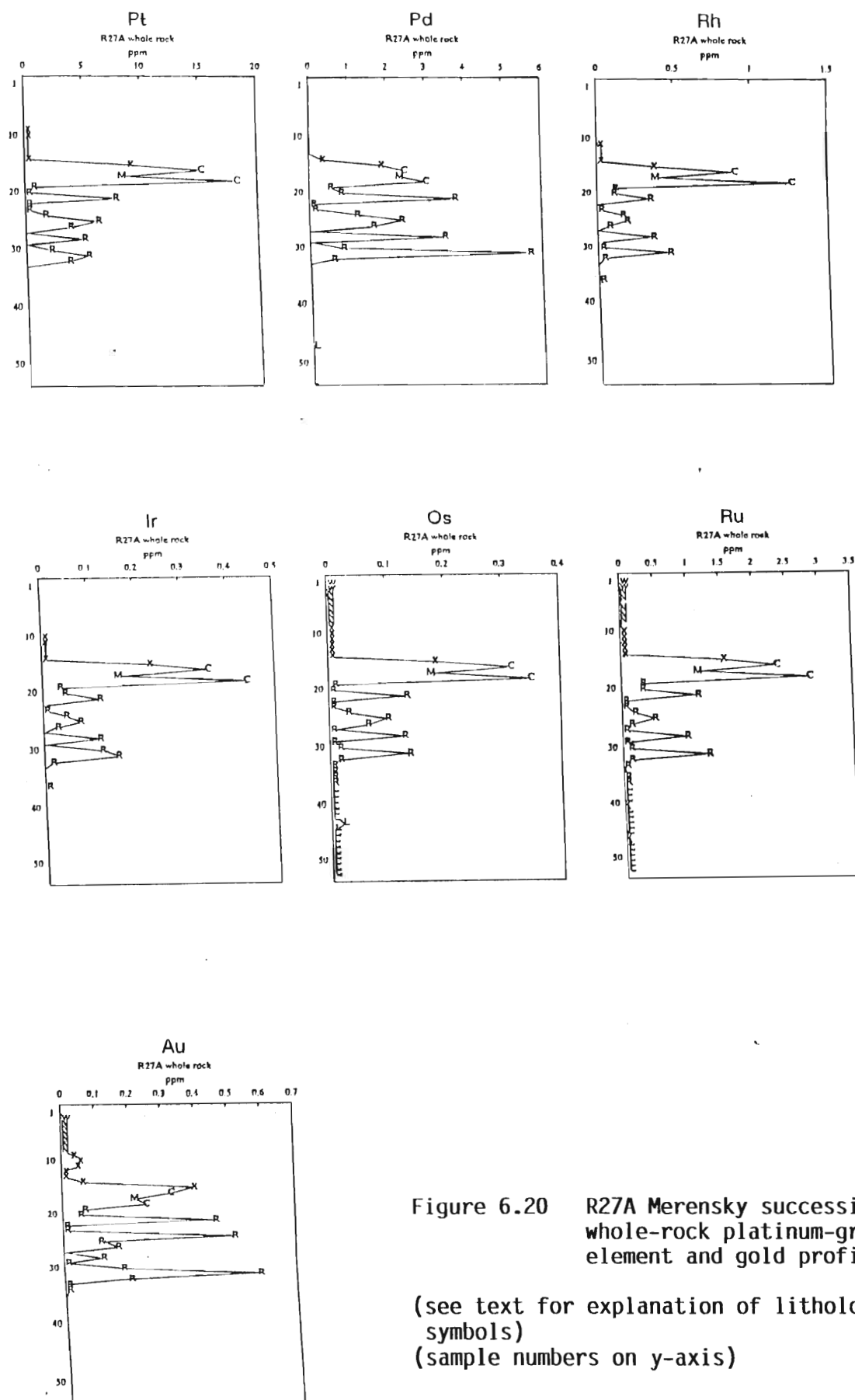
Figure 6.20   R27A Merensky succession
               whole-rock platinum-group
               element and gold profiles.

(see text for explanation of lithological
 symbols)
(sample numbers on y-axis)

The R27A PGE profiles presented in this study are the first so far examined which relatively accurately delineate the Merensky reef (MR) apart from the overlying Merensky pyroxenite (MP). The PGE profiles are typically jagged or `sawtooth' shaped and show high variability, which may be regarded as a characteristic feature of the Merensky reef. It is of note that elevated PGE abundances appear only some 0,3 to 0,4m (3 to 4 samples) above the Merensky reef basal contact (basal chromitite layer is absent in this reef facies). This position coincides exactly with the commencement of the highly variable major and trace element profiles, ie the ± 1,5m thick middle pyroxenite domain, which is now accurately defined by the variably enriched PGE+Au abundances. Immediately above the uppermost chromitite layer, which defines the Merensky reef top contact, there is an abrupt termination of PGE-enrichment. PGE profiles for the R25A section (0,28m thick MR) are presented in Figure 6.21 for comparison.

With the exception of Pd, all the R27A PGE initially appear to follow similar upward-increasing profiles, with the highest values associated with the chromitite layers. On closer inspection however, there are no increasing or decreasing trends in the PGE profiles. This is consistent with the Pt/Pd ratio profiles in which no trends are observed (see following text). In each case, the higher PGE value of the two chromitite-related peaks coincides with the lower chromitite layer. The profiles are broadly comparable with those of S, Cu and Ni (see Figure 6.4a), with some local offset of PGE and base metal peaks, which suggests some localised late-stage decoupling. Pd follows an almost reverse profile, with the highest values occurring towards the bottom of the reef (rather than at the chromitite layers). Au follows a similar trend to Pd, but unlike the PGE it also shows relatively elevated values at the base of the Merensky pyroxenite, and a higher value in the upper chromitite layer rather than the lower one. Peck & Keays (1990), in their study of the Heazlewood River Complex, found Pd and Au to be both closely related, and show the greatest deviation from patterns shown by the other PGE. They demonstrated the incompatible nature of Pd by its strong negative correlation with whole-rock Mg#, and its strong positive correlation with whole-rock TiO_2. These relationships are confirmed by the R27A data, where a strong, but steeper negative correlation was found with Pd v whole-rock Mg# (Figure 6.22a). Similarly, the strong positive relationship with Pd v whole-rock TiO_2 is consistent with the above findings, however with a somewhat steeper, near linear relationship (Figure 6.22b). A binary plot showing the relationship between the R27A Pd and Au data is presented in Figure 6.22c. In spite of a relatively wide scatter of points, there is a suggestion of a moderate correlation between these elements (see later discussion on
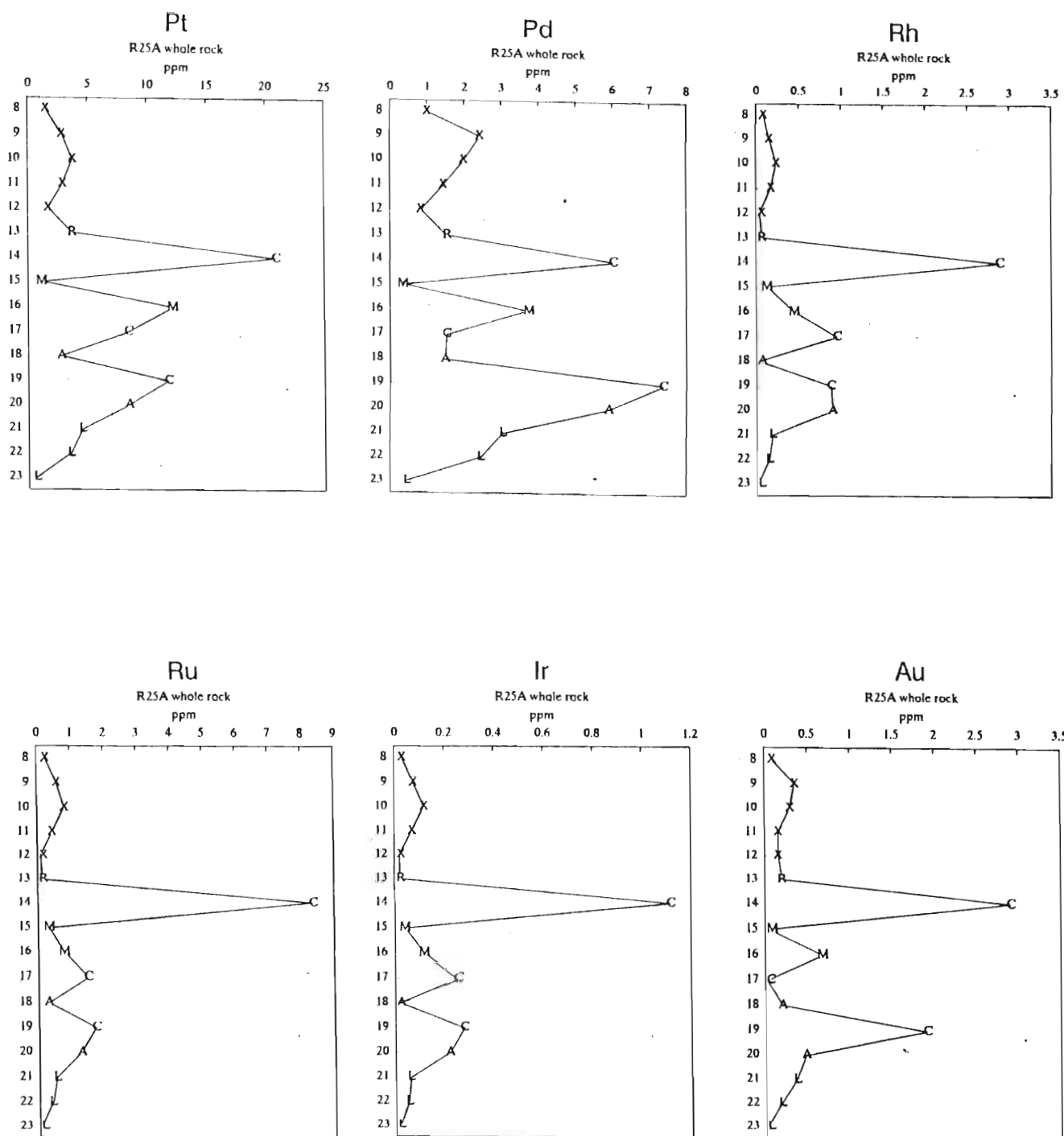
Figure 6.21   R25A Merensky succession whole-rock platinum-group element and gold profiles.
(see text for explanation of lithological symbols)
(sample numbers on y-axis)
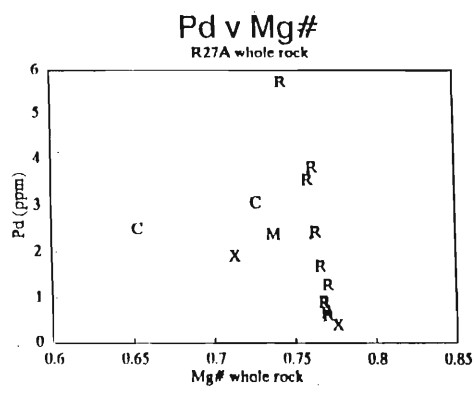
Figure 6.22a   Plot of Pd v whole-rock Mg number.
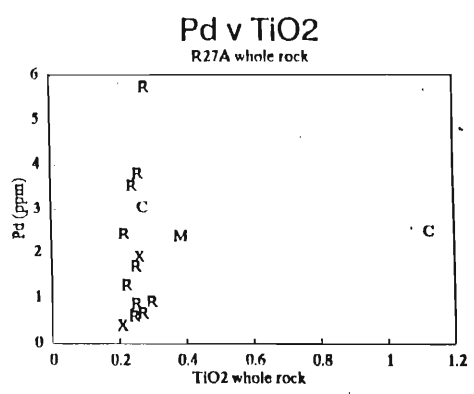
Figure 6.22b   Plot of Pd v whole-rock TiO_2.
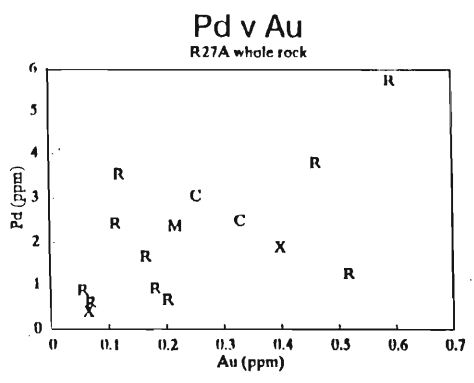
Figure 6.22c   Plot of Pd v Au.

correlation coefficients).

In broad terms the R25A section shows the same basic geochemical features, however, with much of the detail masked due to the considerably thinner Merensky reef. As is typical of the thinner Merensky reef facies, the PGE values extend to greater distances into the footwall and hangingwall, and as such, the Merensky reef itself may not be as clearly geochemically identifiable, save perhaps by the high PGE peak values commonly associated with the chromitite layers. The R25A section is atypical in that a rare chromitite layer is developed within the footwall anorthosite. With the exception of Pd, the highest PGE values are associated with the upper chromitite layer, while values in the reef basal chromitite layer are relatively depleted. The chromitite layer within the footwall anorthosite shows higher values than the basal chromitite layer and is also host to the Pd peak value. It is of interest to note that the immediate footwall anorthosite is highly depleted in PGE. This is consistent with observations discussed in Chapter 4, where it is noted that the footwall anorthosite is typically devoid of BMS relative to the underlying leuconorite. Routine assays of thin and medium reef sequences at RPM Rustenburg Section also consistently show the footwall anorthosite to be PGE-depleted relative to the immediate underlying leuconorite.

The Pt/Pd ratio is a commonly used measure for expressing the relative abundances of Pt and Pd. The R27A Pt/Pd ratio (Figure 6.23a) follows a variable profile through the MR/MP pyroxenite package, but does not show any convincing increasing or decreasing trends. This suggests that the PGE were not fractionated, unlike the Great Dyke, where an upward decreasing trend in the Pt/Pd ratio occurs (A.H.Wilson, *pers comm*). The single very high R27A Pt/Pd value which occurs in the Merensky pyroxenite may be disregarded, as it is likely an abnormal nugget effect due to local dominant PGM control on Pt. The Pt/(Pt+Pd) ratio is also commonly used for expressing the relative abundances of Pt and Pd. The R27A Pt/(Pt+Pd) profile is presented in Figure 6.23b, and similarly shows no distinct trends. The R27A Pt/Pd and Pt/(Pt+Pd) ratios are summarised in Table 6.7. The Pt/Pd and Pt/(Pt+Pd) ratio profiles for the R25A section are shown in Figure 6.24 for comparison, and show similar patterns to the R27A section. These values indicate considerable enrichment of Pt over Pd in all Merensky reef/Merensky pyroxenite components.
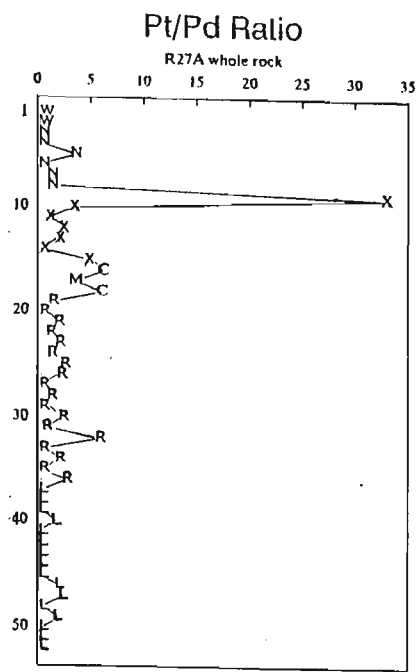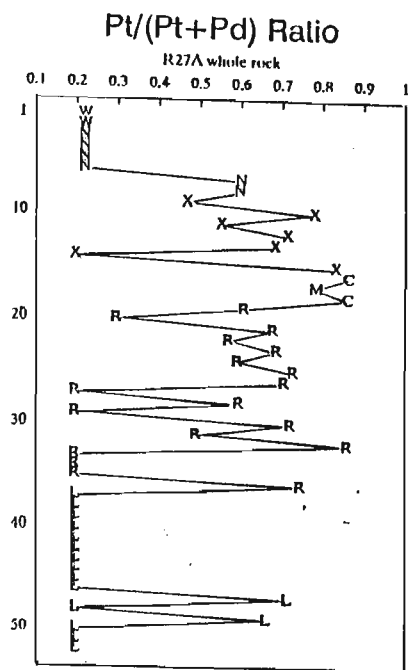
Figure 6.23   R27A Pt/Pd ratio profile (a), and Pt/(Pt+Pd) ratio profile (b).
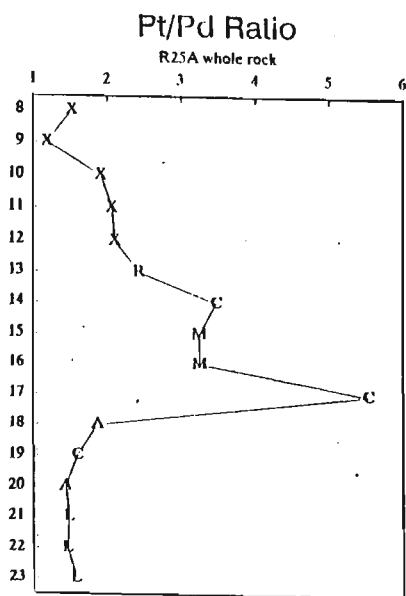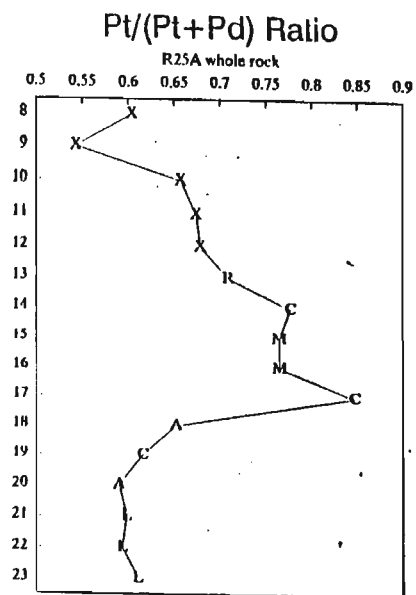
Figure 6.24   R25A Pt/Pd ratio profile (a), and Pt/(Pt+Pd) ratio profile (b).

ROCK UNIT	Pt/Pd	Pt/Pt+Pd
Whole sequence	2,6	0,57
Merensky pyroxenite	2,5	0,60
Merensky reef (inc. chromitite layers)	2,8	0,56
Merensky reef (exc. chromitite layers)	2,4	0,53
Chromitite layers	6,1	0,86

Table 6.7   Mean Pt/Pt and Pt/(Pt+Pd) ratios for the complete R27A succession and components of the Merensky reef/Merensky pyroxenite package.

The variations of total PGE+Au with base metals and silicate mineral compositions in the R27A study section are shown in Figure 6.25. As noted previously, orthopyroxene Mg# and plagioclase Ca# profiles show several patterns of variance progressing up the sequence. Although sharp lithological boundaries exist in places, the changes in mineral composition are gradational, and compositional variance is offset from the lithological contact. These in turn can be correlated with whole-rock data for Cu, Ni and PGE. Also significant is the close geochemical similarity of pyroxenite and pegmatoidal pyroxenite, notwithstanding the textural contrasts. A similar observation has been made at Atok platinum mine (Lee & Butcher, 1990), with high but variable mineral composition and trace element contents. The R25A profiles reveal similar patterns with respect to PGE.

The evolved plagioclase Ca# profile in Figure 6.25 strongly highlights the zone of late-stage hydromagmatic alteration (ie the MR/MP pyroxenite package). It is significant to note that both the elevated Cu & Ni (Figure 6.25a), and elevated PGE+Au values (Figure 6.25b), coincide exactly at a point some 0,4m (4 samples) above the Merensky reef basal contact, where the irregular, variable and evolved plagioclase Ca# profile commences. Although the elevated PGE+Au values decrease immediately below the upper limit of this evolved zone (ie at the upper chromitite layer), the elevated Cu & Ni mineralisation again coincides exactly. This would suggest control on the distribution of the mineralisation, as related to the high degree of pore space which ultimately became filled with late-stage crystallising plagioclase.

Figure 6.26 shows a series of plots of log S v log PGE. These plots are used to evaluate the control of sulphur/sulphide on PGE mineralisation, having already established some of the late-stage effects on the sulphides in the discussion on the trace element geochemistry. The linear distribution of the data indicates positive but varying S control on the PGE mineralisation. It would appear however, that the greatest S control is exercised over Pd and Au. In all samples the Au content is above detection limit and lie on the same straight line as the entire group of Merensky reef samples. It is possible that Pd would also have shown this same trend had the leuconorite samples been above detection limit. These relationships indicate a strong chalcophile character which has previously been well documented (eg Peck & Keays, 1990). The close, straight-line relationships suggest a well constrained S dependence, and these elements may have been incorporated into early sulphide PGM. All the plots show that the Merensky reef (CMR) is S deficient relative to the Merensky pyroxenite (X), for the same amount of PGE. This suggests that the Merensky pyroxenite hosted PGE are dominantly solid-
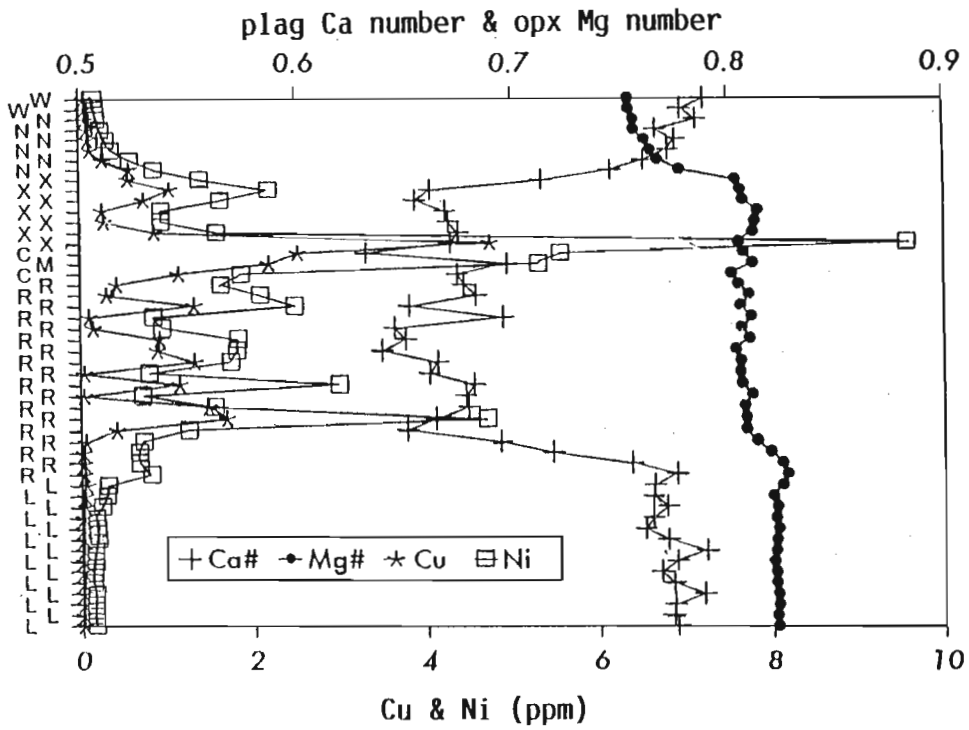
Figure 6.25a   R27A whole-rock Cu and Ni profiles superimposed
                on the orthopyroxene Mg number and plagioclase
                Ca number profiles.   Note the coincidence of the
                elevated Cu and Ni values with changes in mineral
                composition.
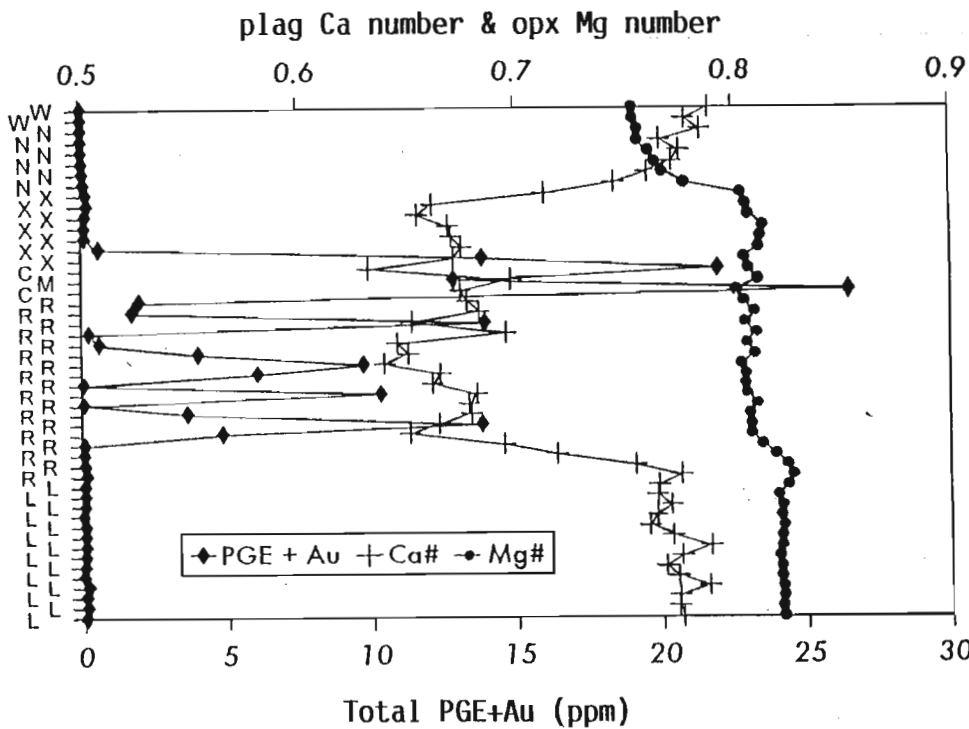
Figure 6.25b   R27A whole-rock total PGE+Au profile superimposed
                on the orthopyroxene Mg number and plagioclase Ca
                number profiles.   Note the coincidence of the
                elevated PGE+Au values with changes in mineral
                composition.
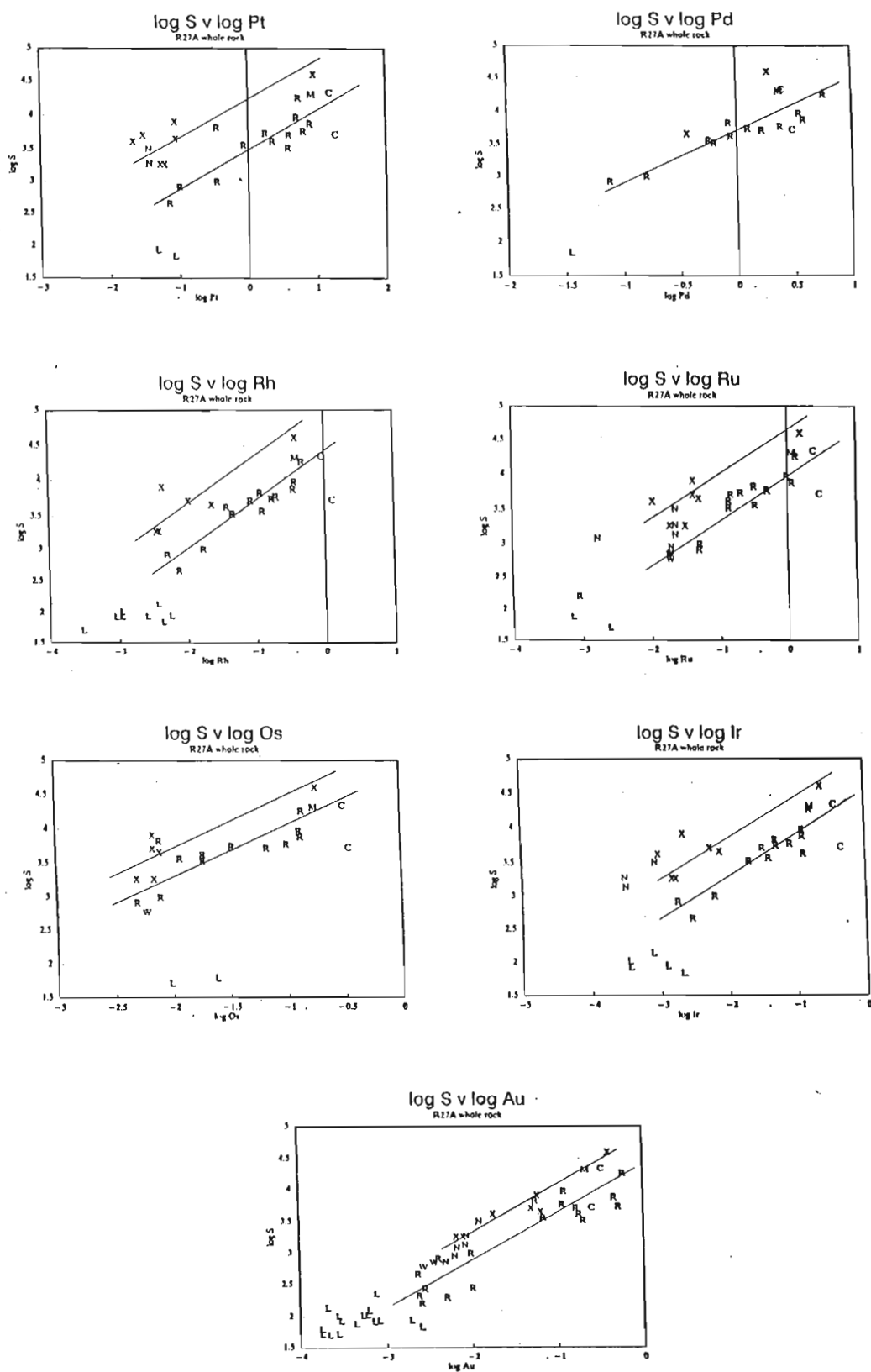
Figure 6.26   R27A whole-rock log S v log PGE plots.   Note the trends shown by the Merensky reef and Merensky pyroxenite, as indicated by the fitted lines. (analyses at detection limit have been excluded)

solution in base metal sulphide controlled (PGE_{ss} in BMS), and the Merensky reef hosted PGE are dominantly, but not exclusively, PGM controlled.

Cu/(Cu+1000PGE) profiles are useful for testing the fundamental control of base metals (Naldrett & Wilson, 1990), and therefore BMS, on PGE distribution (eg Pt and Pd, Figure 6.27). The majority of samples in the bottom ± 0,4m of the Merensky reef are at, or below detection limit. In particular, these diagrams emphasise the broad differences in the PGE-sulphide ratio (expressed here in terms of Cu). The Pt and Pd contents are not controlled by sulphide for all parts of the section, as several distinct fields are evident. It should be noted that the samples with the higher values for the Cu/(Cu+1000Pt) and Cu/(Cu+1000Pd) ratios in no way reflects the below-detection limit concentrations for Pt and Pd, because had these concentrations been known, then even higher values would have resulted. S must be at or above a threshold abundance level in magma in order to form BMS, and to act as a PGE collector, ie S must be at higher level than a possible threshold abundance. PGE (with possible exception of Pd) associated with S below such a threshold value would not form PGE_{ss}, but rather PGM. Notwithstanding the more informative log S v log PGE plots discussed above, the Cu/(Cu+1000PGE) type plot is essentially consistent with the findings that a higher proportion of PGE in the lower portion of the MR/MP package are not PGE_{ss}/BMS controlled, while those higher become increasingly so. The combined result of these two types of plots would suggest that the PGE at the base of the Merensky reef are dominantly PGM controlled, the PGE in the middle and upper Merensky reef both PGM and PGE_{ss} controlled, and the Merensky pyroxenite PGE mostly PGE_{ss} controlled. Overall, this suggests an upward increasing PGE_{ss}/BMS control on PGE through the MR/MP pyroxenite package. This pattern may have evolved due to late-stage alteration of the Merensky reef and the associated or subsequent redistribution of sulphides. Due largely to the constant metal content of the Merensky reef, this phenomenon is only readily detectable in the thick reef facies due to the broader distribution, while in the thin reef facies any detail of this nature is not immediately detectable due to constrained sample resolution, eg the R25A section.

Lee (1985) devised a metal ratio diagram combining Pt, Pd and Cu using a variety of Bushveld related data and average data from similar intrusions (Figure 6.28). Plotting Pt/Cu and Pd/Cu ratios on a logarithmic scale results in composition fields dependent on the relative control of solid solution PGE in BMS and PGM. From this, the Pt/Pd ratio can be empirically derived (Figure 6.28). The lower the PGE/Cu ratio, the greater the amount of PGE held in solid
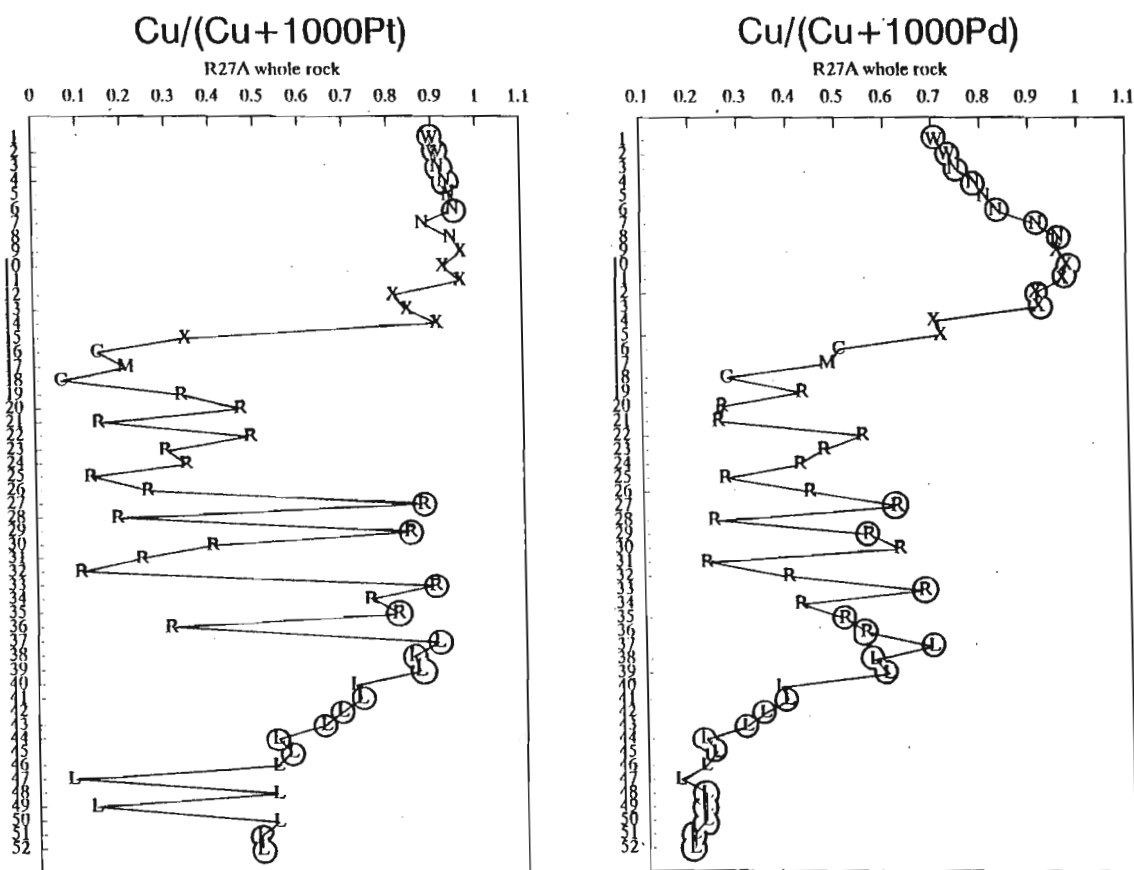
Figure 6.27   R27A whole-rock Cu/(Cu+1000Pt) and Cu/(Cu+1000Pd)
profiles.

(circled symbols indicate samples at detection limit)
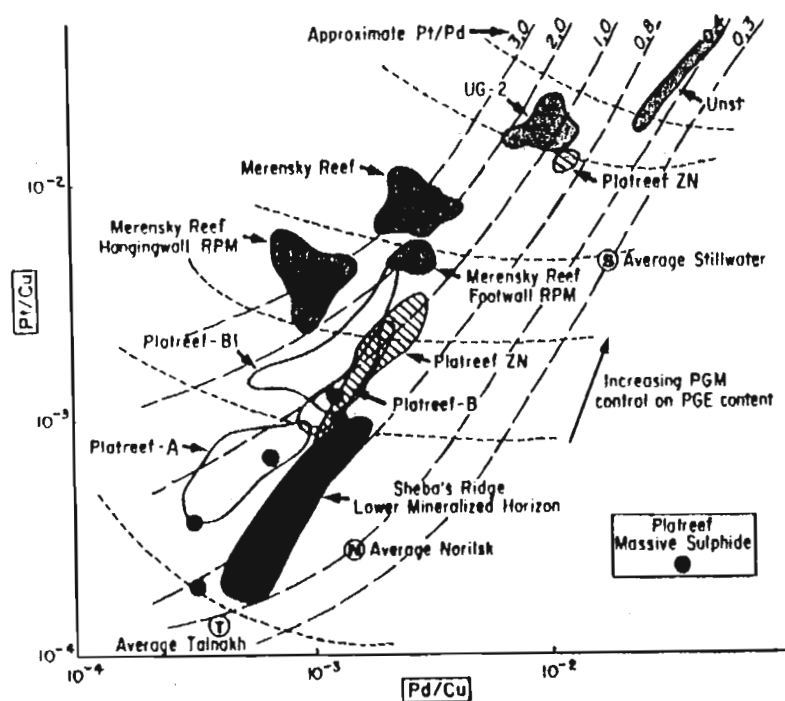
Figure 6.28   Metal ratio diagram using Pt/Cu and Pd/Cu ratios
plotted on a logarithmic scale.   The resulting
composition fields are a function of the ratios
of PGE solid solution in BMS and PGE in PGM.
(after Lee, 1985)

solution in BMS. A high PGE/Cu ratio results where PGM are a significant control. The plot indicates that overall the Merensky reef has a relatively high PGM control on PGE and that the Pt/Pd ratio ranges from 2 to 4, which is consistent with other data so far examined in this work. Figure 6.29 is a similar plot, which shows a comparison between Merensky reef data and data from the Unki area of the Great Dyke, Zimbabwe (Lee, 1990). Compared to the Great Dyke, the Merensky reef shows an overall higher, more tightly constrained PGM control on PGE content, and a higher average Pt/Pd ratio.

Four sets of log Pt/Cu v log Pd/Cu data from various Bushveld Complex sequences are plotted in Figure 6.30 (Lee, 1990). The fields delineated for the silicate cumulates, the Merensky reef, the LG and MG chromitites, and limited UG2 data lie on a trend related to the Pt/Pd ratio of the complex, which is approximately 2,5. The majority of the UG2 data points lie to the right of this trend due to the lower Pt/Pd ratio. This plot is consistent with the more general trends shown in Figure 6.28, with the Footwall and hangingwall of the Merensky reef showing a higher solid solution in BMS control on PGE mineralisation than the Merensky reef. Figure 6.31 shows a plot of log Pt/Cu v log Pd/Cu for the whole-rock R27A data. The Merensky reef and overlapping footwall leuconorite group show a higher PGM control over PGE than the hangingwall Merensky pyroxenite and norite group. The observed data grouping and trends are consistent with the findings of Lee (1985, 1990), and broadly consistent with the interpretations of the log S v log PGE, and Cu/(Cu+1000PGE) plots discussed above, in that greater BMS control of PGE occurs in the Merensky pyroxenite relative to the Merensky reef. However, the log Pt/Cu v log Pd/Cu plot does not show any definite pattern with regards any possible gradational control over PGE by PGM versus solid solution in BMS within the Merensky reef itself. Identification of individual Merensky reef (CMR) samples plotted in Figure 6.31 show an apparently random distribution within the general trend. The footwall leuconorite samples (L), which are above detection limit, show a similar degree of PGM versus PGE_{ss} control to that in the Merensky reef. This suggests that the relatively high PGE and BMS contents observed immediately below the Merensky reef are derived from late-stage migration downwards from the Merensky reef. Routine on-mine sampling shows that this phenomenon occurs to a much greater extent in the thin reef facies environment.

It is appropriate to further address the issue of PGE fractionation. As already observed, the absence of trends in the R27A and R25A Pt/Pd ratio profiles strongly suggest that the Merensky reef PGE were not fractionated. Consistent with this observation are the results of a series of
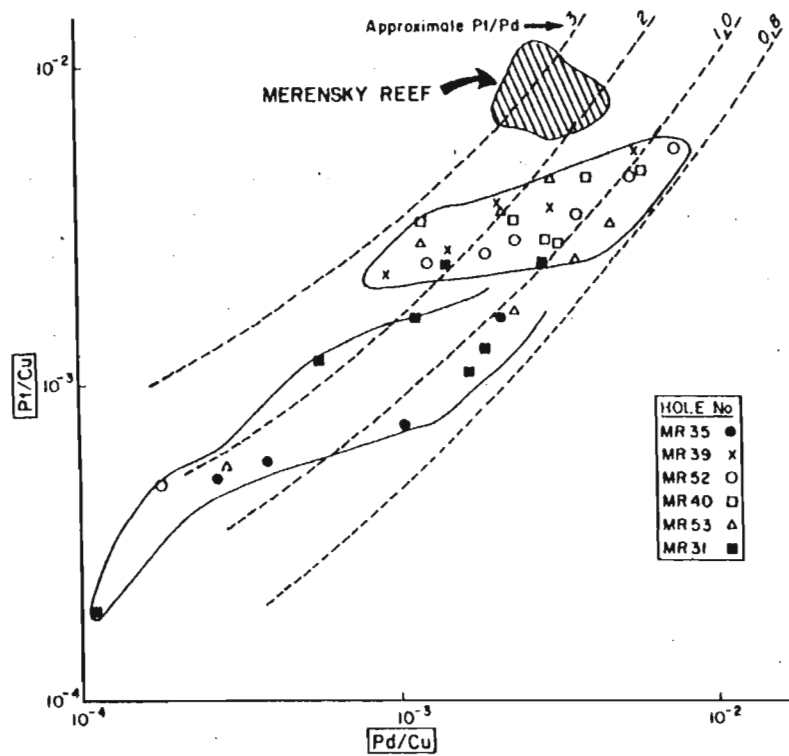
Figure 6.29   Logarithmic Pt/Cu v Pd/Cu plot for the Unki area of the Great Dyke, Zimbabwe, with the Merensky reef field for comparison. (modified after Lee, 1990)
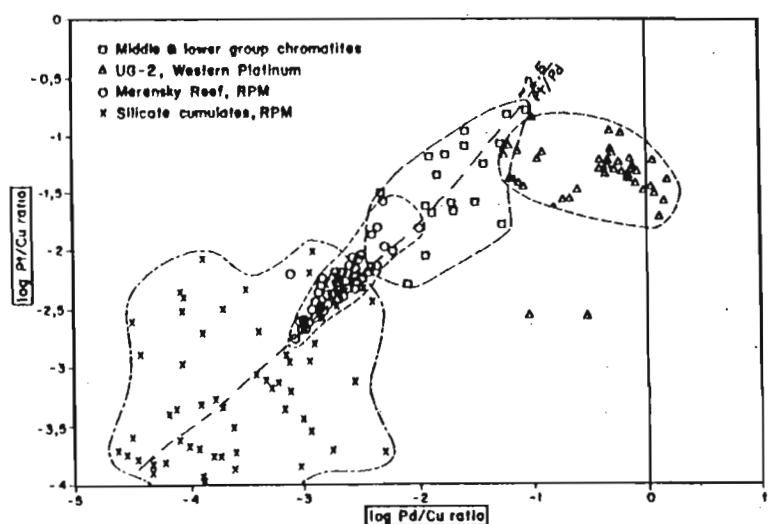
Figure 6.30   Log Pt/Cu v log Pd/Cu metal ratio diagram for
               various Bushveld Complex rocks.
               (after Lee, 1990)
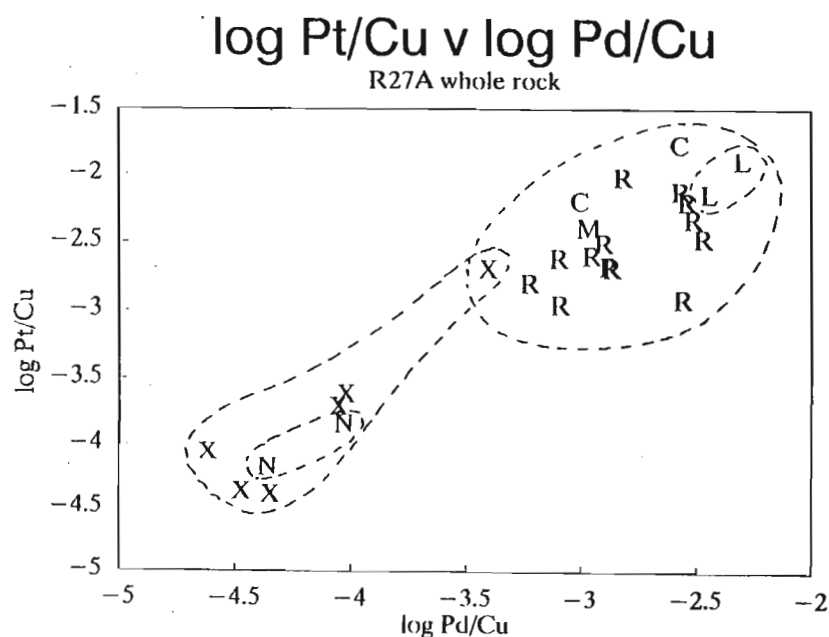
Figure 6.31   Log Pt/Cu v log Pd/Cu plot for the R27A whole
               -rock data.
               CMR = Merensky reef   L = footwall leuconorite
               X   = Merensky pyroxenite
               N   = hangingwall norite
               (analyses at detection limit have been excluded)

binary plots of log S v log tenor PGE for the R27A section (Figure 6.32). These plots are useful for testing for PGE (and base-metal) fractionation by converting back to 100% sulphide (log tenor PGE = log[ppmPGE * [100/[wt%S/0,36]]) (A.H.Wilson, *pers comm*). A negative slope straight-line trend would suggest fractionation control. However, in all cases the values above detection limit constitute a scatter of points with no observable trend, thereby suggesting that no PGE or base-metal fractionation took place.

Correlation analysis for PGE and trace elements reveals specific lithological control on the resulting geochemical relationships. Correlation coefficients (at 95% confidence limits) were calculated for PGE+Au pairs (Table 6.8), and for PGE+Au and trace element pairs (Table 6.9) for the entire R27A sampled sequence, and for the Merensky reef alone.

The PGE+Au interelement correlation coefficients are generally lower in the Merensky reef compared to the entire sequence. These lower coefficients may suggest that late-stage decoupling or alteration to the Merensky reef has occurred. In both cases Pd correlates poorly with the other PGE, and not at all with Os, but shows a relatively high correlation with Au. Similarly Au shows poor correlations with all the PGE, save for Pd. This indicates that Pd decoupled from the other PGE. Evidence in this study has already shown that PGE fractionation did not occur. This would then suggest that the observed Pd distribution was a secondary, late-stage event, whereby it may have gone into platinum-group mineral (PGM) association. This would be consistent with the higher Pd values obtained towards the base of the Merensky reef. The remaining five PGE show high inter-correlation coefficients (>0,9).

The PGE correlations with the base elements (Table 6.9) do not show any general decrease in coefficients within the Merensky reef. With the notable exceptions of Pd and Au, all PGE show relatively high correlations with Cr_2O_3, which is consistent with the high PGE peak values associated with the chromitite layers. The Merensky reef correlations, as expected, show increases in these coefficients, and further decreases for Pd and Au. Next to Cr_2O_3, the PGE-Zn correlations are also relatively high. This is not a function of any direct relationship between PGE and Zn, but rather a function of the high Zn content of chromite, with which the PGE have already been shown to correlate.

It would be expected that the PGE-S correlations would be high if total S control existed over PGE mineralisation. However, these values are low, with only Pd and Au showing relatively
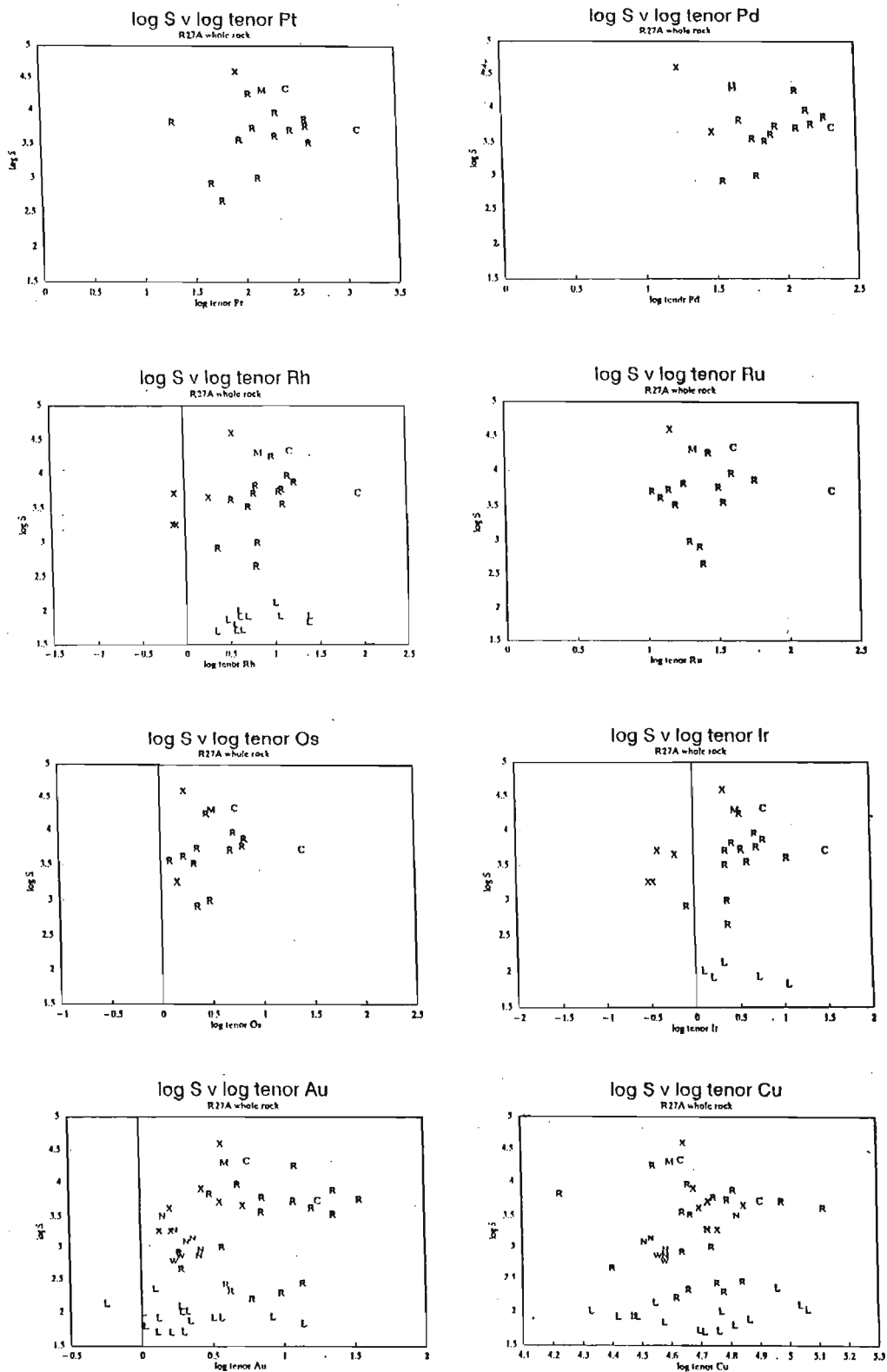
Figure 6.32   R27A whole-rock log S v log tenor PGE, Au and Cu.
Note that there are no convincing trends.
(analyses at detection limit have been excluded)

	Pt	Pd	Rh	Ru	Os	Ir	Au
Pt	1,0000	0,6633	0,9488	0,9546	0,9829	0,9626	0,6198
Pd	0,6633	1,0000	0,6045	0,3416	-0,049	0,6371	0,7710
Rh	0,9488	0,6045	1,0000	0,9668	0,9626	0,9660	0,5778
Ru	0,9546	0,3416	0,9668	1,0000	0,9711	0,9893	0,4588
Os	0,9829	-0,049	0,9626	0,9711	1,0000	0,9867	0,5311
Ir	0,9626	0,6371	0,9660	0,9893	0,9867	1,0000	0,6372
Au	0,6198	0,7710	0,5778	0,4588	0,5311	0,6372	1,0000

Table 6.8a   Correlation coefficients for PGE+Au pairs,
             Borehole R27A whole sequence.
             n_{Pt} = 31 n_{Pd} = 23 n_{Rh} = 29 n_{Ru} = 10
             n_{Os} = 12 n_{Ir} = 36 n_{Au} = 52
             (linear regression at 95% confidence)
             (analyses at detection limit have been excluded)

	Pt	Pd	Rh	Ru	Os	Ir	Au
Pt	1,0000	0,5709	0,9459	0,9547	0,9765	0,9479	0,4380
Pd	0,5709	1,0000	0,5634	0,3746	-0,042	0,5484	0,7152
Rh	0,9459	0,5634	1,0000	0,9874	0,9724	0,9705	0,4160
Ru	0,9547	0,3746	0,9874	1,0000	0,9735	0,9893	0,4442
Os	0,9765	-0,042	0,9724	0,9735	1,0000	0,9932	0,1220
Ir	0,9479	0,5484	0,9705	0,9893	0,9932	1,0000	0,4320
Au	0,4380	0,7152	0,4160	0,4442	0,1220	0,4320	1,0000

Table 6.8b   Correlation coefficients for PGE+Au pairs,
             Borehole R27A Merensky reef (CMR).
             n_{Pt} = 17 n_{Pd} = 16 n_{Rh} = 16 n_{Ru} = 9
             n_{Os} = 8 n_{Ir} = 17 n_{Au} = 21
             (linear regression at 95% confidence)
             (analyses at detection limit have been excluded)

	Pt	Pd	Rh	Ru	Os	Ir	Au
As	,6433	,3672	,5729	,4454	,7045	,6270	,5223
S	,6027	,5289	,5088	,3100	,4853	,6473	,7066
Ni	,6249	,5614	,5328	,3132	,5143	,6695	,7296
Cu	,6558	,5264	,5339	,4273	,5358	,6937	,7382
Zn	,6798	,3718	,6941	,7153	,8469	,6982	,5068
Co	,5186	,5608	,4536	,1571	,5312	,5582	,6636
Pb	,6271	,4445	,5830	,3311	,5668	,6168	,5392
Cr_2O_3	,8034	,3180	,8468	,8162	,8451	,8292	,3854

Table 6.9a   Correlation coefficients for PGE+Au and base element
pairs, Borehole R27A whole sequence.
$n_{Pt} = 31$ $n_{Pd} = 23$ $n_{Rh} = 29$ $n_{Ru} = 10$
$n_{Os} = 12$ $n_{Ir} = 36$ $n_{Au} = 52$
(linear regression at 95% confidence)
(analyses at detection limit have been excluded)

	Pt	Pd	Rh	Ru	Os	Ir	Au
As	0,6687	0,1312	0,5272	0,4312	0,5648	0,6190	0,2801
S	0,5860	0,6623	0,5318	0,3541	0,2918	0,5905	0,6494
Ni	0,5831	0,6696	0,5373	0,3559	0,2967	0,5921	0,6386
Cu	0,6981	0,6504	0,5810	0,5971	0,4056	0,6916	0,7034
Zn	0,7346	0,1051	0,7338	0,7512	0,8488	0,7694	0,2142
Co	0,4010	0,5836	0,3760	0,0909	0,1340	0,4205	0,5966
Pb	0,6080	0,3852	0,5212	0,3264	0,3252	0,5666	0,4132
Cr_2O_3	0,8357	0,2223	0,8520	0,8583	0,9243	0,8689	0,2628

Table 6.9b   Correlation coefficients for PGE+Au and base
element pairs, Borehole R27A Merensky reef (CMR).
$n_{Pt} = 17$ $n_{Pd} = 16$ $n_{Rh} = 16$ $n_{Ru} = 9$
$n_{Os} = 8$ $n_{Ir} = 17$ $n_{Au} = 21$
(linear regression at 95% confidence)
(analyses at detection limit have been excluded)

high correlation of the order of 0,64. Pt, Rh and Ir show poor correlation of approximately 0,5, while Os and Ru show very low correlation in the order of 0,3. This evidence, together with other evidence already presented in this study, is consistent with sulphide solid solution control being only part of the mineralisation process, and with Pd, the most chalcophile of the PGE, showing the highest S dependence. It is also consistent with the evidence provided by the Zr v S relationship, which demonstrates redistribution of both late silicate liquid and sulphide. Sulphide melt can deposit PGM at moderately high temperatures; these PGM could remain attached to, or encapsulated in silicate, while sulphide melt migrated into intercrystal spaces with cooling. Isolated PGM are well known in these mineralised sequences, providing textural evidence of sulphide migration.

The As-PGE correlations are similar to the S-PGE correlations, with minor differences. For instance, Pt correlates more highly with As than with S, Pd and Au-As considerably lower, Ir and Ru-As slightly higher, and Os-As considerably higher. Both the PGE pairs correlations and the PGE-base element correlations illustrate the differing behaviour of Pd and Au, supporting a late-stage decoupling event. The Os-PGE and Os-base element correlations constitute the next most obvious deviation from average PGE behaviour.

6.5 SUMMARY AND CONCLUSIONS

Detailed centimetre-scale sampling of seemingly monotonous rock sequences has proved to be a valuable technique in revealing fine-scale geochemical processes (Wilson, 1992). This technique has been applied to four diverse Merensky reef intersections, of which the thick Merensky reef section R27A was selected as the reference section.

Whole rock geochemistry shows major differences between the norites and the pyroxenite package. The major elements essentially reflect the differences in modal mineral composition, while the trace elements show anomalous enrichment in incompatible elements, particularly within the Merensky reef/Merensky pyroxenite package. Whole-rock and mineral profiles typically show variable 'sawtooth' shaped patterns in the pyroxenites and smooth profiles in the norites, while binary plots consistently show a clear lithologically related three-way grouping of data. This suggests that the different rock types are separate geochemical entities with little geochemical inter-relationship. There is however evidence of interaction between lithologies

where transitional compositions overlap lithological contacts. Major inconsistencies exist in mineral compositions between orthopyroxene (as Mg#) and plagioclase (as Ca#). Orthopyroxene Mg# and plagioclase Ca# profiles follow significantly different trends, with the greatest geochemical deviation being observed in the plagioclase. The re-equilibration of orthopyroxene with trapped liquid cannot explain the Merensky reef/Merensky pyroxenite pyroxene compositions. Unlike the Great Dyke no trends are observed in the relationship between whole-rock Zr (or P) and orthopyroxene Mg#.

The Merensky reef is unique amongst PGE occurrences in that metal content is constant, where in thick reef the mineralisation is diluted by silicate phases (low grade), and is highly concentrated in thin reef facies (high grade). This suggests that when the magma was introduced it was already largely unmixed, already contained a fixed metal content combined with a fixed amount of sulphide, and therefore, the sulphide liquid was independent of the variable volume of silicate liquid.

There is ample evidence to suggest that the Merensky succession, in particular the Merensky reef, was exposed to late-stage hydromagmatic *in situ* recrystallisation, alteration and re-equilibration, as follows:

a) In terms of major and trace element abundances and behaviour, the texturally diverse Merensky reef and overlying Merensky pyroxenite are geochemically indistinct.

b) Zr, P, Y, Nb, La, K and similar late-stage low temperature elements are concentrated in the Merensky reef/Merensky pyroxenite sequence relative to the footwall and hangingwall norites.

c) Whole-rock and mineral major and trace element abundances in the pyroxenite sequence, and in the Merensky reef in particular, show highly and sharply variable profiles relative to the adjacent norites.

d) The upward Ca-enrichment of plagioclase through the Merensky reef/Merensky pyroxenite package, which is the reverse of what would be expected, where the plagioclase chemistry is controlled by late-stage equilibration with trapped intercumulus liquid.

e) The erratic nature of the Cu/Ni ratio in the Merensky reef/Merensky pyroxenite sequence. The ratio is influenced by the abundance of orthopyroxene and the composition of the base metal sulphides.

f) The distinct offset of the Zr and P peaks with the Cu, Ni & S peaks, indicating late-stage decoupling of sulphides and incompatible elements.

g) Lack of correlation between Zr & S, due to late-stage migration of sulphide melt and displacement of trapped intercumulus material. There is thus little evidence to suggest co-entrapment of incompatible elements and sulphide.

h) The orthopyroxene CaO, Na_2O & Al_2O_3 profiles are variable and erratic, indicating a late-stage modification of the orthopyroxene compositions.

i) A positive correlation exists between orthopyroxene NiO and whole-rock NiO. This provides evidence for late Ni exchange or re-equilibration between base metal sulphides and orthopyroxene.

j) The plagioclase Ca# is highly evolved and follows a reverse trend and erratic profile through the Merensky reef/Merensky pyroxenite package.

k) The relationship between orthopyroxene TiO_2 and plagioclase Ca# suggests systematic interaction with trapped intercumulus fluid within the Merensky reef/Merensky pyroxenite sequence.

l) Elevated PGE and base metal values coincide with the most highly altered and chemically variable zone of the Merensky reef/Merensky pyroxenite package.

m) There is localised decoupling of PGE and S, Cu & Ni peaks.

n) Some compositional variances are offset from lithological contacts.

o) There is evidence for late-stage decoupling of Pd (& Au) from the other PGE.

The relationship of S to the PGE and base metal mineralisation has been investigated in some detail. Log S v log PGE plots show that the greatest S control within the PGE is exercised, not unexpectedly, over Pd and Au, where a moderate correlation exists. Correlation between S and the remaining PGE is relatively low. The Merensky reef is S-deficient relative to the Merensky pyroxenite for the same amounts of PGE, which suggests that the PGE in the Merensky pyroxenite have a higher level of PGE$_{ss}$ in BMS control than the PGE in the Merensky reef. The Cu/(Cu+1000PGE) plot indicates a relative lack of sulphide towards the base of the Merensky reef and therefore is consistent with a possible dominant PGM control. The combined results of these two types of plots suggests that, the PGE mineralisation at the base of the Merensky reef is largely, but not exclusively PGM controlled, the middle and upper Merensky reef PGE are both PGM and PGE$_{ss}$ in BMS controlled, and that the Merensky pyroxenite hosted PGE are mostly PGE$_{ss}$ in BMS controlled. Overall, this shows an upward-increasing PGE$_{ss}$ in BMS control on the PGE mineralisation through the Merensky reef/Merensky pyroxenite package. The grouping shown in the log Pt/Cu v log Pd/Cu plot is broadly consistent with this interpretation, where a strong differentiation between the Merensky reef and Merensky pyroxenite is observed. It also shows evidence for submagmatic migration of PGE$_{ss}$ and PGM into the immediate footwall leuconorite.

There is significant evidence that the PGE within the Merensky succession were not fractionated. This is indicated by the Pt/Pd ratios, and the log S v log tenor PGE plots in which no trends are observed. The broad geochemical evidence presented in this study would support a petrogenetic model involving magma injection already enriched at the source with a quantity of combined sulphur and metal. Therefore during subsequent magma chamber fractionation and accumulation of incompatible elements, no S unmixing and no PGE scavenging took place. It is possible that during the magmatic stage that PGE and S showed high inter-correlation. During subsequent late-stage hydromagmatic processes, this relationship was variably altered according to the relative chalcophile nature of individual PGE and the partitioning of PGE into lower temperature phases such as PGE arsenides, bismuthides and tellurides along the lines of a process similar to that described by Coghill & Wilson, 1993 in their study of the Great Dyke. There is some evidence to suggest that the bulk of the late-stage recrystallisation, redistribution and alteration within the Merensky reef was fluid-driven.

CHAPTER 7

CONCLUSIONS

While the Bushveld Complex and the mineralised Merensky reef are similar to other PGE-bearing mafic and ultramafic layered complexes in terms of lithology and PGE enrichment, there are a number of features which make it unique. Such contrasts have so far complicated efforts to achieve consensus on a petrogenetic model for the Merensky reef. Several diverse models have been proposed over the years, ranging from orthomagmatic to hydrothermal. In addition, much effort has been devoted to potholed Merensky reef with no comparative base of what may be regarded as normal Merensky reef. As a consequence of this diversity, the final objective of this study is to collate the more important constraining evidence, derived from a study of normal Merensky reef, into a most likely genetic model-type fit.

The Merensky reef at RPM Rustenburg Section is a base metal sulphide and platinum-group element enriched pegmatoidal feldspathic orthopyroxenite with a variable number of thin associated chromitite layers. Currently economic Merensky reef is extremely variable in thickness (0,04 - 2m), and with this are associated a number of other variations which are largely characteristic of a particular reef facies. The reef facies have been described in this study as the thin, through to thick reef facies. Generally, the thick reef facies show the highest textural variability, in which there is the most abundant field evidence for late-stage hydromagmatic *in situ* recrystallisation, alteration and local redistribution of component minerals. The petrographic observations are consistent with this evidence.

Whole-rock and mineral separate geochemistry shows that the Merensky reef and overlying Merensky pyroxenite are virtually indistinguishable from one another, despite the textural contrasts. This also provides strong evidence that *in situ* isochemical recrystallisation is a likely origin of the Merensky reef pegmatoidal feldspathic pyroxenite. Similar conclusions were reached by Lee and Butcher (1990) in their study of the eastern Bushveld Merensky reef at Atok, and by Mathez *et al* (1994) in a more recent study at Atok. The platinum-group element distribution is the only geochemical basis for identifying the Merensky reef.

The Merensky reef has a sharp contact with the footwall and shows a regressive and paraconformable relationship. This suggests that the reef may have been emplaced as a separate event. Where a basal chromitite layer is developed, reaction has taken place with the footwall leuconorite resulting in the formation of an anorthosite layer of variable thickness, which is considered to form part of the Merensky Unit (Nicholson & Mathez, 1991; Brown, 1991). Where a basal chromitite occurs, the anorthosite is depleted in BMS and PGE relative to the immediately underlying leuconorite. The fact that subeconomic to economic PGE concentrations occur within the immediate footwall leuconorite, ie over and above the normal background values, is suggestive of migration of BMS and PGE from the overlying Merensky reef. Such migration is most likely to have occurred during the submagmatic stage. The relatively high correlation between Zr and S observed in the footwall leuconorites (contrasting with the overlying MR/MP package) suggests co-trapped residual magma and base metal sulphides with very limited, if any, recrystallisation and redistribution of BMS during the subsequent hydromagmatic stage. There is virtually no field, petrographic or geochemical evidence that would suggest that late-stage exsolved hydrous fluid played an important role in the evolution of the footwall leuconorite.

Contrasting features between the Merensky reef and other layered PGE deposits include high Pt/Pd and Ni/Cu ratios, high individual and total PGE grades, the lack of fractionation trends in the base and precious metal enrichment patterns, and the constant metal content relative to variable reef width. For these reasons any detailed petrogenetic model would appear to be specific to the Merensky reef. Lee and Butcher (1990), in their Sr isotope study of the Atok Merensky reef sequence, have also suggested the possibility of the Merensky reef having been emplaced as a unique layer, where they draw certain parallels with the Rhum sill intrusion model proposed by Bedard et al (1988). They envisage that the Merensky reef may represent the emplacement of a PGE + S-rich melt in the form of a sill, derived from a magma chamber that became increasingly enriched in PGE and related elements as melt was removed and emplaced to form the cumulates of the Critical Zone. The melt entrained trace amounts of sulphide (with PGE) which has resulted in the background levels observed in the layered rocks (Lee & Tredoux, 1986).

Abundant field and geochemical evidence has emerged in this study which may be used to constrain the petrogenesis of the Merensky reef. The results and interpretations would suggest that the evolution of the Merensky reef and related rocks includes components of both the

orthomagmatic and hydrothermal processes, resulting in a complex multi-stage sequence of events, involving magmatic, submagmatic and hydromagmatic stages.

Magmatic and Emplacement Stage: The field and geochemical evidence supports orthomagmatic processes as the initial control on PGE enrichment observed in the Merensky reef, in which sulphide mineralisation, early concentrations of PGE and formation of primary, high temperature PGM assemblages occurred. Subsequent processes have to some extent modified the textures and mineral assemblages and therefore obscured this evidence. It is proposed that the source magma of the Merensky reef was enriched in PGE, S, semi-metals (As, Te & Bi) and base metals. Broadly consistent with the processes described by Lee and Butcher (1990), and more specifically those by Coghill and Wilson (1993), it is envisaged that during the initial stage the PGE atoms entrained in the magma combined to form high temperature PGM assemblages and metastable PGE + (As, Te, Bi, S) clusters. This was followed by liquation and precipitation of sulphide, into which direct partitioning of remaining free PGE atoms and PGE+semi-metal clusters occurred. This resulted in a mixture of a fixed amount of monosulphide solid solution (and therefore PGE, PGM and base metals), magma, and a variable quantity of nucleating olivine and orthopyroxene crystals, which was subsequently injected into the magma chamber. The sulphide liquid was therefore effectively independent of the variable volume of silicate liquid and crystal mush, thereby producing the almost constant total metal content, irrespective of the width of the ore zone. The constant metal content is an important characteristic of the Merensky reef. Rapid mixing of the supernatant liquid, relieved of its charge of sulphide and early formed crystals, combined with the resident magma to continue crystallising to form the observed differentiated sequence.

There is no direct evidence from this study to support the magma chamber mixing events of Hoatson & Keays (1989) and Naldrett *et al* (1990), with the associated implications of sulphide unmixing, PGE scavenging and partitioning (based on the so-called R-factor), and sulphide settling. These processes are therefore not regarded as essential to the Merensky reef petrogenetic process, which is consistent with the observed fixed metal content of the reef. In addition, the Sr isotope study at Atok by Lee and Butcher (1990), in which similar data from Rustenburg (Kruger & Marsh, 1982) was compared, did not provide isotopic evidence of magma mixing at the observed PGE enrichment levels.

It is proposed that the parent magma to the Merensky reef was injected into the magma chamber and emplaced as a separate and unique layer with little or no mixing with the resident contents of the chamber until suspended silicates and sulphide liquid had separated. The liquid to solid status of the resident contents of the magma chamber above, or below the level of emplacement is not known, and therefore, the exact mechanism of emplacement could only be speculated on at this stage.

Submagmatic Stage: The submagmatic stage was initiated by a state of disequilibrium which arose through progressive cooling and crystallisation of the evolving mixture of silicate minerals, sulphide and trapped melt in the emplaced layer. This resulted in the dissociation and exsolution from the monosulphide solid solution of PGM, PGE and the semi-metals As, Bi and Te. Some local remobilisation is likely to have taken place at this stage, whereby some PGE would have migrated with sulphides. At the same time sulphide containing PGE in solid solution are likely to have migrated into the leuconorite footwall. The Merensky reef chromitite layers, which are considered to have formed by reaction at this stage, typically carry higher PGE concentrations than the surrounding pyroxenite. It is suggested that chromite could have acted as an efficient collector of PGE during the submagmatic stage, and likely to have continued into the hydromagmatic stage. As a further result of the state of disequilibrium, peritectic reaction resulted in the replacement of the bulk of the olivine by orthopyroxene.

Overall, there is a progressive change in orthopyroxene composition upwards through the sequence, with the compositions ranging from En_{82} in the footwall leuconorite, to En_{81} in the Merensky reef/Merensky pyroxenite, to En_{76} in the hangingwall norite. The change in plagioclase composition shows a completely different, somewhat erratic pattern, with compositions ranging from An_{77} in the footwall leuconorite, to An_{67} in the MR/MP package, back to An_{77} in the hangingwall norites. The more sodic plagioclase in the Merensky reef relates to its textural form, which is in clear contrast with the plagioclase in the norites, and results from late-stage crystallisation of this mineral.

Hydromagmatic Stage: With further cooling of the Merensky succession, hydrous fluid was exsolved from the intercumulus silicate liquid. This fluid is proposed to be primarily responsible for the *in situ* isochemical recrystallisation of the Merensky reef silicates, and for the final stages of the local migration, redistribution and reaction of both the primary, and the dissociated and exsolved PGE, PGM, semi-metals and base metal sulphides. The field, petrographic and

geochemical evidence strongly indicates that the late-stage hydrous fluid gave rise to reactions between the silicate components, and between silicate components and the fluid itself, whereby their original compositions, particularly that of the intercumulus plagioclase, was altered. This may also explain the variable sawtooth element profiles within the Merensky reef/Merensky pyroxenite interval, and by the minor changes in mineral composition through the succession. All evidence of hydrous activity is confined to the pyroxenite package, with no evidence of this occurring in the footwall or hangingwall norites.

Various studies and observations, eg Lee & Butcher (1990), have shown that the Merensky reef/Merensky pyroxenite package and the Bastard pyroxenite are geochemically, isotopically and texturally similar (even to the extent of a pegmatoidal layer being occasionally developed at the base of the Bastard pyroxenite (Mathez et al, 1994)), save for the elevated PGE content of the Merensky reef. Similarly with the Merensky hangingwall and footwall norites, the Bastard footwall anorthosite and hangingwall norite do not show any evidence of hydromagmatic effects. This, along with abundant other evidence (largely the trace element geochemistry), suggests that the exsolved hydrous intercumulus fluid was internally derived in each case, and the reaction effects confined to the respective pyroxenite packages. The concept of externally derived migrating hydration fronts (eg Nicholson & Mathez, 1991) is thus questionable on the basis of insufficient geochemical evidence. There is indication that limited migration of sulphide liquid away from the Merensky reef took place. There is no evidence of external components or fluid being added to the Merensky reef.

There is geochemical and textural evidence for other late-stage hydromagmatic processes, including, re-equilibration and exchange between base metal sulphides and silicates, the decoupling of sulphide and incompatible elements, and the decoupling of individual PGE and base metal sulphides. It is probable that interstitial, low-temperature phases rich in incompatible elements crystallised during this stage, eg phlogopite, zircon, apatite and rare earth minerals, along with the crystallisation of low-temperature PGM arsenides, bismuthides, tellurides and late-stage sulphides.

The geochemistry uniquely defines and characterises the Merensky succession despite the considerable variability in thickness and associated petrological features. This type of fundamental study will provide a basis for further comparitive studies of the Merensky reef, and will have implications for the approach to the study of similar layered PGE deposits.

REFERENCES

Allen S.W.(1986) Comparison of different Merensky reef types and Value Distributions at RPM Rustenburg Section West.
JCI Geologists Technical Meeting, 1, p31-70 (unpublished).

Amosse J., Allibert M., Fischer W. & Piboule M.(1990) Experimental study of the solubility of platinum and iridium in basic silicate melts - Implications for the differentiation of platinum-group elements during magmatic processes.
Chem. Geol., 81, p45-53.

Asif M. & Parry S.J.(1989) Elimination of Reagent Blank Problems in the Fire-assay Pre-concentration of the Platinum Group Elements and Gold With a Nickel Sulphide Bead of Less Than One Gram Mass.
Analyst, 114, p1057-1059.

Asif M. & Parry S.J.(1990) Nickel Sulphide Fire Assay for the Collection of the Platinum Group Elements and Gold From Chromitites Using Reduced Bead Size.
Mineralogy & Petrology, 42, p321-326.

Ballhaus C.G. & Stumpfl E.F.(1985) Occurrence and petrological significance of graphite in the Upper Critical Zone, western Bushveld Complex, South Africa.
Earth & Planetary Science Letters, 74, p58-68.

Ballhaus C.G., Cornelius M. & Stumpfl E.F.(1988) The Upper Critical Zone of the Bushveld Complex and the Origin of Merensky-Type Ores - A Discussion.
Econ. Geol., 83, p1082-1091.

Ballhaus C.G. & Stumpfl E.F.(1986) Sulfide and platinum mineralization in the Merensky Reef: evidence from hydrous silicates and fluid inclusions.
Contrib. Mineral. Petrol., 94, p193-204.

Barnes S.J.(1986) The effect of trapped liquid crystallisation on cumulus mineral compositions in layered intrusions.
Contrib. Mineral. Petrol., 93, p524-531.

Barnes S.J. & Campbell I.H.(1988) Role of late magmatic fluids in Merensky-type platinum deposits: A discussion.
Geology, 16, p488-491.

Barnes S.J. & Keays R.R.(1992) Distribution of sulphides and PGE within the porphyritic websterite zone of the Munni Munni Complex, Western Australia.
Aust. J. Earth Sci., 39, p289-302.

Barnes S.J. & Naldrett A.J.(1985) Geochemistry of the J-M (Howland) Reef of the Stillwater Complex, Minneapolis Adit Area. I. Sulfide Chemistry and Sulfide-Olivine Equilibrium.
Econ. Geol., 80, p627-645.

Bedard J.H., Sparks R.S.J., Renner M., Cheadle M.J. & Hallworth M.A.(1988) Peridotite sills and metasomatic gabbros in the eastern layered series of the Rhum Complex.
Geol. Soc. London Jour., 145, p207-224.

Boudreau A.E., Mathez E.A. & McCallum I.S.(1986) Halogen Geochemistry of the Stillwater and Bushveld Complexes: Evidence for Transport of the Platinum-Group Elements by Cl-Rich Fluids.
J. Petrol., 27, p967-986.

Boudreau A.E. & McCallum I.S.(1992) Concentration of Platinum-Group Elements by Magmatic Fluids in Layered Intrusions.
Econ. Geol., 87, p1830-1848.

Brown R.T.(1991) The inter-relationship between the variability of the Merensky reef and its footwall stratigraphy at Frank Shaft, Rustenburg Platinum Mines.
JCI Geologists Technical Meeting, 6, p24-44 (unpublished).

Buchanan D.L. & Nolan J.(1979) Solubility of Sulfur and Sulfide Immiscibility in Synthetic Tholeiitic Melts and their Relevance to Bushveld-Complex Rocks.
Canadian Mineralogist, 17, p483-494.

Burger A.J. & Coertze F.J.(1975) Age determinations: April 1972 -March 1974.
South Africa Geol. Survey Annals, 10, p135-141.

Cameron E.N.(1982) The Upper Critical Zone of the Eastern Bushveld Complex - Precursor of the Merensky Reef.
Econ. Geol., 77, p1307-1327.

Campbell I.H. & Barnes S.J.(1984) A Model for the Geochemistry of the Platinum-Group Elements in Magmatic Sulfide Deposits.
Canadian Mineralogist, 22, p151-160.

Campbell I.H., Naldrett A.J. & Barnes S.J.(1983) A Model for the Origin of the Platinum-Rich Sulfide Horizons in the Bushveld and Stillwater Complexes.
J. Petrol., 24, p133-165.

Cawthorne R.G. & McCarthy T.S.(1985) Incompatible Trace Element Behaviour in the Bushveld Complex.
Econ. Geol., 80, p1016-1026.

Chai G. & Naldrett A.J.(1992) Characteristics of Ni-Cu-PGE Mineralization and Genesis of the Jinchuan Deposit, Northwest China.
Econ. Geol., 87, p1475-1495.

Chunnett G.K.(1987) Structural Variations in Normal Merensky Reef.
JCI Geologists Technical Meeting, 2, p213-224 (unpublished).

Coats C.J.A. & Johannessen P.(1992) Platinum, Palladium, Gold, and Copper-Rich Stringers at the Strathcona Mine, Sudbury: Their Enrichment by Fractionation of a Sulfide Liquid.
Econ. Geol., 87, p1584-1598.

Coertze F.J., Burger A.J., Walraven F., Marlow A.G. & McCaskie D.R.(1978) Field relations and age determinations in the Bushveld Complex.
Geol. Soc. S. Afr. Trans, 81, p1-11.

Coetzee H. & Kruger F.J.(1989) The geochronology, Sr- and Pb- isotope geochemistry of the Losberg Complex, and the Southern Limit of the Bushveld Complex Magmatism.
S. Afr. J. Geol., 92, p37-41.

Coghill B.M. & Wilson A.H.(1993) Platinum-group minerals in the Selukwe Subchamber, Great Dyke, Zimbabwe: implications for PGE collection mechanisms and post-formational redistribution.
Mineralogical Magazine, 57, p613-633.

Craig J.R. & Vaughan D.J.(1981) Ore Microscopy and Ore Petrology.
John Wiley & Sons, 406pp.

Eales H.V., Marsh J.S., Mitchell A.A., De Klerk W.J., Kruger F.J. & Field M.(1986) Some geochemical constraints upon models for the crystallisation of the upper critical zone - main zone interval, northwestern Bushveld Complex.
Mineralogical Magazine, 52, p63-79.

Eales H.V., Teigler B. & Maier W.D.(1993) Cryptic variations of minor elements Al, Cr, Ti, Mn in Lower and Critical Zone orthopyroxenes of the Western Bushveld Complex.
Mineralogical Magazine, 57, p257-264.

Elliott W.C., Grandstaff D.E., Ulmer G.C. & Buntin T.(1982) An Intrinsic Oxygen Fugacity Study of Platinum-Carbon Associations in Layered Intrusions.
Econ. Geol., 77, p1493-1510.

Faurie J.N. & Von Gruenewaldt G.(1979) Zaaiplaats project. Pretoria Univ., Pretoria, Inst. Geol. Research Bushveld Complex, Ann. Rept. 1978, p11-15 (unpublished).

Hamilton P.J.(1977) Sr-isotope and trace element studies of the Great Dyke and Bushveld mafic phase and their relation to early Proterozoic magma genesis in southern Africa.
J. Petrol., 18, p24-52.

Hamlyn P.R. & Keays R.R.(1986) Sulfur Saturation and Second-Stage Melts: Application to the Bushveld Platinum Metal Deposits.
Econ. Geol., 81, p1431-1445.

Harmer R.E. & Sharpe M.R.(1985) Field relations and strontium isotope systematics of the marginal rocks of the east Bushveld Complex.
Econ. Geol., 80, p813-837.

Hiemstra S.A.(1979) The Role of Collectors in the Formation of the Platinum Deposits in the Bushveld Complex.
Canadian Mineralogist, 17, p469-482.

Hoatson D.M. & Keays R.R.(1989) Formation of Platiniferous Sulfide Horizons by Crystal Fractionation and Magma Mixing in the Munni Munni Layered Intrusion, West Pilbara Block, Western Australia.

Econ. Geol., 84, p1775-1804.

Hunter R.H.(1987) Textural equilibrium in layered igneous rocks.   *In* Parsons I. (ed.), Origins of Igneous Layering, p473-503.   D.Reidel Publishing Company.

Irvine T.N.(1982) Terminology for Layered Intrusions.
J. Petrol., 23, p127-162.

Irvine T.N., Keith D.W. & Todd S.G.(1983) The J-M Platinum-Palladium Reef of the Stillwater Complex, Montana: II. Origin by Double-Diffusive Convective Magma Mixing and Implications for the Bushveld Complex.
Econ. Geol., 78, p1287-1334.

Keays R.R. & Campbell I.H.(1981) Precious Metals in the Jimberlana Intrusion, Western Australia: Implications for the Genesis of Platiniferous Ores in Layered Intrusions.
Econ. Geol., 76, p1118-1141.

Kinloch E.D. & Peyerl W.(1990) Platinum-Group Minerals in Various Rock Types of the Merensky Reef: Genetic Implications.
Econ. Geol., 85, p537-555.

Klemm D.D., Ketterer S., Reichardt F., Steindl J. & Weber-Diefenbach K.(1985) Implication of vertical and lateral compositional variations across the Pyroxene marker and its associated rocks in the upper part of the Main Zone in the Eastern Bushveld Complex.
Econ. Geol., 80, p1007-1015.

Kruger F.J.(1990) The stratigraphy of the Bushveld Complex: a reappraisal and the relocation of the Main Zone boundaries.
S. Afr. J. Geol., 93, p376-381.

Kruger F.J.(1991) Authors Reply to Discussion on the Stratigraphy of the Bushveld Complex: a reappraisal and the relocation of the Main Zone boundaries.
S. Afr. J. Geol., 94, p187-190.

Kruger F.J.(1992) The Origin of the Merensky Cyclic Unit: Sr-Isotopic and Mineralogical Evidence for an Alternative Orthomagmatic Model.
Economic Geology Research Unit, Information Circular No. 247, University of the Witwatersrand, 12pp (unpublished).

Kruger F.J. & Marsh J.S.(1982) Significance of $^{87}Sr/^{86}Sr$ ratios in the Merensky cyclic unit of the Bushveld Complex.
Nature, 298, p53-55.

Kruger F.J. & Marsh J.S.(1985) The Mineralogy, Petrology, and Origin of the Merensky Cyclic Unit in the Western Bushveld Complex.
Econ. Geol., 80, p958-974.

Le Bas M.J. & Streckeisen A.L.(1991) The IUGS systematics of igneous rocks.
J. Geol. Soc. London, 148, p825-833.

Lee C.A.(1983) Trace and Platinum-Group Element Geochemistry and the Development of the

Merensky Unit of the Western Bushveld Complex.
Mineral. Deposita, 18, p173-190.

Lee C.A.(1985) PGE distribution patterns in the Platreef, Potgietersrus Part II. Pt, Pd, Cu, S and Ni contents and characterization of Platreef facies.
JCI Research Unit Rep. No.196 (unpublished).

Lee C.A.(1989) Pt, Pd, Ir and Au distribution in the critical zone and part of the main zone, Rustenburg Section, Rustenburg Platinum Mines, and their relevance in evaluating PGE targets.
JCI Research Unit Report No. 237/89 (unpublished).

Lee C.A.(1990) Platinum-Group Element Geochemistry in Geological Modelling and Resource Evaluation.
JCI Geologists Technical Meeting, 5, p97-114 (unpublished).

Lee C.A. & Tredoux M.(1986) Platinum-group element abundances in the lower and lower critical zones of the eastern Bushveld Complex.
Econ. Geol., 81, p1087-1095.

Lee C.A. & Parry S.J.(1988) Platinum-group element geochemistry of the lower and middle group chromitites of the eastern Bushveld Complex.
Econ. Geol., 83, p1127-1139.

Lee C.A. & Butcher A.R.(1990) Cyclicity in the Sr Isotope Stratigraphy through the Merensky and Bastard reef units, Atok Section, Eastern Bushveld Complex.
Econ. Geol., 85, p877-883.

Leeb du-Toit A.(1986) The Impala Platinum Mines.
In: Anhaeusser C.R., and Maske S., Eds., *Mineral Deposits of Southern Africa, II*, Geol. Soc. S. Afr., Johannesburg, p1091-1106.

Lurie J.(1986) Mineralization of the Pilanesberg Alkaline Complex.
In: Anhaeusser C.R., and Maske S., Eds., *Mineral Deposits of Southern Africa, II*, Geol. Soc. S. Afr., Johannesburg, p2215-2228.

Macdonald A.J.(1987) Ore Deposit Models #12. The Platinum Group Element Deposits: Classification and Genesis.
Geoscience Canada, 14, p155-166.

Mathez E.A., Dietrich V.J., Holloway J.R. & Boudreau A.E.(1989) Carbon Distribution in the Stillwater Complex and Evolution of Vapor During Crystallization of Stillwater and Bushveld Magmas.
J. Petrol., 30, p153-173.

Mathez E.A., Agrinier P. & Hutchinson R.(1994) Hydrogen Isotope Composition of the Merensky Reef and Related Rocks, Atok Section, Bushveld Complex.
Econ. Geol., 89, p791-802.

Mathez E.A.(1994) Magmatic metasomatism and formation of the Merensky reef, Bushveld Complex.

Nature (in press).

McBirney A.R. & Noyes R.M.(1979) Crystallization and Layering of the Skaergaard Intrusion.
J. Petrol., 20, p487-554.

McCandless T.E. & Ruiz J.(1991) Osmium isotopes and crustal sources for platinum-group mineralization in the Bushveld Complex, South Africa.
Geology, 19, p1225-1228.

Middlemost E.A.K.(1991) Towards a comprehensive classification of igneous rocks and magmas.
Earth-Science Reviews, 31, p73-87.

Mitchell A.A. & Scoon R.N.(1991) Discussion on 'The stratigraphy of the Bushveld Complex: a reappraisal and relocation of the Main Zone boundaries'.
S. Afr. J. Geol., 94, p183-186.

Mogessie A., Stumpfl E.F. & Weiblen P.W.(1991) The Role of Fluids in the Formation of Platinum-Group Minerals, Duluth Complex, Minnesota: Mineralogic, Textural, and Chemical Evidence.
Econ. Geol., 86, p1506-1518.

Morimoto M.(1988) Nomenclature of pyroxenes.
Fortschr. Miner., 66, p237-252.

Mossom R.J.(1986) The Atok Platinum Mine.
In: Anhaeusser C.R., and Maske S., Eds., *Mineral Deposits of Southern Africa, II*, Geol. Soc. S. Afr., Johannesburg, p1143-1154.

Mostert A.B., Hofmeyr P.K. & Potgieter G.A.(1982) The Platinum-Group Mineralogy of the Merensky Reef at the Impala Platinum Mines, Bophuthatswana.
Econ. Geol., 77, p1385-1395.

Mountain B.W. & Wood S.A.(1988) Chemical Controls on the Solubility, Transport, and Deposition of Platinum and Palladium in Hydrothermal Solutions: A Thermodynamic Approach.
Econ. Geol., 83, p492-510.

Naldrett A.J. & Cabri L.J.(1976) Ultramafic and Related Mafic Rocks: Their Classification and Genesis with Special Reference to the Concentration of Nickel Sulfides and Platinum-Group Elements.
Econ. Geol., 71, p1131-1158.

Naldrett A.J.(1989) Magmatic Sulfide Deposits.
Oxford University Press, 186pp.

Naldrett A.J. & Wilson A.H.(1990) Horizontal and vertical variations in noble-metal distribution in the Great Dyke of Zimbabwe: A model for the origin of the PGE mineralization by fractional segregation of sulfide[a].
Chem. Geol., 88, p279-300.

Naldrett A.J. & Barnes S-J.(1986) The behaviour of platinum group elements during fractional crystallization and partial melting with special reference to the composition of magmatic sulfide ores.
Fortschr. Miner., 64, p113-133.

Naldrett A.J., Gasparrini E.C., Barnes S.J., Von Gruenewaldt G. & Sharpe M.R.(1986) The Upper Critical Zone of the Bushveld Complex and the Origin of Merensky-type Ores.
Econ. Geol., 81, p1105-1117.

Naldrett A.J., Brugmann G.E. & Wilson A.H.(1990) Models for the Concentration of PGE in Layered Intrusions.
Canadian Mineralogist, 28, p389-408.

Nicholson D.M. & Mathez E.A.(1991) Petrogenesis of the Merensky Reef in the Rustenburg section of the Bushveld Complex.
Contrib. Mineral. Petrol., 107, p293-309.

Norrish K. & Hutton (1969) An Accurate X-Ray Spectrographic Method for the Analysis of a Wide Range of Geological Samples.
Geochim. Cosmochim. Acta, 33, p431-453.

Paktunc A.D., Hulbert L.J. & Harris D.C.(1990) Partitioning of the Platinum-Group and other Trace Elements in Sulfides from the Bushveld Complex and Canadian Occurrences of Nickel-Copper Sulfides.
Canadian Mineralogist, 28, p475-488.

Peck D.C. & Keays R.R.(1990) Insights into the behaviour of precious metals in primitive, S-undersaturated magmas: evidence from the Heazlewood River Complex, Tasmania.
Canadian Mineralogist, 28, p553-577.

Parry S.J.(1992) The role of neutron activation with radiochemistry in geoanalysis.
J. Geochemical Exploration, 44, p321-349.

Schurmann L.W. & Von Gruenewaldt G.(1991) The Petrogenesis of the Upper Critical Zone in the Boshoek Section of the Western Bushveld Complex.
Institute for Geological Research on the Bushveld Complex, Research Report No. 94, University of Pretoria, 25pp (unpublished).

Schwellnus J.S.I., Hiemstra S.A. & Gasparrini E.(1976) The Merensky Reef at the Atok Platinum Mine and its Environs.
Econ. Geol., 71, p249-260.

Sharpe M.R.(1985) Strontium isotope evidence for preserved density stratification in the main zone of the Bushveld Complex, South Africa.
Nature, 316, p119-126.

South African Committee for Stratigraphy (SACS) (1980) Stratigraphy of South Africa. Part 1 (Comp. L.Kent). Lithostratigraphy of the Republic of South Africa, South West Africa/Namibia, and the Republics of Bophuthatswana, Transkei and Venda: Handb. Geol. Surv. S. Afr., 8.

Streckeisen A.(1976) To each plutonic rock its proper name.
Earth-Science Reviews, 12, p1-33.

Stumpfl E.F. & Tarkian M.(1976) Platinum Genesis: New Mineralogical Evidence.
Econ. Geol., 71, p1451-1460.

Stumpfl E.F. & Ballhaus C.G.(1986) Stratiform platinum deposits: New data and concepts.
Fortschr. Miner., 64, p205-214.

Tankard A.J., Jackson M.P.A., Eriksson K.A., Hobday D.K., Hunter D.R. & Minter W.E.L.(1982) Crustal Evolution of Southern Africa, 3.8 Billion Years of Earth History.
Springer-Verlag, New York, 523pp.

Thompson J.B.(1991) Modal Space: Applications to Ultramafic and Mafic Rocks.
Canadian Mineralogist, 29, p615-632.

Vermaak C.F.(1976) The Merensky reef - thoughts on its environment and genesis.
Econ. Geol., 71, p1270-1298.

Vermaak C.F. & Hendriks L.P.(1976) A Review of the Mineralogy of the Merensky Reef, with Special Reference to New Data on the Precious Metal Mineralogy.
Econ. Geol., 71, p1244-1269.

Viljoen M.J. & Hieber R.(1986) The Rustenburg Section of Rustenburg Platinum Mines Limited, with Reference to the Merensky Reef.
In: Anhaeusser C.R., and Maske S., Eds., *Mineral Deposits of Southern Africa, II*, Geol. Soc. S. Afr., Johannesburg, p1107-1134.

Viljoen M.J., de Klerk W.J., Coetzer P.M., Hatch N.P., Kinloch E. & Peyerl W.(1986) The Union Section of Rustenburg Platinum Mines Limited, with Reference to the Merensky Reef.
In: Anhaeusser C.R., and Maske S., Eds., *Mineral Deposits of Southern Africa, II*, Geol. Soc. S. Afr., Johannesburg, p1061-1090.

Von Gruenewaldt G., Sharpe M.R. & Hatton C.J.(1985) The Bushveld Complex: Introduction and Review.
Econ. Geol., 80, p803-812.

Wager L.R. & Brown G.M.(1968) Layered Igneous Rocks.
Oliver & Boyd, Edinburgh, 588pp.

Wagner P.A.(1929) Platinum Deposits and Mines of South Africa.
Oliver & Boyd, Edinburgh, 326pp.

Walraven F.(1986) A Note on the Stratigraphic Terminology of the Bushveld Complex.
In: Anhaeusser C.R., and Maske S., Eds., *Mineral Deposits of Southern Africa, II*, Geol. Soc. S. Afr., Johannesburg, p1039-1040.

Wilson A.H.(1982) The Geology of the Great Dyke, Zimbabwe: Crystallization, Layering, and Cumulate Formation in the P1 Pyroxenite of Cyclic Unit 1 of the Darwendale Subchamber.
J. Petrology, 33, p611-663.

Wilson A.H., Naldrett A.J. & Tredoux M.(1989) Distribution and controls of platinum group element and base metal mineralization in the Darwendale subchamber of the Great Dyke, Zimbabwe.
Geology, 17, p649-652.

Wilson A.H. & Tredoux M.(1990) Lateral and Vertical Distribution of Platinum-Group Elements and Petrogenetic Controls on the Sulfide Mineralization in the P1 Pyroxenite Layer of the Darwendale Subchamber of the Great Dyke, Zimbabwe.
Econ. Geol., 85, p556-584.

Zientek M.L., Fries T.L. & Vian R.W.(1990) As, Bi, Hg, S, Sb, Sn and Te geochemistry of the J-M Reef, Stillwater Complex, Montana: constraints on the origin of PGE-enriched sulfides in layered intrusions.
J. Geochemical Exploration, 37, p51-73.

APPENDIX I

SAMPLING AND ANALYSES

APPENDIX I

SAMPLING AND ANALYSES

1. SAMPLE PREPARATION

Major elements were analysed using the lithium tetraborate fusion disc method of Norrish and Hutton (1969).   Trace elements were analysed using pressed powder pellets.

Sampling was done from continuous AXT borehole core (diameter = 32,51mm, mass = approx 23g/cm) drilled through the study sections.   Sampling intervals were appropriately determined and samples accurately cut using a core splitter (core splitter used in preference to diamond saw to avoid loss of material).   The samples were then cleaned with acetone, 220 silicon carbide paper, detergent and immersed in water in a BRANSONIC 32 ultrasonic cleaner before crushing with a 5x3 KEEGOR roll jaw crusher (crusher jaws cleaned with acetone between samples).   The crush was statistically split to approximately 200g samples using the cone and quartering method.   Portions of this were used for whole-rock and mineral separate geochemical analyses respectively.   All dry sample preparation was carried out in a laboratory with powerful extractor fan facilities to prevent any dust contamination.

Whole rock: The crush was milled for 1 minute using a SIEBTECHNIK T.250 swing mill, part of the resulting sample being used for preparation of fusion discs and pressed powder pellets for use in X-Ray Fluorescence (XRF) analysis for major and trace elements (R24A, R25A, R26A & R27A samples).   Part of the milled sample was also used for whole rock PGE + Au analysis (R27A samples only) by Neutron Activation (NAA), the remainder being retained for possible further work.

Mineral separates: Crush from R27A samples was milled for 2 seconds and then sieved through 212 and 149 mesh, producing 3 grain size fractions.   About 25g of the middle 149 - 212 fraction was collected and retained for mineral separation. These samples were repeatedly washed with deionised water (with beakers immersed in ultrasonic cleaner) to remove dust, and then oven dried.

Electromagnetic mineral separation was performed using a FRANTZ ISODYNAMIC L-1 magnetic separator.   Plagioclase was separated out in the initial separation sequence. Instrument settings were as follows:

Plagioclase Separation

1st run
Left-right tilt angle: 22° Left (constant throughout)
Vibrator setting: 6   (constant throughout)

Forward-back tilt angle: 15° Back
Current: 0,65 A
2nd and 3rd runs
Forward-back tilt angle: 10° Back
Current: 1,0 A

The resultant unseparated residue consisting of orthopyroxene, clinopyroxene, phlogopite/biotite, base metal sulphides (BMS), a small amount of remaining plagioclase, chromite *etc*, was collected and washed in concentrated HCl to remove BMS and then well rinsed with deionised water.   From this, orthopyroxene was separated out with instrument settings as follows:

Orthopyroxene Separation

1st run
Left-right tilt angle: 22° Left (constant throughout)
Vibrator setting: 6   (constant throughout)
Forward-back tilt angle: 23,5 to 24° Back
Current: 0,55 to 0,6 A

2nd run
Forward-back tilt angle: 23,5 to 24° Back
Current: 0,7 A

3rd, 4th and 5th runs
Forward-back tilt angle: 22 to 24° Back
Current: 0,62 to 0,65 A

6th, 7th and 8th runs
Forward-back tilt angle: 23,5 to 24° Back
Current: 0,55 to 0,6 A

The respective mineral separates were prepared into fusion discs for XRF analysis of major elements.   The remaining residue has been retained for possible further work.

Preparation of fusion discs: Approximately 0,5g of sample is placed into a clean silica crucible (crucible cleaned in hot dilute HCl) and oven dried at 100°C.   The crucible is then placed into a furnace at 1000°C for 4 hours, producing an ashed sample, which is slowly cooled in a dessicator.   The spectroflux (Johnson Matthey Spectroflux 105) used in the preparation of fusion discs is first preheated in platinum crucibles at 1000°C and then about 0,4g of the ashed sample added, as close as possible to the ratio of sample mass/flux mass = 2,2.   The samples are fused at 1000°C and the resultant product cast in a brass die maintained at a temperature of 250°C.   Discs are annealed for about 3 hours on a heated asbestos plate and then slowly cooled.   Each new batch of flux is homogenised and a new set of standards made up.   Fusion discs are individually sealed in plastic bags and any other contact with the surfaces avoided.

Preparation of pressed powder pellets: Approximately 8g of finely milled sample is mixed with 0,6ml of Mowiol solution (2,5g/l) and homogenised using an agate mortar and pestle.   The homogenised sample is placed at the bottom of a thick-walled stainless steel cylinder between

2 steel discs. A steel piston is then placed on top of the upper steel disc. This assembly (with piston protruding from cylinder) is then placed in a hydraulic press and subjected to a pressure of 10 tons for about 10 seconds. This produces a pellet about 5mm thick, which is trimmed and oven dried at 110 to 120°C for 3 to 4 hours. Pellets are individually packed and any other contact with the surface to be irradiated is avoided.

2. X-RAY FLUORESCENCE SPECTROMETRY

The whole-rock and mineral separate major and trace element analyses were performed using the Gold Fields Foundation PHILIPS PW1404/10 X-Ray Fluorescence spectrometer housed at the Department of Geology, University of Natal, Pietermaritzburg. The international standards and limits to which this instrument operates are listed in Table I.1.

3. NEUTRON ACTIVATION

Whole-rock PGE + Au analyses by Neutron Activation (NAA) were conducted by Dr S.J.Parry at the Reactor Centre, Imperial College, London, using a 100kW Consort reactor. Explanation of the methodology and theory of nickel sulphide fire assay collection and NAA used is described by Asif & Parry (1989, 1990) and Parry (1992).

The following detection limits were attained:

Pt ≤ 6 ppb
Pd ≤ 25 ppb
Rh $\leq 0,6$ ppb
Ir $\leq 0,1$ ppb
Os ≤ 2 ppb
Ru ≤ 19 ppb
Au $\leq 0,1$ ppb

Supplementary ultra low level whole-rock PGE analyses by neutron activation were performed by Prof A.H.Wilson at the University of Melbourne, Australia. Detection limits as low as $\pm 0,01$ ppb were attained.

4. BOREHOLE SAMPLING DETAILS

The following lists sample interval details for boreholes R24A, R25A, R26A and R27A, which were used for geochemical analysis.

The symbols in brackets following the sample numbers denote the rock type, as follows. All boreholes were sampled from the top down through the stratigraphic section of interest.

Rock-type symbols:

W = Hangingwall pyroxene anorthosite.
N = Hangingwall norite/leuconorite.
X = Merensky pyroxenite (± medium-grained feldspathic orthopyroxenite).

C = Chromitite layer.
M = Merensky reef pegmatoidal (or partially pegmatoidal) feldspathic orthopyroxenite enclosed by chromitite layers.
R = Other Merensky reef pegmatoidal feldspathic orthopyroxenite.
H = Merensky reef pegmatoidal feldspathic harzburgite.
A = Immediate footwall anorthosite.
L = Footwall leuconorite/norite.

Sample number	Borehole depth (m)	Sample width (cm)
R24A-1 (N)	11,20 - 11,0	20,0
R24A-2 (X)	11,0 - 10,9046	9,54
R24A-3 (X)	10,9046 - 10,8092	9,54
R24A-4 (X)	10,8092 - 10,7138	9,54
R24A-5 (X)	10,7138 - 10,6184	9,54
R24A-6 (X)	10,6184 - 10,523	9,54
R24A-7 (X)	10,523 - 10,4276	9,54
R24A-8 (X)	10,4276 - 10,3322	9,54
R24A-9 (X)	10,3322 - 10,2368	9,54
R24A-10 (X)	10,2368 - 10,1414	9,54
R24A-11 (X)	10,1414 - 10,046	9,54
R24A-12 (X)	10,046 - 9,9515	9,54
R24A-13 (R)	9,9515 - 9,8915	6,0
R24A-14 (C)	9,8915 - 9,8665	2,5
R24A-15 (M)	9,8665 - 9,8165	5,0
R24A-16 (M)	9,8165 - 9,7665	5,0
R24A-17 (C)	9,7665 - 9,7265	4,0
R24A-18 (H)	9,7265 - 9,6415	8,5
R24A-19 (C)	9,6415 - 9,6215	2,0
R24A-20 (A)	9,6215 - 9,5515	7,0
R24A-21 (A)	9,5515 - 9,4815	7,0
R24A-22 (L)	9,4815 - 9,3815	10,0
R24A-23 (L)	9,3815 - 9,2815	10,0
R24A-24 (L)	9,2815 - 9,1815	10,0
R24A-25 (L)	9,1815 - 9,0815	10,0
R24A-26 (L)	9,0815 - 8,9815	10,0
R24A-27 (L)	8,9815 - 8,8815	10,0
R24A-28 (L)	8,8815 - 8,7815	10,0
R24A-29 (L)	8,7815 - 8,6815	10,0
R24A-30 (L)	8,6815 - 8,5815	10,0
R24A-31 (L)	8,5815 - 8,4815	10,0
R24A-32 (L)	8,4815 - 8,3815	10,0
R25A-1 (N)	17,68 - 17,48	20,0
R25A-2 (X)	17,48 - 17,35	13,0
R25A-3 (X)	17,35 - 17,22	13,0
R25A-4 (X)	17,22 - 17,09	13,0
R25A-5 (X)	17,09 - 16,94	15,0
R25A-6 (X)	16,94 - 16,79	15,0

R25A-7 (X)	16,79 - 16,64	15,0
R25A-8 (X)	16,64 - 16,49	15,0
R25A-9 (X)	16,49 - 16,415	7,5
R25A-10 (X)	16,415 - 16,34	7,5
R25A-11 (X)	16,34 - 16,265	7,5
R25A-12 (X)	16,265 - 16,19	7,5
R25A-13 (R)	16,19 - 16,14	5,0
R25A-14 (C)	16,14 - 16,105	3,5
R25A-15 (M)	16,105 - 16,025	8,0
R25A-16 (M)	16,025 - 15,935	9,0
R25A-17 (C)	15,935 - 15,905	3,0
R25A-18 (A)	15,905 - 15,865	4,0
R25A-19 (C)	15,865 - 15,83	3,5
R25A-20 (A)	15,83 - 15,75	8,0
R25A-21 (A)	15,75 - 15,67	8,0
R25A-22 (A)	15,67 - 15,59	8,0
R25A-23 (L)	15,59 - 15,51	8,0
R25A-24 (L)	15,51 - 15,36	15,0
R25A-25 (L)	15,36 - 15,21	15,0
R25A-26 (L)	15,21 - 15,06	15,0
R25A-27 (L)	15,06 - 14,91	15,0
R25A-28 (L)	14,91 - 14,71	20,0
R25A-29 (L)	14,71 - 14,51	20,0
R25A-30 (L)	14,51 - 14,31	20,0
R26A-1 (W)	15,86 - 15,66	20,0
R26A-2 (W)	15,66 - 15,46	20,0
R26A-3 (N)	15,46 - 15,26	20,0
R26A-4 (N)	15,26 - 15,06	20,0
R26A-5 (N)	15,06 - 14,86	20,0
R26A-6 (N)	14,86 - 14,66	20,0
R26A-7 (N)	14,86 - 14,46	20,0
R26A-8 (X)	14,46 - 14,2725	18,75
R26A-9 (X)	14,2725 - 14,085	18,75
R26A-10 (X)	14,085 - 13,8975	18,75
R26A-11 (X)	13,8975 - 13,71	18,75
R26A-12 (X)	13,71 - 13,635	7,5
R26A-13 (X)	13,635 - 13,56	7,5
R26A-14 (X)	13,56 - 13,485	7,5
R26A-15 (X)	13,485 - 13,41	7,5
R26A-16 (C)	13,41 - 13,38	3,0
R26A-17 (M)	13,38 - 13,29	9,0
R26A-18 (C)	13,29 - 13,26	3,0
R26A-19 (A)	13,26 - 13,23	3,0
R26A-20 (L)	13,23 - 13,155	7,5
R26A-21 (L)	13,155 - 13,08	7,5
R26A-22 (L)	13,08 - 13,005	7,5
R26A-23 (L)	13,005 - 12,93	7,5
R26A-24 (L)	12,93 - 12,78	15,0
R26A-25 (L)	12,78 - 12,63	15,0
R26A-26 (L)	12,63 - 12,48	15,0

R26A-27 (L)	12,48 - 12,33	15,0
R26A-28 (L)	12,33 - 12,13	20,0
R26A-29 (L)	12,13 - 11,93	20,0
R26A-30 (L)	11,93 - 11,73	20,0
R26A-31 (L)	11,73 - 11,53	20,0
R26A-32 (L)	11,53 - 11,33	20,0
R26A-33 (L)	11,33 - 11,13	20,0
R26A-34 (L)	11,13 - 10,93	20,0
R26A-35 (L)	10,93 - 10,73	20,0
R27A-1 (W)	19,39 - 19,19	20,0
R27A-2 (W)	19,19 - 18,99	20,0
R27A-3 (N)	18,99 - 18,79	20,0
R27A-4 (N)	18,79 - 18,59	20,0
R27A-5 (N)	18,59 - 18,39	20,0
R27A-6 (N)	18,39 - 18,19	20,0
R27A-7 (N)	18,19 - 17,99	20,0
R27A-8 (N)	17,99 - 17,79	20,0
R27A-9 (X)	17,79 - 17,605	18,5
R27A-10 (X)	17,605 - 17,42	18,5
R27A-11 (X)	17,42 - 17,235	18,5
R27A-12 (X)	17,235 - 17,135	10,0
R27A-13 (X)	17,135 - 17,035	10,0
R27A-14 (X)	17,035 - 16,935	10,0
R27A-15 (X)	16,935 - 16,835	10,0
R27A-16 (C)	16,835 - 16,8	3,5
R27A-17 (M)	16,8 - 16,745	5,5
R27A-18 (C)	16,745 - 16,71	3,5
R27A-19 (R)	16,71 - 16,61	10,0
R27A-20 (R)	16,61 - 16,51	10,0
R27A-21 (R)	16,51 - 16,41	10,0
R27A-22 (R)	16,41 - 16,31	10,0
R27A-23 (R)	16,31 - 16,21	10,0
R27A-24 (R)	16,21 - 16,11	10,0
R27A-25 (R)	16,11 - 16,01	10,0
R27A-26 (R)	16,01 - 15,91	10,0
R27A-27 (R)	15,91 - 15,81	10,0
R27A-28 (R)	15,81 - 15,71	10,0
R27A-29 (R)	15,71 - 15,61	10,0
R27A-30 (R)	15,61 - 15,51	10,0
R27A-31 (R)	15,51 - 15,41	10,0
R27A-32 (R)	15,41 - 15,31	10,0
R27A-33 (R)	15,31 - 15,21	10,0
R27A-34 (R)	15,21 - 15,11	10,0
R27A-35 (R)	15,11 - 15,01	10,0
R27A-36 (R)	15,01 - 14,91	10,0
R27A-37 (L)	14,91 - 14,81	10,0
R27A-38 (L)	14,81 - 14,71	10,0
R27A-39 (L)	14,71 - 14,61	10,0
R27A-40 (L)	14,61 - 14,51	10,0
R27A-41 (L)	14,51 - 14,36	15,0

R27A-42 (L)	14,36 - 14,21	15,0
R27A-43 (L)	14,21 - 14,06	15,0
R27A-44 (L)	14,06 - 13,91	15,0
R27A-45 (L)	13,91 - 13,71	20,0
R27A-46 (L)	13,71 - 13,51	20,0
R27A-47 (L)	13,51 - 13,31	20,0
R27A-48 (L)	13,31 - 13,11	20,0
R27A-49 (L)	13,11 - 12,91	20,0
R27A-50 (L)	12,91 - 12,71	20,0
R27A-51 (L)	12,71 - 12,51	20,0
R27A-52 (L)	12,51 - 12,31	20,0

Element	Tube	KV	Ma	Analytical Line	Analysing Crystal	Collimator	Counter	Peak 2θ	Count Time Sec.	Background 2θ	Count Time Sec.	Standard	Blanks	Detection Limits	Analytical Accuracy
SiO₂	Cr	50	50	Ka	Pet	Coarse	Flow	109.165	60	106.000	30	SiO₂ 100% NIMD 37.02%		0.004%	0.2%
Al₂O₃	Cr	50	50	Ka	"	"	"	145.040	60	139.160	30	NIML 13.90%	SiO₂	0.005%	0.5%
Fe₂O₃	Au	50	50	Ka	Lif200	Fine	"	57.525	40	Blank standards used to calibrate background.		NIML 10.28%	SiO₂ and 60CaO+40SiO₂	0.001%	0.5%
MnO	Au	50	50	Ka	Lif200	"	"	62.990	40			NIML 0.78%	SiO₂ and 60CaO+40SiO₂	0.001%	0.5%
MgO	Cr	50	50	Ka	PX-1	Coarse	"	23.300	60	25.300	30	W-1 6.55%	SiO₂	0.011%	0.3%
CaO	Cr	50	50	Ka	pet	Fine	"	45.240	40	Blank standards		NIML 3.32%	SiO₂ and 40Fe₂O₃60SiO₂	0.0003%	0.2%
K₂O	Cr	50	50	Ka	Pet	"	"	50.720	40	used to calibrate		W-1 0.65%	SiO₂ and 60CaO+40SiO₂	0.0003%	0.2%
TiO₂	Cr	50	50	Ka	Pet	"	"	36.720	40	background		W-1 1.05%	SiO₂ and 60CaO+40SiO₂	0.0004%	0.2%
P₂O₅	Cr	50	50	Ka	Ge	Coarse	"	141.040	60	138.000 / 143.000	30 / 30	BR 1.10%	SiO₂	0.001%	0.2%
Na₂O	Cr	50	50	Ka	PX-1	Fine	"	28.170	60	30.000	30	BR 3.12%	SiO₂	0.018%	2%
Sc	Cr	50	50	Ka	Lif200	"	"	97.730	60	95.850 / 98.555	30 / 30	BCR 33 ppm	SiO₂ and CaCO₃	0.3 ppm	10%
Ba	Cr	50	50	La	Lif220	"	"	115.275	60	114.500 / 116.500	30 / 30	W-1 160 ppm	SiO₂ and MgO	1 ppm	± 20%
Zn	Au	50	50	Ka	Lif200	"	"	41.795	60	39.65 / 46.70	30 / 30	NIMP 100 ppm	SiO₂ and CaCO₃	0.3 ppm	± 10%
Cu	Au	50	50	Ka	Lif200	"	"	45.040	60	39.65 / 46.70	30 / 30	W-1 110 ppm	SiO₂ and CaCO₃	0.2 ppm	± 10%
Ni	Au	50	50	Ka	Lif200	"	"	48.690	60	46.70 / 50.00	30 / 30	BR 260 ppm	SiO₂ and CaCO₃	0.1 ppm	± 10%
Cr	Au	50	50	Ka	Lif200	"	"	69.375	60	68.10 / 70.80	30 / 30	JB1 400 ppm	SiO₂	0.6 ppm	10%
V	Au	50	50	Ka	Lif220	"	"	123.220	60	117.10 / 123.80	30 / 30	W-1 260 ppm	SiO₂	0.5 ppm	± 10%
La	Au	50	50	Ka	Lif220	"	"	138.920	60	132.60 / 141.80	30 / 30	BR 80 ppm	SiO₂	1.5 ppm	15%
Zr	Rh	50	50	Ka	Lif220	"	Scint	32.045	60	29.30 / 34.89	30 / 30	AGV 230 ppm	SiO₂	0.3 ppm	3%
Sr	Rh	50	50	Ka	Lif220	"	"	35.830	60	34.89 / 36.90	30 / 30	W-1 190 ppm	SiO₂	0.2 ppm	3%
Nb	Rh	50	50	Ka	Lif220	"	"	30.420	60	29.45 / 34.80	30 / 30	GSP 23 ppm	SiO₂	0.1 ppm	3%
Y	Rh	50	50	Ka	Lif220	"	"	33.855	60	29.45 / 34.80	30 / 30	NIMG 145 ppm	SiO₂	0.3 ppm	3%
Rb	Rh	50	50	Ka	Lif220	"	"	37.960	60	34.80 / 41.10	30 / 30	NIMG 320 ppm	SiO₂	0.4 ppm	2%
U	Rh	50	50	Ka	Lif220	"	"	37.300	100	36.90 / 41.10	30 / 30	NIMG 15 ppm	SiO₂	0.1 ppm	20%
Th	Rh	50	50	Ka	Lif220	"	"	39.250	100	36.90 / 41.10	30 / 30	GSP 105 ppm	SiO₂	0.5 ppm	20%
Pb	Au	50	50	Ka	Lif220	"	Flow/Scint	40.225	60	39.80 / 41.50	30 / 30	GSP 54 ppm	SiO₂	1 ppm	± 10%
Ga	Au	50	50	Ka	Lif220	"	"	56.165	60	55.50 / 57.20	30 / 30	GSP 23 ppm	SiO₂	0.2 ppm	10%
Co	Au	50	50	Ka	Lif220	"	"	77.890	60	77.40 / 79.00	30 / 30	NIMD 210 ppm	SiO₂	1 ppm	± 10%

Table I.1   Operating standards of the Philips PW1404/10 X-Ray Fluorescence Spectrometer.

APPENDIX II

WHOLE-ROCK MAJOR AND TRACE ELEMENT DATA

Major Element values for profile R27A whole rock (Wt %)

Sample	Rock	SiO2	Al2O3	Fe2O3	MnO	MgO	CaO	Na2O	K2O	TiO2	P2O5	Cr2O3	NiO	Total	LOI
1	W	49.53	27.52	3.04	0.05	3.77	13.62	2.01	0.14	0.0741	0.01	0.0638	0.0268	99.86	0.13
2	W	49.42	27.19	3.17	0.06	4.01	13.56	1.93	0.13	0.0829	0.01	0.0511	0.029	99.63	0.16
3	N	49.61	26.83	3.18	0.06	4.17	13.69	2.01	0.13	0.08	0.01	0.0648	0.0297	99.86	0.92
4	N	49.53	26.49	3.46	0.06	4.5	13.35	1.98	0.13	0.0836	0.01	0.075	0.0347	99.7	0.08
5	N	49.75	26.01	3.83	0.06	5.14	12.88	2.03	0.13	0.0739	0.01	0.0766	0.0435	100.02	0.28
6	N	49.89	24.5	4.31	0.07	6.06	12.79	1.95	0.12	0.079	0	0.1007	0.0522	99.93	0.11
7	N	50.14	22.56	5.28	0.09	7.73	12	1.72	0.12	0.0962	0.01	0.1334	0.0697	99.93	0.09
8	N	50.96	17.71	7.77	0.13	11.84	9.75	1.47	0.11	0.1121	0.01	0.1953	0.1162	100.16	0.12
9	X	52.45	7.64	12.02	0.22	21.79	4.76	0.44	0.09	0.1722	0.01	0.3665	0.1847	100.14	0.17
10	X	52.77	5.13	12.75	0.21	22.89	4.47	0.27	0.15	0.2321	0.03	0.4054	0.2904	99.61	1.42
11	X	53.16	6.89	11.83	0.21	22.45	4.24	0.53	0.12	0.2048	0.11	0.3684	0.2178	100.33	3.71
12	X	53.47	7.25	11.34	0.21	22.43	4.25	0.5	0.16	0.1999	0.01	0.3702	0.1203	100.31	0.12
13	X	53.43	6.61	11.29	0.21	22.85	4.64	0.44	0.14	0.2118	0.03	0.3956	0.1211	100.36	0.16
14	X	53.24	6.51	11.83	0.22	23.03	4.02	0.37	0.13	0.209	0.01	0.3788	0.2062	100.15	0.16
15	X	50.2	4.9	15.93	0.22	22.24	3.6	0.18	0.14	0.261	0.01	0.4387	1.3153	99.43	0.21
16	C	41.9	5.5	18.95	0.24	20.01	4.3	0.04	0.08	1.1233	0.02	5.6255	0.7257	98.5	0.42
17	M	50.56	4.22	14.28	0.21	22.51	5.32	0.22	0.18	0.3852	0.12	1.1022	0.7024	99.81	0.21
18	C	45.93	11.03	12.71	0.2	18.94	4.93	0.6	0.1	0.2712	0	4.0489	0.2465	99.02	0.25
19	R	51.41	7.44	12.28	0.2	23.13	4.16	0.37	0.28	0.2453	0.01	0.5969	0.2175	100.34	0.88
20	R	52.6	5.65	12.83	0.22	23.83	3.8	0.29	0.13	0.2514	0.01	0.3632	0.2797	100.26	0.59
21	R	51.51	6.76	12.89	0.21	23.14	4.2	0.38	0.12	0.2605	0.01	0.312	0.3356	100.12	0.9
22	R	52.19	8	11.46	0.2	22.09	4.86	0.56	0.08	0.2164	0	0.3509	0.1075	100.13	0.24
23	R	52.85	7.04	11.92	0.21	22.47	4.03	0.73	0.24	0.2725	0.01	0.3186	0.1221	100.2	0.13
24	R	51.78	7.53	11.92	0.21	22.46	4.63	0.5	0.09	0.2231	0.01	0.3306	0.2412	99.92	0.3
25	R	52.85	9.77	10.42	0.18	18.87	5.26	0.97	0.43	0.2166	0.29	0.2915	0.2487	99.8	0.01
26	R	52.71	8.85	10.93	0.18	20.1	4.66	0.74	0.52	0.2506	0.1	0.5001	0.2315	99.77	0.14
27	R	53.64	6.61	11.76	0.22	22.55	3.92	0.55	0.27	0.2925	0.02	0.376	0.1007	100.3	0.34
28	R	52.54	8.16	11.81	0.21	20.87	4.58	0.66	0.22	0.2427	0.01	0.3331	0.3936	100.03	0.17
29	R	54.5	7.31	11.04	0.19	20.97	4.21	0.75	0.62	0.3076	0.01	0.3357	0.0899	100.35	0.85
30	R	53.38	6.96	11.49	0.2	21.38	4.63	0.66	0.37	0.2971	0.02	0.3672	0.2036	99.94	0.7
31	R	51.5	8.25	11.43	0.17	18.6	7.5	0.79	0.28	0.2821	0.02	0.5225	0.6472	100.01	0.23
32	R	53.36	8.99	10.7	0.18	20.03	5.02	0.89	0.32	0.2707	0.02	0.3201	0.1649	100.26	0.78
33	R	53.27	6.77	11	0.21	21.85	5.71	0.51	0.13	0.2461	0.01	0.4485	0.0914	100.23	0.44
34	R	53.5	7.36	10.98	0.2	21.64	4.81	0.64	0.27	0.2551	0.01	0.4478	0.0843	100.2	0.1
35	R	52.45	9.67	10.4	0.18	20.63	5.13	0.7	0.23	0.2167	0.01	0.4337	0.0853	100.14	0.48
36	R	50.86	11.27	10.16	0.17	20.28	5.85	0.82	0.15	0.157	0.01	0.2783	0.1046	100.11	0.78
37	L	51.15	20.75	4.86	0.09	9.94	11.17	1.65	0.15	0.1374	0.02	0.1893	0.0395	100.15	0.39
38	L	50.54	20.54	5.01	0.09	10.65	10.51	1.44	0.11	0.0868	0.01	0.166	0.0379	99.2	0.23
39	L	50.48	22.21	4.12	0.08	8.7	12.06	1.59	0.12	0.0961	0	0.1592	0.0305	99.64	0.27
40	L	49.8	25.43	3.25	0.06	6.21	12.6	1.89	0.14	0.0804	0.01	0.0995	0.0202	99.59	3.3
41	L	50.15	24.96	3.39	0.06	6.69	12.62	1.85	0.13	0.0782	0	0.1108	0.0219	100.08	0.42
42	L	50.09	24.97	3.48	0.07	6.81	12.57	1.83	0.13	0.0857	0.01	0.117	0.0262	100.18	0.44
43	L	50.08	25.72	3.19	0.06	6.18	12.66	1.87	0.13	0.0656	0	0.099	0.0185	100.06	0.41
44	L	49.95	25.85	3.19	0.06	6.2	12.66	1.78	0.13	0.0665	0.01	0.1016	0.0193	100.02	0.27
45	L	49.81	26.78	2.78	0.05	5.28	13.13	1.94	0.14	0.0753	0.01	0.0772	0.0155	100.08	0.25
46	L	49.84	26.94	2.7	0.04	5.06	13.22	1.95	0.14	0.0667	0.01	0.087	0.0154	100.06	0.16
47	L	49.94	25.72	3.16	0.06	6.03	12.74	1.85	0.14	0.0709	0.01	0.1029	0.0198	99.83	0.21
48	L	49.87	26.12	2.94	0.05	5.54	12.98	1.93	0.15	0.0753	0.01	0.0924	0.018	99.77	0.12
49	L	50.02	25.85	3.13	0.06	5.95	12.79	1.83	0.15	0.0807	0.01	0.1031	0.0179	99.98	0
50	L	50.17	26.1	3.08	0.06	5.88	12.82	1.89	0.15	0.0809	0.01	0.1076	0.0167	100.35	0.21
51	L	50.09	25.54	3.23	0.06	6.18	12.74	1.84	0.15	0.0823	0.01	0.1157	0.0184	100.05	0.17

Trace Element values for profile R27A whole rock (ppm)

Sample	Rock	Nb	Y	Rb	Zr	Sr	Pb	Ga	Co	As	Zn	Cu	Ni	Ba	Sc	V	La	S
1	W	0.4	3.7	1.4	8	405	0	17	16	1.07	23	60	175	76	5	28	2.4	570
2	W	0.1	4.6	0.8	6.6	403.7	0	17	18	1.16	26	68	196	80	4	29	0	682
3	N	0	4.1	0.9	5.4	397.6	0	16	18	0	23	74	209	79	5	32	2	697
4	N	0	3.5	1.4	6.3	396.1	0	17	22	0.66	24	92	249	84	6	40	0.7	865
5	N	0	4.2	0.9	6.2	384.8	0	15	23	0.66	29	105	308	86	6	30	1.3	1163
6	N	0	3.5	1.4	6.3	361.9	2.73	15	31	0.34	31	124	368	71	9	43	1.7	1304
7	N	0	4.8	1	6.1	334.9	1.44	15	38	1.63	36	267	585	77	12	57	3.1	1811
8	N	0	5.5	0.6	7.2	265.6	4.41	12	68	1.49	54	573	855	83	20	87	4.1	3092
9	X	0	6.6	2.3	8.3	104.2	3.97	10	140	3.56	85	558	1384	85	39	155	0.9	4025
10	X	0.7	10.3	6.3	19.9	66.9	0	10	168	1.25	87	1037	2175	96	47	191	6.7	7809
11	X	0.4	8.7	4	14	95.9	0.97	8	154	2.71	82	741	1618	91	38	164	8.6	4987
12	X	0.8	8.1	4.4	27.6	100.9	5.43	8	136	2.49	78	262	942	108	40	164	4.9	1767
13	X	1.1	9.4	4.6	19.8	89.8	0	8	140	1.04	79	282	939	91	43	170	5.5	1767
14	X	1.2	8.5	4.3	15.2	91.3	9.28	8	145	2.32	79	863	1578	89	41	169	7.6	4416
15	X	0.5	9.3	6	23.8	61.1	8.52	10	326	4.22	80	4739	9573	87	40	174	6.2	38518
16	C	0.5	9.9	2.9	14.7	45.6	15.97	16	226	4.73	197	2515	5557	73	40	1007	7.2	20888
17	M	1	13.5	7.7	26.3	46.6	12.04	10	219	4.22	90	2182	5301	135	47	288	9.8	19655
18	C	0.4	6.1	1.8	9.2	127.3	7.01	15	136	3.41	133	1142	1860	81	27	392	5	5154
19	R	1.2	7.8	12.3	47.7	92.9	6.56	10	168	3.06	83	426	1626	141	36	166	0.7	3507
20	R	0.2	9.8	4.4	17.5	68.9	2.05	9	179	2	85	305	2081	94	43	181	5.1	6490
21	R	0.1	9.2	5	18.7	90.3	0	9	196	1.69	86	1314	2477	90	39	160	5.6	7278
22	R	0	8.2	1.2	14.1	113.8	3.79	10	141	2.22	81	95	846	85	37	149	0	793
23	R	0.9	8.7	8.7	30.1	99.7	0	8	144	1.76	87	145	945	160	39	164	6.4	954
24	R	0	7.9	1.3	14.3	108.9	5.04	9	159	1.88	83	916	1825	86	36	154	3.1	5323
25	R	2.5	14.4	15.9	19.6	146.6	12.57	11	131	3.6	72	886	1806	138	29	124	15.4	5704
26	R	1.9	9	23.2	21.7	121.8	7.5	10	150	2.61	77	1316	1732	150	30	146	7.1	5014
27	R	1.7	9.8	11.4	26.5	88.5	0	8	129	1.24	88	41	791	132	41	182	8.3	259
28	R	0.4	9.6	7.9	31.3	116.1	3.9	10	196	2.27	82	1139	2988	106	35	153	11.7	8973
29	R	2.1	10.4	23.7	51.4	98.6	0	9	121	2.15	80	32	713	207	39	165	11.9	192
30	R	1.6	11	15.7	45.9	93.8	1.89	8	139	2.86	83	1476	1545	143	40	170	4.8	4058
31	R	0.9	11.2	9.3	29.5	118.1	7.87	10	200	2.3	68	1685	4696	139	39	176	4.3	17360
32	R	2.2	9.4	12.4	28.3	132.4	0	10	131	3.07	78	414	1243	146	35	154	2.6	3197
33	R	0	10	4.9	17.8	91.2	0	9	125	1.34	80	52	720	78	44	184	0.6	270
34	R	0.8	10.3	9.9	29.9	105.2	0	9	120	2.1	82	18	666	157	39	175	4.4	156
35	R	1.3	7.2	8.9	24.6	137.8	0	10	122	1.7	76	26	674	121	31	142	2.7	205
36	R	1.2	6.8	4.3	16.2	174.5	0	10	130	1.18	73	31	811	88	24	103	1.8	441
37	L	0	5.8	1.2	10.5	328.8	0.15	15	39	2.06	50	56	304	106	12	64	0	222
38	L	0	4.5	0.2	6.3	309.8	0	14	42	0.1	35	33	289	75	11	55	2.3	103
39	L	0	4.5	0.3	6.1	335.5	0	16	34	2.22	29	37	232	74	11	53	3.4	122
40	L	0	3.8	1.2	7.5	381.3	0	16	25	0.38	23	15	159	84	7	33	0	74
41	L	0	3.7	1.4	6.5	376.2	1.37	13	24	0.67	23	16	172	69	7	37	0.8	98
42	L	0	3.9	2.2	7.8	370.6	0	16	29	2.21	39	13	184	72	7	38	3	133
43	L	0.1	3.4	0.6	5	386.9	0	15	23	0.92	24	11	151	77	5	30	0	61
44	L	0	3.4	1.1	6.4	383.4	0	18	25	0.31	25	7	149	81	5	34	3.3	51
45	L	0	3.6	1.8	6.3	398	0	17	18	0	24	8	133	83	5	28	2.8	50
46	L	0	3.8	0.8	7.4	402	3.15	15	17	0.15	22	7	124	74	5	26	0	49
47	L	0	4.2	1.3	7.5	386.2	0	16	24	0.31	26	7	153	71	6	33	3.1	67
48	L	0	3.4	2.1	9	395.7	2.03	16	19	0.8	28	7	142	64	6	32	0	82
49	L	0.4	4	2.5	8.2	389.7	0.53	16	23	0.01	25	7	150	60	5	31	0.6	85
50	L	0	4.7	0.9	8.2	389.9	0	17	23	0.63	23	7	151	72	6	30	0	83
51	L	0.4	4.3	2.5	8.9	383.9	0	16	22	0	24	6	166	68	7	33	0.8	82
52	L	0	4	2.2	9.9	372	2.06	15	27	0	26	6	180	72	8	36	0	101

Trace Element values for profile R26A whole rock (ppm)

Sample	Rock	Zr	Sr	Nb	Y	Rb	Zn	Cu	Ni	Ba	S	P
1	W	5.3	398.5	0.2	4.6	2	21.7	93.8	156.5	73.2	683.8	68.832
2	W	6.8	390.4	0	2.5	2.6	22.5	101.1	171.7	76.3	711.6	50.101
3	N	5	397.2	0	2	1.3	22.5	118.7	190.6	71.4	844.8	46.692
4	N	5.5	385.6	0	4.3	1.7	26.8	137.4	237.9	67.5	959.9	35.698
5	N	5.5	373	0.4	3.3	1.7	31.5	191.7	311.6	71.2	1354	58.283
6	N	7.1	351.1	0	3.6	2.9	34.7	280.1	507	65.6	1843.2	45.96
7	N	12	288.2	0.2	4.4	4.5	48.1	499.3	808.6	88.1	2975.1	60.679
8	X	15.4	120.1	0.9	6.5	6.9	64.9	600.9	1164.3	75.1	4073.1	119.55
9	X	28.5	69.8	2.6	8.9	15.3	86.9	1183.5	2334.2	98	9115.7	176.206
10	X	21.1	70	0.6	7.4	9.7	82	1088.2	1937.4	71.2	7514.3	263.496
11	X	28.3	77.1	0.9	9.9	10	81.7	455.8	983.4	63.1	2466.7	1758.288
12	X	17.9	93.1	0	5.9	7.3	82.8	406.7	852.8	54.2	1767.4	54.671
13	X	16.6	75.5	0.3	8	4.9	81.3	2856.7	4256.3	42.7	17825.9	255.404
14	X	21.6	53	0.3	10.3	7.7	71.6	3220.5	4877	65.4	23857.1	71.512
15	X	24.6	59.3	1	8.5	10.2	81.1	2814.5	8666.9	75	31746.5	41.845
16	C	11.1	120.5	0.5	6.5	4.7	75.2	2953.7	6969.1	47.9	24426.9	46.884
17	M	10.3	44.4	0	7.2	2.4	57.5	9422.6	17145	31.4	91375.1	42.699
18	C	6.1	128.6	0	4.2	1.8	221.1	2138.4	3752.8	53.5	12320.8	46.317
19	A	3.4	412.5	0	1.3	2.8	16.6	1446.6	2087.9	93	7204.6	30.561
20	L	6.4	340.9	0.8	3.2	3.3	34	1772.6	2767.4	83.5	10142.8	51.342
21	L	6.6	391.9	0	2.2	2.6	18	11.8	120.4	89.9	202	41.482
22	L	6.9	378.8	0	4.2	1.8	19.7	12.4	130.5	84.4	167	34.982
23	L	6.3	371.1	0	2.5	2.2	20.3	22.9	144.4	103.1	248.7	36.863
24	L	16.8	282.7	0	3.6	5.3	37.9	38.8	265	76.9	250.9	196.866
25	L	9.3	318.7	0	3	3.2	35	33.2	217.5	90.1	319.8	96.638
26	L	9	255.2	0	3.9	3.1	44.6	53.8	315.6	61	306.1	65.082
27	L	7.8	299.4	0	2.3	3.4	37.6	75.3	263.7	72.4	334.4	30.399
28	L	12	293.3	0	3.3	3.2	38.8	133.5	372.1	76.2	847.6	92.981
29	L	8.4	300.2	0	4.2	2.7	37.3	118.6	350.4	78.3	642.1	40.501
30	L	6.4	337.9	0	3.8	2.2	29.1	920.7	1487.3	86	5537.5	29.227
31	L	9	341	0	2.5	2.7	26.4	16.9	170.2	80.2	235.6	37.795
32	L	8.9	297.3	0	3.8	3.5	34.2	17.9	234.1	62.1	184.4	38.223
33	L	8.4	294.3	0	3.5	3.5	36.5	21	239	69	214	89.486
34	L	9.3	284.6	0	3.3	3.2	37.2	19.5	273	71.3	462.1	65.277
35	L	8.3	318.3	0	3.1	2.6	30.4	15.8	194.9	94.2	284.8	40.126

Trace Element values for profile R25A whole rock (ppm)

Sample	Rock	Zr	Sr	Nb	Y	Rb	Zn	Cu	Ni	Ba	S	P
1	N	39.1	181.9	0.4	6.6	19.7	57.9	550.2	874.2	98.6	4505.6	81.659
2	X	11.7	126	0	6.7	4.2	78.9	560.5	1206.1	53.9	4015.3	50.994
3	X	13	95.1	0.4	7.2	2.4	102.8	696.5	1481	45.9	5328.3	44.672
4	X	12.8	67.9	0	7.3	2.9	89.9	1289	2176.8	27.8	9689.8	37.412
5	X	10.5	62.2	0.3	7.7	2.1	103.9	1255.2	2203	33.4	8993.2	44.843
6	X	12.1	55.9	0.8	8.4	4.5	113.9	332.5	1034.1	50.1	2855.9	75.168
7	X	13.1	59.5	0.4	7.5	5.4	93.3	299.5	950.6	43.8	2473	83.026
8	X	11.8	72.5	0	6	4	83.2	1445.5	2821.5	34.2	10922.4	60.219
9	X	10.1	56.4	0	6.5	2.1	83.8	3069.1	4904.2	37.7	21423.9	43.989
10	X	9.1	57	0	5.4	1.7	76.8	2606.3	4786.2	25.8	20834.9	24.342
11	X	10.7	73.7	0.4	7.9	2.3	76	1646.1	2592.7	25.5	10945.5	99.342
12	X	20.5	49.7	0.4	14.2	5.2	59.9	1015.7	1735.3	34.1	6642.9	167.849
13	R	18	85.4	0	13.3	3.8	64.2	1354.8	1834.6	41.6	7522.1	52.019
14	C	6.2	141	0	3.7	2.4	202	2247.8	2501.3	34.8	8506.1	35.191
15	M	7.1	155.4	0.4	3	1.5	58.2	86.8	1071.8	27.4	1461.6	51.677
16	M	8	88.5	0	4.5	2.8	53.7	2439.2	3201.9	29.7	11336.6	30.663
17	C	5.8	212.5	0	1.9	1.9	125.6	503.4	1183.1	46.6	2511.3	32.628
18	A	3.9	329.1	0	3	2	446.6	732.5	803	84.5	2618.1	30.663
19	C	9.4	270.1	0.8	3.8	1.9	131.3	3632.6	6222.5	55.2	14002.9	30.407
20	A	5.2	412.7	0	2.1	2.6	16.5	2311.7	3319.8	83	13826.6	32.97
21	L	3.4	414.2	0	3	1	13.8	1503.5	2445	77.6	9166.6	22.89
22	L	4.3	379.6	0	2	2.2	17.1	1183.2	2331.9	70.4	8252.5	22.719
23	L	5.7	328.5	0	1.8	2.2	28.2	251.7	505.9	51.6	1323.9	20.228
24	L	4.7	326.7	0	2.5	1.1	28.7	51.4	232.6	77.6	294.8	24.822
25	L	5.6	284.9	0	2.4	2.2	38.1	246	711.3	66.7	1878.9	25.843
26	L	6.8	283.7	0	4.2	2.4	44.6	559.8	1399.4	54.8	5312.1	23.839
27	L	5.1	285.4	0.2	3.5	2.2	42.1	36.4	243.3	57.1	272.6	25.553
28	L	4.8	270.6	0	2.8	1.5	41.8	26.5	256.5	59.8	261.4	23.067
29	L	6.2	302.1	0	3.2	2.5	34.4	20.4	212.1	68.3	199.3	21.891
30	L	4.8	330.2	0	3	0.8	27.9	17.5	174.2	64.3	149.1	22.575

Trace Element values for profile R24A whole rock (ppm)

Sample	Rock	Zr	Sr	Nb	Y	Rb	Zn	Cu	Ni	Ba	S	P
1	N	9.3	212.8	0	5.8	2	61.1	528	954.2	69.9	3148.4	51.933
2	X	10	76.3	0	6.3	6.5	76.1	598.8	1353.9	60.4	4542.8	28.357
3	X	11.9	65.6	0.5	8.8	5.7	79.6	633.8	1457.2	63.5	4774.8	29.553
4	X	16.5	79.1	0.5	7.3	4.6	82.8	1349.6	2307.6	57.6	9036.1	70.52
5	X	29	75.2	0	7.7	6.2	81.2	1388.2	2268.4	48.3	8680.2	47.712
6	X	23	69.2	1.4	9	12.8	83.4	657.4	1294.5	93.2	4087.1	1218.41
7	X	26.4	61.4	1.8	8.5	14.3	81.5	363.6	1035.9	78.6	2605.9	67.151
8	X	43.1	73.1	0.7	8.4	13.9	79.7	324.8	944.4	72.5	2505.6	149.097
9	X	30.3	80.8	1.9	8.2	12.6	80.8	984.7	1447	119.9	4363.9	64.67
10	X	18.8	82.4	0	6.7	8	84.9	3195	5450.6	49.4	21341.3	53.084
11	X	25.5	51.4	0	7	7.2	84.1	5362.7	2958.5	43.1	20290.9	82.238
12	X	15	78.5	0.6	7.4	9.5	86.1	1946.7	3772.5	69.9	14740.9	47.028
13	R	25.3	41.1	0.3	10.1	12	81.6	2047.7	6400.5	66.7	21861.3	78.119
14	C	5.3	67	0	4.7	1.5	280.3	2364.8	5429.5	24.6	17249.9	21.399
15	M	33.2	47.4	0.9	12.2	6.6	93.7	387.8	1250.1	45.3	2922.1	1037.656
16	M	9.1	90.4	0	5.2	2.7	77.2	194.4	895	17.3	1333.1	280.907
17	C	10	96.6	0	3.6	3.4	294.2	3739.1	3275.4	34.5	10590	97.669
18	H	12.5	94.7	0	3.3	3	72.4	3269.5	7114.4	36.6	23702.9	73.254
19	C	7.6	170.9	0.8	5.2	5.2	71.9	4464.5	14341	41.6	48678.5	44.714
20	A	5.5	408.5	0	2	3.7	17.3	261.2	350.2	79.7	1154.3	29.384
21	A	3.3	417.4	0	2.8	2.7	14.2	61.9	131.7	86.5	226.3	25.701
22	L	5.2	389	0	2.3	3.2	20.4	1175.3	1860.9	83.6	7320.9	27.176
23	L	4.6	347.2	0	3.1	2.9	25.2	1650.3	3748.4	78.3	14352.1	22.708
24	L	7	340.1	0	3.3	3.3	27	49.8	178.2	81.8	223.2	41.011
25	L	9	302.8	0	4.1	2.9	33.7	51.2	230	62.9	248.9	104.894
26	L	10.9	297	0.7	3.4	3.1	39.6	36.1	223.7	72	193.4	72.007
27	L	9	294.6	0	3.9	2.1	34.1	36.5	233.3	66.3	171	48.602
28	L	7.5	282.3	0	3.1	4.1	34.9	34.7	247.8	72.1	162.6	24.257
29	L	6.3	284.4	0	3.6	1.6	35.6	32.4	248	68.8	165.3	23.659
30	L	11.1	277.5	0.1	4.1	3.5	36.7	20	253.5	69.3	160.4	116.767
31	L	7.5	311.2	0.3	3.1	3.2	30.7	23.8	206.5	63.6	183.2	139.745
32	L	5.6	319.7	0.1	3.4	3	30.2	19.5	190.2	65.7	126.9	33.909

APPENDIX III

MINERAL SEPARATE MAJOR ELEMENT DATA

Major Element values for profile R27A orthopyroxene (Wt%)

Sample	Rock	SiO2	Al2O3	Fe2O3	FeO	MnO	MgO	CaO	Na2O	K2O	TiO2	Cr2O3	NiO	ZnO	Mg#
1	W	53.55	1.47	1.84	14.88	0.33	25.68	1.63	0	0	0.2264	0.3317	0.0835	0	0.7546
2	W	53.54	1.46	1.84	14.91	0.33	25.78	1.59	0	0	0.228	0.3218	0.0868	0	0.755
3	N	53.69	1.43	1.83	14.8	0.34	25.9	1.6	0	0	0.2219	0.3265	0.0868	0	0.7572
4	N	53.48	1.4	1.83	14.78	0.33	25.86	1.54	0.03	0	0.2277	0.3165	0.0902	0	0.7571
5	N	53.63	1.38	1.78	14.44	0.32	25.94	1.59	0	0	0.2115	0.3439	0.0924	0	0.762
6	N	53.72	1.4	1.76	14.27	0.32	26.03	1.72	0.03	0	0.2041	0.3591	0.0948	0	0.7648
7	N	53.74	1.43	1.74	14.09	0.31	26.19	1.71	0.04	0	0.2011	0.3647	0.0971	0	0.7681
8	N	54.03	1.48	1.68	13.57	0.3	26.69	1.64	0.02	0	0.1952	0.3785	0.1018	0	0.778
9	X	54.26	1.52	1.5	12.11	0.27	27.83	1.68	0.06	0	0.1857	0.4468	0.1072	0	0.8037
10	X	54.38	1.38	1.48	11.95	0.26	27.86	1.65	0.09	0	0.2115	0.4332	0.1204	0	0.8059
11	X	54.38	1.4	1.47	11.88	0.26	27.9	1.66	0.36	0	0.2131	0.44	0.1172	0	0.8071
12	X	54.54	1.48	1.42	11.52	0.25	28.29	1.66	0.04	0	0.1947	0.4662	0.1075	0	0.814
13	X	54.39	1.48	1.43	11.56	0.25	28.14	1.65	0	0	0.1946	0.4669	0.1063	0	0.8126
14	X	54.53	1.37	1.44	11.66	0.26	28.23	1.56	0	0	0.2062	0.4483	0.1177	0	0.8118
15	X	54.53	1.31	1.49	12.06	0.26	27.95	1.52	0.05	0	0.2366	0.4214	0.1481	0	0.8051
17	M	54.42	1.4	1.47	11.94	0.26	28.05	1.65	0.1	0	0.2238	0.4261	0.1334	0	0.8072
19	R	54.48	1.47	1.44	11.67	0.25	28.17	1.68	0.02	0	0.2259	0.4072	0.118	0	0.8114
20	R	54.25	1.37	1.53	12.37	0.26	28.06	1.49	0	0	0.2455	0.4091	0.145	0	0.8017
21	R	54.48	1.27	1.51	12.19	0.26	28.24	1.37	0	0	0.2719	0.3841	0.13	0	0.805
22	R	54.63	1.31	1.47	11.92	0.26	28.46	1.34	0.06	0	0.2666	0.4182	0.111	0	0.8097
23	R	54.7	1.17	1.5	12.12	0.27	28.23	1.34	0	0	0.2781	0.3791	0.1155	0	0.8058
24	R	54.61	1.3	1.46	11.82	0.26	28.4	1.42	0.07	0	0.2456	0.4431	0.1217	0	0.8107
25	R	54.66	1.23	1.48	12.02	0.26	28.08	1.45	0	0	0.2595	0.3946	0.1354	0	0.8064
26	R	54.55	1.47	1.45	11.73	0.26	28.07	1.68	0.05	0	0.2272	0.4267	0.127	0	0.81
27	R	54.73	1.21	1.5	12.12	0.27	27.87	1.41	0	0	0.2599	0.3879	0.1166	0	0.8038
28	R	54.59	1.24	1.49	12.09	0.27	28.16	1.43	0	0	0.2565	0.3904	0.1191	0	0.8059
29	R	54.6	1.28	1.49	12.05	0.27	28.02	1.47	0.05	0	0.2419	0.3955	0.111	0	0.8056
30	R	54.7	1.35	1.48	11.97	0.26	27.97	1.49	0	0	0.2311	0.409	0.1172	0	0.8063
31	R	54.64	1.47	1.44	11.67	0.25	28.08	1.81	0.07	0	0.2197	0.4282	0.1228	0	0.8109
32	R	54.57	1.31	1.47	11.91	0.26	28.05	1.48	0.04	0	0.2389	0.4077	0.1178	0	0.8076
33	R	54.55	1.26	1.47	11.91	0.26	28.18	1.46	0	0	0.2507	0.4117	0.1086	0	0.8083
34	R	54.65	1.37	1.47	11.87	0.26	28.12	1.55	0.05	0	0.2336	0.4168	0.1013	0	0.8084
35	R	54.52	1.52	1.43	11.55	0.26	28.2	1.66	0.05	0	0.2055	0.4404	0.1011	0	0.8131
36	R	54.47	1.65	1.38	11.17	0.25	28.42	1.76	0.01	0	0.1999	0.4251	0.1008	0	0.8193
37	L	54.36	1.57	1.34	10.86	0.26	28.67	1.51	0	0	0.1911	0.4374	0.0912	0	0.8247
38	L	54.81	1.52	1.34	10.84	0.26	29.15	1.46	0	0	0.1824	0.433	0.0888	0	0.8273
39	L	54.98	1.47	1.35	10.97	0.26	29	1.42	0.03	0	0.1883	0.4373	0.0847	0	0.8249
40	L	54.65	1.66	1.38	11.15	0.27	28.56	1.59	0	0	0.2145	0.4284	0.0826	0	0.8203
41	L	54.78	1.64	1.36	10.99	0.26	28.53	1.7	0.03	0	0.197	0.4358	0.0833	0	0.8222
42	L	54.73	1.57	1.37	11.08	0.26	28.63	1.62	0	0	0.2131	0.3981	0.0815	0	0.8216
43	L	54.75	1.61	1.35	10.97	0.27	28.59	1.65	0	0	0.1906	0.453	0.0813	0	0.8229
44	L	54.63	1.56	1.36	11.04	0.26	28.56	1.62	0	0	0.2032	0.4486	0.0789	0	0.8218
45	L	54.59	1.59	1.37	11.08	0.26	28.66	1.62	0.12	0	0.2076	0.4451	0.0796	0	0.8217
46	L	54.78	1.6	1.37	11.12	0.26	28.55	1.65	0.12	0	0.2132	0.4552	0.0792	0	0.8207
47	L	54.92	1.57	1.36	11.04	0.26	28.53	1.64	0.01	0	0.2117	0.4499	0.0792	0	0.8216
48	L	54.82	1.64	1.37	11.05	0.26	28.54	1.67	0.02	0	0.2189	0.4462	0.0795	0	0.8215
49	L	54.6	1.55	1.37	11.06	0.26	28.7	1.6	0.29	0	0.2197	0.4446	0.0796	0	0.8222
50	L	54.75	1.64	1.36	11.02	0.26	28.66	1.67	0	0	0.2138	0.4486	0.0809	0	0.8225
51	L	54.41	1.6	1.36	11.05	0.26	28.6	1.67	0	0	0.2153	0.4469	0.0832	0	0.8219
52	L	54.55	1.57	1.36	11.04	0.26	28.67	1.58	0	0	0.2191	0.4381	0.0848	0	0.8223

Major Element values for profile R27A plagioclase (Wt%)

Sample	Rock	SiO2	Al2O3	Fe2O3	FeO	MnO	MgO	CaO	Na2O	K2O	TiO2	Cr2O3	NiO	ZnO	Ca#
1	W	49.24	32.25	0	0.12	0	0.17	15.52	2.29	0.17	0.03	0	0	0	0.7893
2	W	49.19	32.26	0	0.12	0	0.2	15.52	2.44	0.17	0.03	0	0	0	0.7786
3	N	49.5	32.27	0	0.12	0	0.2	15.51	2.34	0.17	0.03	0	0	0	0.7856
4	N	49.38	32.26	0	0.11	0	0.18	15.48	2.6	0.17	0.03	0	0	0	0.767
5	N	49.36	32.32	0	0.09	0	0.2	15.42	2.46	0.18	0.03	0	0	0	0.776
6	N	49.53	32.22	0	0.09	0	0.19	15.42	2.51	0.18	0.03	0	0	0	0.7725
7	N	49.47	32.17	0	0.09	0	0.18	15.29	2.65	0.18	0.03	0	0	0	0.7613
8	N	50	31.76	0	0.12	0	0.22	14.86	2.8	0.21	0.03	0	0	0	0.7458
9	X	50.6	30.83	0	0.41	0.01	0.33	13.79	3.06	0.23	0.03	0	0	0	0.7136
10	X	52.79	29.44	0	0.43	0	0.32	12.75	3.6	0.36	0.04	0	0	0	0.6619
11	X	52.87	29.21	0	0.21	0	0.25	12.91	3.76	0.44	0.05	0	0	0	0.6549
12	X	52.76	29.88	0	0.09	0	0.26	13.06	3.57	0.43	0.04	0	0	0	0.6691
13	X	52.96	29.76	0	0.09	0	0.25	12.96	3.52	0.47	0.04	0	0	0	0.6705
14	X	53.58	29.27	0	0.16	0	0.31	12.71	3.38	0.48	0.05	0	0	0	0.6752
15	X	51.24	28.33	0	1.86	0	0.31	12.39	3.35	0.39	0.07	0	0	0	0.6715
17	M	55.87	25.54	0	0.41	0	0.32	11.21	3.6	1.18	0.14	0	0	0	0.6325
19	R	51.56	29.7	0	0.28	0.02	0.93	13.32	3.19	0.52	0.05	0	0	0	0.6977
20	R	51.57	29.04	0	0.92	0.01	1.14	12.57	3.35	0.41	0.06	0	0	0	0.6747
21	R	51.3	29.74	0	0.5	0.01	1.11	13	3.42	0.31	0.07	0	0	0	0.6775
22	R	51.1	30.58	0	0.27	0.01	0.83	13.53	3.47	0.25	0.05	0	0	0	0.6831
23	R	53.27	29.14	0	0.12	0	0.44	12.36	3.64	0.66	0.05	0	0	0	0.6524
24	R	51.02	30.7	0	0.2	0	0.27	13.69	3.31	0.27	0.04	0	0	0	0.6957
25	R	55.73	27.19	0	0.3	0	0.33	11.47	3.48	0.79	0.2	0	0	0	0.6456
26	R	60.53	23.48	0	0.16	0	0.44	10.01	2.97	1.39	0.05	0	0	0	0.6507
27	R	54.53	28.25	0	0.15	0	0.45	12.01	3.74	0.45	0.05	0	0	0	0.6397
28	R	52.44	29.54	0	0.24	0	0.37	12.91	3.59	0.33	0.07	0	0	0	0.6653
29	R	54.36	28.61	0	0.18	0	0.41	12.13	3.43	0.83	0.06	0	0	0	0.6616
30	R	53.04	29.22	0	0.31	0	0.37	12.93	3.33	0.47	0.05	0	0	0	0.6822
31	R	52.57	29.8	0	0.2	0	0.3	13.12	3.44	0.57	0.05	0	0	0	0.6783
32	R	53.17	29.33	0	0.28	0	0.33	12.73	3.32	0.7	0.1	0	0	0	0.6794
33	R	52.81	29.81	0	0.19	0	0.3	12.9	3.6	0.37	0.05	0	0	0	0.6645
34	R	53.51	29.13	0	0.2	0	0.26	12.56	3.72	0.47	0.05	0	0	0	0.6511
35	R	52.55	29.46	0	0.29	0.01	0.66	13.19	3.21	0.52	0.04	0	0	0	0.6943
36	R	50.79	30.88	0	0.34	0.02	0.51	14.18	3.07	0.31	0.06	0	0	0	0.7186
37	L	49.77	32.09	0	0.02	0	0.27	15.17	2.72	0.2	0.03	0	0	0	0.7551
38	L	49.33	32.29	0	0.02	0	0.3	15.41	2.46	0.18	0.03	0	0	0	0.7759
39	L	49.35	32.26	0	0	0	0.27	15.41	2.61	0.19	0.03	0	0	0	0.7655
40	L	49.34	32.19	0	0.08	0	0.35	15.41	2.62	0.19	0.03	0	0	0	0.7648
41	L	49.36	32.24	0	0.1	0	0.38	15.49	2.54	0.18	0.03	0	0	0	0.7712
42	L	49.24	32.28	0	0.12	0	0.33	15.52	2.64	0.19	0.04	0	0	0	0.7647
43	L	49.32	32.06	0	0.11	0	0.35	15.56	2.7	0.18	0.03	0	0	0	0.7611
44	L	49.32	32.02	0	0.11	0	0.39	15.58	2.55	0.17	0.03	0	0	0	0.7716
45	L	49.19	31.91	0	0.12	0	0.34	15.51	2.29	0.16	0.03	0	0	0	0.7892
46	L	49.22	32.36	0	0.12	0	0.33	15.58	2.49	0.18	0.03	0	0	0	0.7757
47	L	49.25	32.08	0	0.12	0	0.33	15.55	2.59	0.18	0.03	0	0	0	0.7685
48	L	49.34	32.2	0	0.12	0	0.4	15.56	2.51	0.18	0.03	0	0	0	0.7741
49	L	49.48	32.37	0	0.12	0	0.3	15.54	2.31	0.19	0.04	0	0	0	0.7881
50	L	49.42	32.05	0	0.13	0	0.35	15.48	2.49	0.19	0.04	0	0	0	0.7746
51	L	49.36	32.14	0	0.13	0	0.35	15.48	2.5	0.19	0.04	0	0	0	0.7739
52	L	49.33	32.07	0	0.13	0	0.38	15.46	2.47	0.19	0.04	0	0	0	0.7758

APPENDIX IV

PLATINUM-GROUP ELEMENT DATA

PGE + Au values for profile R27A whole rock (ppm)

Sample	Rock	Rh	Pd	Pt	Ir	Os	Ru	Au	TotPGE	Pt/Pt+Pd	Pt/Pd
1	W	0.0006	0.025	0.007	0.0001	0.006	0.019	0.0027	0.0577	0.21875	0.28
2	W	0.0006	0.025	0.007	0.0001	0.002	0.019	0.0036	0.0537	0.21875	0.28
3	N	0.0006	0.025	0.007	0.0001	0.002	0.019	0.005	0.0537	0.21875	0.28
4	N	0.0006	0.025	0.007	0.0001	0.002	0.02	0.0064	0.0547	0.21875	0.28
5	N	0.0006	0.00855	0.0317	0.000197	0.002	0.00171	0.0108	0.05371	0.21875	3.707602
6	N	0.0006	0.025	0.007	0.00032	0.004	0.023	0.0085	0.05992	0.21875	0.28
7	N	0.0006	0.025	0.0374	0.00031	0.004	0.023	0.0088	0.09031	0.599359	1.496
8	N	0.0006	0.025	0.0367	0.00085	0.004	0.023	0.0124	0.09015	0.594814	1.468
9	X	0.0006	0.00421	0.139	0.00103	0.004	0.0108	0.0394	0.08546	0.466951	33.01663
10	X	0.0044	0.025	0.0877	0.0022	0.007	0.042	0.0591	0.1683	0.778172	3.508
11	X	0.0106	0.025	0.0306	0.0054	0.007	0.042	0.0505	0.1206	0.55036	1.224
12	X	0.0039	0.025	0.0618	0.0015	0.0071	0.019	0.0081	0.1183	0.711982	2.472
13	X	0.0036	0.025	0.0533	0.0017	0.005	0.032	0.0067	0.1206	0.680715	2.132
14	X	0.023	0.368	0.0893	0.0075	0.008	0.051	0.065	0.5468	0.195277	0.242663
15	X	0.377	1.88	9.192	0.234	0.185	1.56	0.401	13.428	0.830202	4.889362
16	C	0.9	2.47	15.237	0.359	0.316	2.36	0.33	21.642	0.860507	6.168826
17	M	0.381	2.35	8.417	0.164	0.177	1.153	0.218	12.642	0.781741	3.581702
18	C	1.27	3.03	18.288	0.441	0.35	2.86	0.254	26.239	0.857867	6.035644
19	R	0.123	0.566	0.865	0.0389	0.012	0.334	0.0695	1.9389	0.604472	1.528269
20	R	0.115	0.847	0.353	0.0489	0.008	0.324	0.056	1.6959	0.294167	0.416765
21	R	0.349	3.79	7.905	0.124	0.135	1.16	0.463	13.463	0.67593	2.085752
22	R	0.0051	0.078	0.102	0.0018	0.005	0.051	0.0041	0.2429	0.566667	1.307692
23	R	0.0172	0.162	0.351	0.0062	0.008	0.052	0.0099	0.5964	0.684211	2.166667
24	R	0.17	1.25	1.787	0.0507	0.034	0.208	0.519	3.4997	0.58841	1.4296
25	R	0.196	2.4	6.334	0.0813	0.102	0.503	0.115	9.6163	0.725212	2.639167
26	R	0.0838	1.66	3.916	0.0318	0.068	0.15	0.167	5.9096	0.702296	2.359036
27	R	0.0006	0.025	0.006	0.0002	0.003	0.03	0.00284	0.0648	0.193548	0.24
28	R	0.365	3.51	5.093	0.123	0.131	0.981	0.122	10.203	0.592003	1.450997
29	R	0.0006	0.025	0.006	0.0002	0.003	0.03	0.00515	0.0648	0.193548	0.24
30	R	0.0378	0.886	2.247	0.127	0.019	0.139	0.182	3.4558	0.717204	2.536117
31	R	0.471	5.71	5.423	0.161	0.139	1.31	0.594	13.214	0.48711	0.949737
32	R	0.046	0.632	3.796	0.02	0.019	0.139	0.203	4.652	0.857272	6.006329
33	R	0.0006	0.025	0.006	0.0002	0.003	0.03	0.0103	0.0648	0.193548	0.24
34	R	0.0006	0.0129	0.0286	0.000135	0.003	0.00091	0.0101	0.0648	0.193548	2.217054
35	R	0.0006	0.025	0.006	0.0002	0.003	0.03	0.00243	0.0648	0.193548	0.24
36	R	0.0076	0.025	0.072	0.0029	0.003	0.03	0.00236	0.1405	0.742268	2.88
37	L	0.0006	0.025	0.006	0.0002	0.003	0.03	0.00077	0.0648	0.193548	0.24
38	L	0.0006	0.025	0.006	0.0002	0.003	0.03	0.00061	0.0648	0.193548	0.24
39	L	0.0006	0.025	0.006	0.0002	0.003	0.03	0.00064	0.0648	0.193548	0.24
40	L	0.0006	0.00086	0.00153	0.000132	0.003	0.00073	0.000179	0.0648	0.193548	1.77907
41	L	0.0006	0.025	0.006	0.0002	0.003	0.03	0.00028	0.0648	0.193548	0.24
42	L	0.0037	0.025	0.006	0.00077	0.003	0.03	0.00021	0.06847	0.193548	0.24
43	L	0.0006	0.025	0.006	0.0002	0.024	0.03	0.00018	0.0858	0.193548	0.24
44	L	0.0006	0.025	0.006	0.0002	0.0096	0.03	0.00028	0.0714	0.193548	0.24
45	L	0.0005	0.025	0.006	0.0002	0.003	0.03	0.00018	0.0647	0.193548	0.24
46	L	0.0003	0.00048	0.00101	0.000287	0.003	0.00249	0.000113	0.0645	0.193548	2.104167
47	L	0.0044	0.035	0.085	0.00207	0.003	0.03	0.00256	0.15947	0.708333	2.428571
48	L	0.0009	0.025	0.006	0.00036	0.003	0.03	0.0003	0.06526	0.193548	0.24
49	L	0.0057	0.025	0.048	0.00123	0.003	0.03	0.00197	0.11293	0.657534	1.92
50	L	0.0026	0.025	0.006	0.00017	0.003	0.03	0.00084	0.06677	0.193548	0.24
51	L	0.0011	0.025	0.006	0.0002	0.003	0.03	0.00073	0.0653	0.193548	0.24
52	L	0.0011	0.025	0.006	0.00035	0.003	0.03	0.00054	0.06545	0.193548	0.24

PGE + Au values for profile R25A whole rock (ppm)

Sample	Rock	Pt	Pd	Rh	Ir	Ru	Au	TotalPGE	Pt/Pd	Pt/Pt+Pd
8	X	1.54	1.01	0.09	0.031	0.26	0.091	3.022	1.524752	0.603922
9	X	2.9	2.44	0.16	0.076	0.6	0.36	6.536	1.188525	0.543071
10	X	3.84	2	0.24	0.12	0.84	0.3	7.34	1.92	0.657534
11	X	3	1.45	0.18	0.07	0.46	0.16	5.32	2.068966	0.674157
12	X	1.77	0.84	0.044	0.019	0.1	0.16	2.933	2.107143	0.678161
13	R	3.8	1.56	0.075	0.02	0.16	0.2	5.815	2.435897	0.708955
14	C	21	6.04	2.89	1.12	8.38	2.91	42.34	3.476821	0.776627
15	M	1.17	0.36	0.13	0.042	0.35	0.029	2.081	3.25	0.764706
16	M	12.2	3.75	0.45	0.12	0.8	0.68	18	3.253333	0.76489
17	C	8.47	1.53	0.95	0.26	1.52	0.019	12.749	5.535948	0.847
18	A	2.79	1.49	0.026	0.019	0.31	0.2	4.835	1.872483	0.651869
19	C	11.8	7.38	0.88	0.28	1.75	1.91	24	1.598916	0.615224
20	A	8.5	5.91	0.9	0.22	1.3	0.48	17.31	1.43824	0.589868
21	L	4.54	3.05	0.19	0.061	0.54	0.37	8.751	1.488525	0.598155
22	L	3.58	2.45	0.15	0.054	0.41	0.19	6.834	1.461224	0.593698
23	L	0.72	0.46	0.019	0.019	0.064	0.018	1.3	1.565217	0.610169